U.S. Department
of Transportation

**Federal Railroad
Administration**

STUB SILL TANK CAR RESEARCH PROJECT
RESULTS OF A 15,000-MILE OVER-THE-ROAD TEST

**Office of Research and
Development
Washington, D.C. 20590**

DOT\FRA\ORD\95-11

September 1995

This document is available to the
U.S. public through the National
Technical Information Service
Springfield, Virginia 22161

DISCLAIMER

This document is disseminated under the sponsorship of the Department of Transportation in the interest of information exchange. The United States Government assumes no liability for the contents or use thereof. The United States Government does not endorse products or manufacturers. Trade or manufacturers' names appear herein solely because they are considered essential to the object of this report.

METRIC CONVERSION FACTORS

Approximate Conversions to Metric Measures

Symbol	When You Know	Multiply by	To Find	Symbol
		LENGTH		
in	inches	*2.50	centimeters	cm
ft	feet	30.00	centimeters	cm
yd	yards	0.90	meters	m
mi	miles	1.60	kilometers	km
		AREA		
in^2	square inches	6.50	square centimeters	cm^2
ft^2	square feet	0.09	square meters	m^2
yd^2	square yards	0.80	square meters	m^2
mi^2	square miles	2.60	square kilometers	km^2
	acres	0.40	hectares	ha
		MASS (weight)		
oz	ounces	28.00	grams	g
lb	pounds	0.45	kilograms	kg
	short tons (2000 lb)	0.90	tonnes	t
		VOLUME		
tsp	teaspoons	5.00	milliliters	ml
Tbsp	tablespoons	15.00	milliliters	ml
fl oz	fluid ounces	30.00	milliliters	ml
c	cups	0.24	liters	l
pt	pints	0.47	liters	l
qt	quarts	0.95	liters	l
gal	gallons	3.80	liters	l
ft^3	cubic feet	0.03	cubic meters	m^3
yd^3	cubic yards	0.76	cubic meters	m^3
		TEMPERATURE (exact)		
°F	Fahrenheit temperature	5/9 (after subtracting 32)	Celsius temperature	°C

* 1 in. = 2.54 cm (exactly)

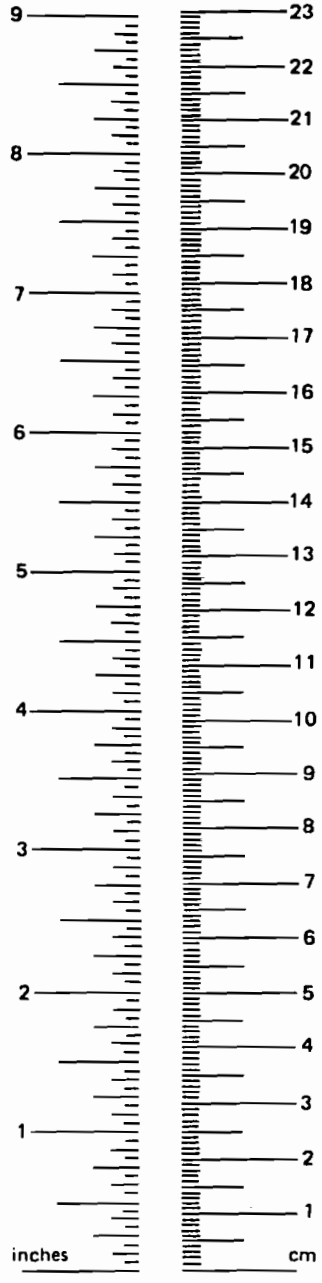

Approximate Conversions from Metric Measures

Symbol	When You Know	Multiply by	To Find	Symbol
		LENGTH		
mm	millimeters	0.04	inches	in
cm	centimeters	0.40	inches	in
m	meters	3.30	feet	ft
m	meters	1.10	yards	yd
km	kilometers	0.60	miles	mi
		AREA		
cm^2	square centim.	0.16	square inches	in^2
m^2	square meters	1.20	square yards	yd^2
km^2	square kilom.	0.40	square miles	mi^2
ha	hectares (10,000 m^2)	2.50	acres	
		MASS (weight)		
g	grams	0.035	ounces	oz
kg	kilograms	2.2	pounds	lb
t	tonnes (1000 kg)	1.1	short tons	
		VOLUME		
ml	milliliters	0.03	fluid ounces	fl oz
l	liters	2.10	pints	pt
l	liters	1.06	quarts	qt
l	liters	0.26	gallons	gal
m^3	cubic meters	36.00	cubic feet	ft^3
m^3	cubic meters	1.30	cubic yards	yd^3
		TEMPERATURE (exact)		
°C	Celsius temperature	9/5 (then add 32	Fahrenheit temperature	°F

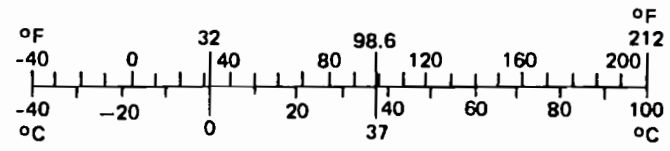

1. Report No.	2. Government Accession No.	3. Recipient's Catalog No.
FRA\ORD\95-11		

4. Title and Subtitle	5. Report Date
Stub Sill Tank Car Research Project Results of a 15,000-mile Over-the-Road Test	September 1995
	6. Performing Organization Code
7. Authors Lowell T. Cogburn	8. Performing Organization Report no.
9. Performing Organization Name & Address Association of American Railroads Transportation Technology Center P. O. Box 11130 Pueblo, CO 81001	10. Work Unit No. (TRAIS)
	11. Contract Or Grant No. DTFR53-93-C-00001 TO 108, Task 2
12. Sponsoring Agency Name & Address U.S. Department of Transportation Federal Railroad Administration Office of Research and Development 400 Seventh Street SW Washington, D.C. 20590	13. Type Of Report Or Period Covered August 1994 through April 1995
	14. Sponsoring Agency Code DOT/FRA/RDV-32

15. Supplemental Notes

16. Abstract

The Federal Railroad Administration (FRA) contracted with the Association of American Railroads (AAR), Transportation Test Center (TTC) — now known as the Transportation Technology Center — Pueblo, Colorado, to study in-revenue service loads on stub sill constructed tank cars. Over 162,000 of these cars have been placed into service since 1950. The FRA has been investigating incidents of fatigue cracking at the attachment of the stub sill to the tank shell of these cars. As a result, the FRA has undertaken a program to work with industry representatives to further investigate the causes of the fatigue cracking and recommend preventative measures.

Results from the over-the-road (OTR) testing showed that the highest surge pressures experienced never exceeded 40 psi. OTR testing resulted in obtaining vertical coupler force and longitudinal coupler force histograms for typical environments experienced by tank cars. Representative time history events were obtained that suggest a possible source of VCF's responsible for a high percentage of total fatigue damage experienced by tank cars.

17. Key Words	18. Distribution Statement
Vertical Coupler Force, Fatigue Damage, NCF Histogram LCF Histogram, Impact Time Histories, OTR testing FEEST Data	This document is available through National Technical Information Service Springfield, VA 22161

19. Security Classification (of the report)	20. Security Classification (of this page)	21. No Of Pages	22. Price
Unclassified	Unclassified	285	

Form DOT F 1700.7 (8-72)

Executive Summary

The Federal Railroad Administration (FRA) has been investigating incidents of fatigue cracking of the stub sill and at the attachment of the stub sill to the tank shell of stub sill type tank cars. Over 162,000 of these cars have been placed in service since 1950. The FRA has also issued Emergency Order #17, which asks the railroad industry to investigate further failures of stub sill tank cars and recommend preventative measures.

The FRA contacted with the Association of American Railroads (AAR), Transportation Test Center (TTC) — now known as the Transportation Technology Center — Pueblo, Colorado, to study effect of in-revenue-service loads on this type tank cars. The AAR TTC was tasked to investigate and define the forces imposed on the structure and validate the AAR'S Freight Equipment Environmental Sampling Test (FEEST). Data collected during the 1988 FEEST included vertical coupler force (VCF) levels, which were characterized by a high force level "hump" in the histogram. When used in a previous fatigue analysis project (performed by the AAR TTC for FRA), the hump resulted in a severe reduction of the expected fatigue life of stub sill tank cars. Because of this, the validity of the FEEST data, contained in the *AAR Manual of Standards and Recommended Practices*, has been questioned.

To validate or redefine the forces measured during FEEST, a representative stub sill tank car was fitted with a remote data acquisition system to record the same type of information obtained during FEEST. Primarily, the data consisted of significant longitudinal and vertical coupler loads during in-service conditions. The instrumented tank car used for testing collected data for approximately 15,000 in-service miles and traversed approximately the same basic route as was used during FEEST. This report presents the data collected in the over-the-road (OTR) test conducted from August, 1994 to March, 1995.

The OTR testing resulted in obtaining histograms and representative time history data that was very similar to the FEEST data except for the absence of the hump in the VCF histograms. However, VCF's were still indicated that would reduce the fatigue life in the critical area.

A significant contribution to the reduction of the critical area fatigue life was found to be a high number of relatively low-frequency (i.e., waveform frequency) VCF events. The source of these events was hypothesized to be caused by the changes in the vertical stiffness of the track such as those changes that occur at crossings. The change in track stiffness results in temporarily producing a dynamic height differential between the two adjacent cars as the wheels roll over the area. That difference in height develops the VCF. The ability of the couplers to sustain relatively large VCFs is demonstrated with actual test data acquired during the OTR test. Elimination in the number of these events or a reduction in the force levels produced by these events would result in significant increases in the fatigue life of stub sill tank cars.

Further investigation to verify this hypothesis is recommended. The investigation should include the use of a dedicated instrumented coupler capable of measuring vertical, longitudinal, lateral, and torque coupler forces simultaneously with the vertical wheel motions of the test car and adjacent cars. A more detailed understanding of the source of the low frequency VCFs may allow modifications to the couplers which would provide increased vertical compliance thus eliminating the development of the forces. Ride quality also may be improved by eliminating the VCFs.

The existence of the simultaneous existence of large VCF and longitudinal coupler force during impact conditions was demonstrated with OTR and impact test data. Due to the high stresses produced in the critical region of the stub sill tank car by the VCF, we recommend that a static design case consisting of the simultaneous application of a 60 kip vertical (up and down) load at the sill and a 1000 kip longitudinal coupler force (buff) be considered.

In addition to determining the coupler loading environment, a surge pressure test was conducted concurrently with the OTR test. Surge pressure data was collected for approximately 9,500 miles of in-service conditions during which significant surge pressure events were recorded by the onboard data acquisition system.

Results from the OTR testing showed that the highest surge pressures experienced never exceeded 40 psi. The vast majority of surge pressures were in the 10 to 30 psi range. Impact tests were conducted at the conclusion of the OTR testing to further validate the OTR data. Impact tests produced results very similar to the OTR results. The impact testing showed that high speed impacts (producing longitudinal coupler forces in excess of 1100 kips) did not necessarily produce corresponding high surge pressures.

TABLE OF CONTENTS

1.0 INTRODUCTION 1

1.1 15,000-MILE OTR TEST 3

2.0 OBJECTIVE 3

3.0 PROCEDURES 3

3.1 FEEST2 TEST CAR SELECTION 3

3.2 TEST ROUTE AND LADING 5

3.3 DATA ACQUISITION SYSTEMS 5

3.4 DATA ACQUISITION POWER SYSTEM 6

3.5 INSTRUMENTATION DATA MODES 6

3.5.1 Rainflow Mode 6

3.5.2 Burst (Time) History Mode 8

3.5.3 Peak Valley Mode 9

3.5.4 Time at Level Mode 9

3.6 FEEST2 INSTRUMENTATION 9

3.6.1 Test Car Speed 15

3.6.2 Longitudinal Coupler Force Measurement (LCF1B and LCF2B) 15

3.6.3 Coupler Shank Shear (VCFS) 18

3.6.4 Vertical Sill Bending (VCBA) 21

3.6.5 Vertical Sill Shear (VCFA and VCFB) 25

3.6.6 Striker Carrier (SCTA and SCTB) 30

3.6.7 Yoke Support Plate (YPLA and YPLB) 30

3.6.8 Side Bearing Load Measurements 32

3.6.9 Truck Bolster Vertical Load Measurements (BOLA and BOLB) 34

3.6.10 Micro Strain Measurements 37

3.6.11 Tank Internal Surge Pressure Measurement 42

3.7 COUPLER JACKING TESTS 43
3.8 VCF MEASUREMENT EVOLUTION COUPLER LOAD INVESTIGATION TESTS 44
3.9 TEST PROCEDURE 54
3.9.1 Parameter Operational Status 55
3.9.2 Test Lading 57
3.10 SURGE PRESSURE IMPACT TESTS 57
3.10.1 Surge Pressure Impact Test Configurations 57

4.0 TEST RESULTS 59
4.1 RELATIVE FATIGUE LIFE ANALYSIS RESULTS 60
4.2 TEST HISTOGRAMS 66
4.3 FEEST2 TEST BURST HISTORY DATA 95
4.4 FEEST2 CONSIST LOCATION 108
4.5 FEEST2 OUTAGE AND TEMPERATURE MEASUREMENTS 110
4.6 FEEST2 SURGE PRESSURE DATA 111
4.7 SURGE PRESSURE IMPACT TESTS RESULTS 114
4.8 FEEST2 SHOCK WATCH DATA 120
4.8.1 Surge Pressure Impact Tests Shock Watch Data 121
4.9 CRITICAL REGION STRAINS 125
4.10 IMPACT TEST DATA 135
5.0 CONCLUSIONS AND RECOMMENDATIONS 136

APPENDIX A — Histograms for the Loaded Portion of the OTR Testing A-0
APPENDIX B — Histograms for the Unloaded Portion of the OTR Testing B-0
APPENDIX C — OTR Surge Pressure Response Data C-0
APPENDIX D — Shock Watch Data Obtained During the OTR Test D-0
APPENDIX E — Leg to Leg Speed Distribution E-0
APPENDIX F — OTR Leg 9 Burst History Data F-0
APPENDIX G — OTR Loaded and Empty Impact Events G-0

TABLE OF FIGURES

Figure 1. Locations of Test Measurements for the FEEST2 Tests 10

Figure 2. LCF Measurement LCF1B Calibration Check 17

Figure 3. Coupler Shank Shear Measurement VCFS 18

Figure 4. VCF Measurement VCFS Calibration Check 19

Figure 5. VCFS Cross Axis Sensitivity Check 20

Figure 6. Sill Bending Measurement VCBA 22

Figure 7. VCBA VCF Sensitivity 23

Figure 8. VCBA LCF Sensitivity 24

Figure 9. Sill Shear Measurements VCFA and VCFB 25

Figure 10. VCFA and VCFB Calibration 27

Figure 11. VCFA LCF Sensitivity 28

Figure 12. VCFB LCF Sensitivity 29

Figure 13. Locations of VCF Instrumentation for the FEEST2 Test 31

Figure 14. Yoke Plate Load Calibration Points 32

Figure 15. Side Bearing Load Measurement Installation 33

Figure 16. Side Bearing Load Measurement Installation 33

Figure 17. Truck Bolster Load Measurements 35

Figure 18. Truck Bolster Load Measurement Circuits 36

Figure 19. Strain gage Locations -- Sill bending, Critical Region Rosette 37

Figure 20. SG3A VCF Sensitivity 40

Figure 21. Critical Region Strain LCF Sensitivity 41

Figure 22. Surge Pressure Transducer Installation 42

Figure 23. Jacking Calibration Configurations 44

Figure 24. FEEST1 Assumed VCF Load Path 47

Figure 25. Shear Diagram For Assumed VCF Load Path 48

Figure 26A. Comparison of VCF Measurements B-End 51

Figure 26B. Comparison VCF Measurements A-End 52

Figure 26C. Low Frequency VCF Measurement Comparisons 53

Figure 27. Surge Pressure Impact Configuration A and B 58

Figure 28. Surge Pressure Impact Test Configuration C 58

Figure 29. Loaded VCF Histograms 70
Figure 30. Unloaded VCFB Histograms 71
Figure 31. Loaded and Unloaded FEEST2 VCFB Histograms 72
Figure 32. Loaded LCF1B Histograms 73
Figure 33. Unloaded LCF1B Histograms 74
Figure 34. Loaded and Unloaded FEEST2 LCF1B Histograms 75
Figure 35. LCF Average Values for the Loaded Configuration 79
Figure 36. LCF Average Values for the Unloaded Configuration 80
Figure 37. LCF Leg to Leg Values for the Loaded Configuration 81
Figure 38. VCF Histogram Comparisons 82
Figure 39. VCFA and VCFB Equivalent Coupler Force Comparisons 83
Figure 40. Loaded Vertical Bolster Loads Histogram Comparisons 84
Figure 41. Unloaded Vertical Bolster Loads Histogram Comparisons 85
Figure 42. Loaded Sill Bending VCBA Histogram 86
Figure 43. VCBA Equivalent Sill Force Histogram 87
Figure 44. Loaded LCF Distribution 90
Figure 45. Unloaded LCF Distribution 91
Figure 46. Loaded VCF Distribution (VCFA) 92
Figure 47. Loaded VCF Distribution (VCFB) 93
Figure 48. Unloaded VCF Distribution (VCFB) 94
Figure 49. Leg 9 Typical Coupling Event 100
Figure 50. Leg 9 Typical Low Frequency VCF Event 101
Figure 51. Low Frequency High Magnitude VCF Event 102
Figure 52. Low Frequency High Speed VCF Event 103
Figure 53. VCF Sticktion Event 104
Figure 54. Largest VCF Event Recorded 105
Figure 55. Leg 9 Typical Low Frequency VCF Event 106
Figure 56. Leg 9 Typical "Smooth" Coupling Event 107
Figure 57. FEEST2 Surge Pressure Peak Valley Results 113
Figure 58. Surge Pressure Repeatability 8 mph 117
Figure 59. Surge Pressure Repeatability 9 mph 118
Figure 60. Surge Pressure Repeatability 9 mph 119

Figure 61. Surge Pressure Impact Test 9 mph Configuration A 124
Figure 62. Critical Region Strain Response to Impact 126
Figure 63. Coupler Force Response To Impact 127
Figure 64. Critical Region Stress Response to Impact 128
Figure 65. Critical Region Stress Response to Impact on Leg 10 130
Figure 66. Critical Region Stress Response During Leg 10 131
Figure 67. Loaded VCF Fatigue Life Distribution for VCFB 132
Figure 68. Loaded LCF Fatigue Life Distribution for LCF1B 133
Figure 69. LCF VCF Phase Relationship During Impact 135

LIST OF TABLES

Table 1. FEEST2 Test Car Characteristics 4
Table 2. FEEST2 Test Measurements Recorded by SOMAT 1 (B end) 11
Table 3. FEEST2 Test Measurements Recorded by SOMAT 2 (A-end) 11
Table 4. FEEST2 Test Strain Environment Measurements Recorded by SOMAT 3 12
Table 5. Surge-Pressure FEEST2 Test Measurements Recorded by SOMAT4 12
Table 6. Data Modes for Measurements Recorded by SOMAT 1 13
Table 7. Data Modes for Measurements Recorded by SOMAT 2 13
Table 8. Data Modes for Measurements Recorded by SOMAT 3 14
Table 9. Data Modes for Measurements Recorded by SOMAT 4 14
Table 10. VCF Sensitivities for Various Calibration Methods 26
Table 11. Yoke Support Plate Sensitivities vs Location 31
Table 12. Stress Level Relations In The Critical Region 38
Table 13. Operational Mileages By Measurement For SOMAT 1 55
Table 14. Operational Mileages By Measurement For SOMAT 2 56
Table 15. Operational Mileages By Measurement for SOMAT's 3 and 4 56
Table 16. Relative Leg and Cumulative Fatigue Mileages for VCFB 62
Table 17. Relative Leg and Cumulative Fatigue Mileages for VCFA 63
Table 18. Relative Leg and Cumulative Fatigue Mileages for LCF1B 64
Table 19. FEEST2 Test Consist Information 109
Table 20. FEEST2 Outages and Water-Methanol Temperatures 110
Table 21. Surge Pressure Impact Test Configurations and Results 115
Table 22. Leg 7 Shock Watch Data 121
Table 23. Surge Pressure Impact Tests Shock Watch Data 122

1.0 INTRODUCTION

The Federal Railroad Administration (FRA) contracted with the Association of American Railroads (AAR), Transportation Test Center (TTC) — now known as the Transportation Technology Center — Pueblo, Colorado, to study in-revenue service loads on stub sill construction tank cars. The FRA has been investigating incidents of fatigue cracking in stub sill tank cars. These cars comprise nearly all tanks build since the 1950's and total over 162,000 units. Fatigue cracking at the attachment of the stub sill to the tank shell has been found in a number of these tanks throughout the industry. The FRA has therefore undertaken a program to work with industry representatives to investigate the causes of the fatigue cracking and recommend preventative measures.

In 1990, the FRA tasked the AAR-TTC under contract DTFR53-82-C-00282, Task Order 43, to study fatigue crack growth in stub sill tank cars. TTC's Simuloader (fatigue test fixture) was used to replicate 300,000 miles of fatigue-significant tank car service. The fatigue loads used were obtained by combining the representative tank car waveforms gathered during an over-the-road (OTR) test with the AAR's 1988 Freight Equipment environmental Sampling Test (hereafter referred to as FEEST1) modified to conform with the OTR waveforms. The modification consisted of the addition of vertical coupler forces (VCF) to the FEEST1 parameters. This test program indicated that the VCF was the primary contributor to crack initiation and propagation in the head and sill pads of a stub sill tank car without a head brace.

The AAR has been publishing the FEEST1 data, since June 1988, in the *AAR Manual of Standards and Recommended Practices*, Section C, Part II, Chapter II, "Road Environment Percent Occurrence Spectrum— Fatigue Design of New Freight Cars." Prior to June 1988, the environmental load data for tank cars were found in the original Freight Car Fatigue Analysis (FCFA) guidelines (AAR Report 245, dated May 1977). The FCFA data was based on 1970 road test data using range-mean cycle counting methods. The FEEST1 uses the more conservative rainflow cycle counting techniques. The FCFA study recorded a maximum VCF of 12.5 kips for an E-type coupler. The FEEST1 recorded 50 kips on the

same type coupler. The relatively high load levels and repeatability recorded during the FEEST1 study have been questioned.

Past testing focused on stub sill tank cars without head braces. However, many in-service tank cars have been fitted with head bracing designed to reduce the stress concentration at the sill/tank shell interface. The effectiveness of these designs at limiting fatigue cracks at the tank to sill junction has not been investigated quantitatively. The VCF may no longer be the primary fatigue-causing force in these modified tanks.

The FRA funded the development of finite element models of stub sill tank car designs for the evaluation of stresses resultant from VCF input. These models have also made comparative studies of head brace alternatives. Little validation of these models has been performed with actual data from a railcar.

Stub Sill Tank Car Research test programs have been undertaken to address the concerns raised about the FEEST1 data, head brace designs, and finite element model validation. To accomplish these tasks, the following test phases have been developed, corresponding to Tasks 2 through 4, as defined in the FRA statement of work for contract DTFR J3-93-C-00001, TO108.

Task 2: 15,000-MILE OTR TEST OF A STUB SILL TANK CAR

Task 3: STUB SILL TANK CAR FATIGUE TEST

Task 4: STUB SILL TANK CAR SQUEEZE TEST

This document covers only Task 2, the 15,000-mile OTR test.

1.1 15,000-MILE OTR TEST

This document presents the results of the Stub Sill Tank Car 15,000-mile OTR test, which was co-funded by the Railway Progress Institute (RPI), FRA, and AAR. References in this report to "FEEST2" refer to data or events that were associated with the OTR testing performed from August 1994 until March 1995. The test program was designed to collect revenue-service load and strain environment data for a stub sill tank car, principally to confirm or replace the loads characterized in 1986 under the FEEST1 test program. The original data collected in 1986 will be referred to as "FEEST1" in this report. The test car, provided by RPI, was instrumented in a fashion similar to the instrumentation used during the AAR FEEST1 tests. Prior to OTR testing, coupler load investigation tests were performed to study and optimize the instrumentation. OTR test data was recorded by an onboard unattended data collection system. Additional instrumentation also allowed surge pressure relief nozzle environmental data to be recorded.

2.0 OBJECTIVE

The objective of this test program was to measure and record approximately 15,000 miles of revenue-service loads for a stub sill tank car, principally to confirm or replace the tank car loads spectra characterized in the 1986 FEEST1 test program. Additionally, the test car was instrumented to collect surge pressure data in order to characterize the internal tank pressures experienced during in-service operations.

3.0 PROCEDURES

3.1 FEEST2 TEST CAR SELECTION

The RPI Tank Car Committee selected a member tank car manufacturer at random to provide a car for the program. As a result, Union Tank Car Company provided a DOT 111A100W-3 tank car previously used in revenue service. The car was thoroughly inspected upon arrival at TTC for proper operation and no defects were found. To help with the surge pressure study, the car's original 75 psi safety valve was replaced with a 165-pound frangible disk, and the car was reclassified to combustible prior to entering interchange. Table 1 lists the test car characteristics.

Table 1. FEEST2 Test Car Characteristics

Classification	DOT E11309 -- placard combustible liquid
Car number	UTLX 67571
Typical load	Vegetable oil
Total mileage upon receipt	128,000 miles
Year built	March 1981
Sill Test	February 1993
Tank Test	1991 -- 100 psi
Safety Vent	165 frangible disk
Insulation	4" fiber glass; #11 gage jacket
Coils	16 runs of external coils
Reinforcing pads	5/8" x 16" extending 10' inboard of body
Draft gear	M901E
B-end coupler	Type E double shelf, instrumented
A-end coupler	Type E double shelf, no instrumentation
Truck type	100-ton Barber S-2
Side bearings as-received	Friction block
Side bearings as-tested	Friction block modified with load cells
Brake system	Rod through
Spring group	D-3 springs
Shell	7/16" - A515
Diameter	111" OD
Capacity	23,535 gallons
Weight on rail (maximum)	263,000 pounds
Light weight of car	74,500 pounds
Outage tested	1 percent
Weight on rail as tested	262,500 pounds
Length between strikers	52' 9-1/2"
Length between truck centers	41' 10-1/2"
Truck axle centers	5' 10"
B-end coupler height (loaded)	33-1/2"
A-end coupler height (loaded)	34"

3.2 TEST ROUTE AND LADING

The FEEST2 test route was the same route taken, when possible, by the FEEST1 in order to duplicate the loading environment as closely as possible. The test car traversed approximately 15,000 miles of revenue service track during unattended data collection. The 15,000 miles was divided into 11 individual segments which are referred to as legs. The first 10 legs were completed with the tank car loaded (approximately 12,331 miles) and the 11th leg was completed with the tank car empty (approximately 4,179 miles).

The tank car was filled with a water-methanol mixture designed to provide realistic lading volume and density. The initial outage at the beginning of the test was 1.0 percent.

3.3 DATA ACQUISITION SYSTEMS

Four 12-bit SOMAT 3200 data acquisition systems were configured for unattended operation and were mounted on the exterior of the tank car. Two of the SOMAT systems were used to record the FEEST1-type load measurements. A third SOMAT was used to record critical region strain measurements and additional measurements of sill strain added for the Coupler Load Investigation Test. The fourth SOMAT system recorded the surge pressure measurements which consisted of tank surge pressure, longitudinal coupler force, and tank car speed.

Union Tank purchased two Shock Watch MAG3500 impact detectors for the program, which were installed on the A- and B-end of the tank car. The Shock Watch units detected and recorded shocks at levels of 2, 4, 6, and 10 g's (acceleration) and tagged these events with the date and time of the shock event. Units were mounted to the body bolster on the B-end-right and A-end-left sides of the car. These units were not maintained, calibrated or serviced by TTC personnel during the FEEST2 testing; thereby, no assurance of the data accuracy collected by these units is implied by their use during the OTR testing.

A global positioning satellite (GPS) system and cellular phone link was added by AAR/TTC. The GPS system was used to track the location and progress of the tank car during the FEEST2 tests. This system provided accurate location information that was used to monitor the correct routing of the tank car and to schedule the trips required to retrieve the data collected by the SOMAT units (downloading).

3.4 DATA ACQUISITION POWER SYSTEM

The electrical power required for the data collection system was provided by two sources, which acted in parallel to charge the onboard batteries. The first system was an axle driven alternator, providing a charging current to the batteries when the car was in motion. Eighteen solar panels made up the other system, providing a charging current for those periods of time when the tank car was stationary. The electrical storage system consisted of eight marine batteries, providing continuous electrical power directly to the SOMAT units.

3.5 INSTRUMENTATION DATA MODES

The SOMAT units used during the FEEST2 testing were capable of acquiring data in several different modes of operation. Three of these data modes were used to acquire and store data during the test. Data modes associated with each parameter are listed in Tables 2, 3, 4 and 5 and are explained in more detail below. They are presented in order to provide an understanding of the limitations imposed on the data analysis.

3.5.1 Rainflow Mode

The rainflow mode was used to compress time history data into histograms for those channels specified. This methodology compresses data by only recording the number of paired peak/valley combinations that occur within a predetermined range of values referred to as bins. The width of the bins is specified in engineering units. As testing progresses, each bin's count value is incremented by one for each peak/valley occurrence observed. The accumulated count values for all bins are displayed in histograms which contain all the peak/valley occurrences distributed into the appropriate bin values. The

number of bins and the width of the bins are predetermined before the testing begins. The values chosen for the FEEST2 test were selected in order to closely match the FEEST1 values to allow direct comparisons.

Due to the nature of the rainflow algorithm, peak/valley values that may have occurred days apart can be paired together as a single event, as a result of a high positive and high negative value. Indeed, these values do represent a cycle, but as previously mentioned, can occur at different times. For example, under similar conditions, VCF's of -25 kips and +25 kips, which were both generated by impacts that occurred days apart, could be paired together as a 50-kip event in the resulting histogram.

The rainflow ~~mode ran~~ continuously on those measurements that were specified. As a result, any intermittent noise in the instrumentation system or power interruptions that occurred during a leg would be counted as events and stored in memory as count values. The time history data (to be discussed in Section 3.5.2) associated with these events may or may not have been stored if the trigger level were exceeded and computer memory in the SOMAT units were not available. As such, burst history data that was triggered after the memory was full was not stored. These limitations made checking histogram data quality very difficult because the time history information used to develop the histogram was generally not available.

During the FEEST2 testing, the procedure was that if the operation of a SOMAT unit was interrupted at any point during data collection, then the data collected by that individual SOMAT for that leg was considered invalid. Power interruptions did occur on several legs, which will be shown later. If any of the burst histories that were collected showed evidence of noise or intermittent operation, the rainflow data for that leg was considered invalid. This problem points out one of the limitations imposed by an unattended data collection system combined with a real time processing algorithm, such as rainflow. An example of the effects of a very brief amount of "noise" in the instrumentation system on the rainflow counting algorithm will be presented later in this report.

3.5.2 Burst (Time) History Mode

The initial burst history mode (referred to as burst histories or time histories) was used on several measurements to collect time history data. This mode was only active after a selected measurement exceeded a predefined value. This measurement and value together are referred to as the trigger. Once the trigger was exceeded, collection of data was initiated on those channels specified. Due to limitations on real time processing capability, it was found that each SOMAT unit had to have its own individual trigger which was not common with the other SOMAT units. Attempts to have multiple triggers on an individual SOMAT unit were unsuccessful due to the inability of the processor to keep up with the necessary real-time calculations required. This limitation prevents the correlation of burst histories events acquired on one SOMAT unit to events captured on another SOMAT unit.

The burst history mode was used to capture time history data before and after a trigger event. The data before the trigger event is captured by temporally storing the data in a buffer that is written over without being stored in long term memory until the trigger conditions are satisfied. When the trigger condition is satisfied, the data before the trigger event is still resident in a short term storage buffer which is then transferred into long term memory for storage. The burst history mode results in one half of the window length (typical window lengths were 2 or 5 seconds) being filled with data that occurred before the trigger level was exceeded and the last half being filled with data after the trigger event.

The use of triggers implied that only those events that the trigger was sensitive to would be collected. This sensitivity predisposes the data collected to the type of events that produce conditions high enough to cause a trigger. Other events that may cause significant responses in the non-triggering measurements may not have been recorded in the burst history mode due to the trigger being insensitive to that particular type of event. These limitations will be discussed further in the sections on the test data.

Due to memory limitations, the long term buffers used to store events are typically filled during a leg. Once these buffers are filled, no further burst histories are stored. As a result, many of the events that were recorded by the rainflow mode were not captured by the burst history mode.

3.5.3 Peak Valley Mode

The peak valley mode is essentially a time history with only the peaks and valleys being stored. All of the intermediate data is discarded. To specify how peaks and valleys are defined, it is necessary to define a minimum change that must occur between values before a new peak or valley is to be considered. This value is referred to as the hysteresis. This mode ran continuously and required no trigger parameter. This mode was used on the surge pressure measurement.

3.5.4 Time at Level Mode

The time at level mode uses bins which are arranged along the y-axis. When a value is measured, the bin level associated with that value is incremented by 1. The speed measurement used this mode to show the relative time spent at given speeds. Speed values were recorded, approximately once each minute, when the speed was greater than 1 mph.

3.6 FEEST2 INSTRUMENTATION

Figure 1 shows the locations of the test car FEEST2 instrumentation and nomenclature used in this report. Tables 2, 3, 4 and 5 list the measurements along with a description and ranges for all of the measurements — SPEED, LCF1B, VCFB, YPLB, SCTB, SBBR, BOLB — that were active during the OTR tests. Each SOMAT unit also recorded the elapsed time (in seconds) which started at zero after initialization of that individual unit. The names listed in these tables will be used throughout the report when referring to individual measurements. Individual measurement characteristics are described in the following sections. Tables 6, 7, 8 and 9 list the names and data mode for each measurement.

Sections 3.6.3 through 3.6.11 present brief descriptions of each measurement to familiarize the reader with the measurement locations and general characteristics. Due to the complexity in the measurement of the VCF, a history of the evolution of the measurement techniques used during the FEEST2 test is given in Section 3.8.

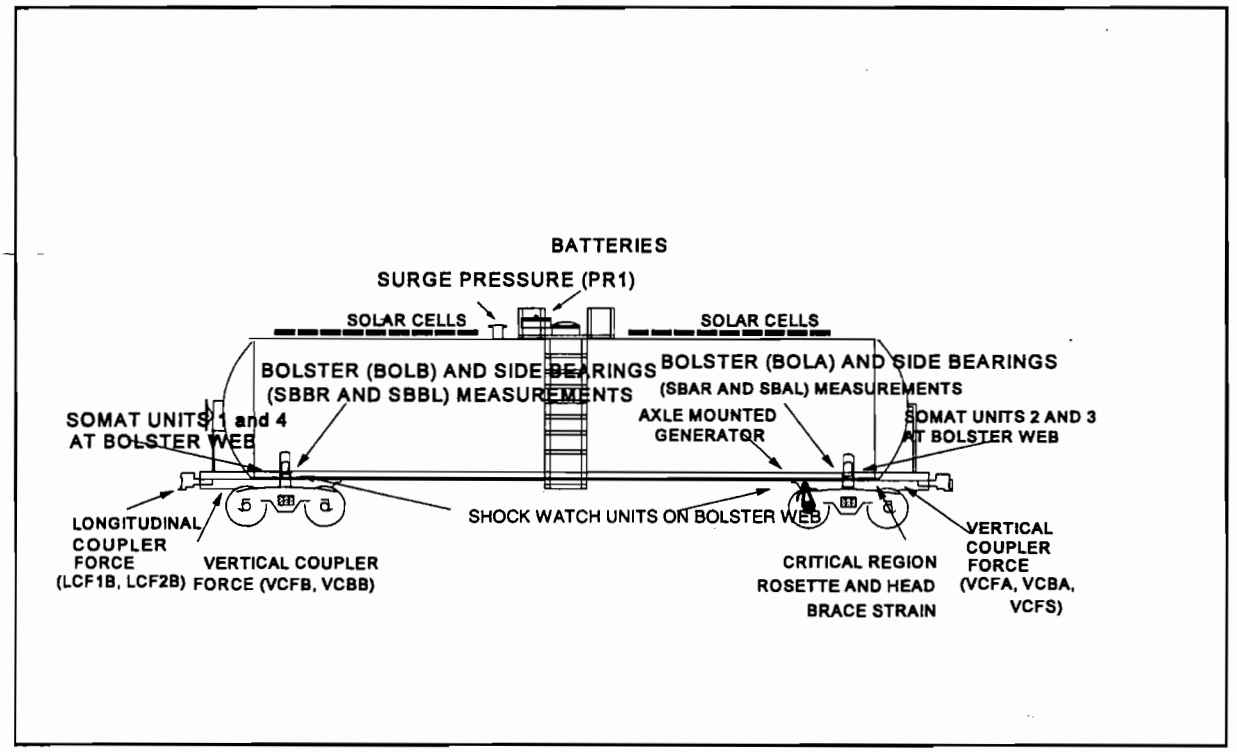

Figure 1. Locations of Test Measurements for the FEEST2 Tests

Table 2. FEEST2 Test Measurements Recorded by SOMAT 1 (B-end)

MEASUREMENT	DESCRIPTION AND LOCATION	TYPE	RANGE
SPEED	Test car speed	tachometer	0-100 mph
LCF1B	B-end, longitudinal coupler force (double shelf coupler)	calibrated strain-gage	+1,000 kips
VCFB (trigger)	Vertical Coupler Load, Sill Shear, B-end	calibrated shear gage	+60 kips
YPLB	Yoke Support Plate Load, B-end	calibrated shear gage	+50 kips
SCTB	Striker/carrier Plate Load, B-end	calibrated strain gage	-50-100 kips
SBBR	Side Bearing Load, B-end, right side	load cell	-20-100 kips
BOLB	Truck Bolster Vertical Load, B-end	calibrated shear gage	-120-280 kips

Table 3. FEEST2 Test Measurements Recorded by SOMAT 2 (A-end)

MEASUREMENT	DESCRIPTION AND LOCATION	TYPE	RANGE
SPEED	Test car speed	tachometer	0-100 mph
VCFA (trigger)	Vertical Coupler Load, Sill Shear, A-end	calibrated shear gage	+60 kips
VCFS	Vertical Coupler Load, Coupler Shank Shear, A-end	calibrated shear gage	+60 kips
YPLA	Yoke Support Plate Load, A-end	calibrated shear gage	+50 kips
BOLB	Truck Bolster Vertical Load, B-end	calibrated shear gage	-120-280 kips
SCTA	Striker/carrier Plate Load, A-end	calibrated shear gage	-50-100 kips

Table 4. FEEST2 Test Strain Environment Measurements Recorded by SOMAT 3

MEASUREMENT	DESCRIPTION AND LOCATION	TYPE	RANGE
SPEED	Test car speed	tachometer	0-100 mph
SG1A	Vertical strain gage in rosette located near stub sill to tank shell interface, A-end	strain gage	+1200 muST
SG2A	Diagonal strain gage in rosette located near stub sill to tank shell interface, A-end	strain gage	+1200 muST
SG3A	Horizontal strain gage in rosette located near stub sill to tank shell interface, A-end	strain gage	+1200 muST
SG4A	Strain gage on head brace, vertical, A-end	strain gage	+200 muST
VCBA (trigger)	Sill bending, A-end	strain gage	+1200 muST

[1]muST = micro strain

Table 5. Surge-Pressure FEEST2 Test Measurements Recorded by SOMAT 4

MEASUREMENT	DESCRIPTION AND LOCATION	TYPE	RANGE
SPEED	Test car speed	tachometer	0-100 mph
LCF2B (trigger unloaded)	B-end longitudinal coupler force (second set of gages on coupler)	calibrated strain-gage	+1,000 kips
PR1 (trigger loaded)	Surge pressure at surge-pressure relief nozzle	pressure	-50 to 300 psia[1]

[1]psia = pounds per square inch, absolute

Table 6. Data Modes for Measurements Recorded by SOMAT 1

MODE	DESCRIPTION	CHANNELS
1	Rainflow Mode Sample rate -- 300 s/s Filter rate -- 30 Hz low pass Rainflow ranges and bins: LCF1B +1000 kips, 20 kip bins VCFB +60 kips, 2.5 kip bins SCTB -50-100 kips, 2.5 kip bins SBBR -20-100 kips, 10 kip bins BOLB -120-280 kips, 10 kip bins	LCF1B, VCFB, SCTB, SBBR, and BOLB
2	Initial-Burst Mode Sample rate -- 300 s/s Filter rate -- 30 Hz low pass Triggered by VCFB (+20 kips) (300) 5-second bursts	SP1, LCF1B, VCFB, YPLB, SCTB, SBBR, BOLB, and time

Table 7. Data Modes for Measurements Recorded by SOMAT 2

MODE	DESCRIPTION	CHANNELS
1	Rainflow Mode Sample rate -- 300 s/s Filter rate -- 30 Hz low pass Rainflow ranges and bins: VCFA +60 kips, 2.5 kip bins VCFS +60 kips, 2.5 kip bins SCTA -50-100 kips, 2.5 kip bins BOLA -120-280 kips, 10 kip bins	VCFA, VCFS, SCTA, and SBAL
2	Time at Level Mode Sample rate -- 1 s/minute Filter rate -- 30 Hz low pass Triggered by SP1>1 mph SP1 0-100 mph, 5 mph bins	SP1
3	Initial-Burst Mode Sample rate -- 300 s/s Filter rate -- 30 Hz low pass Triggered by VCFA (+20 kips) (300) 5-second bursts	SP1, VCFA, VCFS, YPLA, SCTA, and time

Table 8. Data Modes for Measurements Recorded by SOMAT 3 (Stub Sill Strain Environment)

MODE	DESCRIPTION	CHANNELS
1	Rainflow Mode Sample rate -- 300 s/s Filter rate -- 30 Hz low pass Rainflow ranges and bins: SG1A +1200 muST, 40 muST bins SG2A +1200 muST, 40 muST bins SG3A +1200 muST, 30 muST bins SG4A +200 muST, 10 muST bins VCBA +500 muST, 20 muST bins	SG1A, SG2A, SG3A, SG4A, VCBA
2	Initial-Burst Mode Sample rate -- 300 s/s Filter rate -- 30 Hz low pass Triggered by VCBA (+120 muST) (300) 5-second bursts	SP1, SG1A, SG2A, SG3A, SG4A, VCBA, and time

Table 9. Data Modes for Measurements Recorded by SOMAT 4 (Surge-Pressure Measurements)

MODE	DESCRIPTION	CHANNELS
1	Peak-Valley Mode Sample rate -- 1000 s/s Filter rate -- 100 Hz low pass Peak-Valley ranges and bins: PR1 - 50-300 psia 10 psi hysteresis	PR1
3	Initial-Burst Mode Sample rate -- 1000 s/s Filter rate -- 100 Hz low pass Triggered by PR1 (+- 20 psi) (150) 2-second bursts	SP1, LCF2B, PR1, and time

3.6.1 Test Car Speed

An axle-mounted pulse tachometer was used to monitor test car speed and recorded positive speed, regardless of the direction of travel. The unit functioned by producing 60 pulses per revolution of the wheel. The pulses were converted to speed by a pulse converter, which is significant because in the FEEST2 test, a ground fault failure in this transducer caused the reference voltage for all of the SOMAT units (the ground plane) to have a pulsed voltage due to rotation of the wheels. This voltage pulse resulted in a small component being added to the actual measurement values and can be seen in some of the data presented in this report. Due to the small value of this voltage, the effect on the burst history data collected was minor.

In order to mount the transducer on the axle, it was necessary to allow some rotational slack to prevent binding of the transducer. This resulted in speed time history traces that exhibit a very high rate of change of velocity as the slack is being taken up by rotation of the wheel during impact events. Depending upon the direction of the impact and the orientation of this slack, some impact data shows smooth acceleration while other impact data shows a very high accelerations.

3.6.2 Longitudinal Coupler Force Measurement (LCF1B and LCF2B)

A type E, double-shelf instrumented dynamometer coupler, supplied by Miner, was purchased by AAR/TTC for this test program to measure longitudinal coupler force. The coupler was calibrated in a load frame prior to installation in the test car. Two independent sets of strain gages were used to form two independent measurements of longitudinal coupler forces (LCF) on the B-end of the tank car: LCF1B and LCF2B. LCF1B was acquired by SOMAT 1 and was operated in the rainflow mode. LCF2B was acquired by SOMAT 4 and was used to correlate impact conditions with surge pressure events. Correlation between the two LCF measurements during dynamic conditions was very good as demonstrated during impact testing. The accuracy of the calibration procedure used for LCF1B was also checked during squeeze tests conducted before and after the OTR testing. Typical results obtained from one of these tests are presented in Figure 2, which shows the

measured LCF for two separate loading sequences for the measurement LCF1B compared to the LCF as measured by an independent load cell. Due to limitations on restraining the test consist configuration, it was only possible to develop 200-300 kips of compressive/tension load during these squeeze tests. As can be seen in Figure 2, the measurement LCF1B provided very good estimates of the actual LCF (as measured by an independent load cell) imposed on the tank car. The data quality obtained from LCF1B was verified to be within 1 percent of full scale at the beginning and at the end of the FEEST2 testing. The VCF cross axis sensitivity of LCF1B was not tested due to the complexity and safety issues involved in setting up such a test.

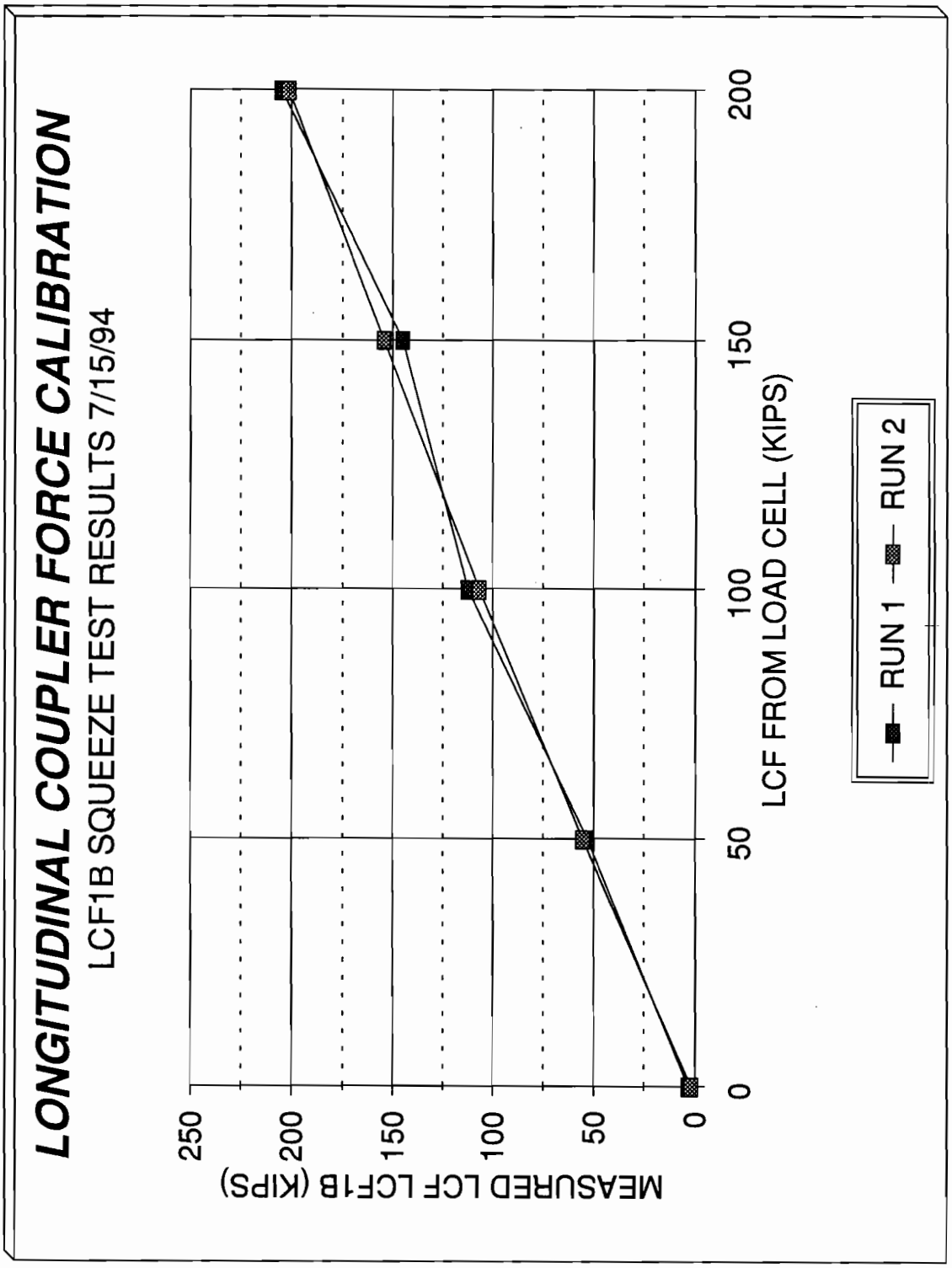

Figure 2. LCF Measurement LCF1B Calibration Check

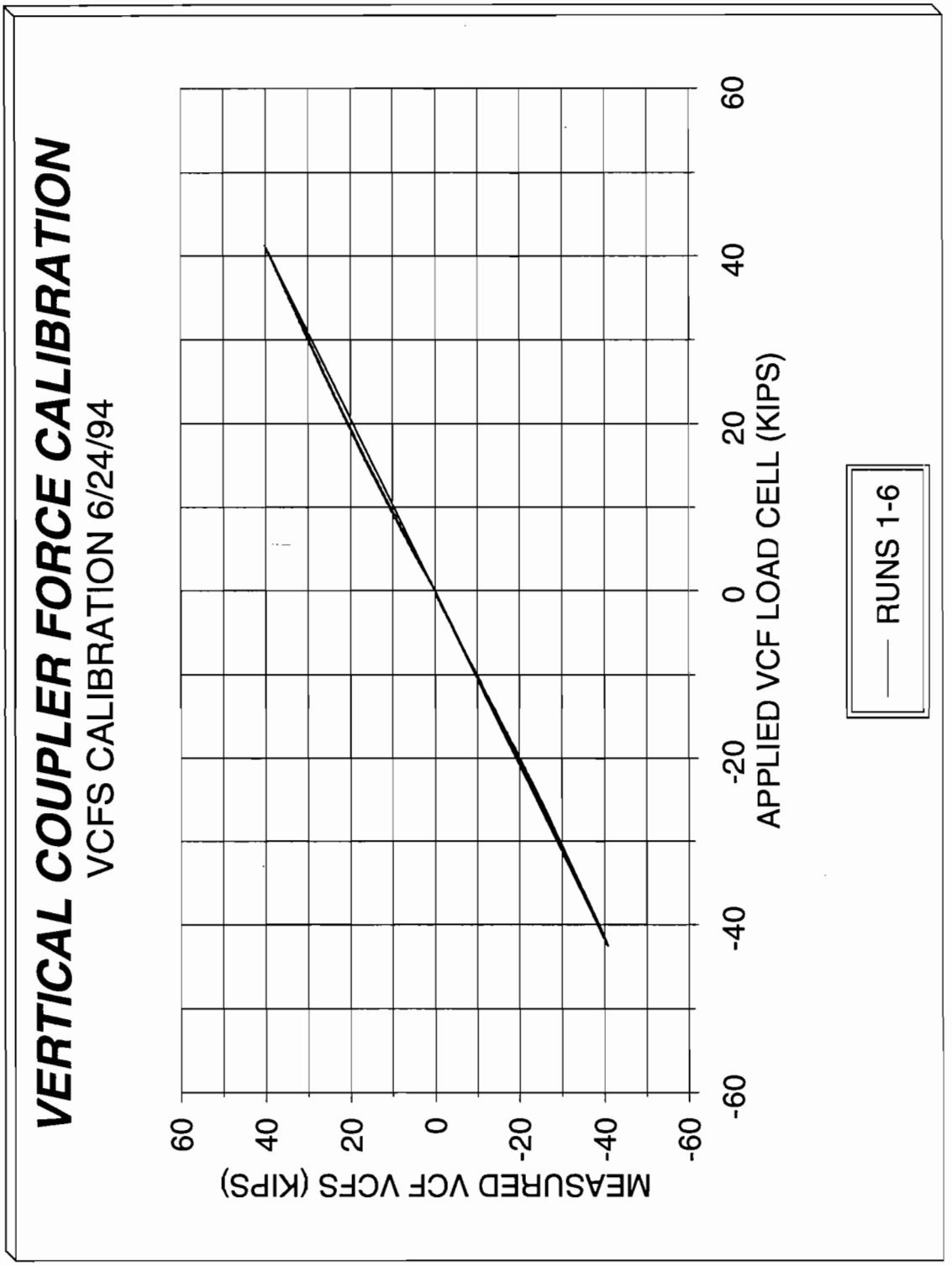

Figure 4. VCF Measurement VCFS Calibration Check

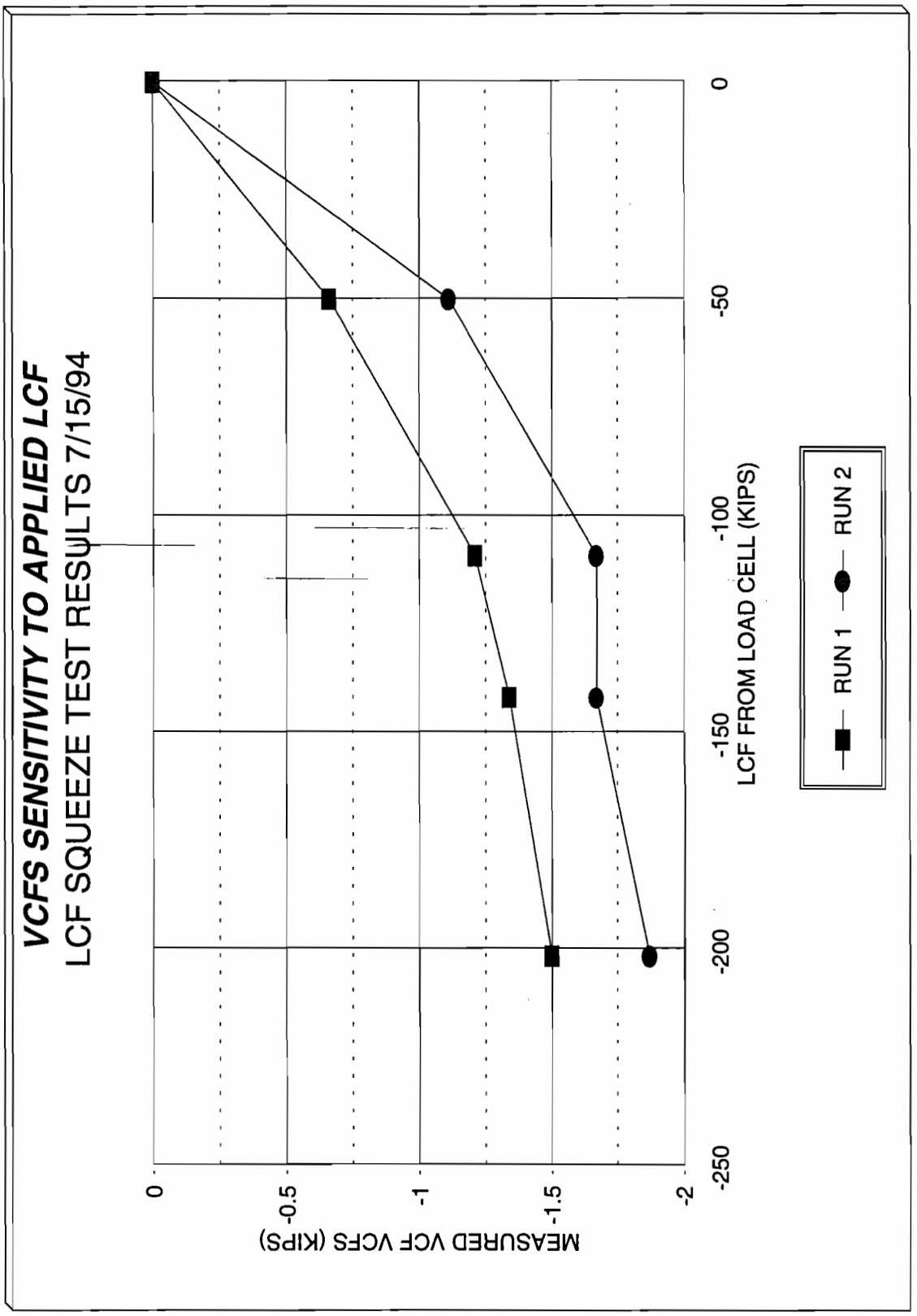

Figure 5. VCFS Cross Axis Sensitivity Check

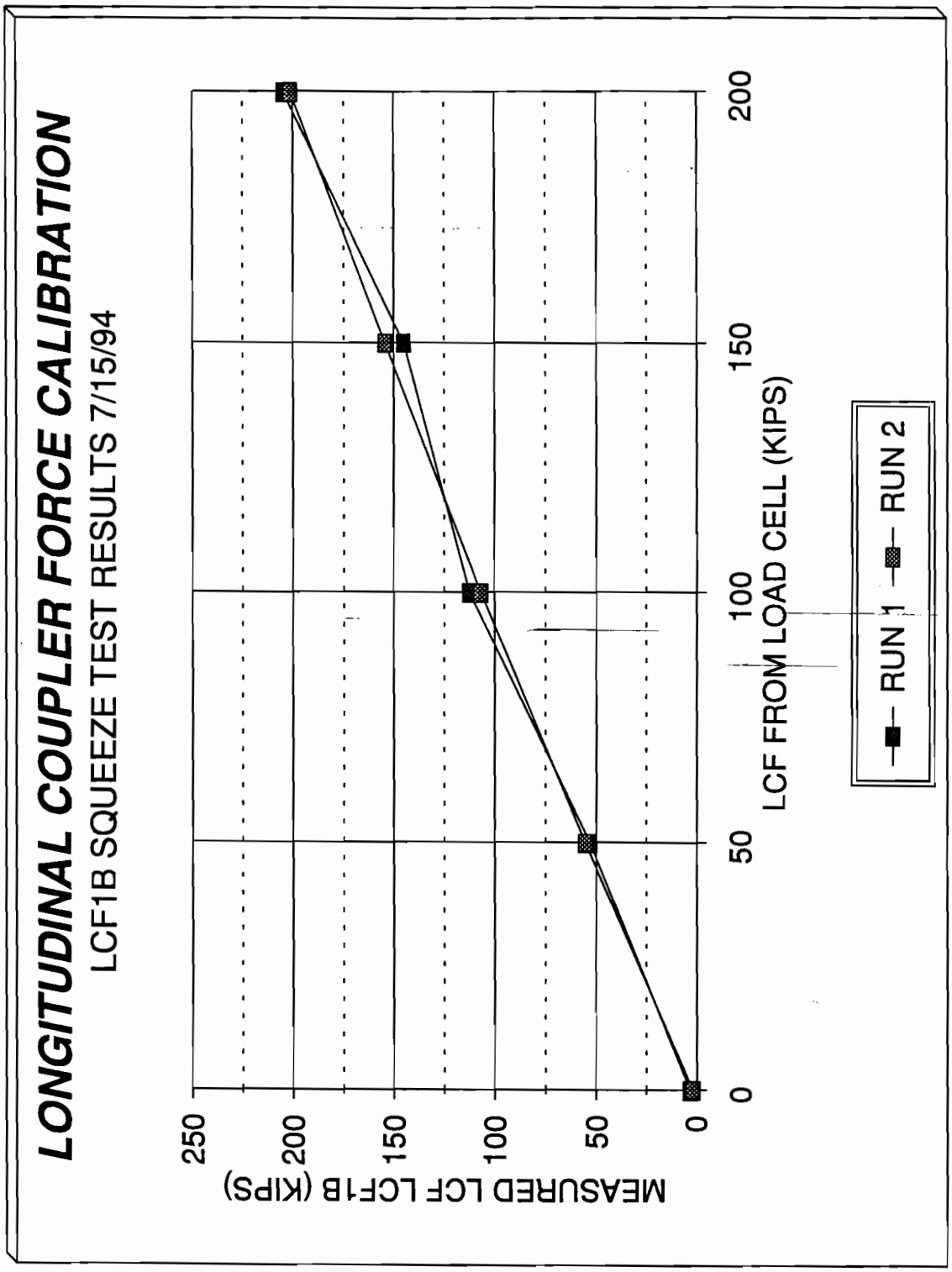

Figure 2. LCF Measurement LCF1B Calibration Check

3.6.3 Coupler Shank Shear (VCFS)

Shear gages were placed on either side of the A-end coupler just behind the knuckle in order to measure the shear load induced by a VCF (see Figure 3). This location was chosen to minimize the effect of the changing load paths caused by draft gear movement. The movement of the draft gear results in changes in the load path through the structure which affects the resulting strains measured by the various VCF measurements. The complexity of the effects on the various VCF measurements caused by the changing load paths resulted in several VCF measurement methodologies, which are discussed in more detail in Section 3.8. This strain gage was used as a backup to the primary VCF measurements of VCFA and VCFB.

The strain gage was calibrated by jacking vertically up and down on the knuckle (Section 3.7 will present detailed information on the calibration procedures). Figure 4 shows the results from 6 separate VCF calibration runs plotted over the top of each other to illustrate the repeatability and accuracy of the measurement. Figure 4 plots the applied load as measured by an independent calibrated load cell against the VCF as measured by the VCFS measurement. The squeeze test referred to in Section 3.6.2 was used to check the cross axis sensitivity of VCFS to applied LCF. Figure 5 shows the results obtained from two separate loading sequences during the squeeze test. It can be seen that the measurement VCFS was relatively insensitive to applied LCF as only 2 kips of VCF were developed at a draft force of 200 kips.

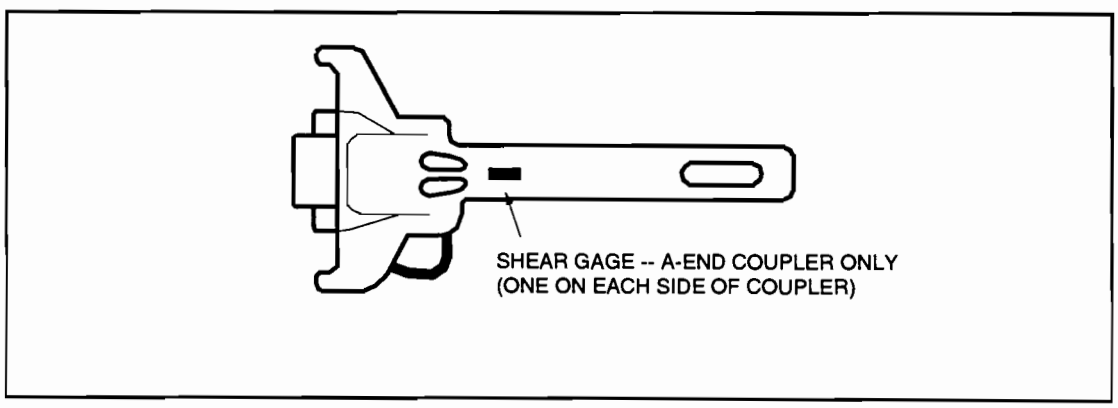

Figure 3. Coupler Shank Shear Measurement VCFS

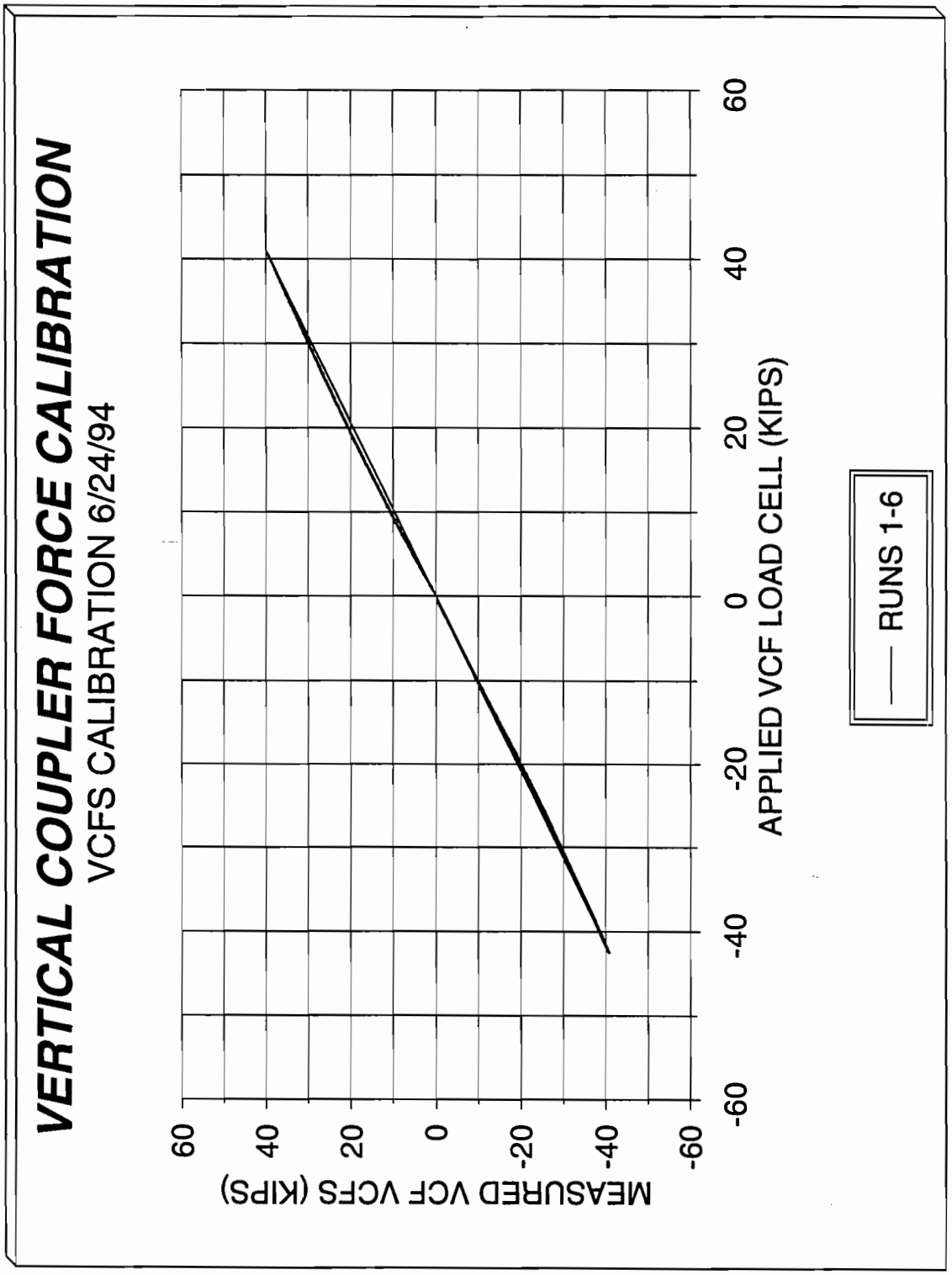

Figure 4. VCF Measurement VCFS Calibration Check

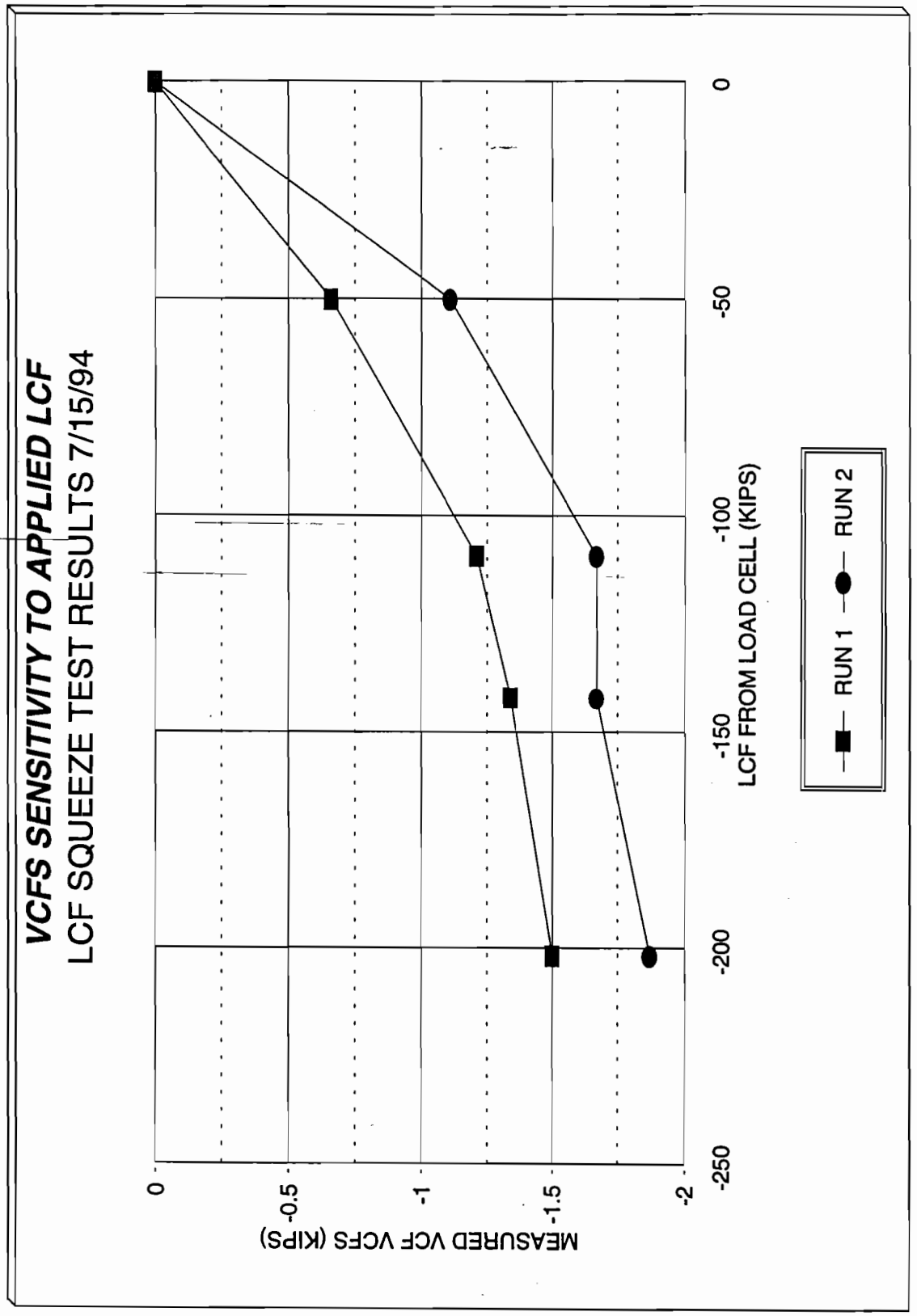

Figure 5. VCFS Cross Axis Sensitivity Check

3.6.4 Vertical Sill Bending (VCBA)

Before the Coupler Load Investigation Test, A-end and B-end sill bending gages (see Figure 6) were installed on the sill in an attempt to determine the strains introduced by bending in the sill. However, due to the variation in the location of the vertical coupler load reaction point within the draft pocket, the output of these gages varied with different load application locations. Only the A-end sill bending gage (VCBA) was used on the FEEST2 test.

This strain gage was not calibrated to measure VCF; its output is presented here in micro strain. However, during the calibration of VCFS, the output of this strain gage was recorded to determine the sensitivity to an applied VCF. Figure 7 shows the results from the same six VCF calibration runs as discussed in Section 3.6.3. It can be seen that the measurement VCBA was very sensitive to VCF inputs and responded in a linear and repeatable manner. This suggests that VCBA could be a good substitute candidate for the measurement of the VCF. Performing a linear regression analysis on the data shown in Figure 7 results in a conversion factor of 5.01 micro strain/kip with a correlation coefficient of .99. However, during the squeeze tests, it was found that this measurement was also sensitive to applied LCF as shown in Figure 8. As shown, the sensitivity to LCF can vary considerably between two different loading sequences by as much as 50 micro strain. Again, this is due to the variability of the VCF load paths through the draft gear and into the sill making it difficult to calibrate to measure pure VCF events. These results show that VCBA is very sensitive to VCF events and less sensitive to LCF events. Recall that this measurement was the trigger for the critical region strain gages SG1A, SG2A, and SG3A.

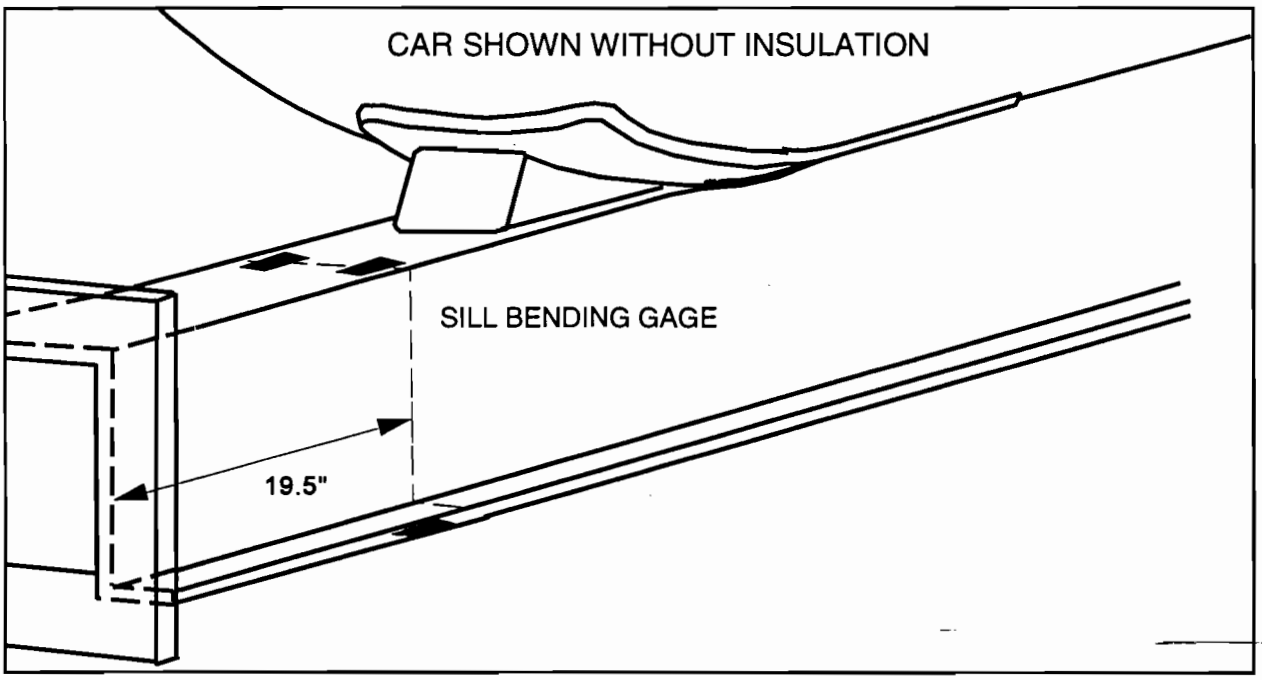

Figure 6. Sill Bending Measurement VCBA

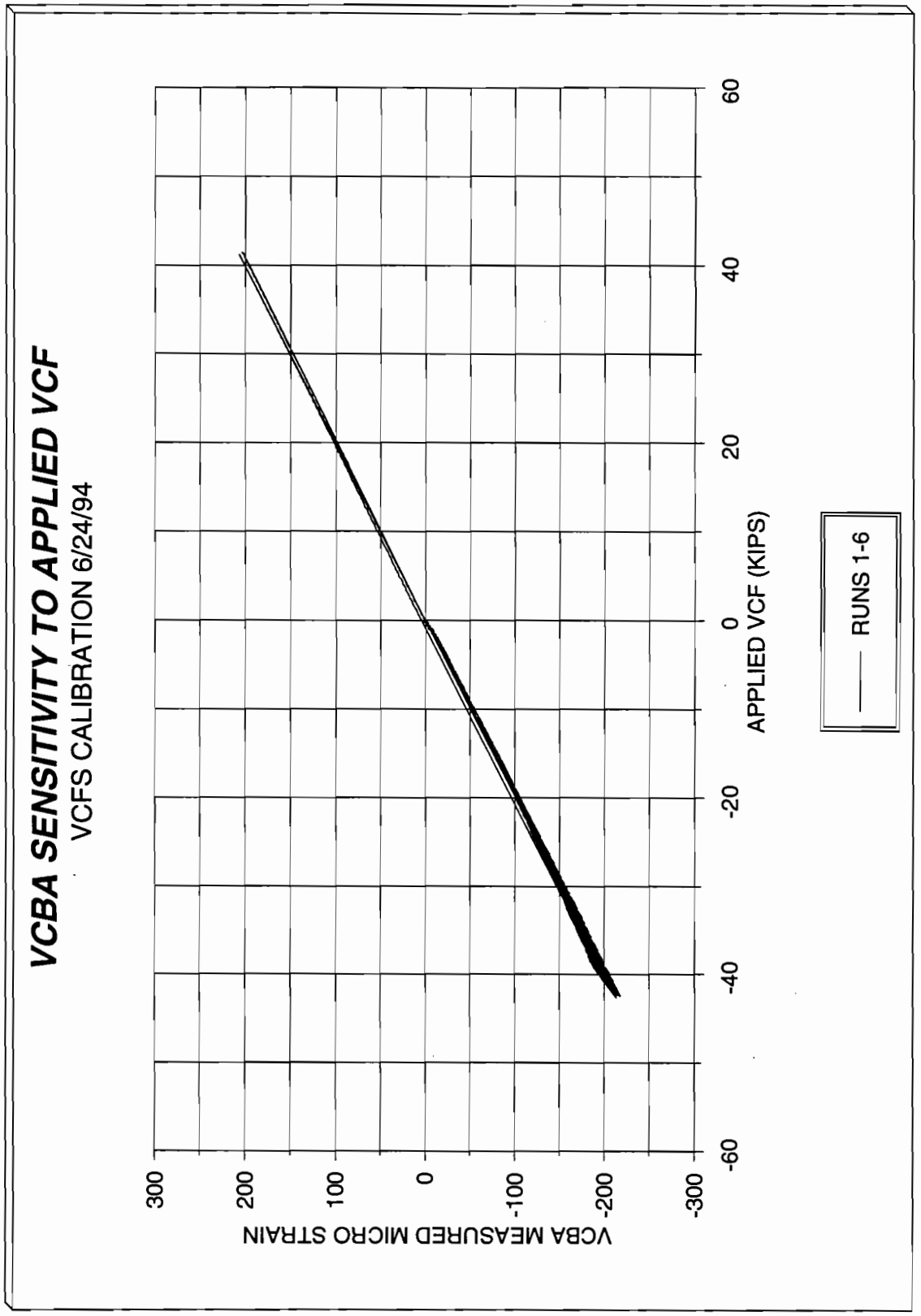

Figure 7. VCBA VCF Sensitivity

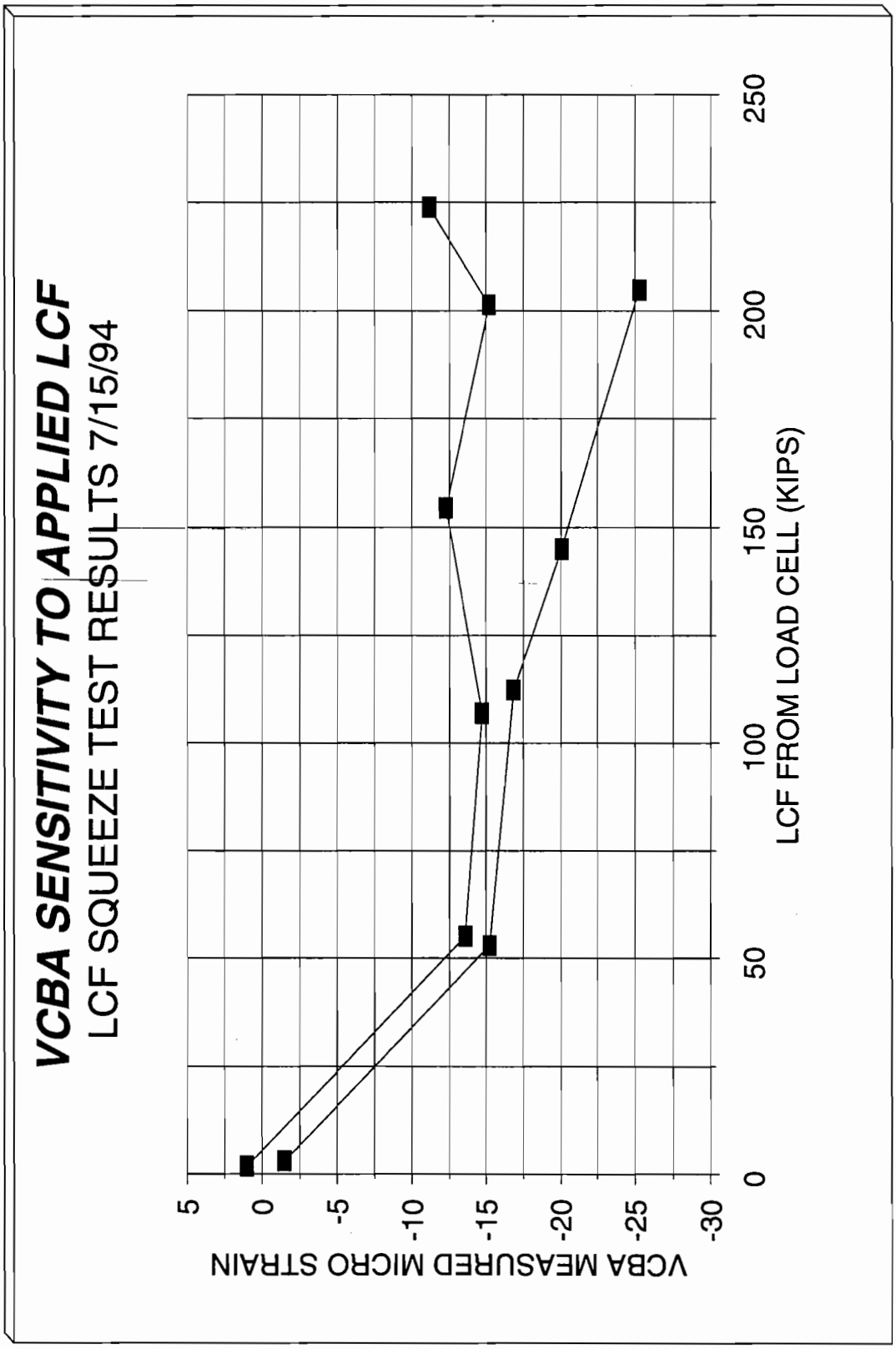

Figure 8. VCBA LCF Sensitivity

3.6.5 Vertical Sill Shear (VCFA and VCFB)

The VCFA and VCFB measurements were chosen to be the primary measurements because of their repeatability and similarity to the FEEST1 instrumentation. The **sill shear forces** induced by **VCFs** were measured at the A- and B-end of the car by a pair of summed shear gages mounted on the neutral axis of the sill between the front and rear draft gear lugs (see Figure 9). These measurements also were sensitive to VCF load path changes but to a lesser extent than the bending gages. Results from several different load application points on the resulting calibration data are shown in Table 10 to illustrate this point. Figure 23 shows the load application point nomenclature used. As shown in Table 10, there is good agreement between the A-end and B-end sensitivities and approximately a 4 to 25 percent change in the sensitivity depending upon the load application point used. Table 10 also shows the variation in sensitivity when the applied load is either down or up on the coupler. Because of this sensitivity difference, the jacking on sill technique was used to reduce the change in sensitivity due to a change in the direction of the applied load.

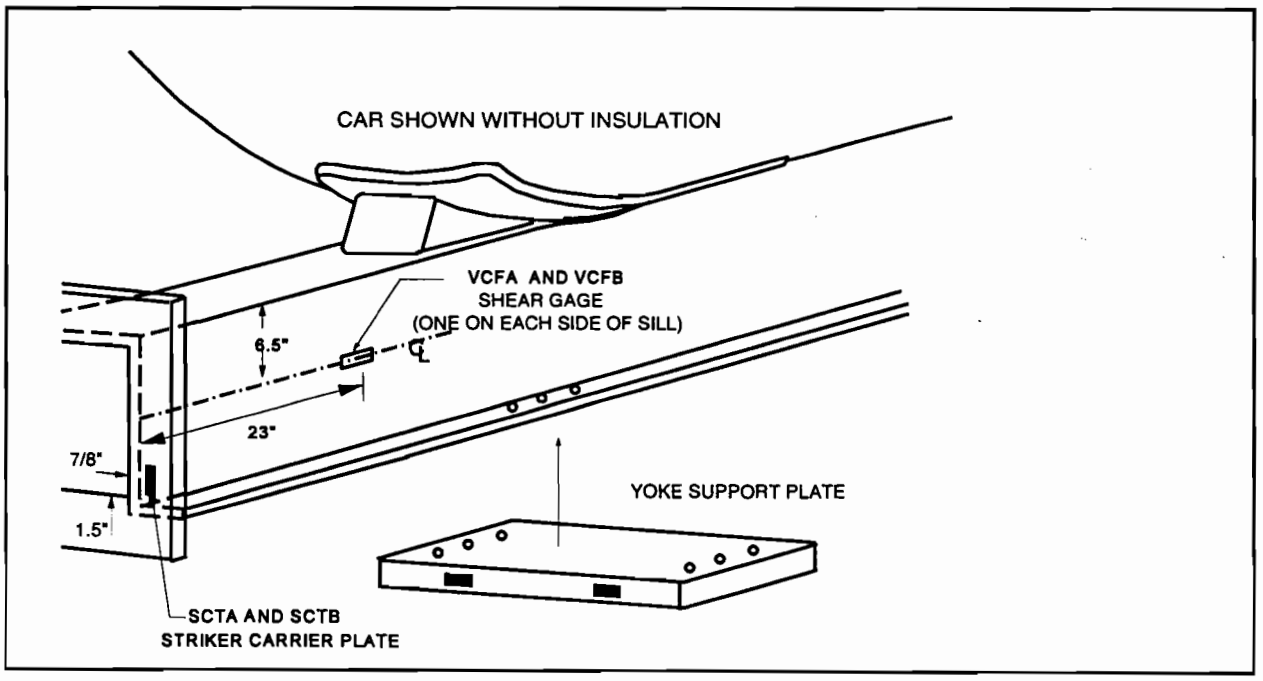

Figure 9. Sill Shear Measurements VCFA and VCFB

Table 10. VCF Sensitivities for Various Calibration Methods

CALIBRATION METHOD	VCFA SENSITIVITY (KLBS/MV/V)	VCFB SENSITIVITY (KLBS/MV/V)
Jacking Up On Sill	164	156
Jacking down on sill	158	153
Jacking Up On Coupler	130	120
Jacking Down On Coupler	152.5	149.2
Jacking Up On Sill *	164	161

* Calibration sensitivities developed at the end of leg 7

To produce the most consistent set of data possible given the variable load path effect, the final set of sensitivities used for these measurements during the FEEST~~2 test were~~ those values that were developed at the end of leg 7 which were based on jacking up on the sill technique of calibration. These values were found to produce the most consistent data along with being relatively simple to calibrate. Figure 10 shows the calibrations for VCFA and VCFB that were developed at the end of leg 7. The calibration quality was excellent as the two curves overlay one another.

VCFA and VCFB measurements produced good estimations of the actual VCF loads applied during static conditions with no applied LCF. Figures 11 and 12 show the response of these measurements applied to LCF for the same runs referenced in Figure 5. As shown, these measurements were slightly more sensitive to applied LCF that was VCFS. However, as opposed to VCFS, the response of the sill shear force measurements VCFA and VCFB to applied LCF is expected due to the vertical forces that result from misalignments in how the LCF is applied. It is hypothesized that some VCF loads may result from coupler key binding as well as coupler carrier reactions. Figure 12 shows that the measurement VCFB is more sensitive to applied LCF with a more defined trend being evident. This was thought to be due to the reduced clearance in the draft gear on the B-end due to the installation of the instrumented coupler. The increased sensitivity at the lower VCF values was also seen in the histograms shown later.

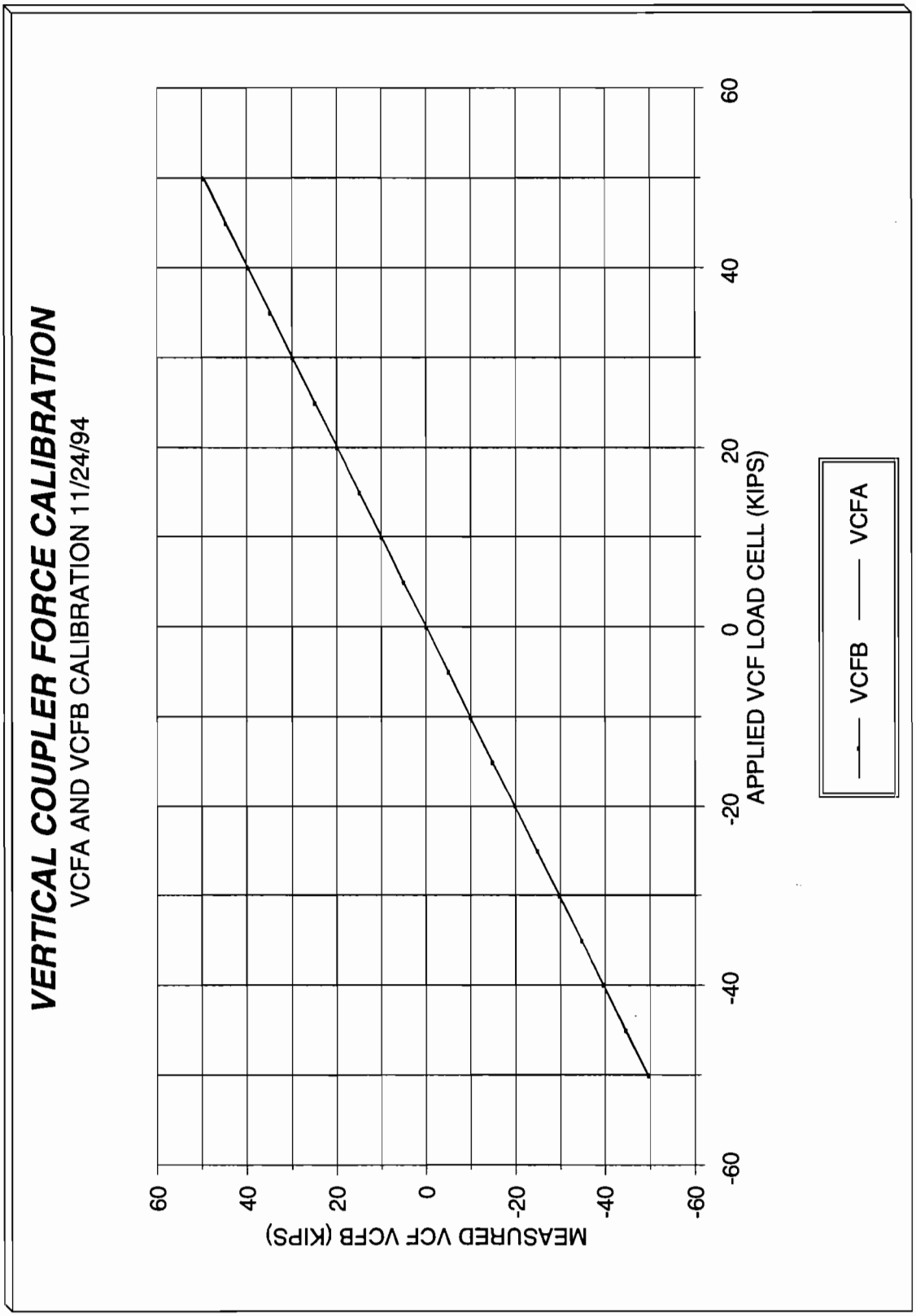

Figure 10. VCFA and VCFB Calibration

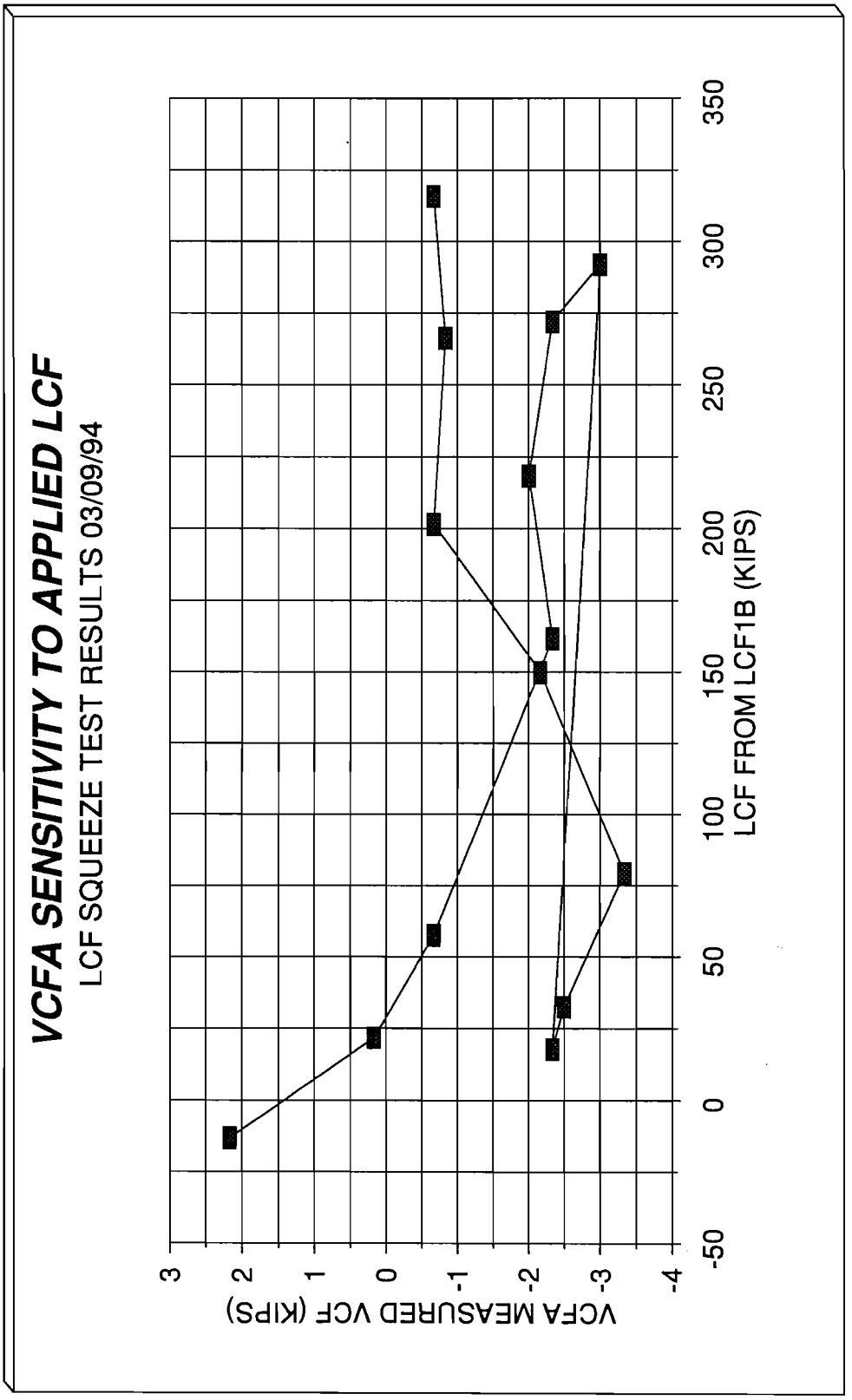

Figure 11. VCFA LCF Sensitivity

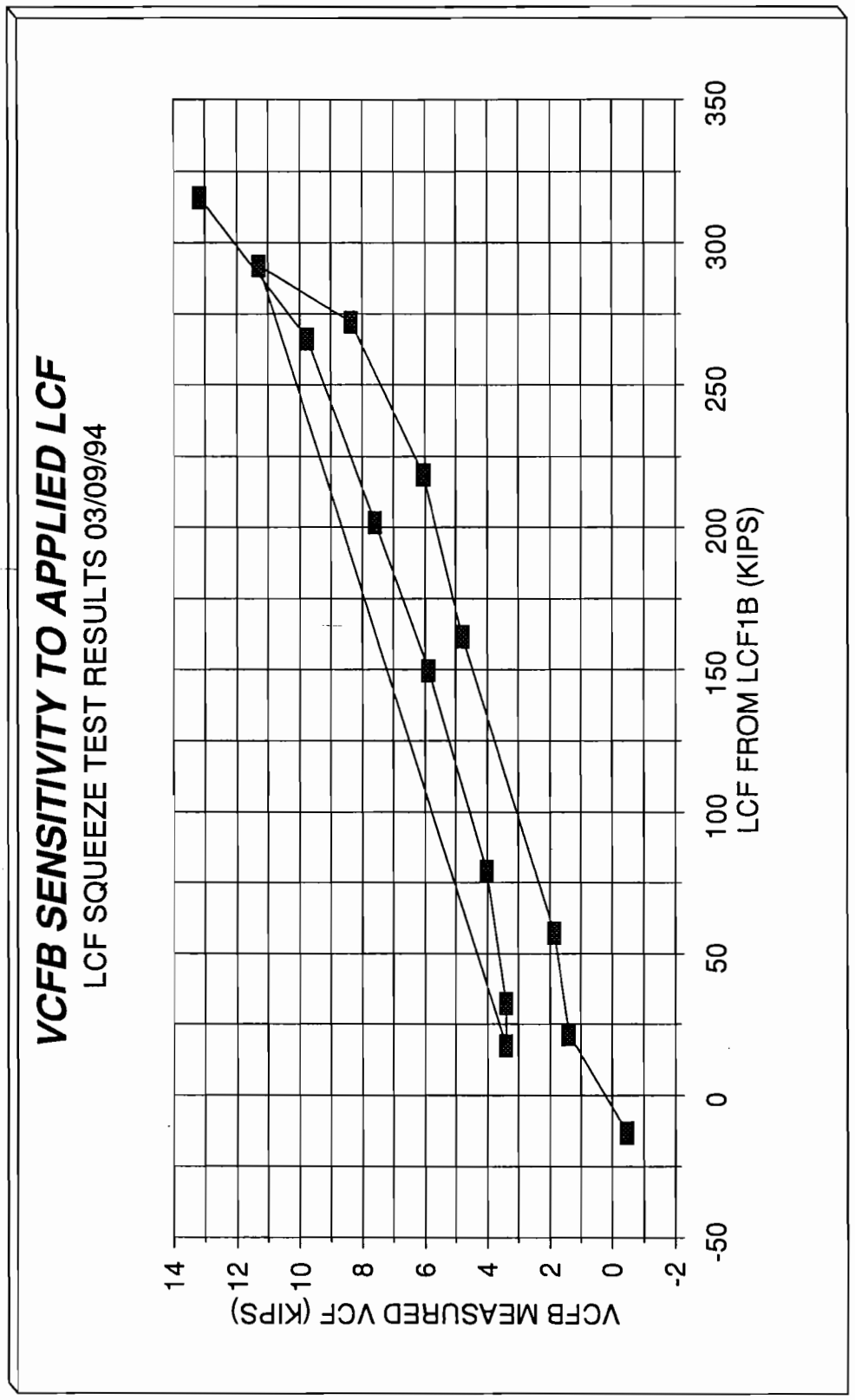

Figure 12. VCFB LCF Sensitivity

3.6.6 Striker Carrier (SCTA and SCTB)

Strain gages were added to the striker/carrier face very early in the test program in an attempt to measure the VCF (see Figure 13 for gage locations). At the time these gages were placed, the complexity of measuring the VCF was not fully understood. As a result, their location made the measurements very sensitive to the direction of the load applied by the coupler. During calibration of these gages, it was observed that these measurements were only sensitive to downward loading on the coupler.

3.6.7 Yoke Support Plate (YPLA and YPLB)

During the initial planning for the Coupler Load Investigation Test, it was noted that for the FEEST1 test, the yoke support plate ~~(Figure 13)~~ was outboard of the sill shear gage. However, with the FEEST2 instrum~~entation~~, the yoke support plate was inboard of the shear gage. Tank and sill geometry prevented moving the sill shear gages, so instead, the A- and B-end yoke support plates were instrumented with shear gages to record vertical force imposed on them by the draft gear. Four shear gages were installed on each plate and configured as a four active arm bridge circuit, as shown in Figure 14. The instrumented yoke plates were calibrated by placing them in an external fixture where calibration loads were applied. Point loads at nine locations around the center were averaged to compute the composite plate sensitivity. Standard deviation was computed for all data to determine measurement error. Table 11 shows a summary of the calibration data.

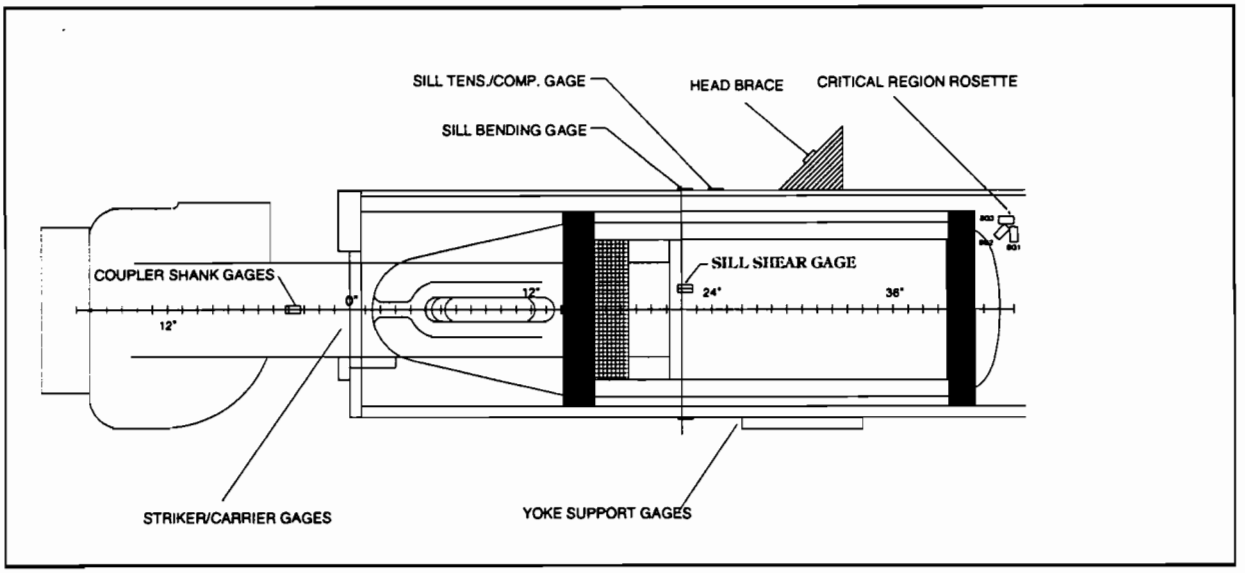

Figure 13. Locations of VCF Instrumentation for the FEEST2 Test

Table 11. Yoke Support Plate Sensitivities vs Location

LOCATION

GAGE	0	1	2	3	4	5	6	7	8
A (KLBS/MV/V)	32.7	29.9	34.3	29.1	26.9	26.9	29.0	39.8	29.3
B (KLBS/MV/V)	37.3	30.1	40.4	32.6	30.5	30.7	38.3	29.6	28.7

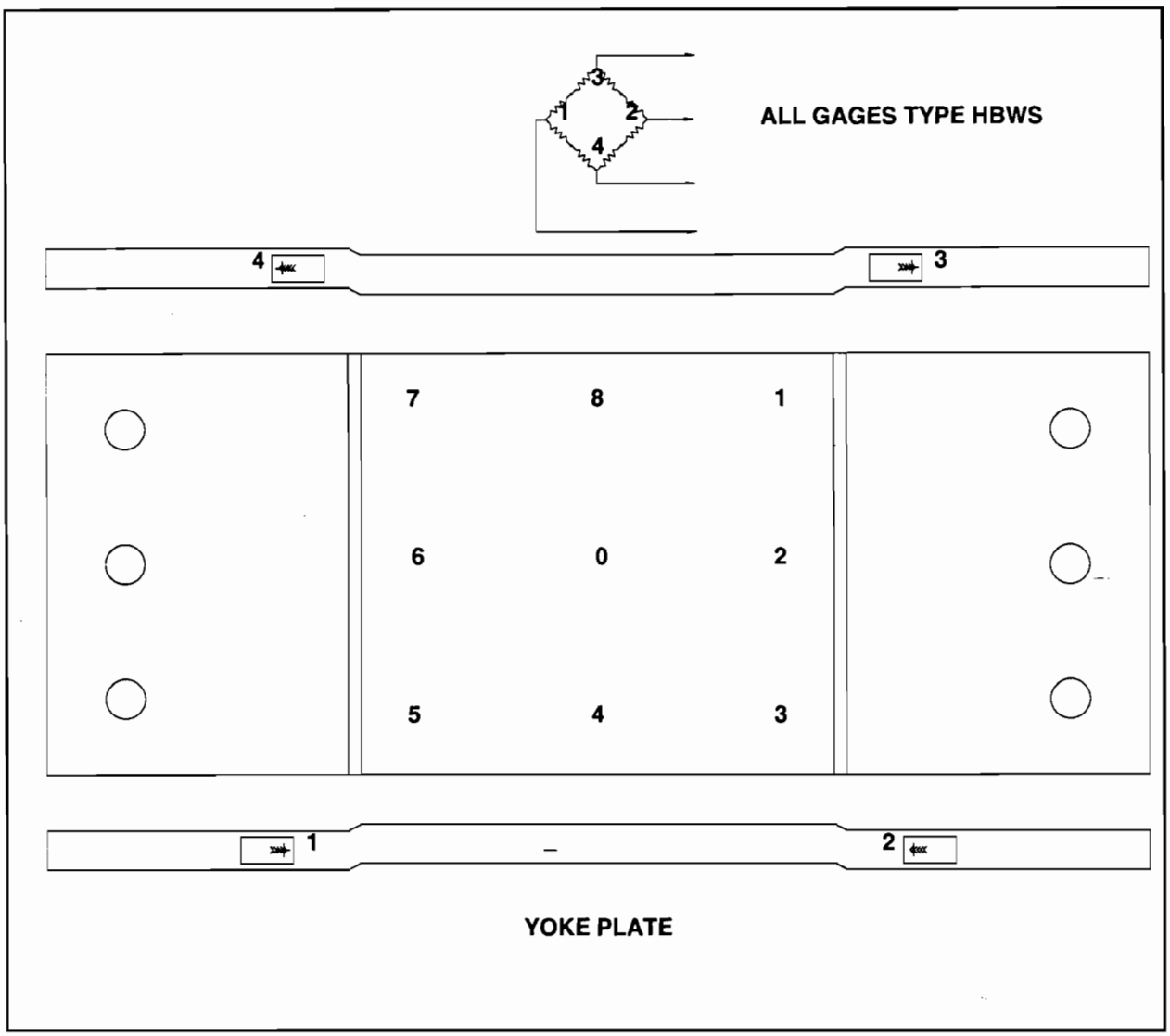

Figure 14. Yoke Plate Load Calibration Points

3.6.8 Side Bearing Load Measurements

Four Side bearing loads were obtained with 100-kip strain-gaged load cells (GSE 100klb compression load cells) inserted within the friction block side bearings. The standard side bearing gap of 1/8 inch was maintained. Figures 15 and 16 depict the side bearing load measurement installation.

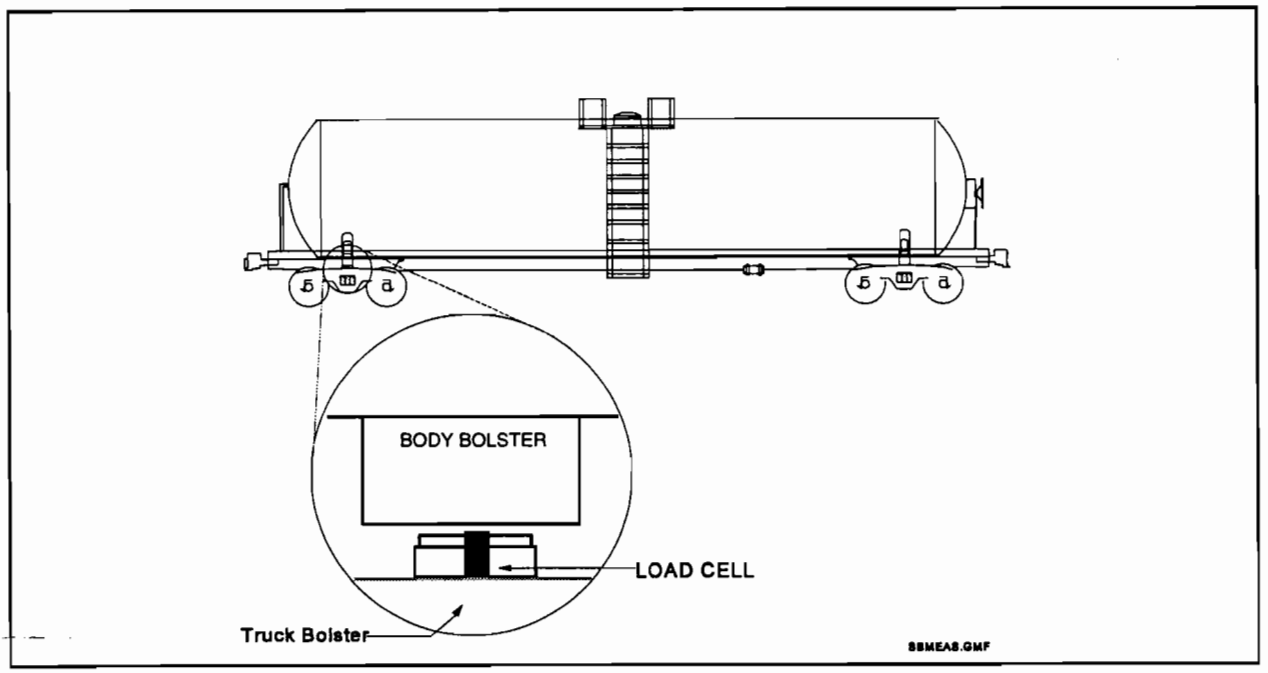

Figure 15. Side Bearing Load Measurement Installation

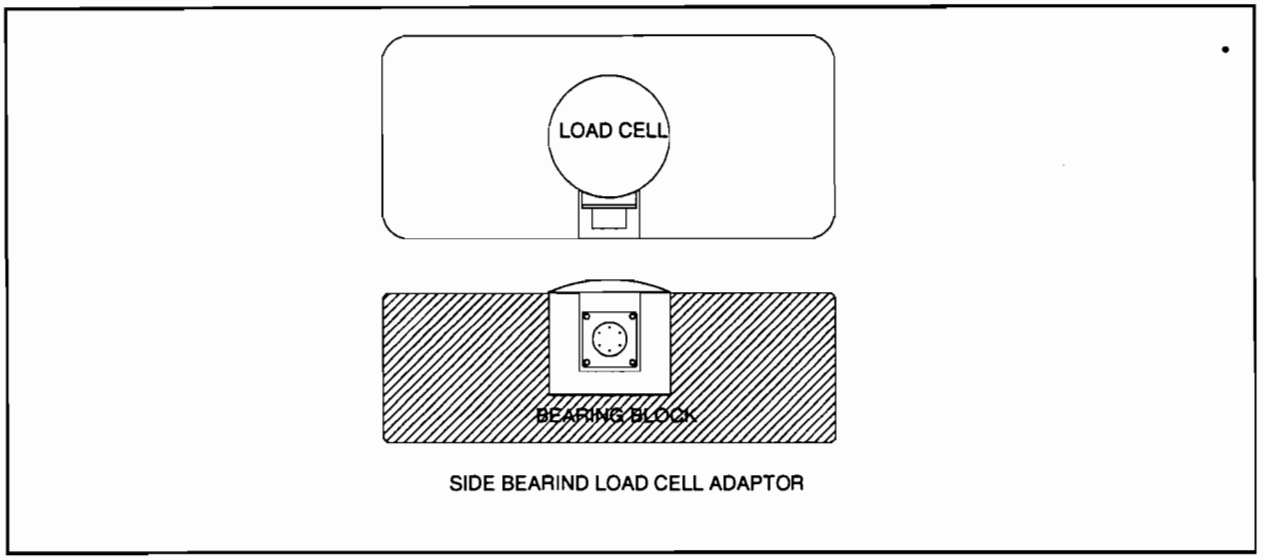

Figure 16. Side Bearing Load Measurement Installation

3.6.9 Truck Bolster Vertical Load Measurements (BOLA and BOLB)

The truck bolster vertical loads were measured with summed shear gages located behind the gibs. Figures 17 and 18 show the installation. Two sets of summed bending strain gages were also installed on the truck bolster to serve as backups in case of gage failure during the FEEST2 test. Each truck bolster was calibrated by placing a 200-kip load cell in the center bowl, then lowering the car body with cranes onto the cell in approximately 20-kip increments while recording the load cell and bolster shear and strain gage outputs. Four load application points were used to calibrate the gages. A linear regression analysis of the resulting data was performed which indicated that the shear output was less sensitive to changes in the load application point. For this reason, the shear circuits were used during the FEEST2 test while the bending circuits served as backups in case of failure of the other circuits.

Figure 17 shows the primary shear and alternative bending force truck bolster vertical load measurements. The bolster calibration technique is also displayed.

The measurements BOLA and BOLB were initially zeroed at the beginning of each leg so as to remove the static weight of the tank car and to remove any static offset caused by settling of the strain gages. This results in only the dynamic and quasi static loads being measured as the static weight of the tank car has been calibrated out of the measurement.

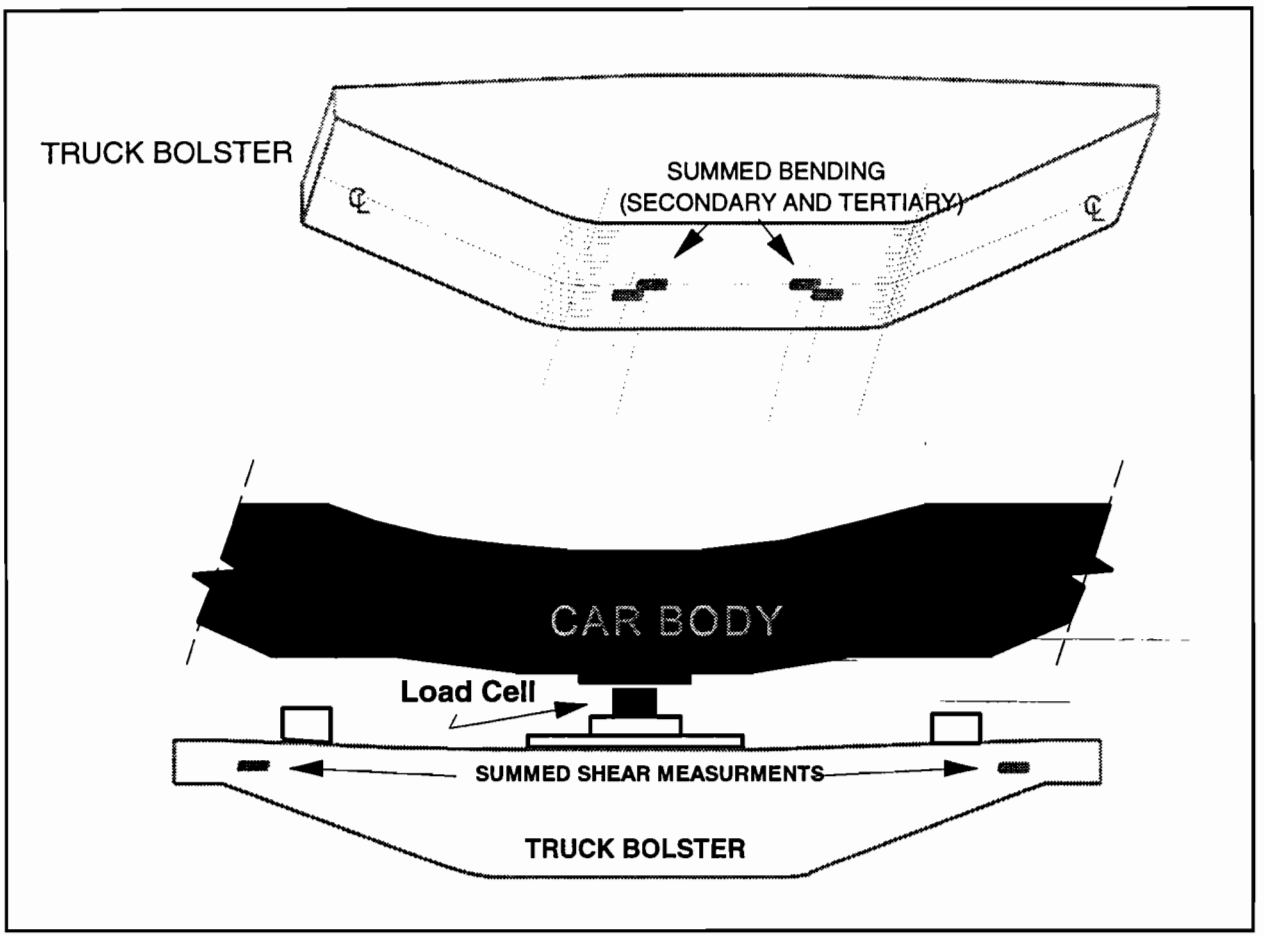

Figure 17. Truck Bolster Load Measurements

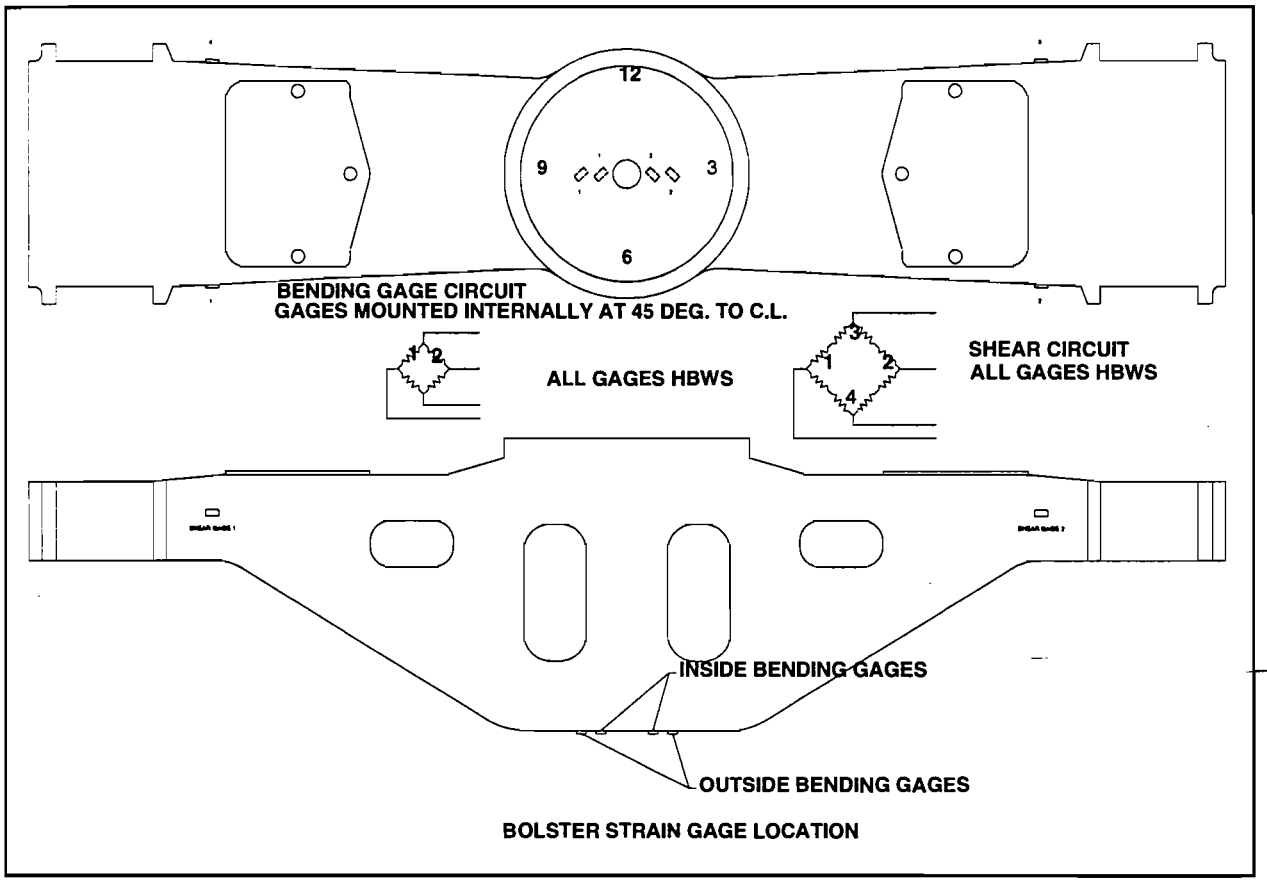

Figure 18. Truck Bolster Load Measurement Circuits

3.6.10 Micro Strain Measurements

Several strain gages were installed to measure the strains in the region thought to be the most critical area and, as such, are referred to as the critical region strain gages (SG1A, SG2A and SG3A). The strain gages were not calibrated but recorded micro strain values. Figure 19 shows the critical region and the strain gage installation location consisting of a strain-gage rosette that measured the strains in the critical sill-to-tank connection region.

The initial Coupler Load Investigation Test data implied that the striker/carrier plate region of the sill was not necessarily the primary point of vertical load transfer. To quantify how much of the vertical load was imparted at the striker or carrier plates, a strain gage was added to the vertical bracing at the sill end (SG4A).

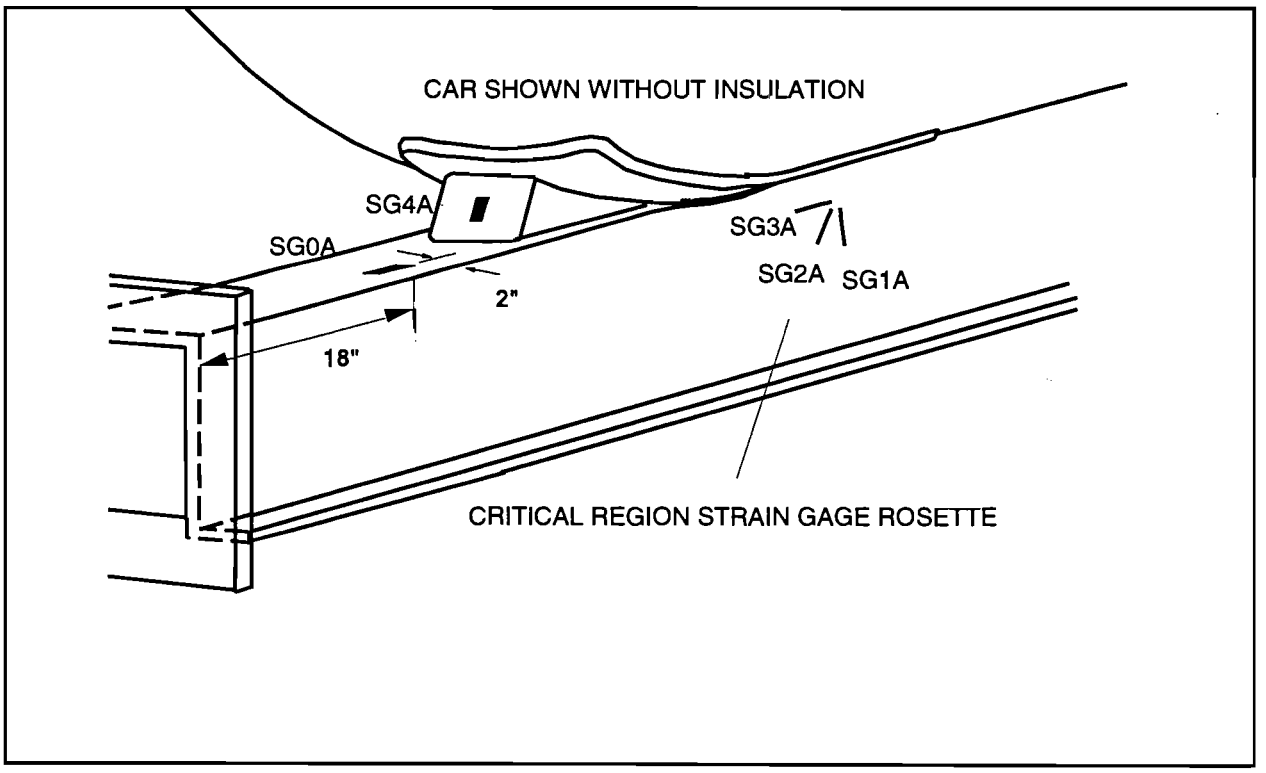

Figure 19. Strain gage Locations — Sill bending, Critical Region Rosette and Head Brace

The sensitivity of the critical region strain gages was established by recording the strain gage outputs during the VCF calibrations and squeeze tests. SG1A and SG2A were found to be only slightly sensitive to applied VCF with typical maximum micro strain values of 30 at VCF values of 40 kips. These measurements were also found to be nonlinear with applied VCF. SG3A was very sensitive to VCF inputs, as shown in Figure 20.

Figure 21 shows the sensitivity of the critical region strains to applied LCF and shows that SG1A is the most sensitive strain gage to LCF. Due to limitations on restraining the test consist, buff and draft forces during the squeeze tests were limited to approximately 300 kips. Because of this, the response of the critical region strains due to LCF above 300 kips can only be extrapolated from this data.

Based on the data, stress levels produced in the critical region by the application of a 40 kip VCF and a 300 kips LCF acting independently can be found. The principal stress levels along with the von Mises stress are shown below in Table 12 for comparison with events to be presented later in this report. It must be kept in mind that due to the non-linear relations and variable load paths that exist, the stress levels shown can vary significantly. However, insight into the fatigue significant events is gained even with this uncertainty.

Table 12. Stress Level Relations In The Critical Region

PARAMETER	300 kip LCF	40 kip VCF
Principal stress S1 (psi)	6741	1426
Principal stress S2 (psi)	-3955	9717
T_{max} (psi)	5348	4145
$\measuredangle$ (degrees) (SG1A = 0°)	33.24	26.12
von Mises Stress (psi)	9367	10500

As can be seen in Table 12, actual VCF events of 40 kips will produce stresses in the critical region greater than the stresses produced by a 300 kip LCF (typical impact value). Assuming a linear relation between the applied LCF and the strains produced in the critical region, extrapolation of the stress levels shown in Figure 12 to LCF values representing more severe impact conditions results in producing the highest stress levels in the critical region.

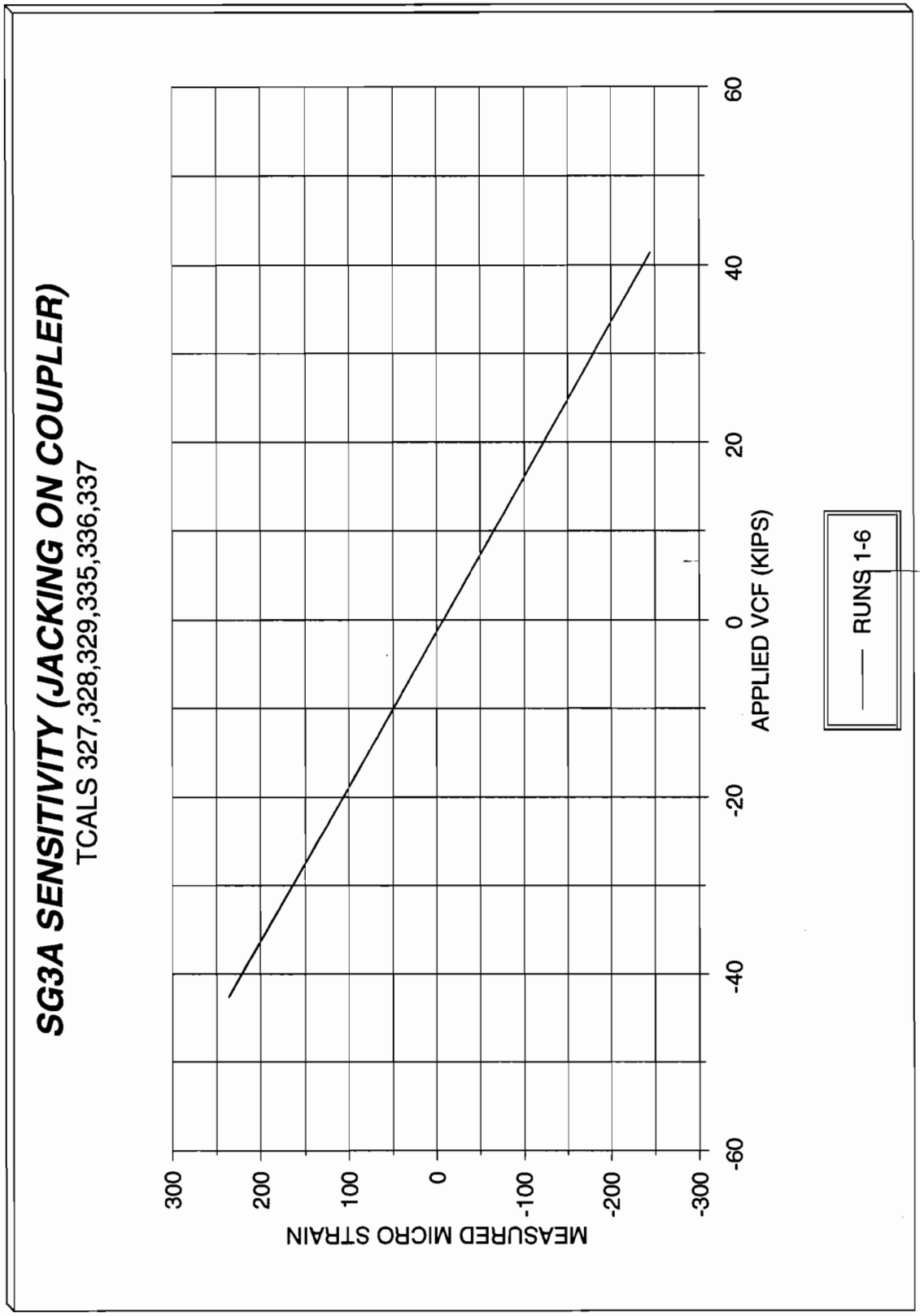

Figure 20. SG3A VCF Sensitivity

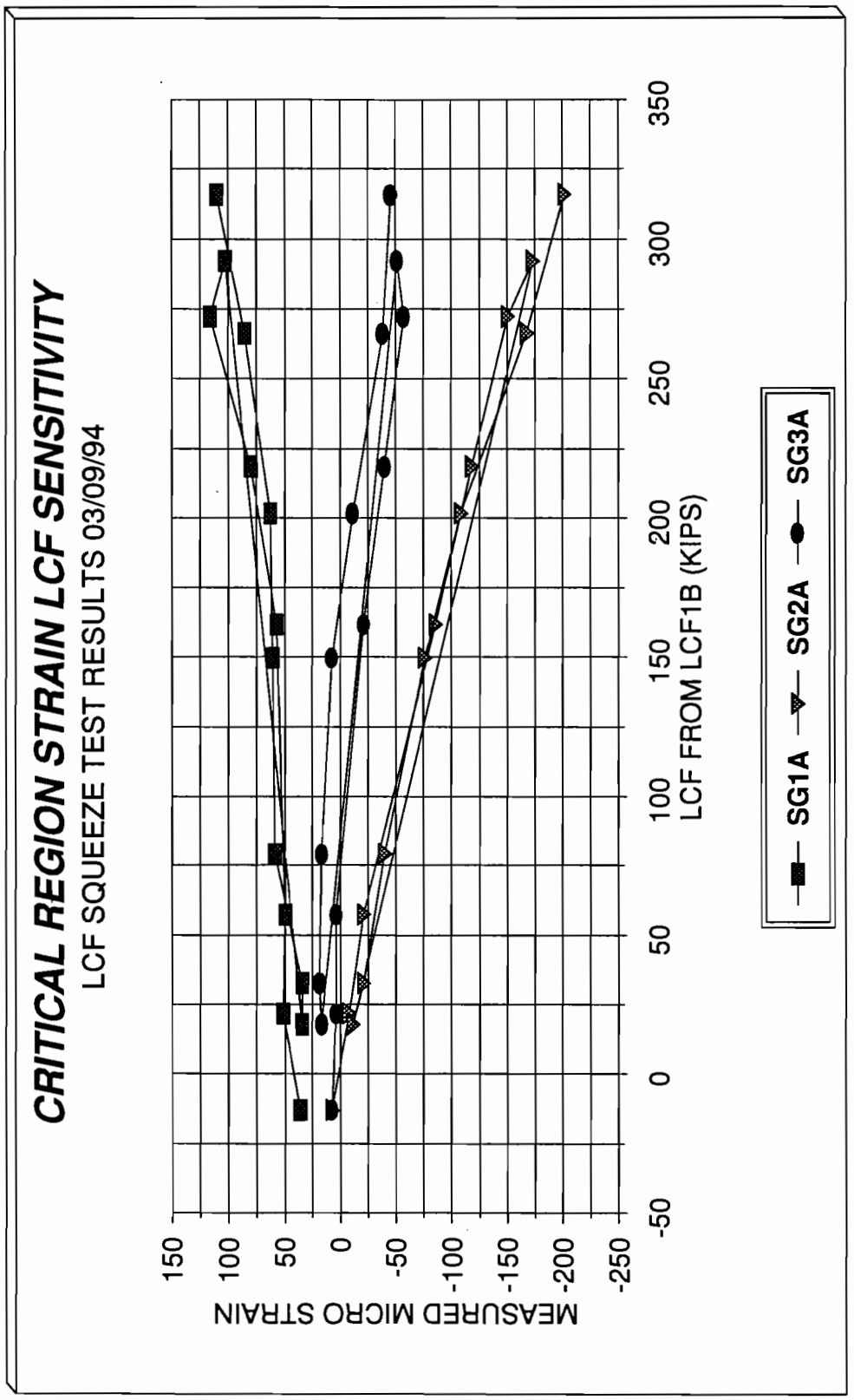

Figure 21. Critical Region Strain LCF Sensitivity

3.6.11 Tank Internal Surge Pressure Measurement

One pressure transducer (Statham PA822-300 300 psia) was used to record tank car surge pressures from 0 to 300 psia at the safety relief valve nozzle. The safety relief valve pipe where the surge pressure transducer was installed contained no baffling of any type. This was done to develop the highest possible surge pressures at the transducer. Figure 22 shows the installation used.

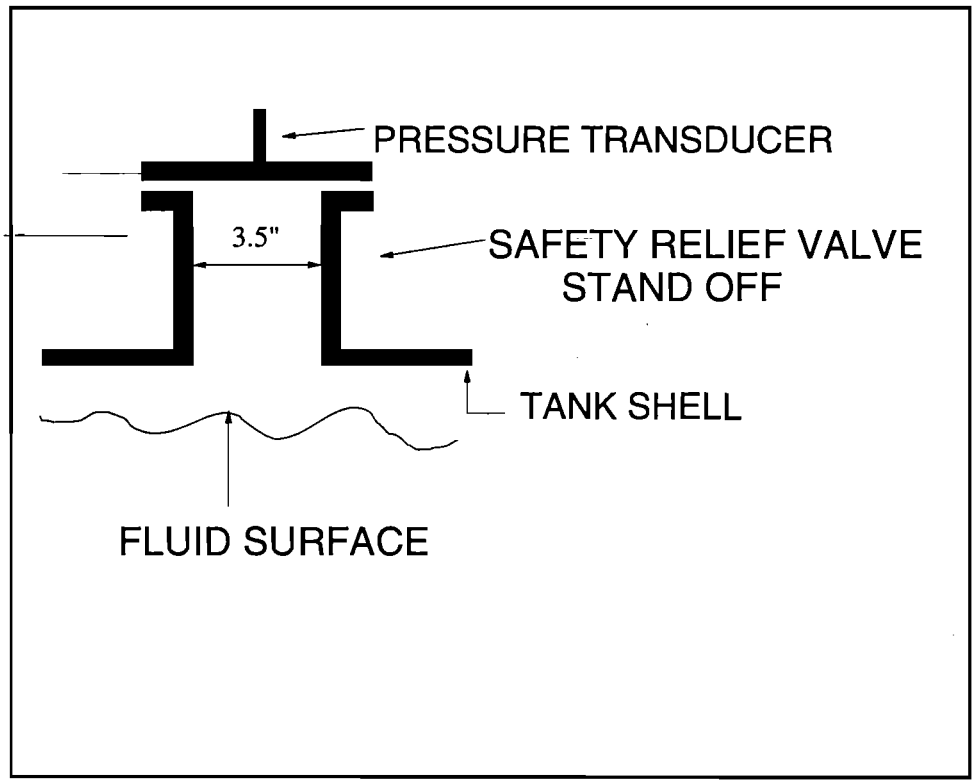

Figure 22. Surge Pressure Transducer Installation

To obtain an accurate measure of internal surge pressure, the original safety relief valve was replaced with a frangible disk. The safety relief valve would have allowed for possible undetectable release of internal tank pressure during surge pressure events. A solid frangible disk assured that the pressure transducer recorded the maximum internal

pressure that was developed. The disk rupture pressure was rated above the test pressure of the tank in an effort to reduce the possibility of a broken disk.

Surge pressure data was also taken in the form of burst history data and peak valley data during the FEEST2 testing and for the dedicated impact tests. The results are presented in Section 4.5

3.7 COUPLER JACKING TESTS

Because of the different methods of measuring VCF, several methods of calibrating the measurements were developed. The primary method of calibrating the measurements was by jacking tests. These tests involved the use of a hydraulic jack combined with a load cell in order to input known forces into the coupler and sill. The output from the various measurements was then calibrated using the known force input. Jacking tests were performed at various positions on the coupler and sill structure to develop calibrations which would most accurately measure the VCF. Basic jacking tests were performed with the aid of a special reaction frame that facilitated downward loading at the coupler or at other points along the sill/draft gear structure. Figure 23 shows a longitudinal view of the sill and the locations of certain strain gage measurements, as well as significant structural features of the tank car along with the main locations used for jacking calibrations. As a result of the evolving understanding and appreciation of the complexity of the vertical load reaction path within the stub sill/draft gear, changes in calibration techniques and procedures were made several times during the test program to obtain the most accurate and repeatable data. Section 3.8 discusses the changes and makes reference to the different methods of calibrating the measurements

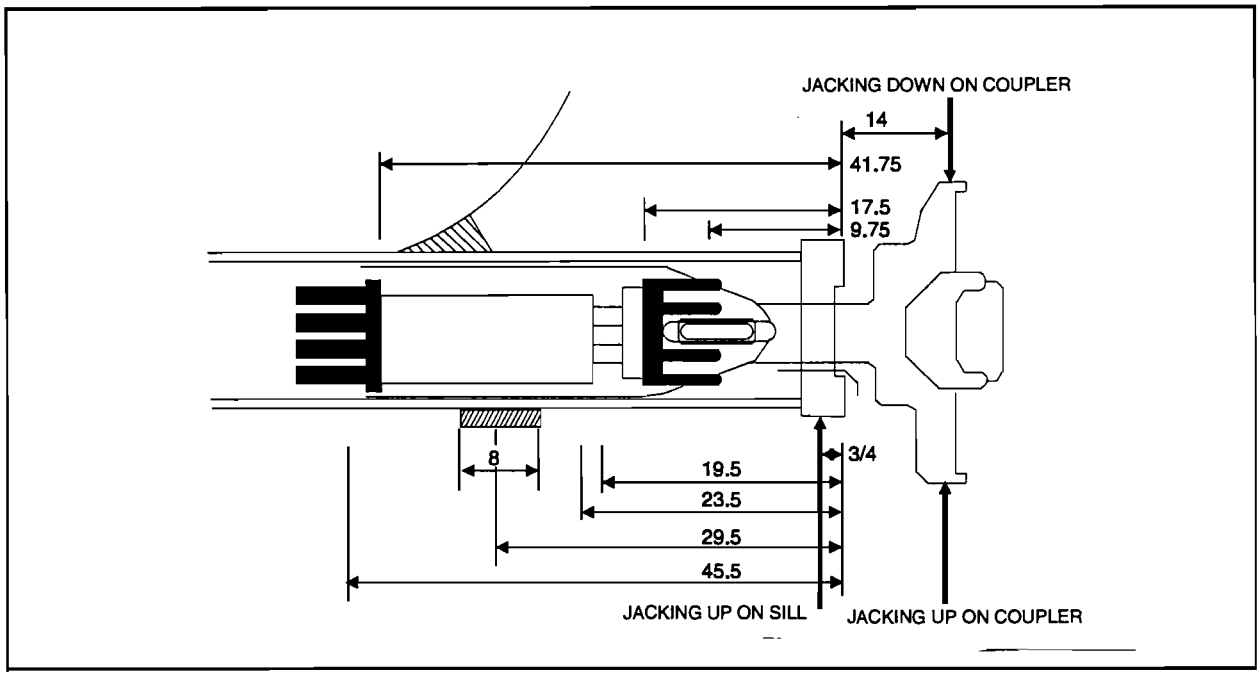

Figure 23. Jacking Calibration Configurations

3.8 VCF MEASUREMENT EVOLUTION — COUPLER LOAD INVESTIGATION TESTS

The test car was initially instrumented for the OTR test in the fall of 1993. The OTR instrumentation was originally designed so as to repeat the configuration used in the 1986 FEEST1 investigation. However, the original instrumentation configuration was enhanced for the Coupler Load Investigation Test to determine if more accurate VCF loads under static and dynamic conditions could be obtained.

The Coupler Load Investigation Test was performed during the spring of 1994, at which time additional instrumentation was added and the existing OTR instrumentation was improved. It had previously been assumed (during the FEEST1) that VCFs are imparted into the sill at the striker/carrier plate as a pure vertical force with a corresponding reaction force being created at the coupler key. Figure 24 shows the free

body diagrams for each component for this assumed VCF load path along with the assumed LCF load path. This VCF load path was assumed during the development of the parameters VCFA and VCFB and was used to develop basic static relations between the VCF and the internal reaction forces.

Referring to Figure 24 and neglecting the weight of the coupler, the equations of static equilibrium are applied to the coupler free body diagram to obtain the static sill force reaction at the striker/carrier (RS) and the sill force reactions at the key slot (RK).

$$\sum M_O = 0 \qquad (V \times B) - RS \times A = 0$$

$$RS = \frac{V \times B}{A} \qquad (1)$$

$$+\uparrow \sum F_Y = 0 \qquad V - RS + RK = 0$$

$$V - \frac{V \times B}{A} + RK = 0$$

$$RK = \frac{V \times B}{A} - V \qquad (2)$$

Substituting in the dimensions for A and B as shown in Figure 23 into Equation 1 gives the equivalent sill force reaction produced by VCF, V.

$$RS = V \times \frac{23.75}{9.00} = V \times 2.63 \qquad (3)$$

The reactions RS and RK are then applied to the sill with the resulting shear diagram as shown in Figure 25. The resulting shear in the sill at the strain gage location for VCFA and VCFB can be seen to be equal to V, the applied coupler force.

Recall that the measurements VCFB and VCFA were calibrated by applying forces at the face of the striker/carrier and calibrating the output of the strain gages to these applied forces. As shown above, the reaction force at the striker/carrier is related to the coupler force by Equation 3. Because of these relations, the measurements VCFA and VCFB do not measure the VCF directly, but rather represent the equivalent force applied at the striker/carrier to an applied VCF. VCFA and VCFB values presented in this report represent the force applied at the striker carrier required to produce the same shear load in the sill that would have been developed by the corresponding VCF. Despite this, the data from VCFA and VCFB is referred to as a VCFs.

The existence of this particular load path was checked at the end of the OTR testing by observing the striker carrier and the coupler for signs of contact. These observations showed that there was very little evidence of contact being made.

Many other possible VCF load paths exist. As many as five different load paths were observed during FAST testing. One such load path observed by Dr. Moyar, who is a technical consultant for the AAR, is that a pure moment may be created at the coupler face between identical adjacent cars. Another load path thought to exist is that the applied VCF is completely reacted out as a couple within the key. By performing the same analysis as was done in Figure 24, the value of the ratio given in Equation 3 can be found to be equal to 1.0 for this load path. The development of a single calibration, which would take into account these different load paths, was not possible to implement with the limited real time processing capability.

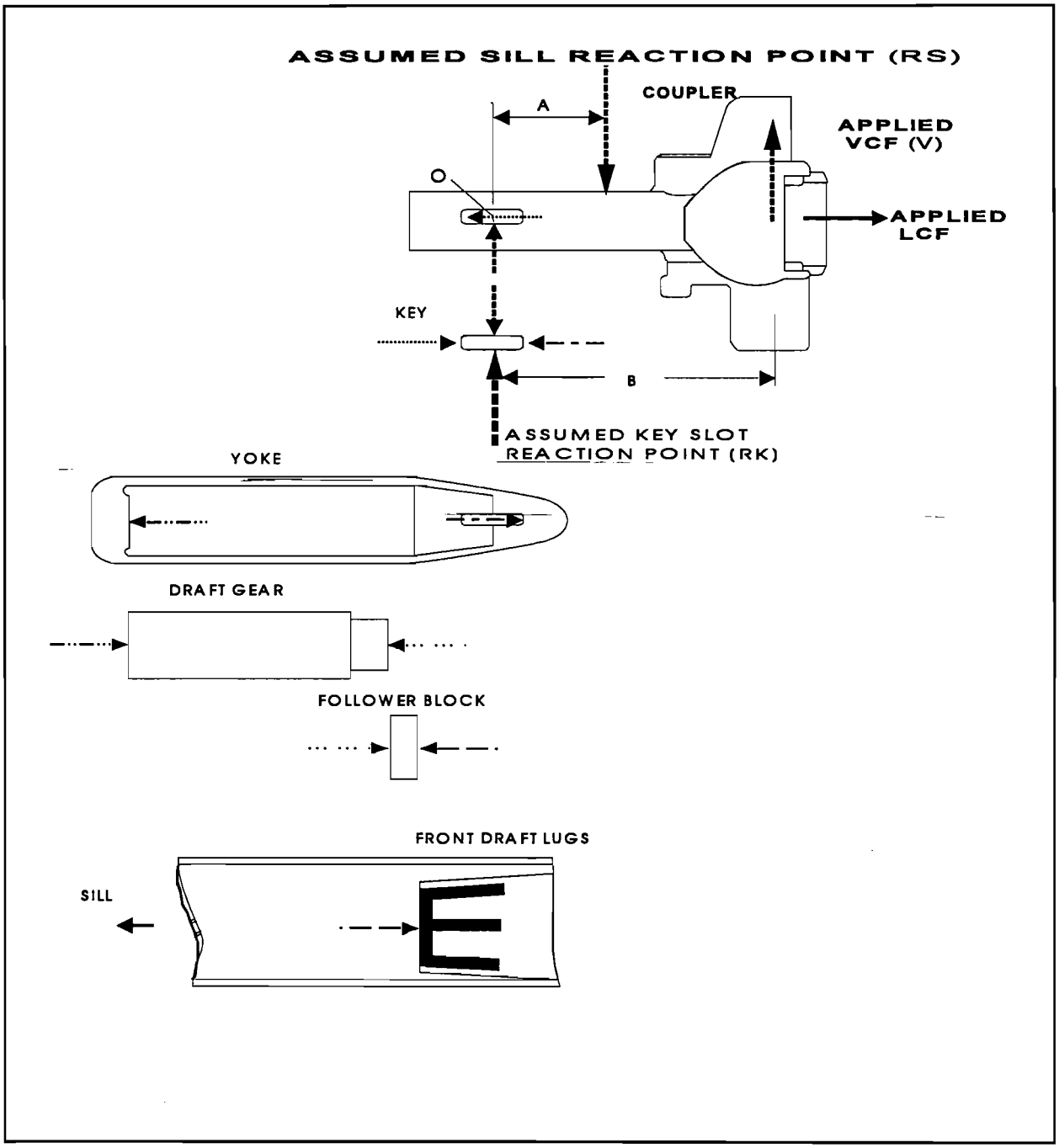

Figure 24. FEEST1 Assumed VCF Load Path

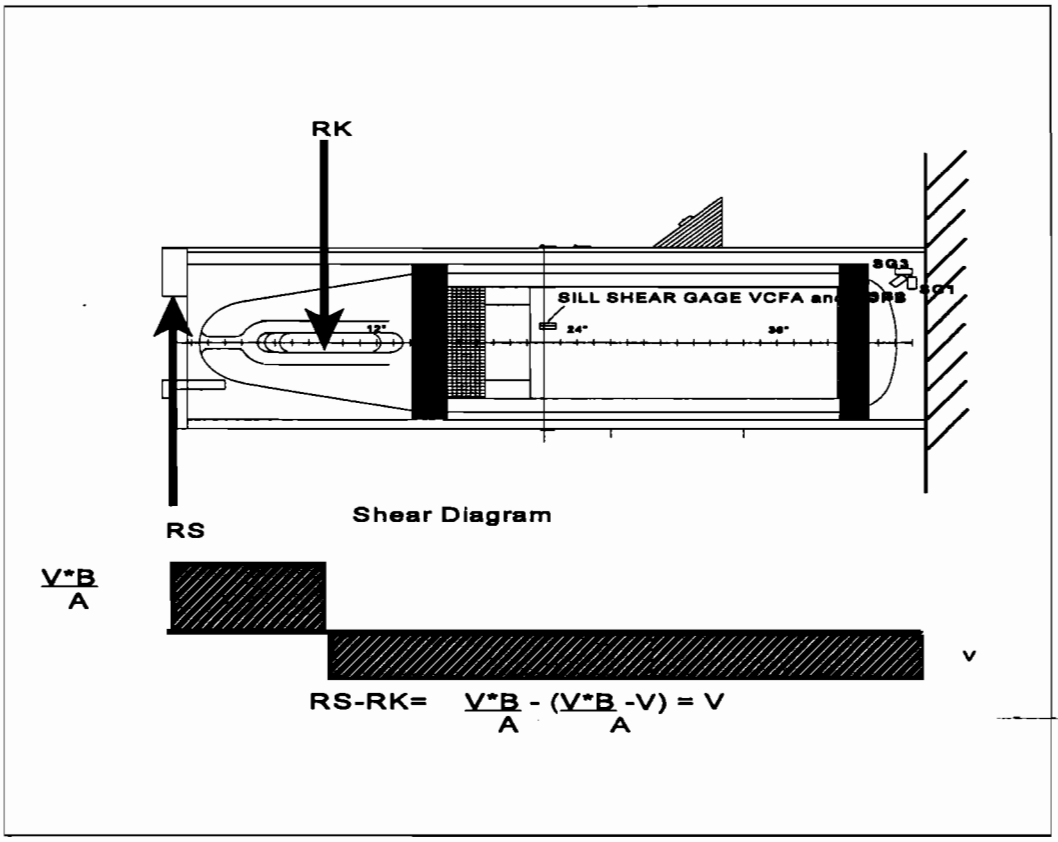

Figure 25. Shear Diagram For Assumed VCF Load Path

To gain more insight into these load paths, the Coupler Load Investigation Test was devised to determine if a suitable compromise could be reached. Of particular interest was the interaction of longitudinal coupler force LCF and VCF loads. This test used simple squeeze and impact tests to help empirically characterize the load paths within the stub sill region of the tank. The adjacent car coupled to the test car during the investigation tests was varied to view the effect of vertical coupler height and sill stiffness on the development of VCF loads. Bolster loads were monitored to determine if an equivalent loading or unloading equal to the sill shear loading occurred. The results from these test showed the variability in the different techniques used to measure the VCF. Because of the these results, the striker/carrier plate strain gages (SCTA and SCTB) were added to better define where along the length of the sill the VCF is imparted. At the recommendation of an RPI member, the shank of the A-end coupler was instrumented with strain gages (VCFS) in an attempt to remove the effects of a changing load paths from the measurement of VCF, as

previously discussed. It also served as a backup to the primary sill shear measurements (VCFA and VCFB).

A reliable measure of VCF in **static** jacking on coupler tests was found to be VCFS and the truck bolster measurements (BOLA and BOLB). Projections of this force based on the bolster gages correlated best with the load cell data from the jacking tests. As may be seen from the longitudinal cross section of the short stub sill design in Figure 25, vertical internal sill reactions to a force applied on the coupler are possible behind or inboard of the position of the sill shear gages (VCFA and VCFB) by a load path passing through the yoke. Any vertical shear reactions occurring behind the location of the strain gages for VCFA and VCFB would not be measured. This load path is thought to exist during dynamic events and is reason to expect differences between the vertical shear measured by the sill gages and the vertical reaction force "felt" by the tank car at the bolster, or at the sill/tank junction. Therefore, for the purpose of dynamic testing, the sill shear gaging was calibrated directly to read shear in the sill at that location. Efforts to extend this calibrated sill shear section inboard towards the tank junction, by considering the modifying effect of a reaction force measured by the specially instrumented yoke plate (sill shear - yoke plate force), were ultimately abandoned because of OTR data recording complexity and the reduced load levels seen by the yoke plate gages.

As discussed, one of the most reliable measures of VCF in static tests was found to be that based on truck bolster load changes. The apparent VCF based on these load changes was used primarily to examine the effect of configuration and equipment variables such as adjacent car type, coupler height or buff versus draft loading in the special squeeze tests.

Due to all of the additional instrumentation, a second set of tests were performed. The objective of the second set of testing was to determine which measurement method was the most reliable in measuring **dynamic and static** coupler forces. The results indicated that the separate methods of measuring VCF that were developed did not produce consistent VCF magnitudes during dynamic events. This result was not unexpected as other independent investigations have had the same result. Figure 26A shows an example of the

differences in VCF measured during a series of dynamic events. The data presented is time correlated data for the measurements VCFB, SCTB and YPLB taken from leg 10 of the OTR testing. The data shown spans 50 seconds of data for 10 separate burst histories.

As mentioned previously, the parameter SCTB was only sensitive to VCF loads in the negative direction (downward) as shown in Figure 26A. For those negative VCF events, relatively good correlation between SCTB and VCFB existed. Figure 26A also shows the VCF as measured by YPLB and illustrates the reduced dynamic response levels. As a result, the data from YPLA and YPLB will not be presented in this report.

Figure 26B shows data for the VCF measurements VCFA and VCFS, which were on the A-end of the car. The two measurements record the same basic dynamic response but the magnitude of the VCF measured by VCFA is higher in magnitude as predicted by Equation 3. Taking the ratio of the predominant peaks in Figure 26B for comparison with the results of Equation 3, ratios between 1 and 2.8 are observed with an average value in the 1.8 range. In addition, there appears to be a static value that is apparent in the time range of 0 to 50 seconds, but not from 75 to 100 seconds. This is the manifestation of the changing load paths.

Figure 26C shows a very low frequency event that occurred during leg 7. The peak VCF, as indicated by the three different measurements, gives the values of VCFS= 26.9, VCFA= 20.1 and BOLA= -32.9. These values show yet another relationship between the VCF measurements such that the measurement VCFS produces the largest VCF.

Due to these differences in the VCF measurements, a meeting was held on July 18, 1994, to determine which set of VCF measurements would be used for the FEEST2 testing. The meeting resulted in the agreement that the VCF measurement limitations were understood and accepted by RPI. It was agreed that each independent VCF measurement technique would be utilized for the FEEST2 test with the sill shear gages (VCFA and VCFB) being the accepted measurement for the VCF fatigue life spectrum.

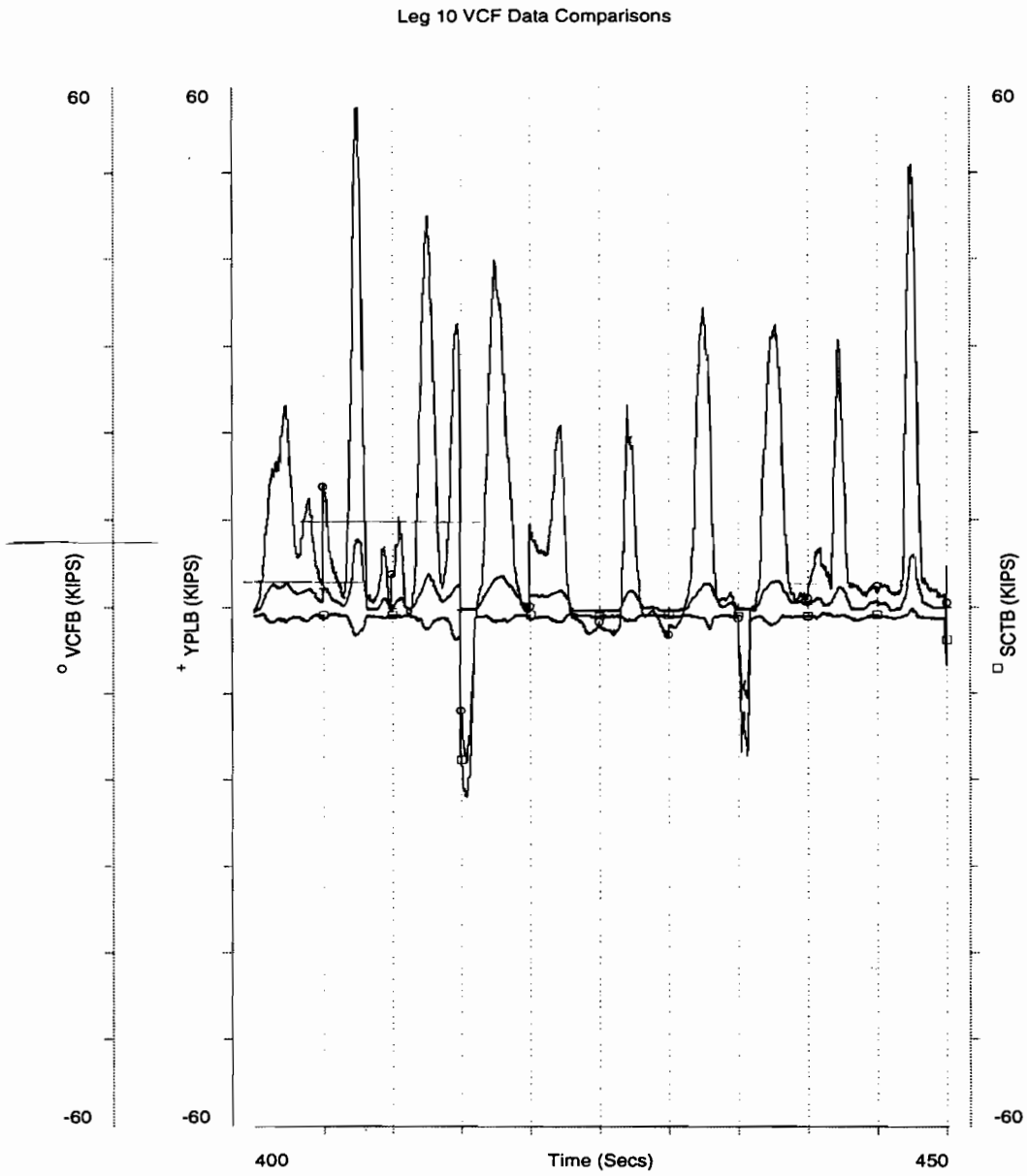

Figure 26A. Comparison of VCF Measurements B-End

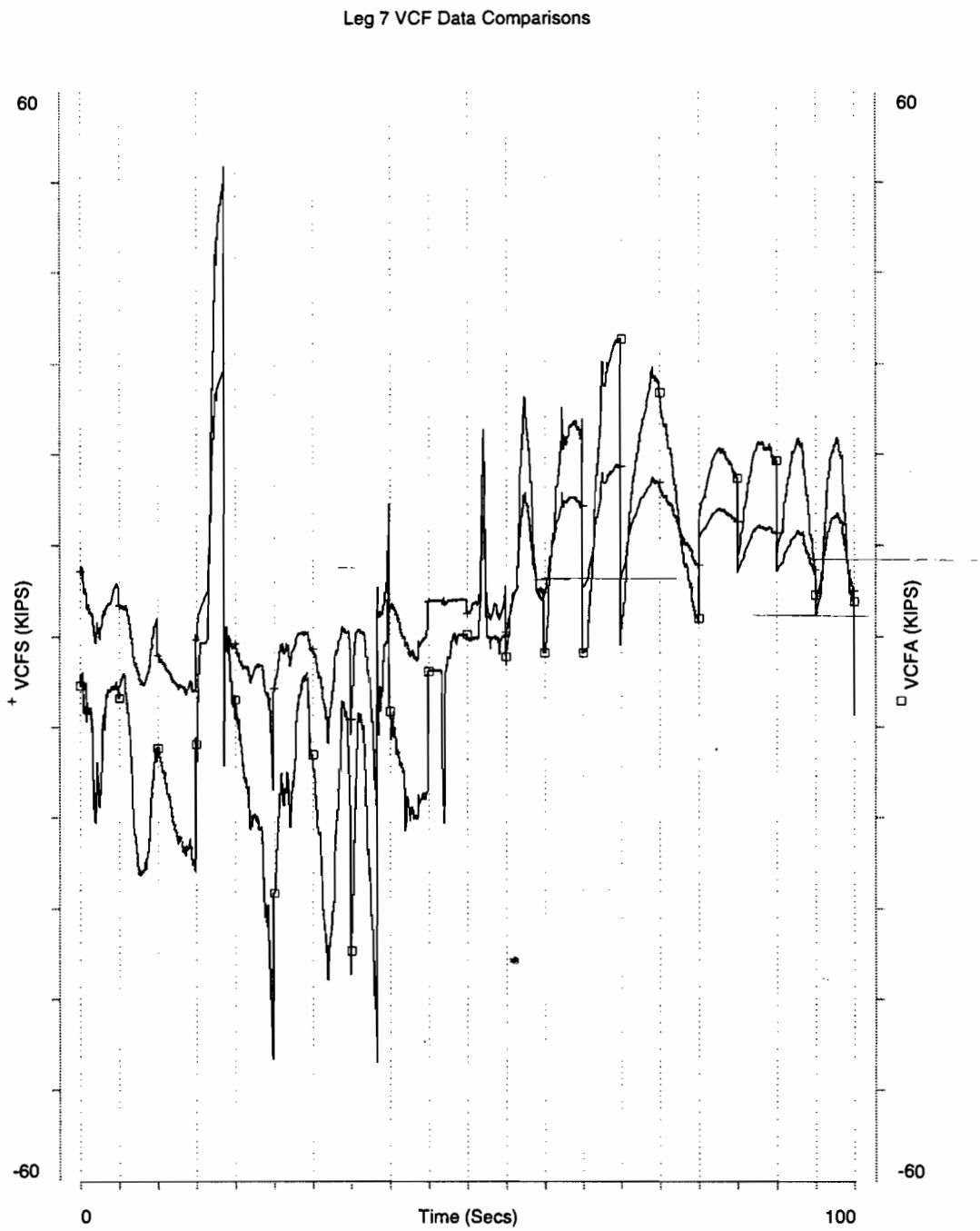

Figure 26B. Comparison VCF Measurements A-End

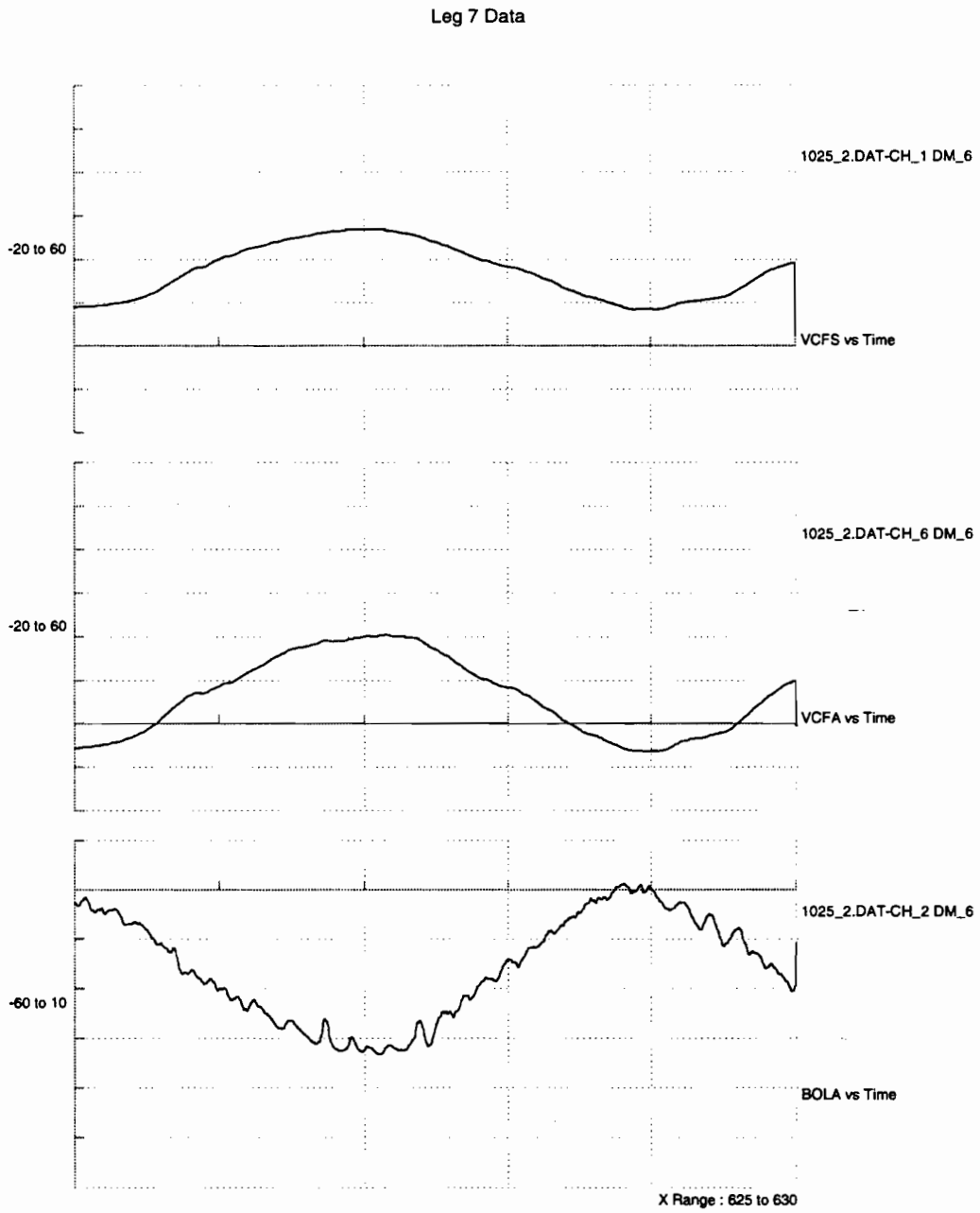

Figure 26C. Low Frequency VCF Measurement Comparisons

3.9 TEST PROCEDURE

The OTR test procedure consisted of collecting data over approximately the same route (when possible) that was used for FEEST1 to match the loading environment as closely as possible. The selected route was broken up into 10 legs. At the end of each leg the data collected by the onboard data collection system was downloaded. As testing proceeded, the distance between download points was progressively increased as confidence in the system was gained. For the loaded portion of testing, the greatest distance traveled between download points was 2,343 miles. For the unloaded portion of the FEEST2 testing at TTC, only one download point was involved resulting in approximately 4,179 miles of unloaded data being collected. The unloaded portion of the FEEST2 testing comprised leg 11.

The test procedure also consisted of remotely monitoring the position of the tank car with the onboard Ground Positioning System (GPS). The GPS system was used to remotely track the location and actual routing of the tank car providing a check on the actual mileages traversed. In addition, the charge on the batteries was monitored remotely to assure sufficient electrical power availability.

The data collected by the SOMATS was recovered by TTC personnel who traveled to each download location and obtained the data stored in the SOMATS. The data was recovered and stored on optical disks for later analysis. Static offset caused by the normal settling of strain gages was removed by resetting the zero point of the measurement.

The temperature of the water-methanol mixture was taken at the bottom, middle, and top of the tank car by using a thermocouple inserted into the manway at each download location. Outage conditions were also measured at each download location.

3.9.1 Parameter Operational Status

The operational status of each measurement was checked at each download location. To perform the fatigue life analysis, it was necessary to keep track of the mileages traveled while each individual measurement was operational. Tables 13, 14 and 15 show the individual measurements and the miles accumulated by individual leg number.

As shown, the side bearing measurements failed early in the FEEST2 test and very little data was collected. Due to the complexity and cost of installing new transducers, these measurements were not made operational once failure occurred. Also shown is the failure of the speed transducer, critical region strains, and VCFA during the unloaded portion of ~~the FEEST2~~ OTR tests.

Table 13. Operational Mileages By Measurement For SOMAT 1

LEG NUMBER	LEG LENGTH (MILES)	BOLB (MILES)	SCTB (MILES)	SBBR (MILES)	VCFB (MILES)	LCF1B (MILES)
1 (loaded)	114.4	114.4	114.4	114.4	114.4	114.4
2 (loaded)	780.5	780.5	780.5	780.5	780.5	780.5
3 (loaded)	1309	1309	1309	0	1309	1309
4 (loaded)	1440.8	1440.8	1440.8	0	1440.8	1440.8
5 (loaded)	878.8	878.8	878.8	0	878.8	878.8
6 (loaded)	919.5	919.5	919.5	0	919.5	919.5
7 (loaded)	483	483	483	0	483	483
8 (loaded)	2343.6	2343.6	2343.6	0	2343.6	2343.6
9 (loaded)	1973.3	1973.3	1973.3	0	1973.3	1973.3
10 (loaded)	2088.5	2088.5	2088.5	0	2088.5	2088.5
11(unloaded)	4179	4179	4179	0	4179	4179
TOTALS:	16510.4	16510.4	16510.4	894.9	16510.4	16510.4
% OPERATIONAL		100	100	5	100	100

Table 14. Operational Mileages By Measurement For SOMAT 2

LEG NUMBER	LEG LENGTH (MILES)	BOLB (MILES)	SCTB (MILES)	SBBR (MILES)	VCFB (MILES)
1 (loaded)	114.4	114.4	114.4	0	114.4
2 (loaded)	780.5	780.5	780.5	0	780.5
3 (loaded)	1309	1309	1309	0	1309
4 (loaded)	1440.8	915	915	0	915
5 (loaded)	878.8	878.8	878.8	0	878.8
6 (loaded)	919.5	919.5	919.5	0	919.5
7 (loaded)	483	483	483	483	483
8 (loaded)	2343.6	0	2343.6	2343.6	2343.6
9 (loaded)	1973.3	0	1973.3	1973.3	1973.3
10 (loaded)	2088.5	0	2088.5	2088.5	2088.5
11(unloaded)	4179	0	0	0	0
TOTALS:	16510.4	5400.2	11805.6	6888.4	11805.6
% OPERATIONAL		32	71.5	41.72	71.5

Table 15. Operational Mileages By Measurement for SOMAT's 3 and 4

LEG NUMBER	LEG LENGTH (MILES)	BOLB (MILES)	SCTB (MILES)	SBBR (MILES)	VCFB (MILES)	SG1A (MILES)	PR1 (MILES)
1 (loaded)	114.4	114.4	114.4	114.4	114.4	114.4	114.4
2 (loaded)	780.5	101	101	101	101	101	780.5
3 (loaded)	1309	1109	1109	1109	1109	1109	1309
4 (loaded)	1440.8	19	19	19	19	19	1440.8
5 (loaded)	878.8	0	0	0	0	0	878.8
6 (loaded)	919.5	919.5	919.5	919.5	919.5	919.5	0
7 (loaded)	483	483	483	483	483	483	483
8 (loaded)	2343.6	2343.6	2343.6	2343.6	2343.6	2343.6	2343.6
9 (loaded)	1973.3	1973.3	1973.3	1973.3	1973.3	1973.3	0
10 (loaded)	2088.5	2088.5	2088.5	2088.5	2088.5	2088.5	2088.5
11 (unloaded)	4179	0	0	0	0	0	NA
TOTALS:	16510.4	9151.3	9151.3	9151.3	9151.3	9151.3	9438.6
% OPERATIONAL		55.5	55.5	55.5	55.5	55.5	77

3.9.2 Test Lading

The test car was initially loaded to a 1-percent outage condition, with a solution of water and methanol. As testing proceeded, no attempt was made to maintain the outage at 1.0% due to changes in the temperature of the water-methanal mixture. The loaded weight configuration of the tank car was:

Car empty weight	74,500 lb
Weight of instrumentation (conservative to ensure total weight is within legal limits)	2,000 lb
Weight of 17,225 gallons of demineralized water	145,469 lb
Weight of 6,065 gallons of methanol	40,531 lb
Total Weight:	262,500 lb

The total weight was verified by weighing the tank car on a certified scale at the start of the FEEST2 test.

3.10 SURGE PRESSURE IMPACT TESTS

At the conclusion of the loaded portion of the FEEST2 testing, impact tests were conducted using three different configurations and at various speeds to characterize OTR surge pressure events recorded with known impact conditions. The speed at impact was measured with radar for checking against the onboard speed sensor.

3.10.1 Surge Pressure Impact Test Configurations

Three configurations were used for the surge pressure impact tests. Configuration A (Figure 27) consisted of three anvil cars (loaded hopper cars). The instrumented tank car was the hammer car with the B-end striking the anvil cars FEEST2 test with the sill shear gages (VCFA and VCFB) being the accepted measurement for the VCF fatigue life

spectrum. Configuration B (Figure 27) was identical to configuration A except that the test car was turned around so that the A-end impacted the anvil car. Configuration C (Figure 28) consisted of the three anvil cars coupled to the test car with another loaded hopper car used as the hammer car. The B-end of the test car was facing the hammer car.

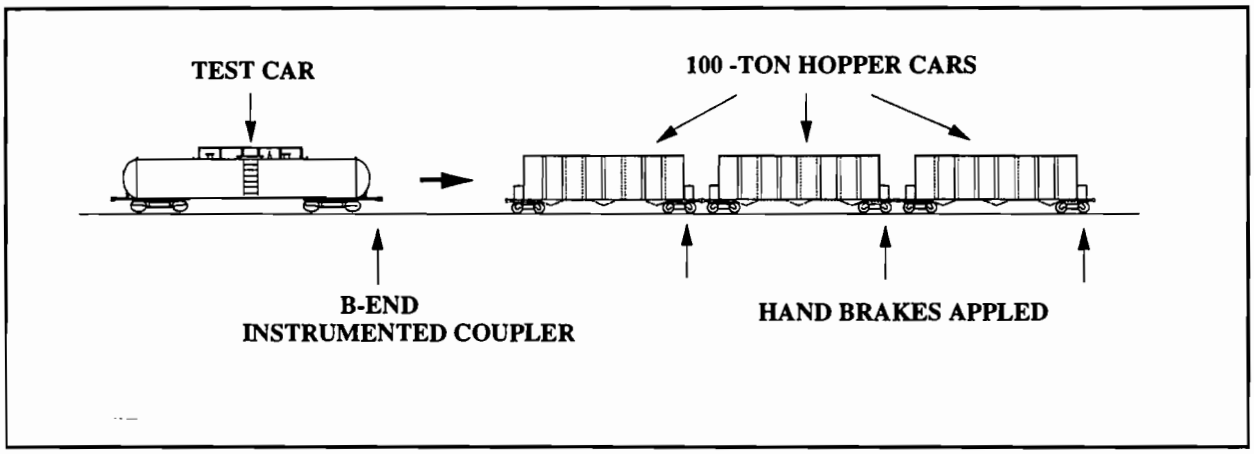

Figure 27. Surge Pressure Impact Configurations A and B

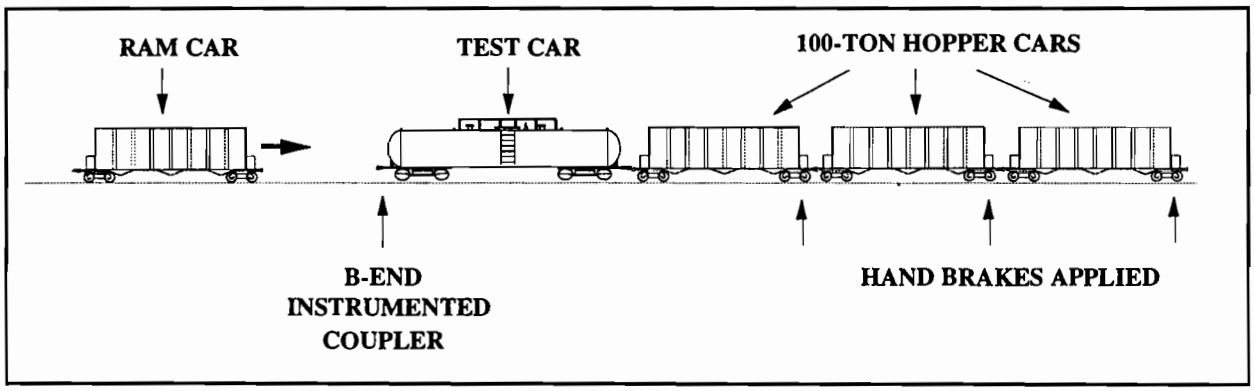

Figure 28. Surge Pressure Impact Test Configuration C

4.0 TEST RESULTS

The FEEST2 testing resulted in obtaining a large amount of in-service loads data in the form of histograms and time history data. In addition, surge pressure events in the form of time history data were also obtained.

As previously mentioned, the calibration factors for the measurements VCFA and VCFB were redefined at the end of leg 7. This change was made in an attempt to resolve a discrepancy in the number and magnitude of events being recorded between the A- and B-ends of the tank car. The initial calibration values used were a composite of several of the calibration jacking point techniques described earlier. The recalibration utilized the jacking up on the sill method which produced the most consistent results.

The recalibration resulted in excellent agreement between the A- and B-end of the car obtained on leg 8. Because of this, all of the data collected before leg 7 was adjusted using the calibration factors developed at the end of leg 7. All of the data presented for VCFA and VCFB in this report has been adjusted for the consistent set of calibrations values developed at the end of leg 7.

In addition to the calibration changes in measurements VCFA and VCFB, the calibration for VCFS also was changed slightly at the end of leg 7 to account for initial settling of the strain gages. The VCFS data taken before leg 7 was not adjusted due to the small change in the calibration. Unfortunately, the strain gages and wiring for the VCFS measurement were destroyed during leg 8 and no data from the measurement VCFS was collected for the remainder of the OTR testing.

The surge pressure transducer was changed several times due to intermittent noise caused by the vibration environment where the transducer was mounted. This intermittent noise did not affect the capturing of individual surge pressure burst history events since the level of the noise floor was below the trigger level of the measurement. However, on several legs, the peak valley data collected showed inconsistent high count values in the low bins, which was the result of the intermittent noise. The peak valley data collected for

the legs that showed high count values caused by the intermittent operation is not included in this report (approximately 23 percent of the total data).

4.1 RELATIVE FATIGUE LIFE ANALYSIS RESULTS

The concept of relative fatigue life was used to estimate the severity of the loads imposed on the tank during each leg and to check data quality. Individual leg and cumulative fatigue lives were calculated using the histograms obtained from the measurements VCFA, VCFB and LCF1B. Drastic changes in the resulting fatigue life indicated a more severe load environment which directly affects the fatigue life of the structural components. This analysis also served as a data quality check as errors in instrumentation would produce inconsistent changes in the resulting fatigue life between measurements.

The AAR Fatigue Life Analysis Package (FLAP) was utilized to calculate the relative fatigue lives. The input measurements used for the fatigue life analysis program are listed below.

Modified Goodman Diagram:

Section Type:

3.1.5.1 Continuous welded I-beam with square end cover plates, welded all around - flexural loading.

$b = 6.3 \quad m = 1.0 \quad k = 0.3$

Sensitivity to loads (arbitrarily chosen):

Vertical coupler forces (VCFB and VCFA) — 5 ksi / 10 kips load

Longitudinal coupler force (LCF1B) — 10 ksi / 100 kips load

Since the sensitivity values chosen were not based on actual stress field data, the resulting fatigue lives are not based on the true stress state. As a result, the mileages shown should only be used for relative comparisons between legs and for tracking general trends in the cumulative data. **The values shown in no way represent predictions of actual fatigue lives that can be expected and are only shown for relative comparisons.** Note that the sensitivity values chosen for the VCF measurements was different than the sensitivity chosen for the LCF preventing comparison between the VCF and LCF fatigue life values. The VCF and LCF loads were **not** combined into a single input; that is, the loads were assumed to act independently.

Tables 16, 17 and 18 show the resulting fatigue lives obtained from the analysis along with the results from FEEST1 for comparison. The FEEST1 fatigue lives were calculated using the same input measurements used for the FEEST2 estimates. This allows direct comparison between FEEST2 and FEEST1 test data.

Table 16. Relative Leg and Cumulative Fatigue Mileage for VCFB

FATIGUE LIVES DERIVED FROM VCFB LOADED DATA

LEG	SEGMENT MILES	CUM. MILES	SEGMENT LIFE (MILES)	CUMULATIVE LIFE (MILES)
1	114	114	298,104	298,104
2	780	894	662,340	572,863
3	1,309	2,203	999,344	767,371
4	1,441	3,644	1,250,190	905,618
5	879	4,524	859,922	896,371
6	920	5,444	1,140,836	930,044
7	483	5,926	195,304	711,768
8	2,343	8,269	421,129	595,416
9	1,974	10,242	447,281	559,702
10	2,089	12,331	603,875	566,696

FEEST 1 CUMULATIVE LIFE 150,358 MILES

FATIGUE LIVES DERIVED FROM VCFB UNLOADED DATA

LEG	SEGMENT MILES	CUM. MILES	SEGMENT LIFE (MILES)	CUMULATIVE LIFE (MILES)
11	4,179	16,510	1,210,775	1,210,775

FEEST1 CUMULATIVE LIFE 2,065,849 MILES

Table 17. Relative Leg and Cumulative Fatigue Mileages for VCFA

FATIGUE LIVES DERIVED FROM VCFA LOADED DATA

LEG	SEGMENT MILES	CUM. MILES	SEGMENT LIFE (MILES)	CUMULATIVE LIFE (MILES)
1	114	114	11,137,050	11,137,050
2	780	894	964,017	1,091,146
3	1,309	2,203	1,642,291	1,363,241
4	915	3,118	3,440,821	1,656,710
5	879	3,998	2,093,856	1,736,342
6	920	4,918	1,839,890	1,754,813
7	483	5,400	179,999	984,393
8	2,344	7,744	641,926	847,536
9	1,973	9,716	1,126,256	892,387
10	2,089	11,806	852,599	885,080

FEEST1 CUMULATIVE LIFE 150,358 MILES

FATIGUE LIVES DERIVED FROM VCFA UNLOADED DATA

LEG	SEGMENT MILES	CUM. MILES	SEGMENT LIFE (MILES)	CUMULATIVE LIFE (MILES)
11	4,179	16,510	not available	not available

FEEST1 CUMULATIVE LIFE 2,065,849 MILES

Table 18. Relative Leg and Cumulative Fatigue Mileages for LCF1B

FATIGUE LIVES DERIVED FROM LCF1B LOADED DATA

LEG	SEGMENT MILES	CUM. MILES	SEGMENT LIFE (MILES)	CUMULATIVE LIFE (MILES)
1	114	114	44,876	44,876
2	780	894	176,000	128,138
3	1,309	2,203	220,677	170,638
4	1,441	3,644	224,520	188,523
5	879	4,524	147,644	178,907
6	920	5,444	155,498	174,469
7	483	5,926	49,638	144,788
8	2,344	8,270	106,517	131,406
9	1,973	10,242	120,494	129,153
10	2,089	12,331	97,699	122,474

FEEST1 CUMULATIVE LIFE 63,250 MILES

FATIGUE LIVES DERIVED FROM LCF1B UNLOADED DATA

LEG	SEGMENT MILES	CUM. MILES	SEGMENT LIFE (MILES)	CUMULATIVE LIFE (MILES)
11	4,179	16,510	81,954	81,954

FEEST1 CUMULATIVE LIFE 270,333 MILES

The most interesting result obtained from the fatigue life analysis for the loaded portion was the dramatic relative reduction in the calculated fatigue life for leg 7. As shown in Tables 16, 17 and 18, the individual fatigue life (referred to as segment life) for all three of the measurements for which fatigue life was calculated showed a large reduction in the fatigue life for leg 7. The cause of this drop in fatigue life can not be stated for certain, but after investigation, it is suspected that the nature of the terrain and track where this data was collected played an important role in the resulting fatigue life. The effect of the distribution of speed during a given leg was checked to see if there was a correlation between a "slow" leg and a "fast" leg by using the time at level data presented in Appendix E. This data shows that Leg 7 was a slow leg as compared to the other legs, however, it is difficult to draw conclusions from this data alone. Comparison of the "Number of Events Per Mile" histograms for the A-end measurements VCFA, VCFS and BOLA (see Appendix A) all show the increased occurrence/load rates that occurred during leg 7. Leg 1 data also showed reduced fatigue life but the results were not as consistent for both of the VCF measurements. This may have been caused by the short length of leg 1.

The unloaded LCF1B fatigue life values shown in Table 18 showed a very large reduction in the expected fatigue life as compared to the FEEST1 values and also showed a more severe load environment than the loaded configuration. This will be discussed in more detail (Section 4.2), when the unloaded histograms are presented.

4.2 TEST HISTOGRAMS

Histograms were developed for all of the measurements which were rainflowed during the OTR testing. Appendix A presents the histograms of the data obtained for each leg during the loaded portion of the testing. Appendix B presents the histograms of the data obtained for the unloaded portion of the FEEST2 testing. Cumulative values represent the total of the individual leg values for the loaded portion. The unloaded portion consisted of only one leg and the resulting values were not combined with the loaded values.

The histogram data is presented in two formats: "Number of Events" and "Number of Events per Mile." The basic data as acquired is referred to as Number of Events and is the total number of peak/valley combinations detected during that leg for each individual bin value. In the second format, the number of events values in each bin were divided by the number of miles over which the data was collected in order to normalize the data to obtain the "Number of Events per Mile" values. This allows a more meaningful value to be used for comparisons and will be the format generally shown. However, division of the low count value by different leg mileages is difficult when making comparisons.

Where applicable, the corresponding FEEST1 data is also presented for ease of comparison. Only the cumulative value for the FEEST1 data is presented. Both the A- and B-end count values for the VCF FEEST1 data were combined into a single file used as input to the fatigue life program to develop the cumulative fatigue life values shown. The cumulative mileage for the VCF FEEST1 measurements was 22,994 miles due to this combining.

Figures 29 and 30 show a summary of the VCF histogram data obtained from the OTR testing. The histograms resulting from the rainflowed data from the measurements VCFA and VCFB normalized for the number of events per mile are shown to allow direct comparison of the rate of occurrences. Note that no data for the measurement VCFA for the unloaded portion of the FEEST2 data is presented due to corrupted data caused by transducer failure. The unloaded B-end data shown (VCFB) was not corrupted and is

considered to be an adequate representation of the VFC loading for the unloaded configuration.

The FEEST2 and FEEST1 VCF loaded data, as shown in Figure 29, are similar up to approximately 40 kips. Above 40 kips, the FEEST2 loaded data was not correlated with the FEEST1 loaded data due to the "hump" in the FEEST1 data. Figure 29 shows that the correlation between the A- and B-end loaded FEEST2 VCF data is very good with significant differences only in the lowest bin values. These differences were most likely caused by the draft gear pocket on the B-end having less vertical clearance than on the A-end. At the conclusion of the OTR testing, the vertical clearance on both ends of the car were measured by applying a upward vertical force on the coupler and measuring the vertical distance traveled before striking the striker carrier face. The A-end traveled 2.0 inches vertically and the B-end traveled 1.375 inches vertically before contact with the striker carrier face.

The effect of the higher occurrence rates in the lower bin values on the fatigue life for the measurement VCFB were determined by removing the lowest bin count values and recalculating the resulting fatigue life using the FLAP program. The FLAP program predicts that the higher count values in the bins below 7.5 kips VCF have an insignificant effect on the resulting fatigue life of the structure. However, this result is a direct consequence of the assumptions made in determining the sensitivity values to be used in the fatigue analysis shown in Section 4.1. Geometric discontinuities and other types of stress risers, such as porosity in welds, could result in smaller loads becoming more significant in initiating and growing cracks in the critical region. A detailed fracture mechanics analysis using these loads would show the relative importance of the loading environment measured.

The VCF histogram obtained from the unloaded portion of the OTR testing is presented in Figure 30. Due to noise in the instrumentation system, the histogram obtained from the measurement VCFA was corrupted and is not presented. Only the data obtained from VCFB is presented with the FEEST1 data for comparison. Figure 30 shows that the

FEEST1 and FEEST2 unloaded VCF histograms are similar. The relative VCF fatigue lives calculated for the unloaded configuration show an increased fatigue life as compared to the loaded fatigue life values but were much less than the values obtained during FEEST1.

As explained in Section 3.5.1 on rainflow algorithm, some of the VCF count values above 60 kips may be due to combining events that occurred separately. The events above 60 kips, shown in Figure 29, are suspected of being formed in this manner. The largest continuous single VCF event that could be found in the burst history data was approximately 60 kips and will be discussed later (Section 4.3).

Appendix A is a listing of the VCF data (loaded data) combined in a single file for both the A- (VCFA) and B-end (VCFB). Appendix B is a listing of the VCF data, which is not combined due to transducer failure, for the unloaded data.

Figure 31 shows a comparison of the loaded and unloaded FEEST2 VCF histograms as measured by VCFB. As shown, the loaded VCF histogram shows higher occurrence rates. Figure 32 presents the cumulative histograms obtained for the LCF measurement LCF1B for the loaded FEEST2 testing along with the loaded FEEST1 data. As can be seen, there was excellent correlation between the FEEST1 and FEEST2 loaded data, except for the events at the 800 kip level in the FEEST1 data. As shown, a very high magnitude event was recorded during the FEEST2 loaded testing that resulted in peak-to-peak LCF of approximately 1060 kips. Assuming that this event was formed during a single impact, from a review of the surge pressure test results, it is estimated that this could have represented an impact occurring at approximately 9 mph. Figures 32 and 33 also show that the total number of LCF events that occurred at and above 500 kips was relatively low (less than 30) for both the loaded and unloaded portions of the FEEST2 testing. The events above 400 kips generally were found to represent impact conditions. Comparison of the fatigue lives for the loaded condition shows that the FEEST2 data was less severe, due in part to the events at 800 kips in the FEEST1 data.

Figure 33 presents the unloaded histograms obtained for the LCF measurement LCF1B for the unloaded FEEST2 testing along with the FEEST1 data. The FEEST2 data can be seen to be more severe which is also shown in the reduced fatigue life of the unloaded configuration compared to the FEEST1 data.

Figure 34 presents a comparison of the FEEST2, LCF loaded versus unloaded data.

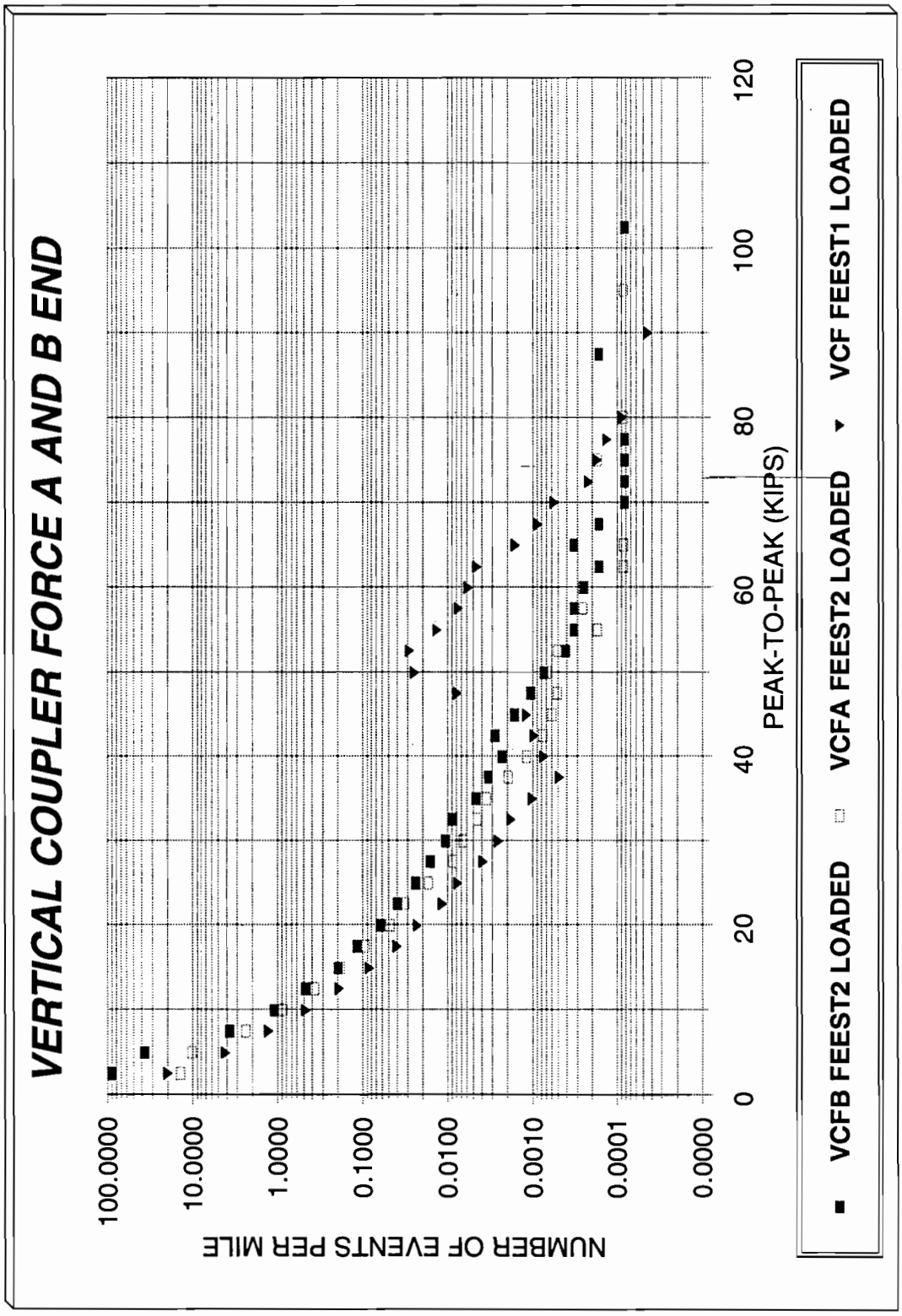

Figure 29. Loaded VCF Histograms

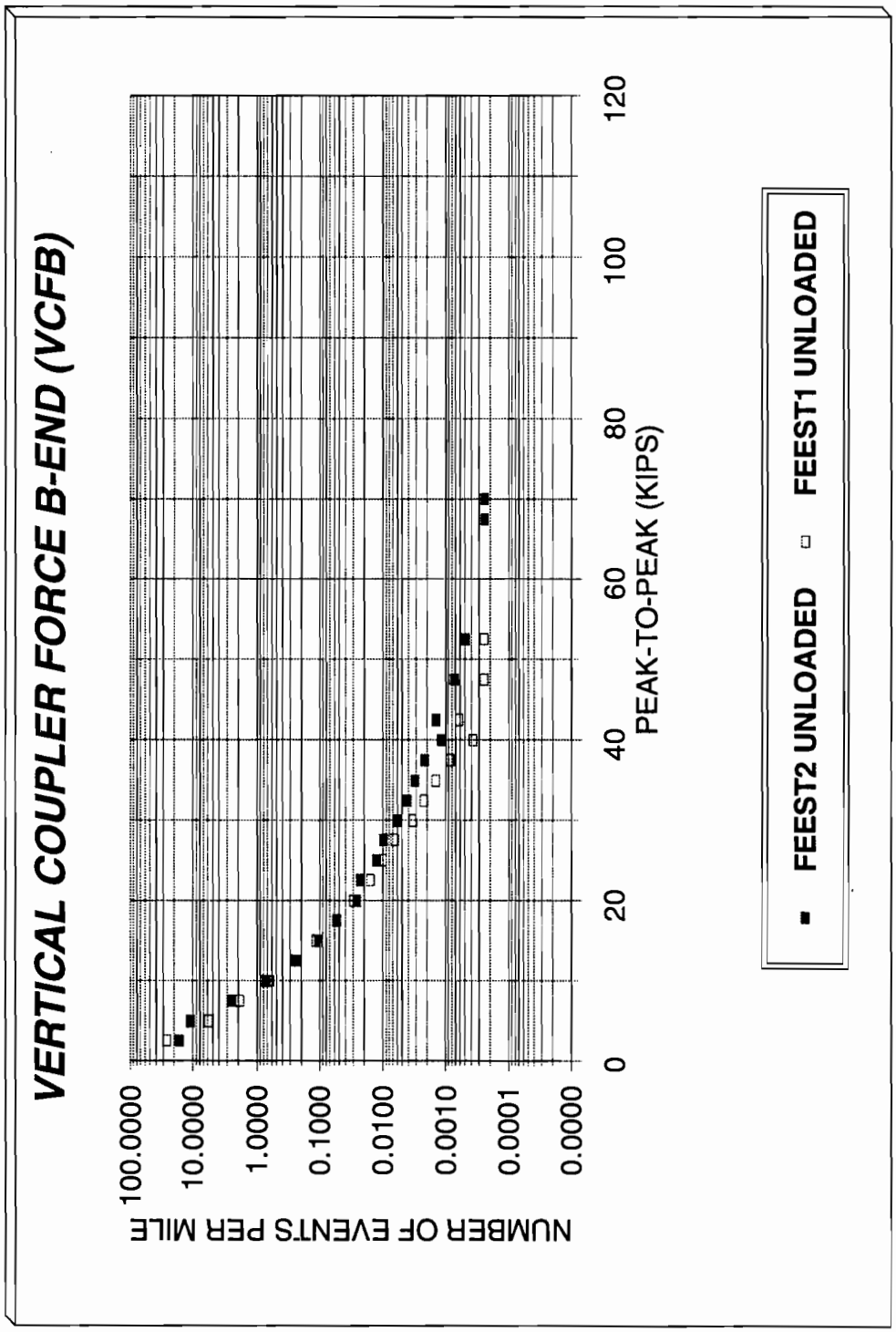

Figure 30. Unloaded VCFB Histograms

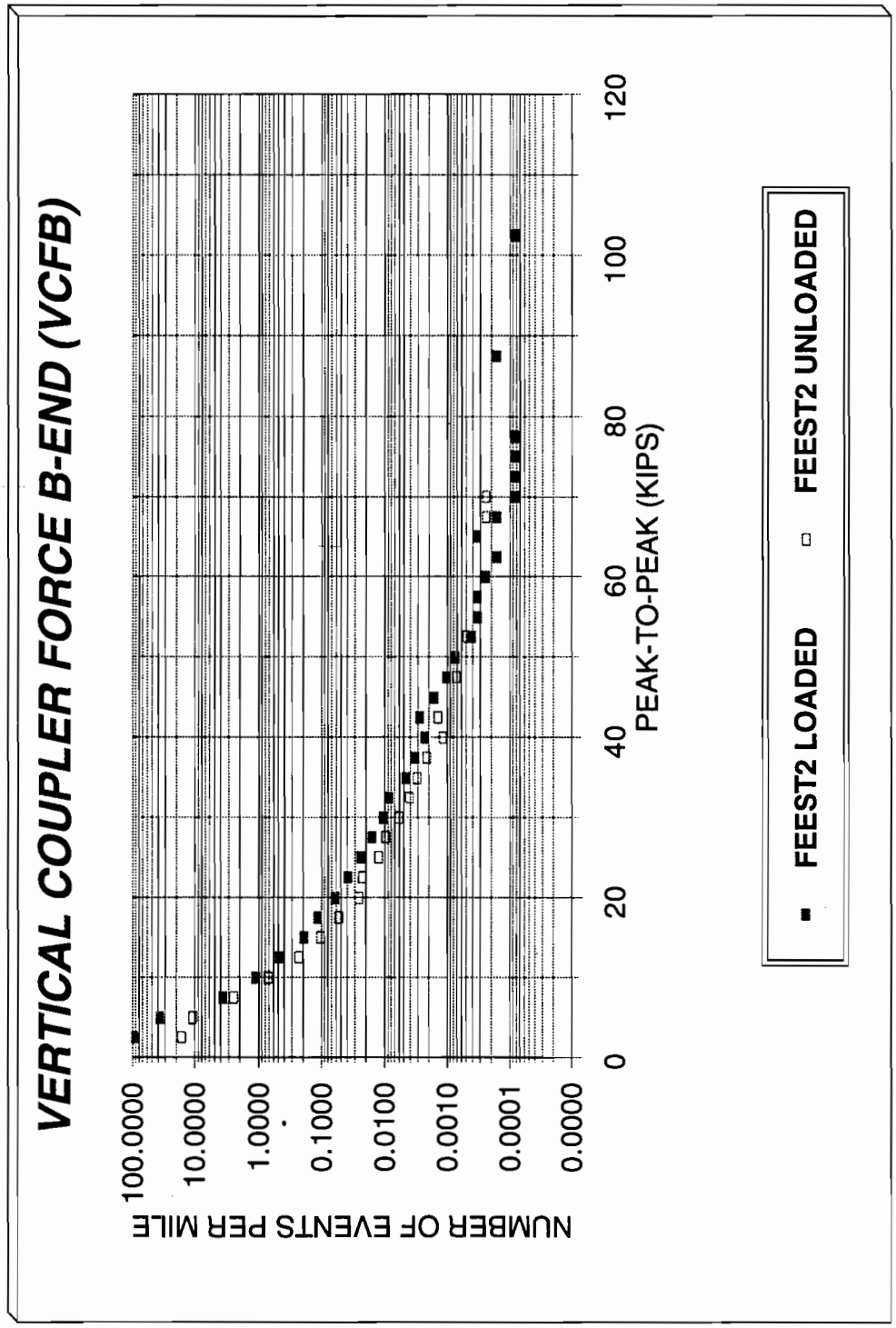

Figure 31. Loaded and Unloaded FEEST2 VCFB Histograms

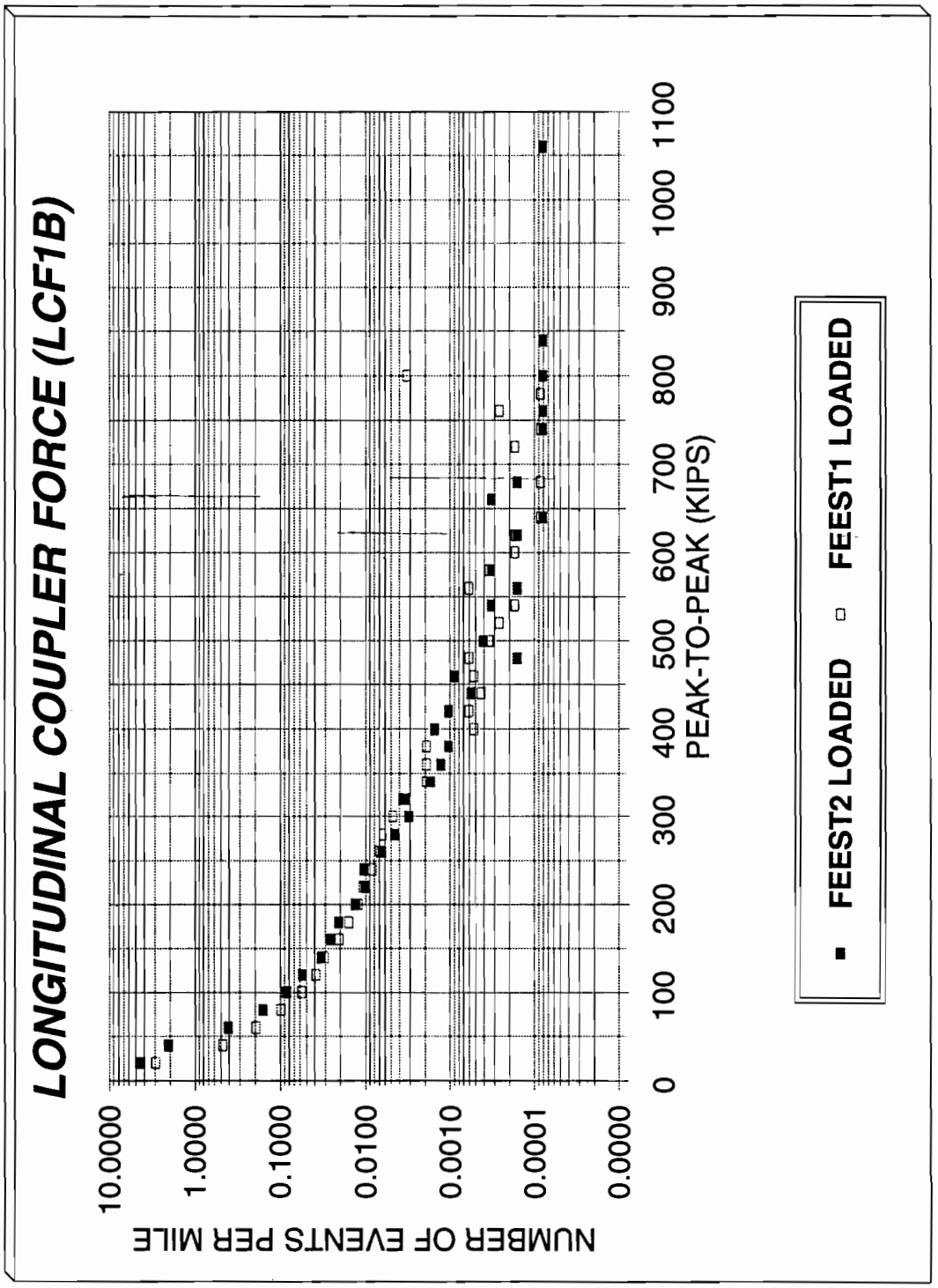

Figure 32. Loaded LCF1B Histograms

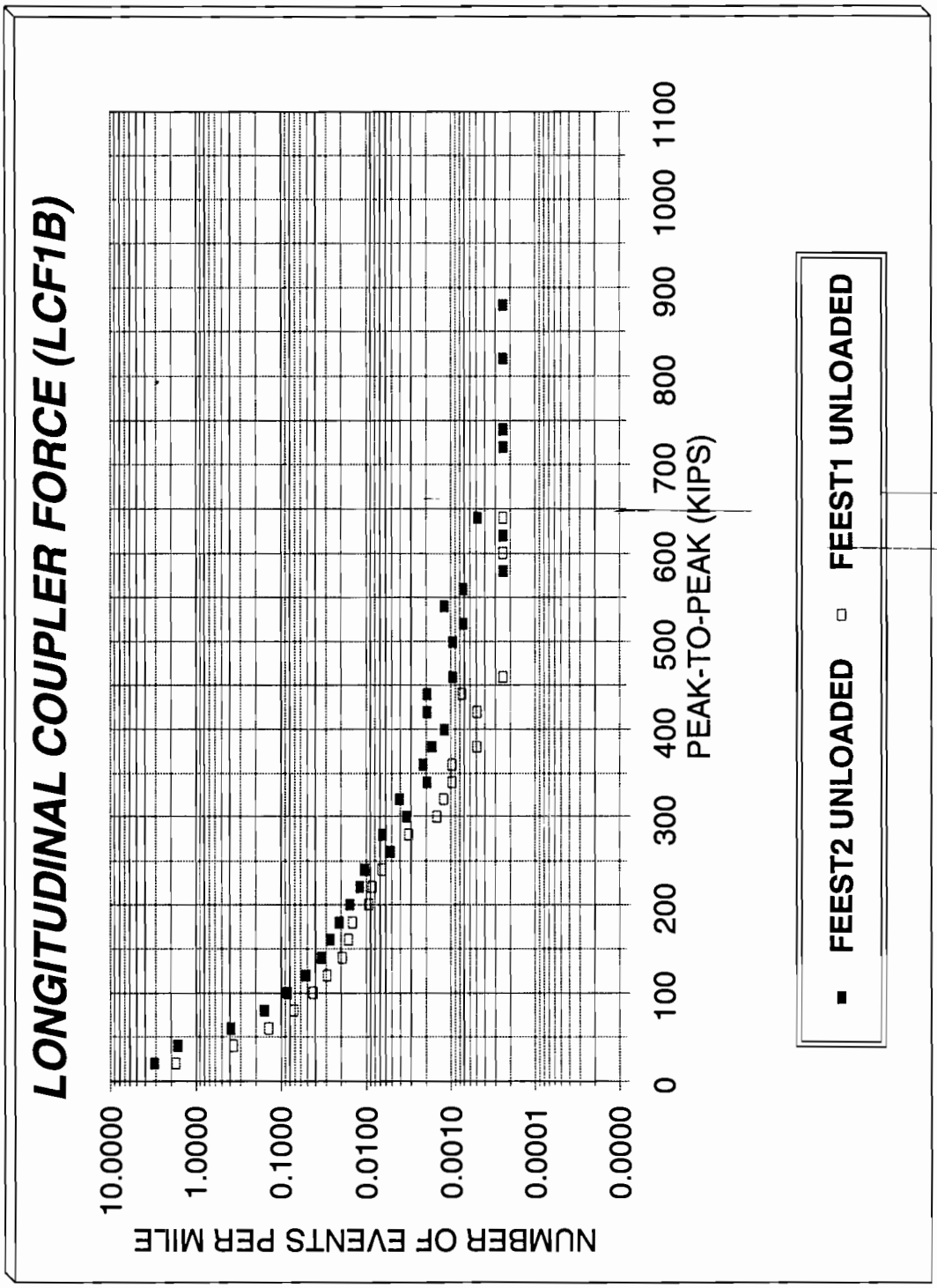

Figure 33. Unloaded LCF1B Histograms

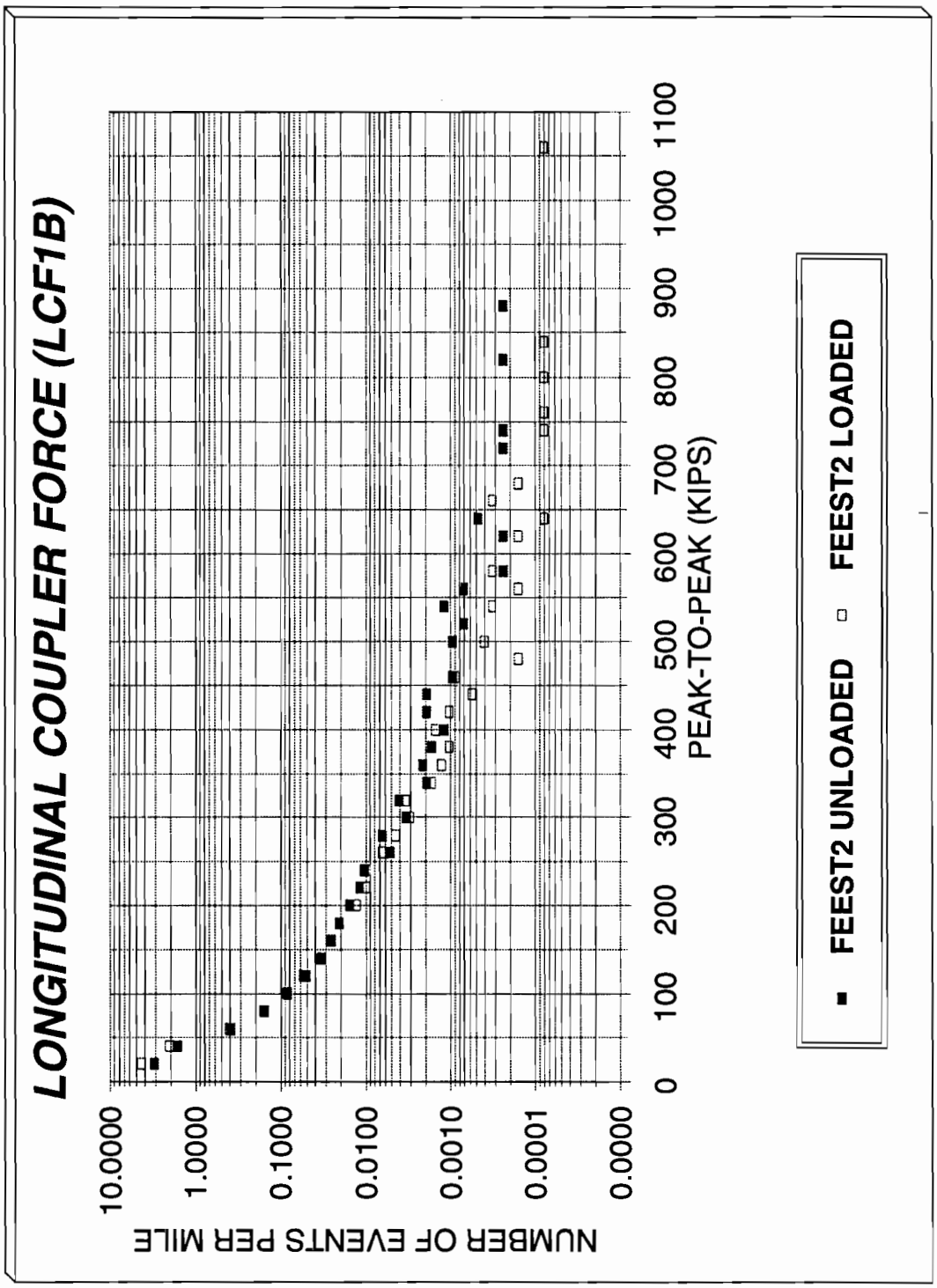

Figure 34. Loaded and Unloaded FEEST2 LCF1B Histograms

The possibility of the LCF instrumentation being the cause of the large reduction in the unloaded fatigue life was checked at the end of the unloaded test by performing a squeeze test. The results of the tests indicated that measurements LCF1B and LCF2B were accurate to within 1 percent of full scale. It showed that the LCF instrumentation was working properly and giving accurate estimates of the LCF during the unloaded OTR testing.

Consist speed may have an effect on loads, which may have caused the unloaded LCF data to be more severe. Since leg 11 data was collected entirely in the western portion of the test area, it was suggested that the unloaded LCF may have been biased to higher values due to the higher speeds typically traveled in the west. The speed distribution data obtained during the FEEST2 test is presented in Appendix E for each leg where data was available. The data shows the relative time spent at speeds as recorded by the time at level mode. Unfortunately the data for unloaded testing (leg 11) is not available due to a speed transducer failure. As shown in Appendix E, legs 9 and 10 spent more time at higher speeds. Routes for legs 9 and 10 were located entirely in the western portion of the test route which tends to support the theory that the unloaded car may have experienced a higher average speed.

The average value of each peak-valley range recorded by the rainflow algorithm for LCF1B during each leg was calculated for the loaded and unloaded configurations. Figure 35 presents the results for the loaded configuration and shows the average value distribution is bimodal with peaks at approximately 175 kips and 25 kips of tensile force. The average value of the unloaded data is shown in Figure 36 and consists of a unimodal distribution centered at approximately 35 kips tension load. By plotting the average distribution for each leg of the loaded data, it was found that the 175 kip tension force distribution peak as shown in Figure 35 was caused by the conditions that only existed on legs 9 and 10. The remaining loaded legs showed unimodal distributions with peaks in the 30 kips of tension region. These results show the large differences in LCF that can exist in any given leg which may in part be attributable to higher speed legs.

Consist location was also tracked during the OTR test. However, changes in consist makeup were found to occur very frequently within a leg, often without accurate consist location data being recorded. It is not possible to correlate the rainflow data with the changes in consist location since the rainflow mode ran continuously during the entire leg. This is because it is not possible to associate specific events in the rainflow data with any other variable such as time or location of the tank car. This point illustrates a limitation imposed by the use of an automatic remote data acquisition system to collect non-stationary data.

Many other random variables also exist which would affect the resulting LCF developed such as handling quality and track condition. Figure 37 shows the leg to leg variation ~~that was~~ experienced during the loaded portion of the testing and demonstrates the variability that can exist. As shown in Figure 37, large differences in occurrence rates are apparent even in the longer length legs such as legs 8, 9 and 10. Since the unloaded LCF loads were influenced by many of the same random variables that are evident in the loaded data, the unloaded data variability can be expected to be similar to the loaded data. Two different statistical procedures were used to test if the LCF environment obtained for the unloaded car was within the expected random variation. These analysis concluded that "the occurrence rates for the loaded and unloaded tank car are statistically the same and that the observed differences can be explained by the random variation. Both the loaded and unloaded tank car have, from a statistical viewpoint, the same occurrence rates." (Excerpt from April 19, 1995, letter from Dan D. Steeples to C.P.L. Barkan, Environmental & Hazardous Materials Research Division, AAR, Washington.) Appendix B lists the unloaded LCF1B data.)

The correlation between the histograms obtained for the various VCF measurement techniques used during the FEEST2 loaded testing is shown in Figure 38. Figure 38 shows the number of events per mile obtained during the loaded portion of the FEEST2 test for the measurements VCFA, VCFB, SCTA, SCTB, and VCFS. As shown, good correlation between like measurements (such as SCTA and SCTB) was obtained during the FEEST2 testing. The correlation between the separate measurement techniques shows significant

differences as explained in Section 3.8. As previously explained, measurements VCFA and VCFB represent the equivalent force applied at the striker carrier required to produce the same shear forces that would be produced by the corresponding coupler load. Figure 39 compares the measurements VCFA and VCFB, corrected to the equivalent coupler force using Equation 3 to VCFS. As shown, the correlation between the two methods produces similar results with the differences attributed to the variation in load paths.

Figure 40 shows the histograms obtained from the loaded FEEST2 testing for the vertical bolster load measurements BOLA and BOLB along with the FEEST1 data. As shown, the FEEST2 bolster loads for the A- and B-end were very similar with each other but were different than the FEEST1 data below 100 kips peak-to-peak. Figure 41 shows the histograms obtained for the unloaded FEEST2 data along with the FEEST1 data. Note that the data for the measurement BOLA FEEST2 unloaded data is not shown due the transducer failure that occurred during leg 11.

Figure 42 shows the cumulative histogram obtained from the FEEST2 loaded testing for the sill bending gage on the A-end (VCBA). Due to a transducer failure, the unloaded data was not available. Figure 43 shows the results of converting the microstrain data to equivalent sill force using the conversion factor in Section 3.6.4 along with VCFA for comparison. This comparison shows the relative increase in bending strains introduced by LCF events as VCBA was shown to be sensitive to LCF. This result indicates that the bending strains induced into the sill are not totally dominated by VCF as LCF also has an influence. The difference between the sill equivalent force derived from VCBA and VCFA is the result of the sensitivity of VCBA to LCF.

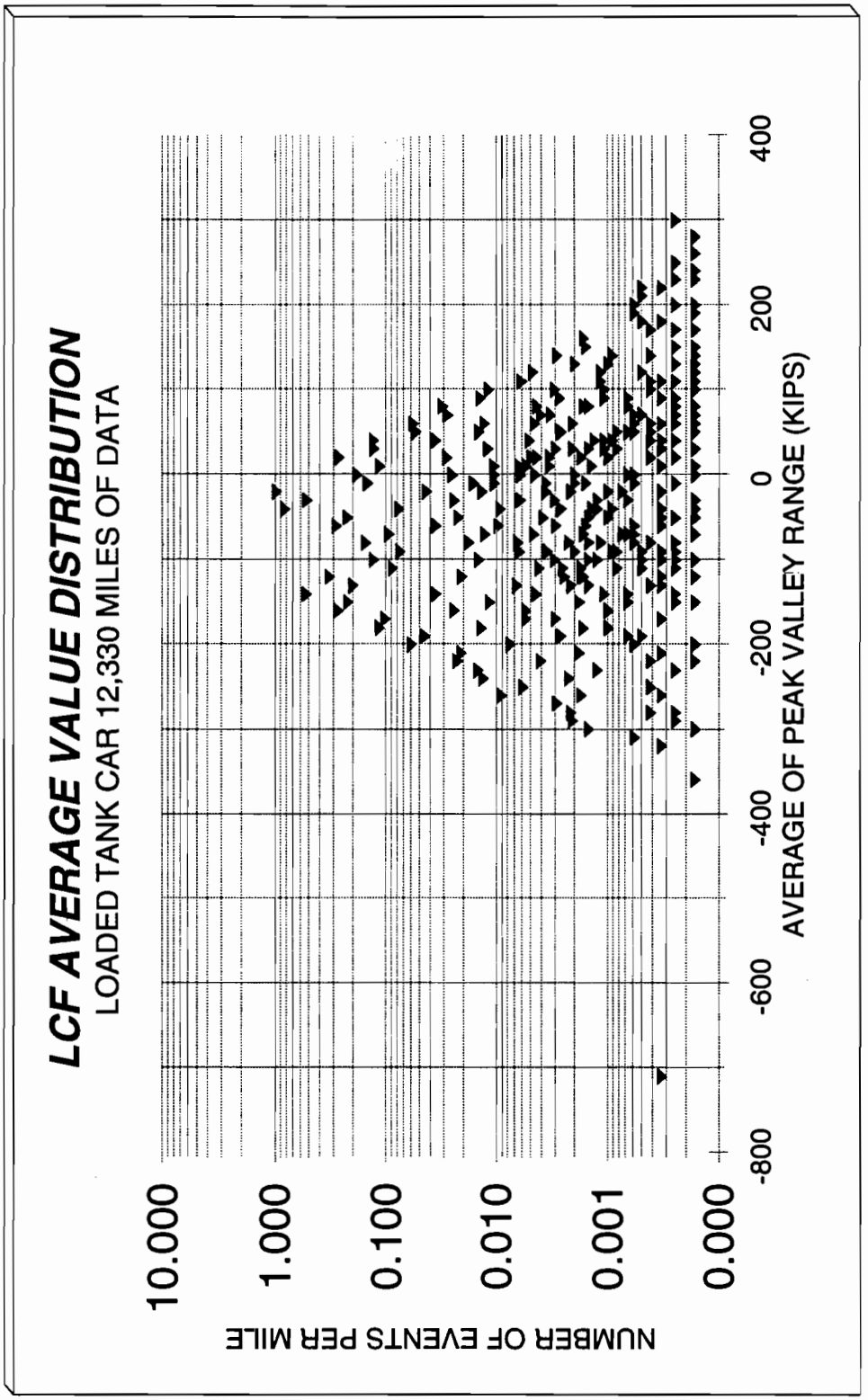

Figure 35. LCF Average Values for the Loaded Configuration

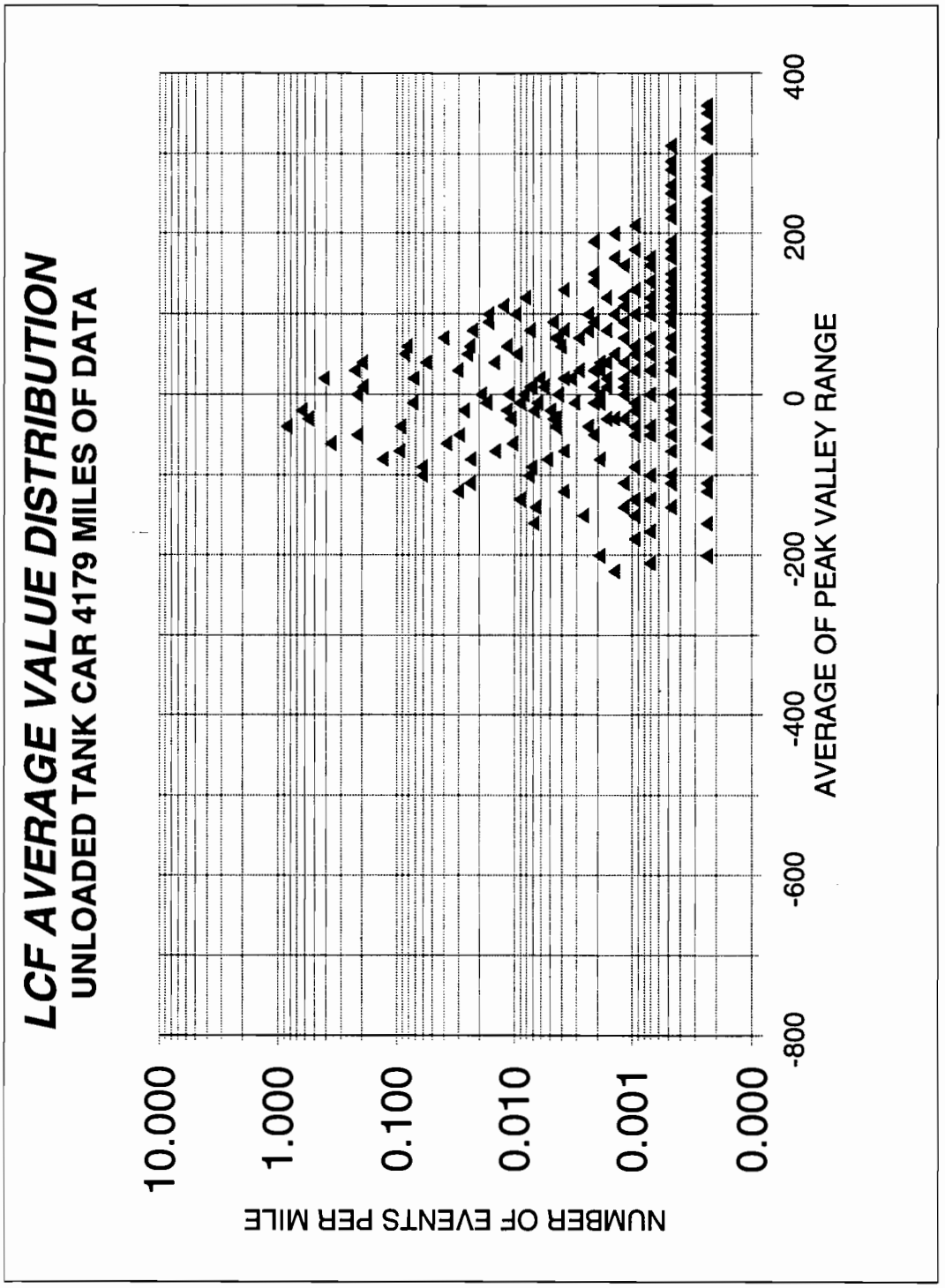

Figure 36. LCF Average Values for the Unloaded Configuration

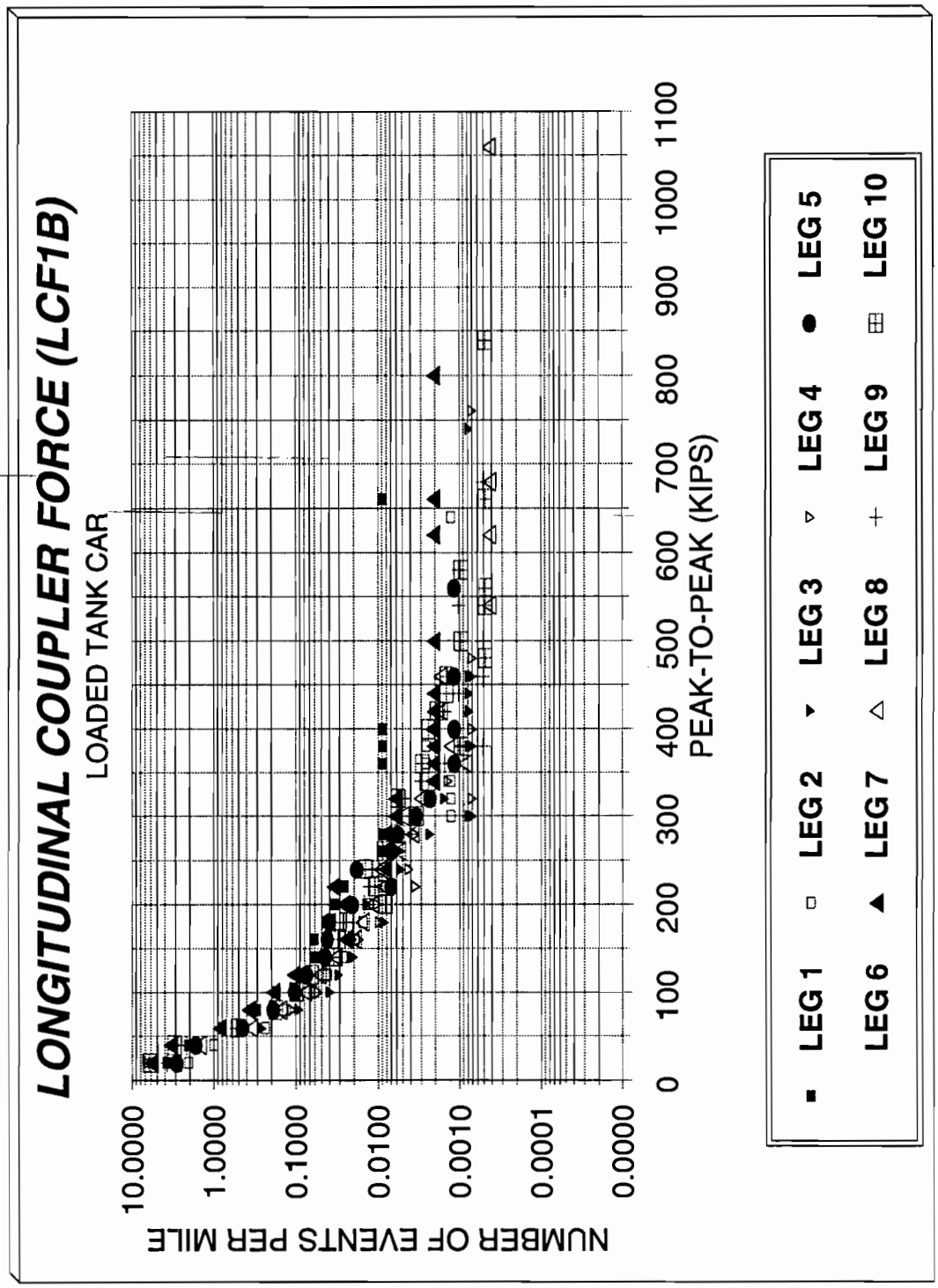

Figure 37. LCF Leg to Leg Values for the Loaded Configuration

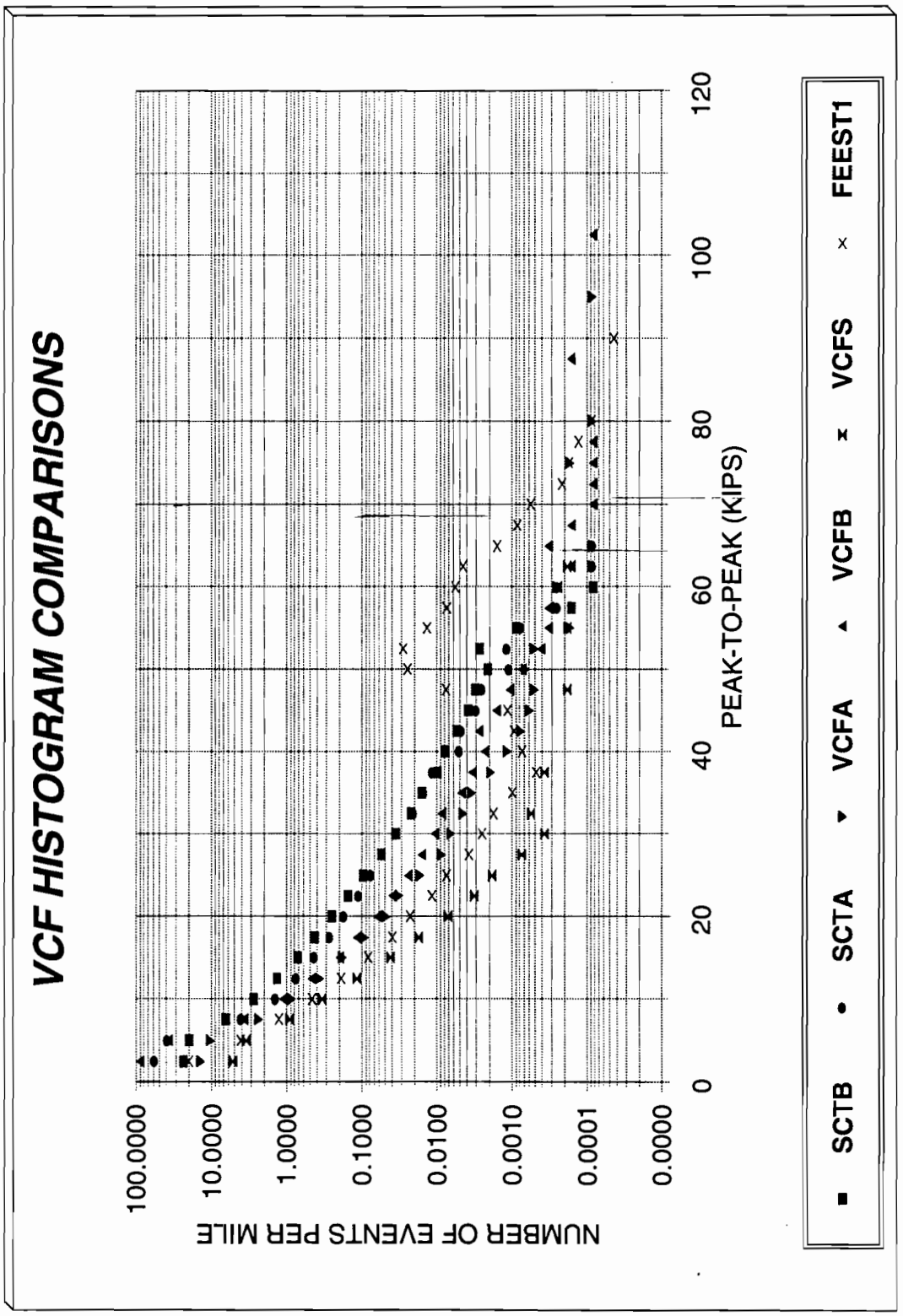

Figure 38. VCF Histogram Comparisons

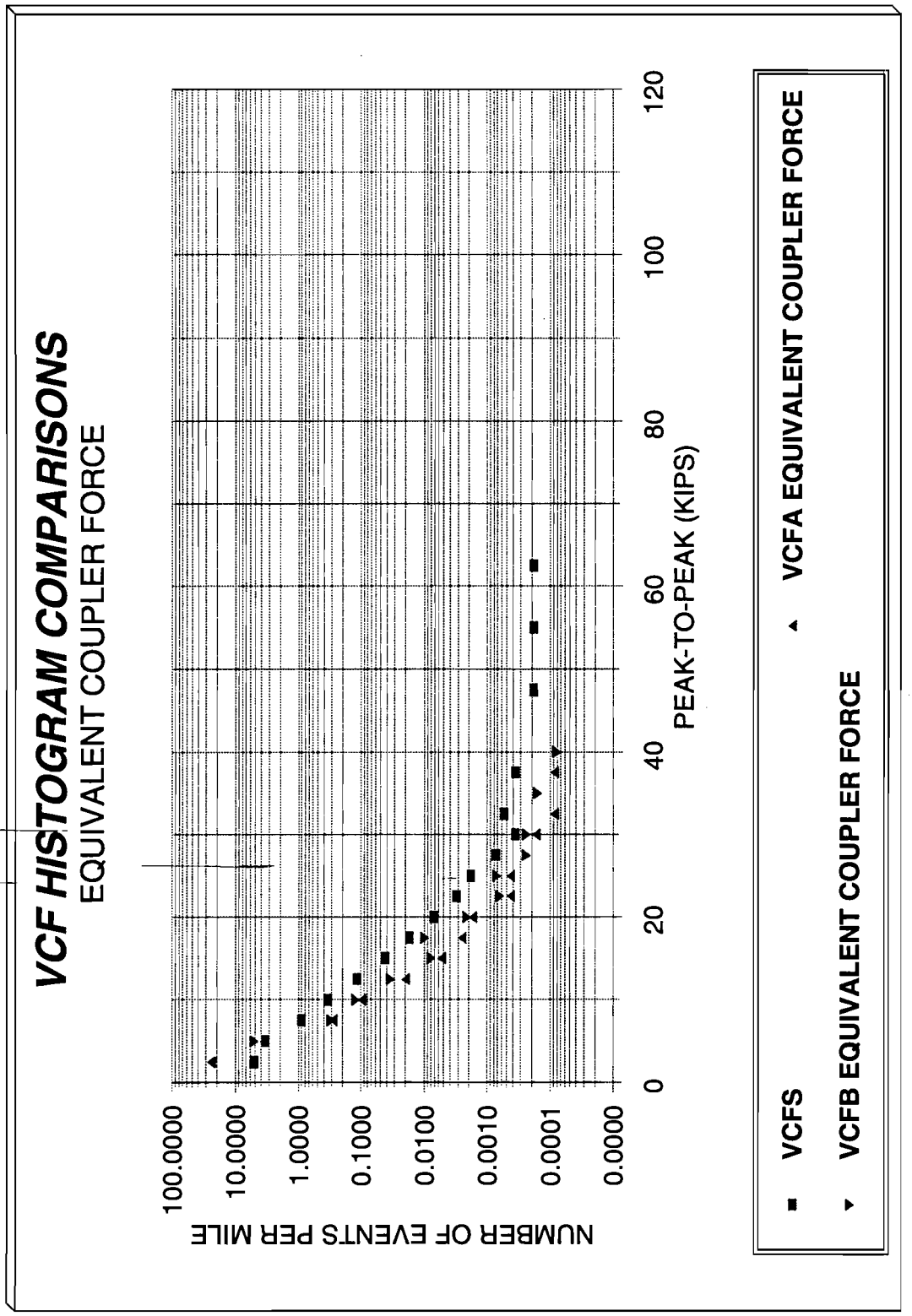

Figure 39. VCFA and VCFB Equivalent Coupler Force Comparisons

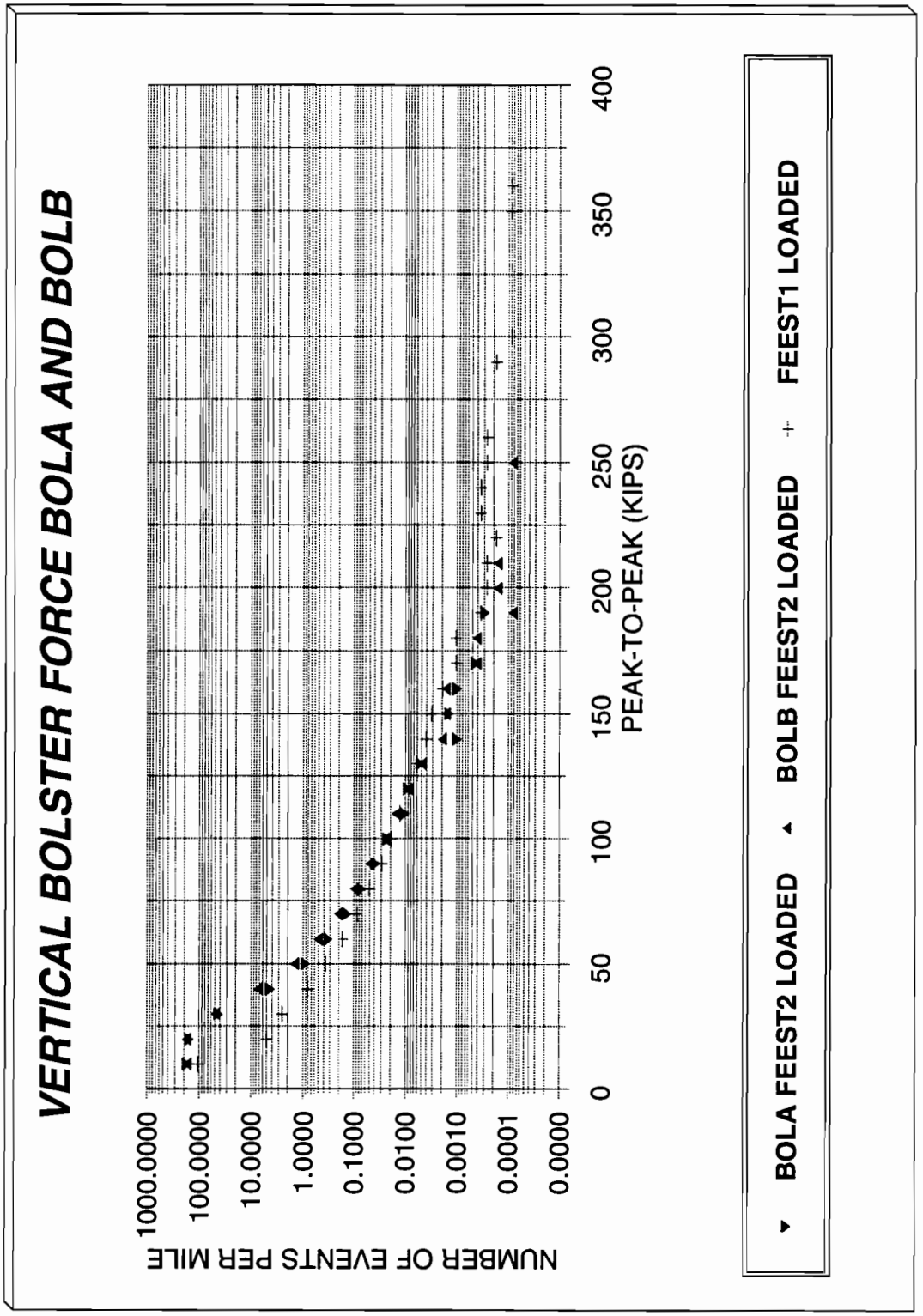

Figure 40. Loaded Vertical Bolster Loads Histogram Comparisons

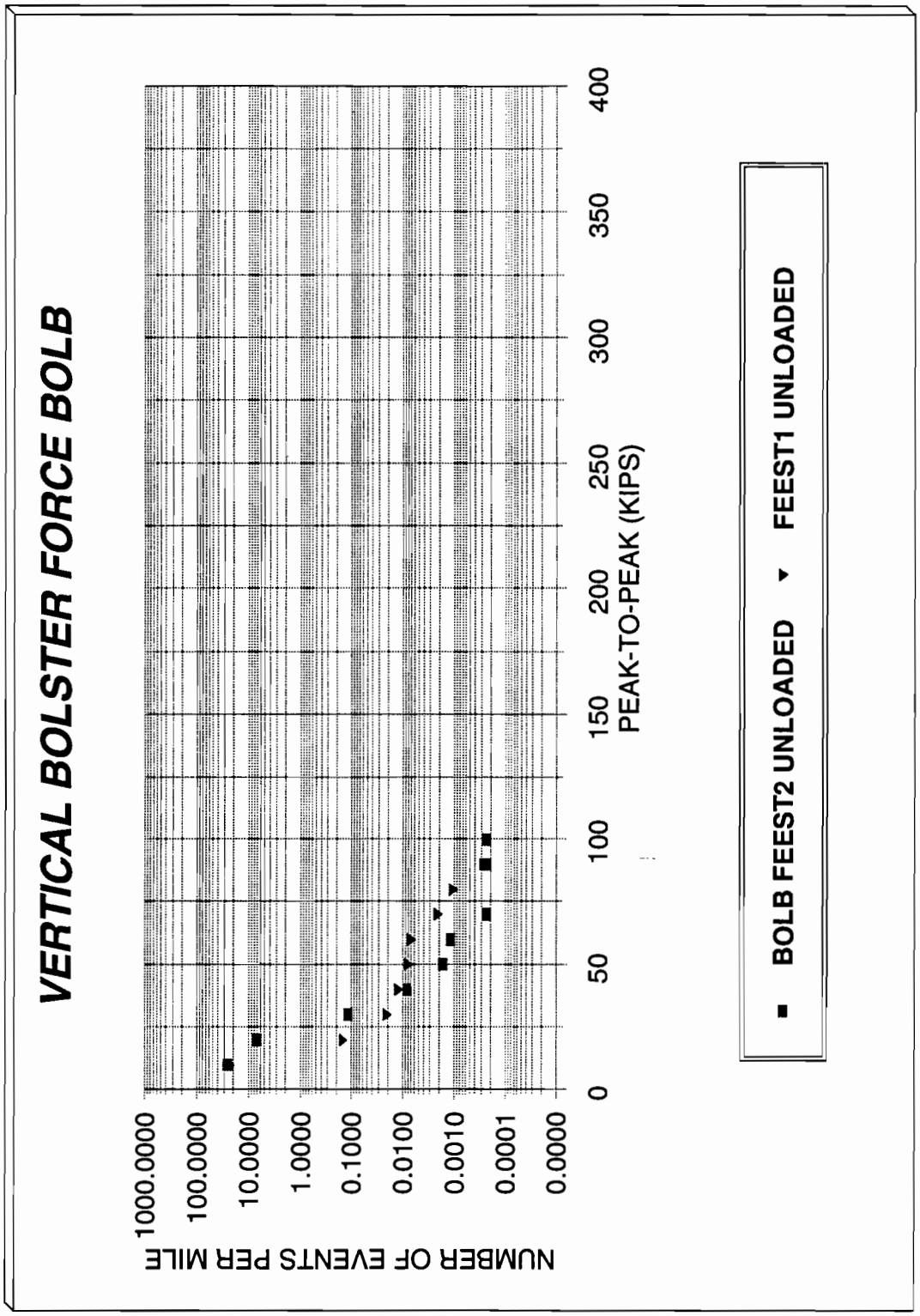

Figure 41. Unloaded Vertical Bolster Loads Histogram Comparisons

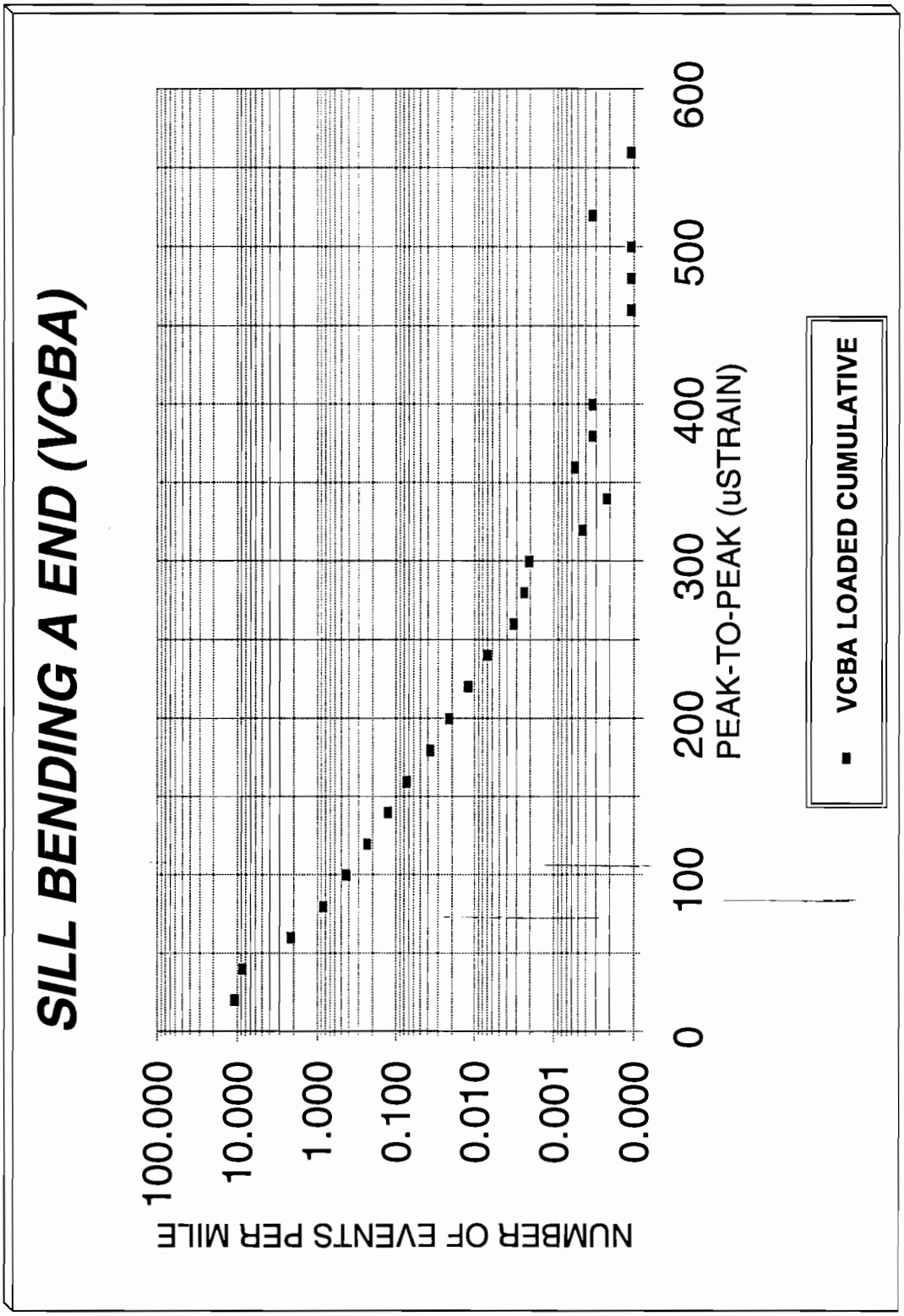

Figure 42. Loaded Sill Bending VCBA Histogram

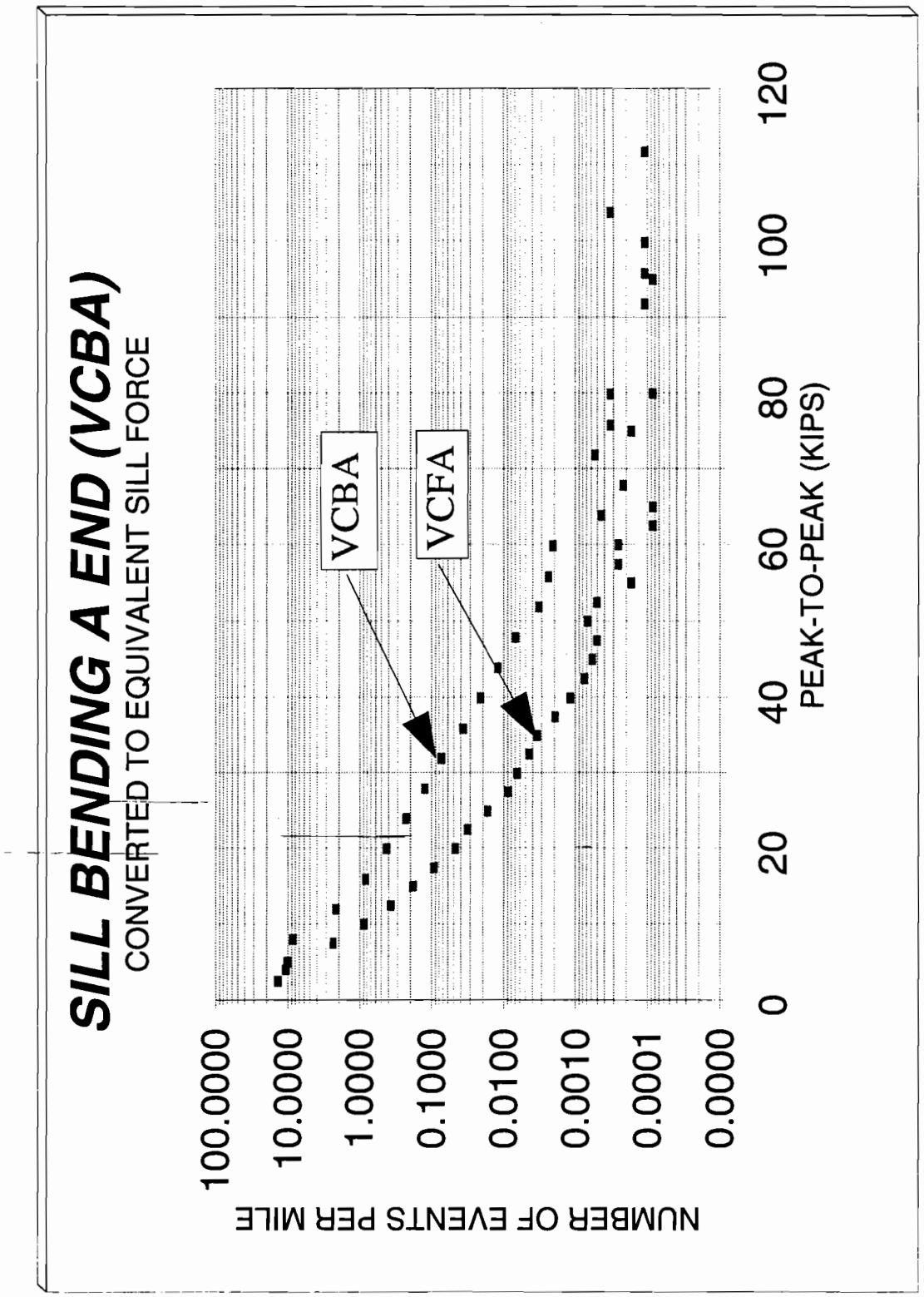

Figure 43. VCBA Equivalent Sill Force Histogram

The histogram format shown in Figures 29-43 only shows the peak-to-peak range of the data and as such does not show the actual peak/valley values and the corresponding average value of the dynamic events recorded. Obviously, the stress distribution at any location is influenced by average values upon which dynamic events are superimposed and must be accounted for in any analysis. The formats of Figures 35 and 36 present these average values but do not show the dynamic range of the data.

By presenting all of the data on one plot, additional insight into the dynamic force environment can be gained. Figures 44 and 45 show all of the LCF rainflow data for the loaded and unloaded configurations as collected on the same plot with the peak/valley range represented by the solid vertical lines and the corresponding number of count values associated with that range represented by the triangle symbols. The peak/valley ranges (in kips) are read on the left-hand axis and the number of events are read on the right-hand axis. Average values of each range are at the midpoint of each vertical peak/valley line. Each vertical peak-valley range line in these plots has a triangle associated with it indicating the number of events that occurred within that range. The triangular grouping of the individual ranges was done in anticipation of using the data to develop time history data that could be used to perform full scale fatigue testing. Each triangular grouping of the individual peak/valley ranges can be reduced to an equivalent peak/valley combination with values based on the average values within each region. This approach greatly reduces that amount of time required to develop force functions for fatigue testing as the number of individual ranges is greatly reduced. Figure 44 shows the bimodal response with the average values as previously discussed. Figures 44 and 45 show that the dynamic environment in draft conditions accounts for the vast majority of the total number events recorded for the loaded and unloaded configurations. It also can be seen that the largest peak/valley ranges occur during buff conditions.

Figure 46 presents the VCF peak-to-peak/number of occurrences data in the same format as Figures 44 and 45. Figure 46 shows the data for the measurement VCFA which indicates an average peak/valley value of VCF of approximately 0 kips. The extreme dynamic range events, shown by the longest vertical peak/valley range lines at the right

of the graph, are characterized by a positive (upward) average value. These conditions were found to exist during impact conditions.

Similarly, Figures 47 and 48 display results for measurement VCFB for the loaded and unloaded configurations.

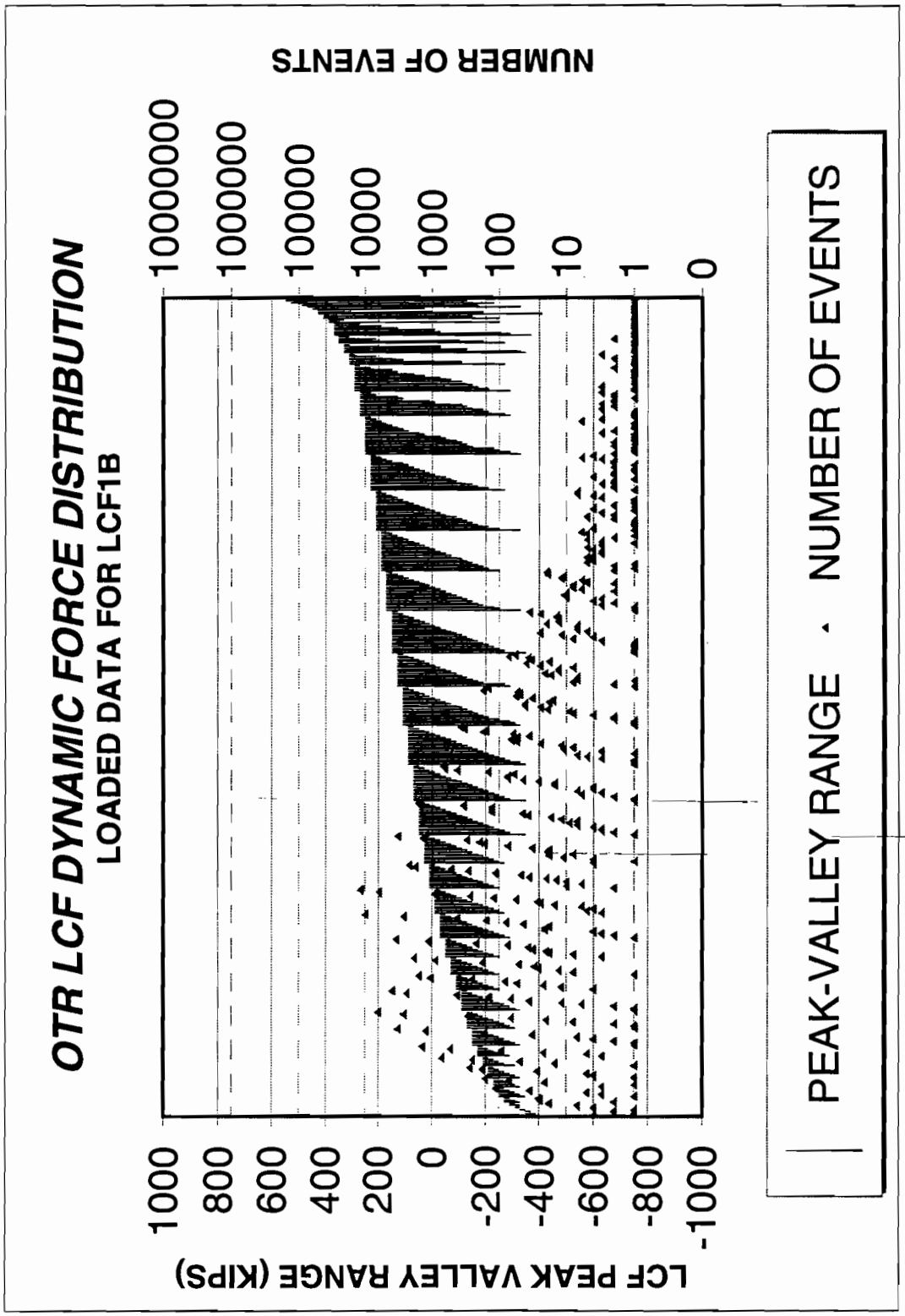

Figure 44. Loaded LCF Distribution

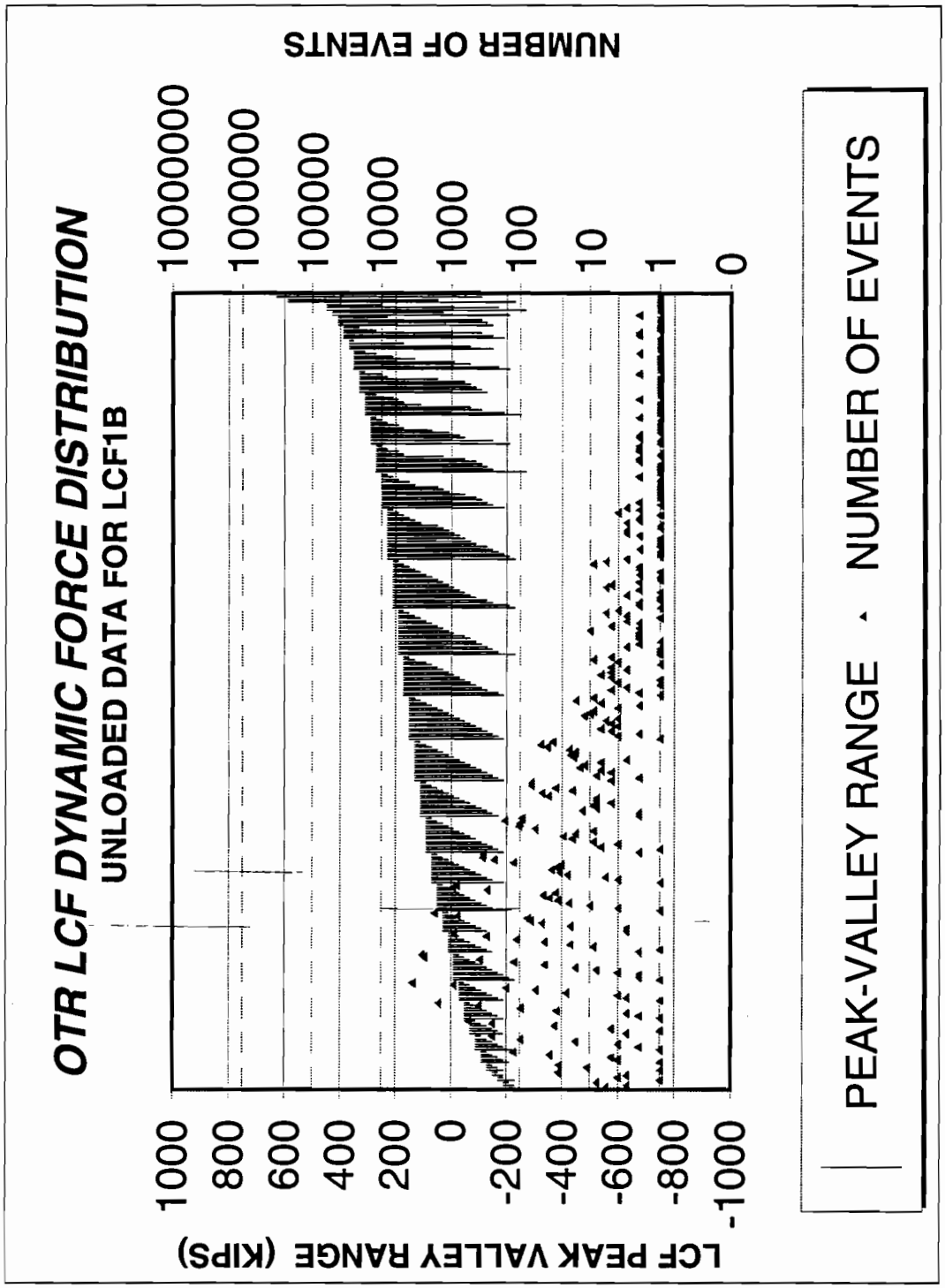

Figure 45. Unloaded LCF Distribution

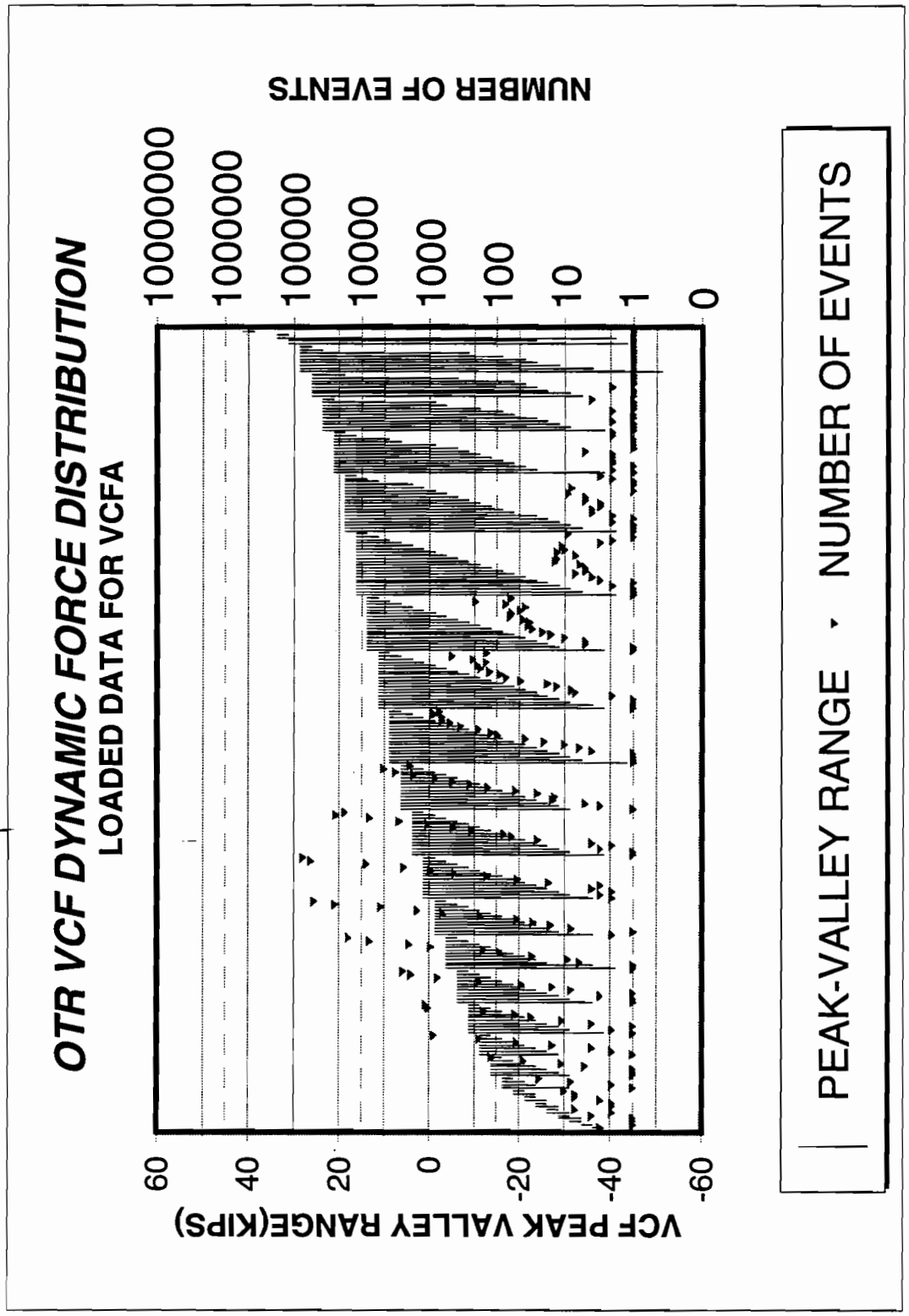

Figure 46. Loaded VCF Distribution (VCFA)

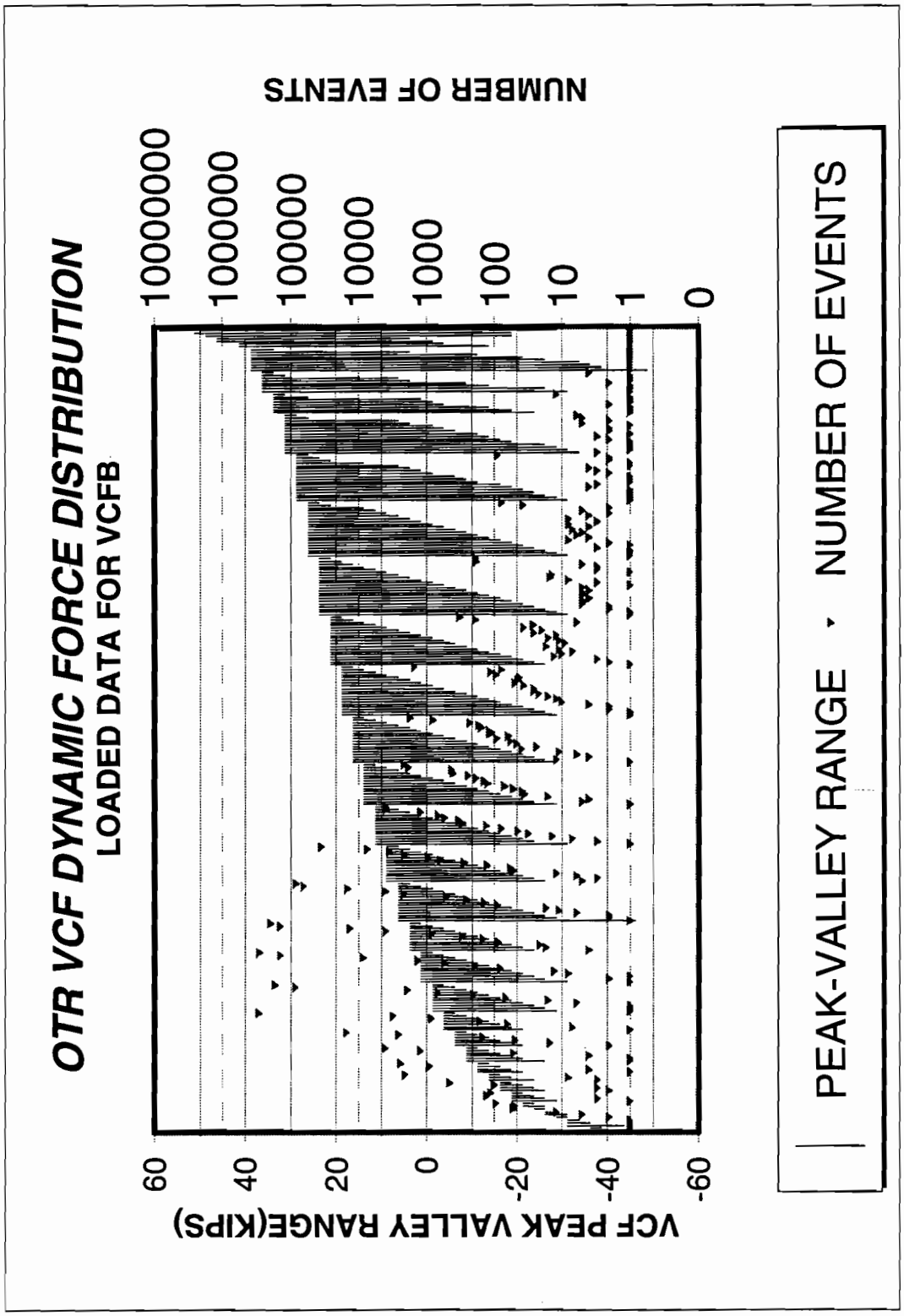

Figure 47. Loaded VCF Distribution (VCFB)

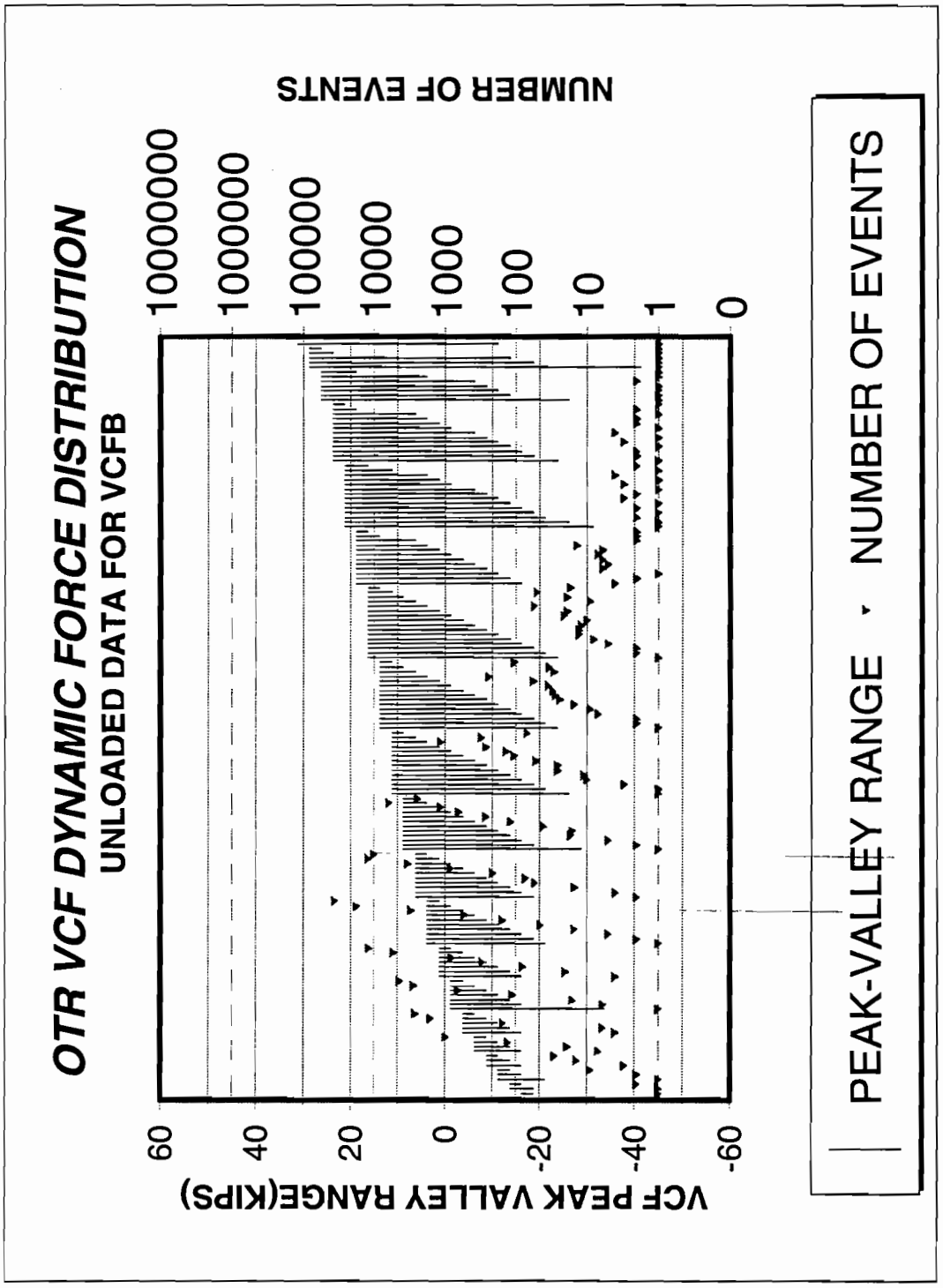

Figure 48. Unloaded VCF Distribution (VCFB)

4.3 FEEST2 TEST BURST HISTORY DATA

This section presents representative burst history data of significant events taken from the FEEST2 data. To convey the general characteristics of the data, all of the data collected (for the measurements VCFB, BOLB, LCF1B and SPEED) during leg 9 is shown in Appendix F.

The format of Figure 49 will be used to illustrate burst history data in this report. The basic layout and meaning of this format is now reviewed. The column of numbers on the left side of the plot indicates the minimum and maximum engineering unit values associated with the scale immediately to the right. The minimum engineering unit value is at the bottom of the scale and the maximum engineering unit value is at the top of the scale. The range between the minimum and maximum values is divided into equal portions. The ***X Range: 0 to 5*** notation at the bottom of the figure is the burst history time (in seconds). This particular burst history was 5 seconds in duration and was the first burst taken as noted by the 0 to 5 X Range. Subsequent bursts will have an elapsed time range with increments of 5 seconds (or 2 seconds as appropriate) which is the window length selected for this measurement. The time range is divided into equal increments of time by the vertical tick marks. The measurement name is shown of the right side of each time history. The measurement names VCFB, BOLB ~~LCF1B and~~ SPEED identify the data shown (see Section 3.6). The leg from which the data was taken along with additional descriptive information is shown at the top of the plots.

Figure 49 shows the first 5-second burst of data which was taken on leg 9 which was an impact event as evidenced by the SPEED measurement and the characteristic longitudinal coupler force signature. The VCF measurement VCFB, and the bolster measurement BOLB both show vertical response characteristics caused by the impact. The bolster response shown is highly damped with a frequency of approximately 4.5 cycles per second (Hz) for the primary mode with a low damped secondary mode at approximately 8-10 Hz. The 8-10 Hz mode is highly attenuated in the measurement VCFB. LCF1B shows multiple peaks that represent the dynamic longitudinal elastic response of the coupler and

tank car at 10 cycles per second. The SPEED parameter shows a near vertical velocity change resulting from slack in the speed transducer. as explained in Section 3.6.1.

The second event captured on leg 9 is shown in Figure 50. This event, characterized by a low frequency VCF with little corresponding longitudinal coupler force, comprised the vast majority of VCF events recorded during the FEEST2 test. For leg 9, approximately 90 percent of the recorded events were of this type. Similar occurrence rates and wave forms existed on the other legs. Some noise is present on the SPEED channel as previously discussed. Figure 51 shows a similar low frequency coupler event taken from leg 10, which produced a large single event VCF of approximately 55 kips. The SPEED measurement shows little change and only a small variation in LCF is shown. The event shows the existence of large VCF events that are not associated with impact conditions or with corresponding LCF dynamics. Figure 52 shows a similar event with the notable difference being the frequency of the event is higher corresponding with the higher speed when the event occurred. Again, these events occur with little or no change in the LCF. From these events, wavelengths based on the respective speed and duration of the event can be calculated as shown below.

Figure	Event Duration (seconds)	Event Speed (mph)	Event Wave Length (feet)
50	.75	13	14.3
51	1.5	8.8	20.0
52	.25	43	15.7

The three events produce wave lengths which are similar and are approximately equal to the spacing between wheel sets on adjacent cars. Based on this result, the hypothesis of relative vertical movement between the couplers on adjacent cars due to changes in the vertical stiffness of the track (such as at crossings) and differential car suspension stiffness is suggested as a source for the low frequency VCF events. Such differences would allow for relative coupler motion to be developed between adjacent cars. If the loads induced by

these events could be reduced or eliminated, which could be accomplished by increasing the vertical compliance of the coupler, the resulting fatigue life would improve.

We recommend that testing of this hypothesis be conducted to determine the exact cause of the low frequency VCF events, and if increased vertical compliance of the coupler reduces these types of loads.

Figure 53 illustrates another VCF event which is characterized by a sudden reduction in the VCF. This demonstrates the ability of the couplers to sustain high VCFs at relatively low LCF. The bolster load burst histories also show the rapid release of VCF. This type of locking of couplers was relatively common in the data and will be referred to as "sticktion." It is difficult to explain how these large VCF events can be developed with such low corresponding LCF values. The actual mechanics of sticktion are unknown at this point. If the sticktion phenomenon could be reduced, fatigue life would improve and VCF events like those shown in Figure 53 would be eliminated.

Figure 54 presents the highest magnitude VCF event captured during the FEEST2 testing. The sticktion phenomenon tended to be the most severe at very low speeds. There was no jitter to cause redistribution of the forces. Again, calculating the wavelength of the event shown in Figure 54 gives approximately 18.5 feet, similar to the spacing between trucks on adjacent cars.

Figure 55 continues the representative data taken from leg 9 and shows another VCF very similar to the events previously shown.

Figure 56 shows a "smooth" coupling event as evidenced by the LCF1B force signature and the SPEED parameter which occurred during leg 7. The VCF and LCF both peak at approximately the same time as opposed to the sticktion event, where significant LCF did not co-exist. Peak VCF and LCF loads can occur at the same time as based on this event.

Because of this, we recommend that a static design loading case consisting of the **simultaneous** application of LCF and VCF be adopted for the design and analysis of stub sill tank cars. The actual values used for this analysis should be based primarily on impact data presented later in this report. This conclusion raises the question as to how many of the VCF and LCF events recorded and shown in the histograms occur simultaneously. Obviously, the simultaneous occurrence scenario will produce much higher stress values in the critical region. Data indicated that the simultaneous occurrence of LCF and VCF almost always was associated with impact type events. The low frequency VCF events were found not to have corresponding LCF values associated with them as previously shown. Based on these conclusions, we recommend that the simultaneous application of LCF and VCF values only be associated with impact events.

The remainder of the leg 9 data was composed of the type of events presented in Figures 49 through 56 with minor variations in response characteristics. The low frequency VCF events comprised the majority of the VCF loads imposed during leg 9 typical of all the data collected. Appendix F shows all of the burst time history data collected during leg 9. Keep in mind, when reviewing the data shown in Appendix F, that the data between the vertical lines represent a single 5-second burst of data and that the data immediately before and following **may or may not be continuous in time**. The data must be viewed as a collection of independent 5-second-long events strung together.

One of the limitations of using an unattended instrumentation system is shown in Appendix F during time from 200 to 400 seconds where there was a static offset in the VCF of sufficient value to cause constant triggering of the measurement VCFB for an extended period. This results in filling the allocated memory with relatively uneventful data. Not all events evident in the histograms have a corresponding burst history as the event may have occurred after the memory space was full. It was very difficult to select a trigger that would capture significant events and not be affected by the static values that exist in the

VCF due to the low frequency high magnitude events. Static VCF values of this magnitude and higher were very common on all of the legs.

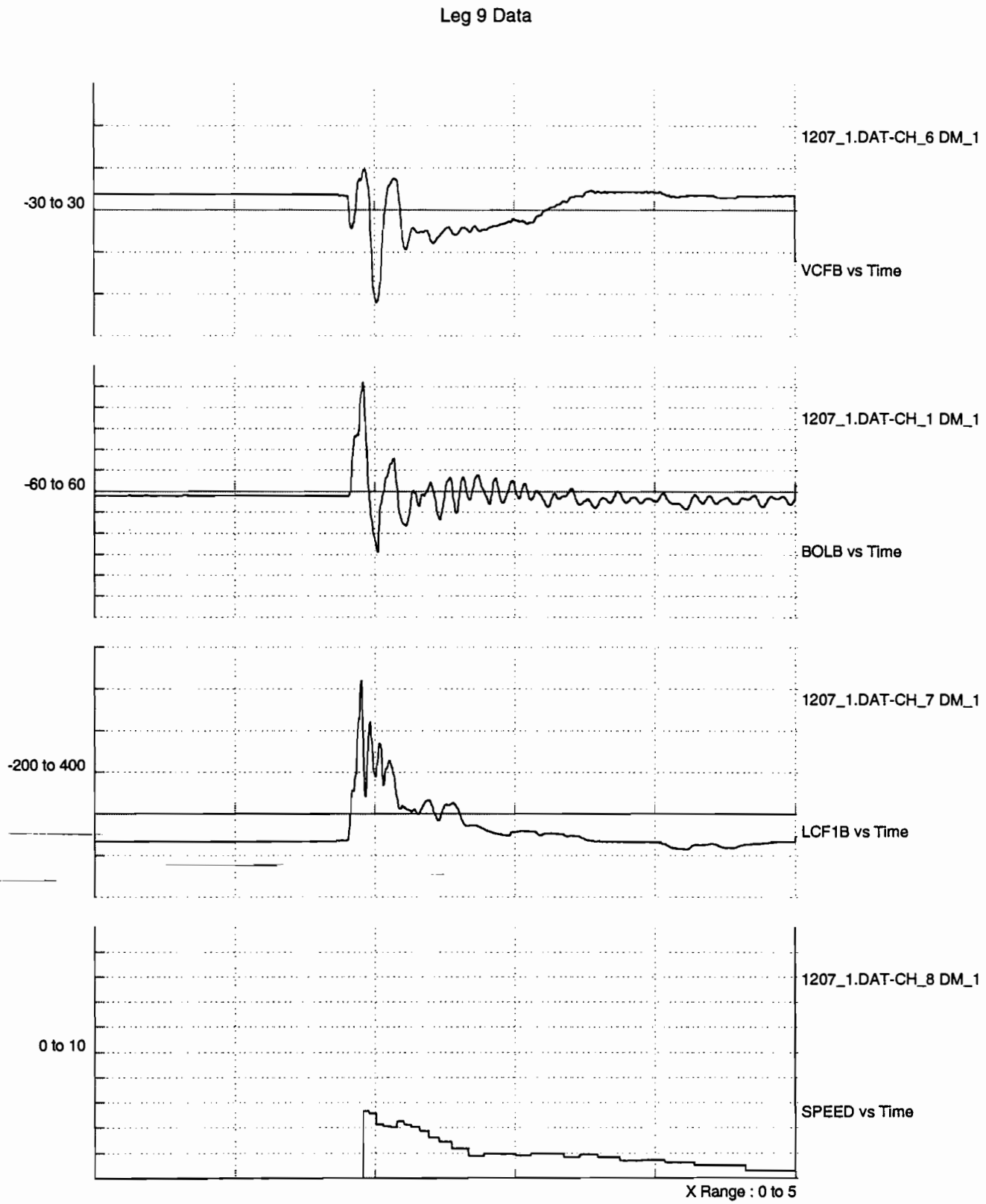

Figure 49. Leg 9 Typical Coupling Event

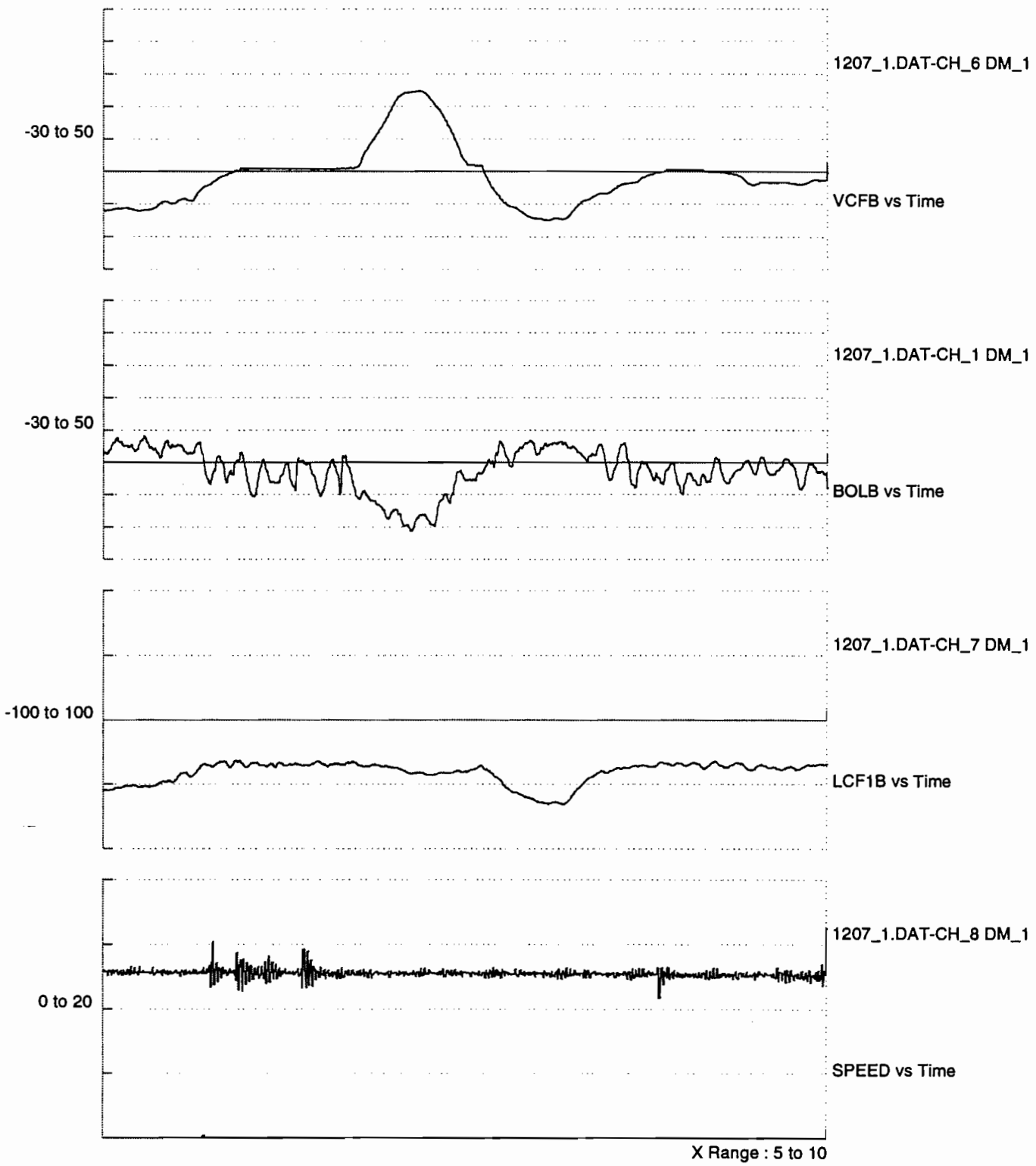

Figure 50. Leg 9 Typical Low Frequency VCF Event

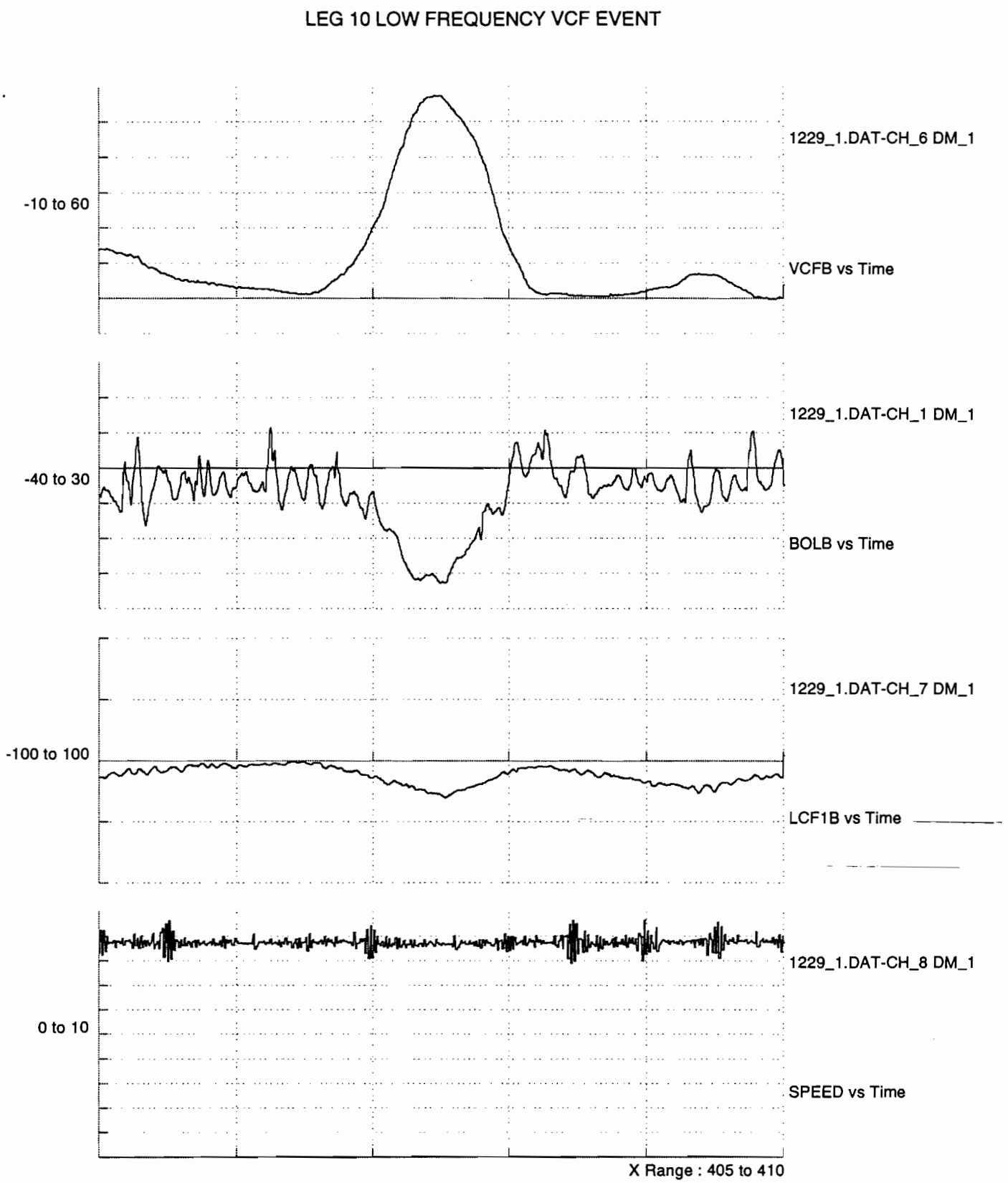

Figure 51. Low Frequency High Magnitude VCF Event

LEG 10 LOW FREQUENCY VCF EVENT

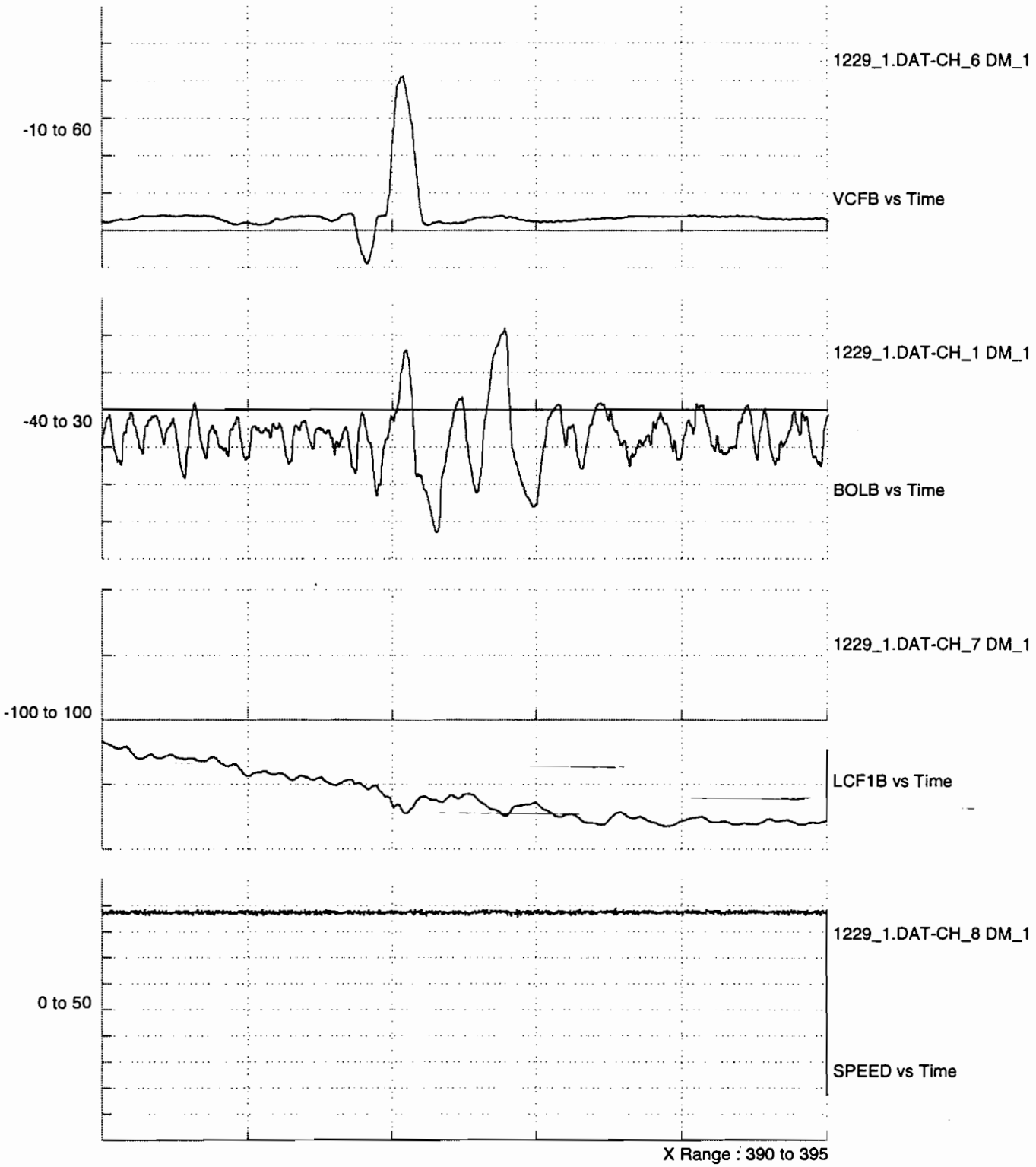

Figure 52. Low Frequency High Speed VCF Event

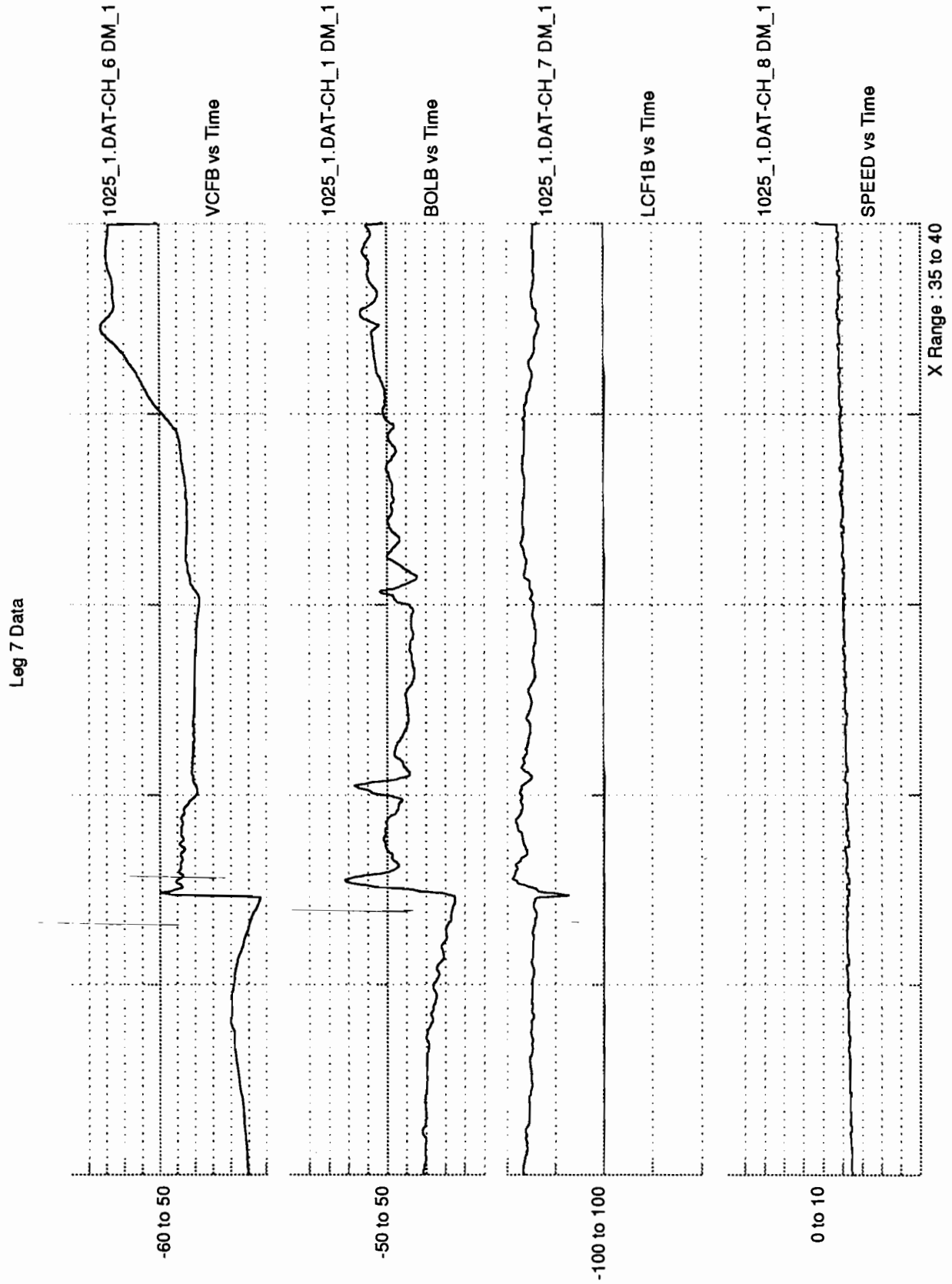

Figure 53. VCF Sticktion Event

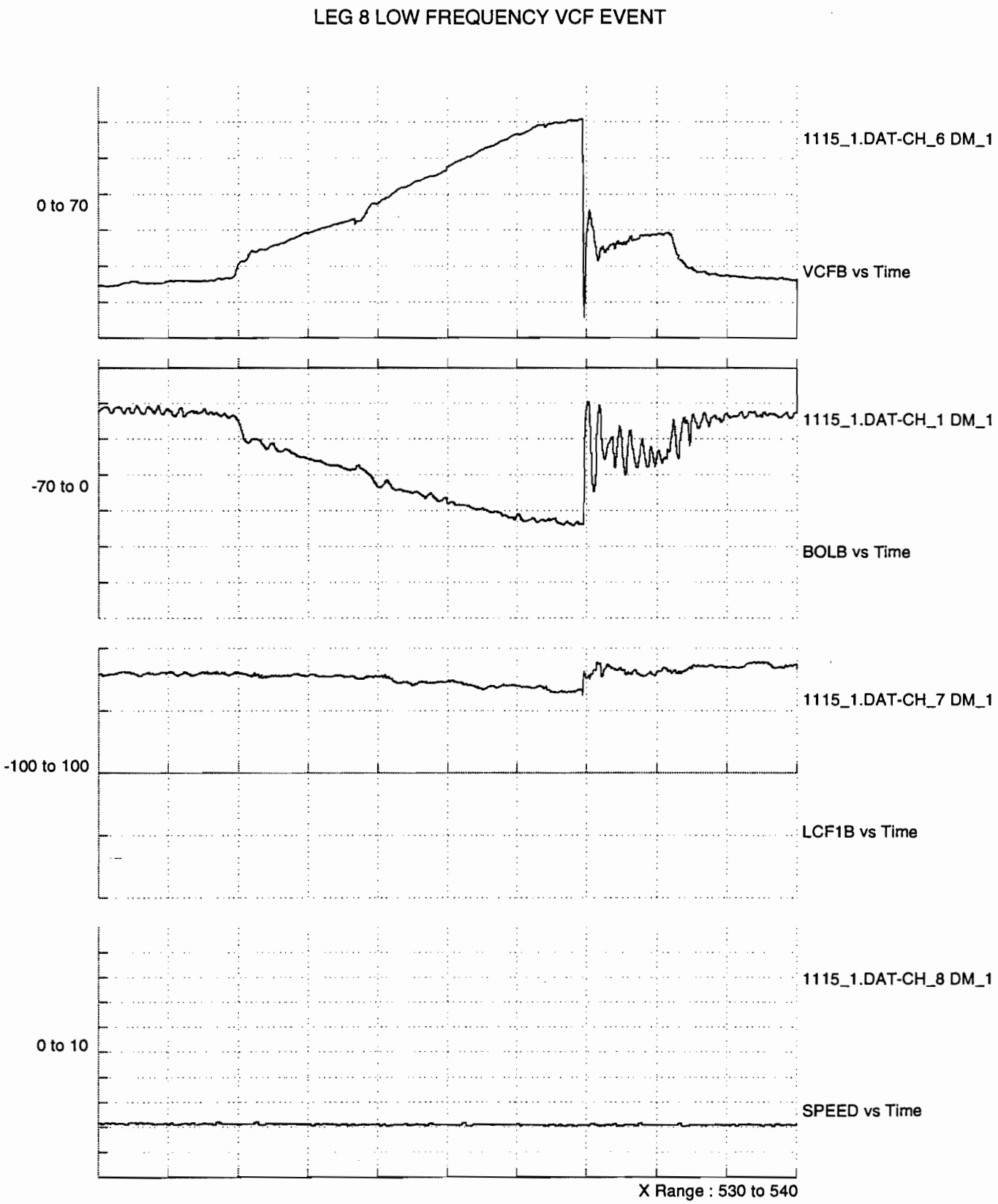

Figure 54. Largest VCF Event Recorded

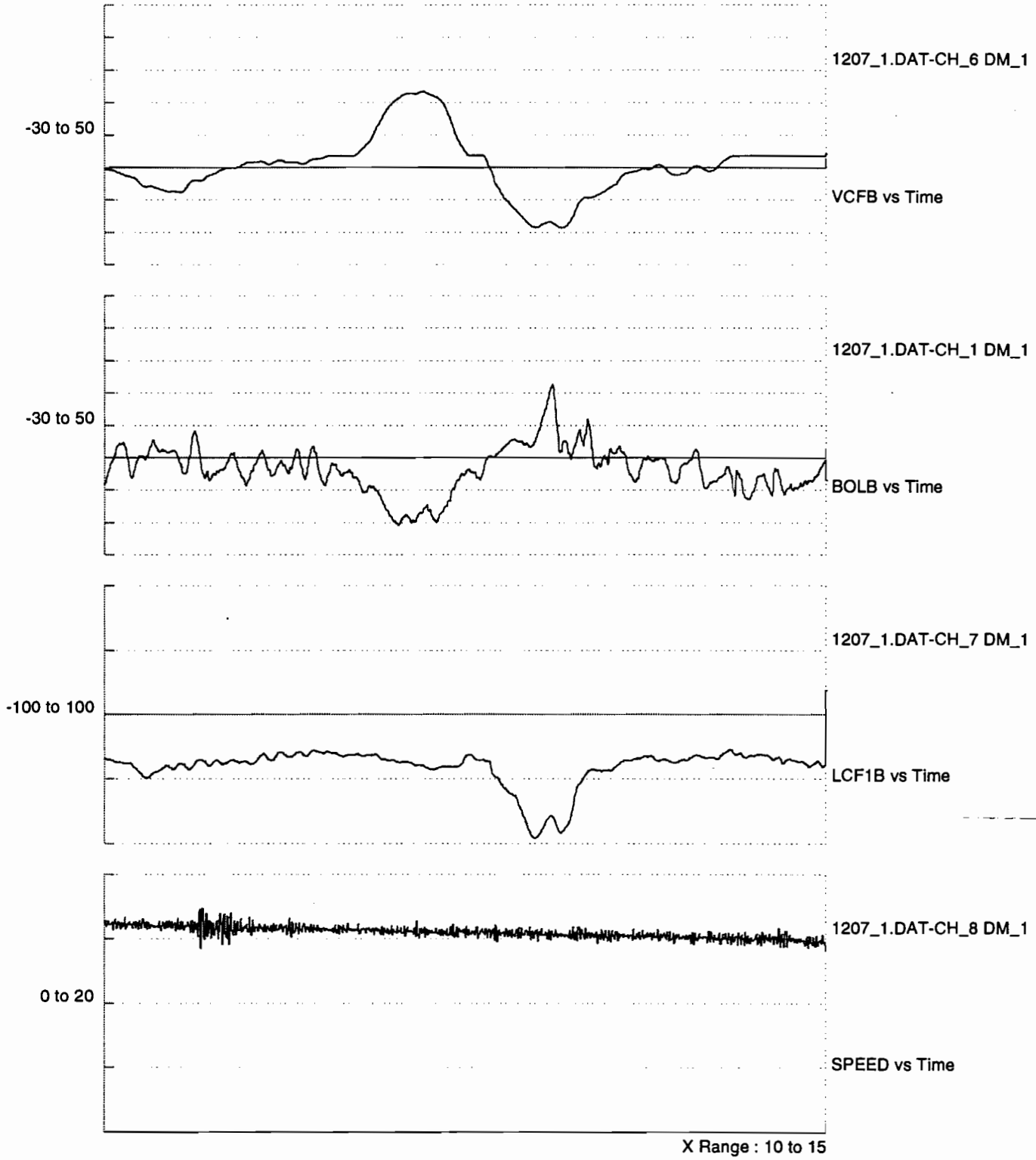

Figure 55. Leg 9 Typical Low Frequency VCF Event

Figure 56. Leg 9 Typical "Smooth" Coupling Event

4.4 FEEST2 CONSIST LOCATION

The location of the test car in the consist was tracked during the FEEST2 testing to determine if consist location influenced the coupler loads environment. Table 19 shows the consist information collected and uses the notation "NA" for legs where the location was not available or was known to have changed during the leg. Many times during the FEEST2 test the actual location of the car listed in the destination consist list was different than that listed at the beginning of the leg. When this occurred, consist data was not considered useful as changes to the consist makeup may have occurred during the leg.

The test car consist location is given as the car count from the last engine. Several of the legs were comprised of different consists as noted by the designations such as leg 2A and 2B.

From this data, no definite trends in the VCF or LCF load environments could be found due to the complexity of time correlation with the rainflow data.

Table 19. FEEST2 Test Consist Information

Leg	Consist Location	Consist Length	Leading Car Tons	Trailing Car Tons
1	47	50	30	110
2A	36	40	30	NA
2B	13	60	74	51
3A	20	21	53	115
3B	50	108	95	130
4A	53	98	NA	135
4B	24	127	35	121
5A	58	90	NA	NA
5B	63	103	NA	NA
5C	101	107	NA	NA
5D	92	106	NA	NA
5	130	131	NA	NA
6A	7	92	NA	NA
6B	14	74	NA	NA
7	NA	NA	NA	NA
8A	73	84	NA	NA
8B	133	164	NA	NA
8C	96	108	NA	NA
8D	104	148	NA	NA
8	NA	NA	NA	NA
9	NA	NA	NA	NA
10	NA	NA	NA	NA

4.5 FEEST2 OUTAGE AND TEMPERATURE MEASUREMENTS

At the end of each leg, the outage conditions and temperature of the water-methanol mixture at the bottom, middle, and top of the tank were recorded. Table 20 shows the outage and temperature data for each download location.

Table 20. FEEST 2 Outages and Water-Methanol Temperatures

LEG	OUTAGE (%)	TOP Temp	MIDDLE Temp	BOTTOM Temp	AVERAGE Temp
1	1.03	87.40	86.10	82.90	85.47
2	1.22	85.10	84.50	80.20	83.27
3	1.3	84.50	84.50	82.40	83.80
4	1.3	83.10	82.70	81.60	82.47
5	1.35	81.30	80.90	80.40	80.87
6	1.22	78.90	78.60	78.00	78.50
7	NA	NA	NA	NA	NA
8	1.67	60.10	58.50	58.00	58.87
9	1.8	56.60	56.60	55.90	56.37
10	1.7	49.40	49.40	49.40	49.40

Some variation in the data was caused by the outage conditions being measured at an unlevel download location, such as leg 6 data. As shown in Table 20, the outage change was almost -1 percent under the long term conditions of the FEEST2 test. If the temperature differential during the test had been in the opposite direction, the surge pressure data would have been very different as a shell full condition could have been produced.

4.6 FEEST2 SURGE PRESSURE DATA

During the loaded portion of the FEEST2 test, 14 surge pressure events were recorded by the data collection system. All 14 of FEEST2 surge pressure events collected are shown in Appendix C. The maximum value of all of the surge pressure events collected was less than 40 psia.

The speed transducer introduced a variable ground level which resulted in the appearance of a low level oscillation in the surge pressure data. The oscillation can be seen in some of the surge pressure events shown in Appendix C. The oscillations had a maximum magnitude of approximately 4 psi at low speeds and diminished to zero at speeds above 10 mph. Due to the small magnitude of oscillation, data quality was not affected seriously . The speed transducer was replaced several times during the test due to the harsh vibration environment where the transducer was located.

All surge pressure events recorded during the FEEST2 testing were the result of impact events. Some of the surge pressure events captured show no corresponding LCF. Impacts that occurred on the A-end of the car with the B-end being uncoupled resulted in no record of LCF response data because only the B-end LCF was acquired by SOMAT 4.

The peak/valley surge pressure data collected for those legs where the data quality was acceptable is presented in Figure 57. The peak/valley data shown corresponds very well with the burst history data and with the surge pressure impact test results, which will be discussed later (Section 4.7).

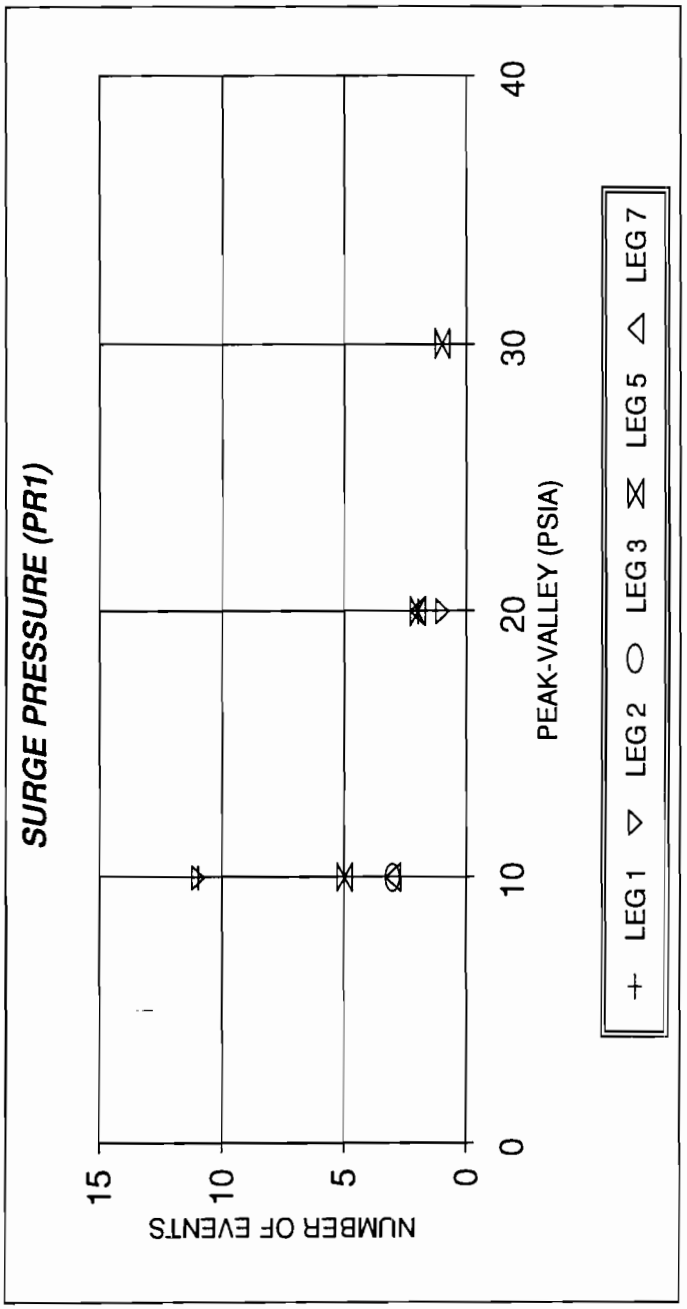

Figure 57. FEEST2 Surge Pressure Peak Valley Results

4.7 SURGE PRESSURE IMPACT TESTS RESULTS

The results of the surge pressure impact testing were in good agreement with the FEEST2 OTR results; no surge pressure events exceeding 40 psi were produced. The majority of the peak surge pressures measured were under 15 psi. The surge pressure test results are presented in Table 21, which shows the configurations and a brief description of the resulting surge pressure impact response data.

Initially, it was thought that the variability of the impact conditions would make defining any trends in the surge pressure data very difficult. For this reason, several impacts at the same speed and configuration were conducted to check for this variability. Figure 58 shows the results of five separate impact tests that were conducted in the A configuration (see Figure 16) at 8 mph. Figure 58 illustrates the relative repeatability of the surge pressure responses that were developed during the impact tests. Figures 59 and 60 show the results of impact tests at 9 mph plus the repeatability of the response data. The repeatable nature of the data demonstrates the accuracy and precision of the test setup. These results also build confidence in the FEEST2 surge pressure burst history data as the same types of response data were obtained.

Figures 59 and 60 show that the surge pressure response data consists primarily of a single large pressure wave followed by much smaller pressure peak with an oscillatory response characteristic. As shown in Table 21, the highest surge pressure event obtained was in the A configuration at an impact speed of 6 mph. The possibility that impact speeds around the 6 mph speed produced higher surge pressures was investigated by performing several impacts at approximately 6 mph. No evidence of surge pressures peaking at a given impact speed were found.

LCF data for several impacts are shown in Table 21 and demonstrate the accuracy of the two separate measurement channels (LCF1B and LCF1B).

Table 21. Surge Pressure Impact Test Configurations and Results

IMPACT NUMBER	TEST CONFIG.	SPEED (mph)	Peak Surge Pressure (psia)	Peak LCF LCF1B (kips	Peak LCF LCF2B (kips)
1	A	2.6	less than 15 psi		
2	A	2.6	less than 15 psi		
3	A	2.6	less than 15 psi		
4	A	2.5	less than 15 psi		
5	A	3.1	less than 15 psi		
6	A	3.9	less than 15 psi		
7	A	4	less than 15 psi		
8	A	3.8	less than 15 psi		
9	A	3.8	less than 15 psi		
10	A	4	less than 15 psi	284.00	223.00
11	A	6.5	less than 15 psi		
12	A	6.3	less than 15 psi		
13	A	6.1	less than 15 psi		
14	A	6	20 psi		324.00
15	A	6	less than 15 psi		
16	A	6	less than 15 psi	327.00	400.00
17	A	8	less than 15 psi		
18	A	7.8	less than 15 psi		
19	A	8	less than 15 psi		
20	A	7.9	less than 15 psi	877.00	832.00
21	A	8.1	less than 15 psi		
22	B	2.5	less than 15 psi		
23	B	3.9	less than 15 psi		
24	B	6	less than 15 psi		
25	B	8.2	less than 15 psi		
26	B	9	less than 15 psi		
27	C	2.4	less than 15 psi		
28	C	3.9	less than 15 psi		
29	C	5.7	less than 15 psi	1150.00	1100.00

Table 21. Surge Pressure Impact Test Configurations and Results – continued

IMPACT NUMBER	TEST CONFIG.	SPEED (mph)	Peak Surge Pressure (psia)	Peak LCF LCF1B (kips)	Peak LCF LCF2B (kips)
30	A	7.7	less than 15 psi		
31	A	9	less than 15 psi		
32	A	9	less than 15 psi		
33	A	8.9	less than 15 psi		

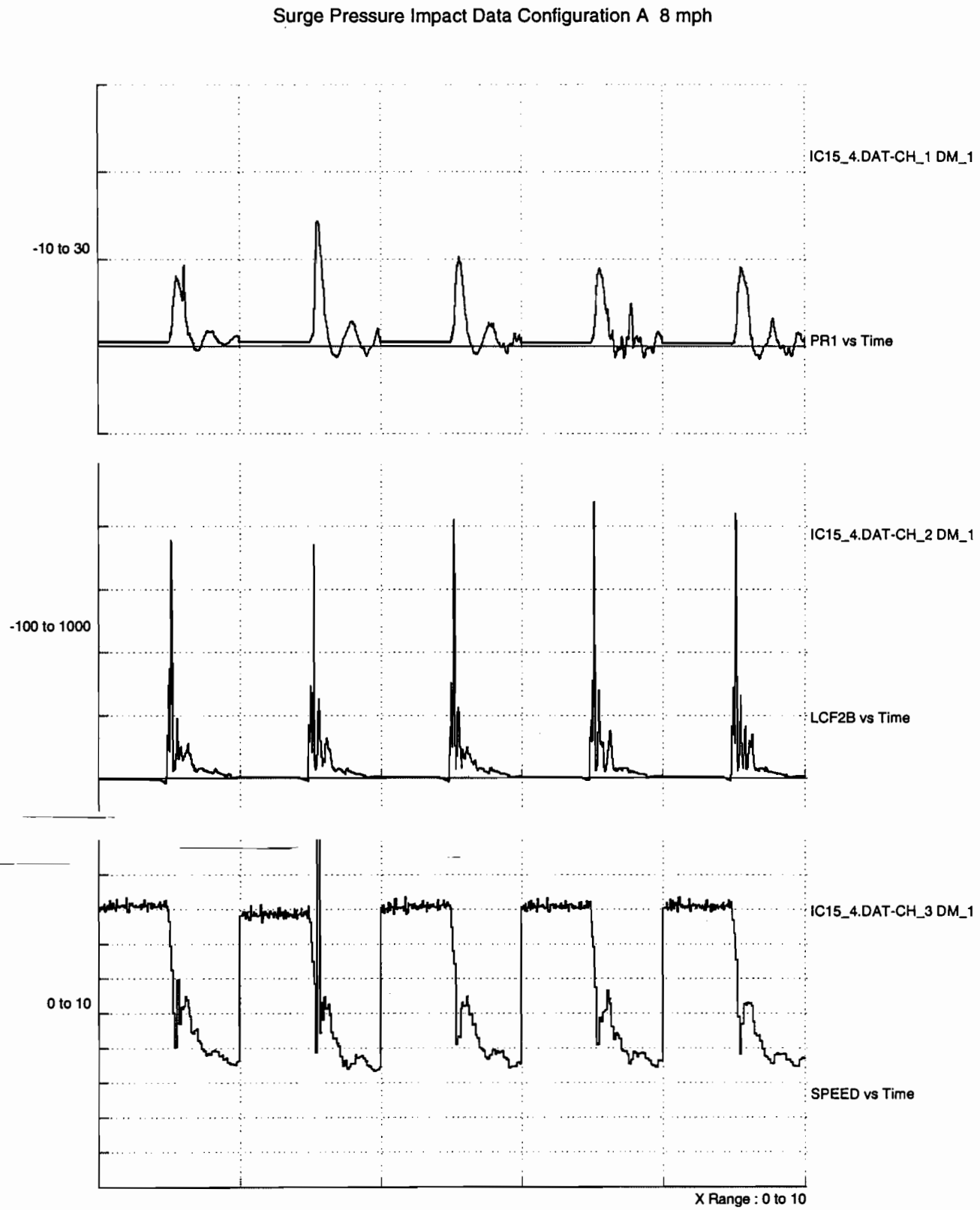

Figure 58. Surge Pressure Repeatability 8 mph

Surge Pressure Impact Data Configuration A 9 mph

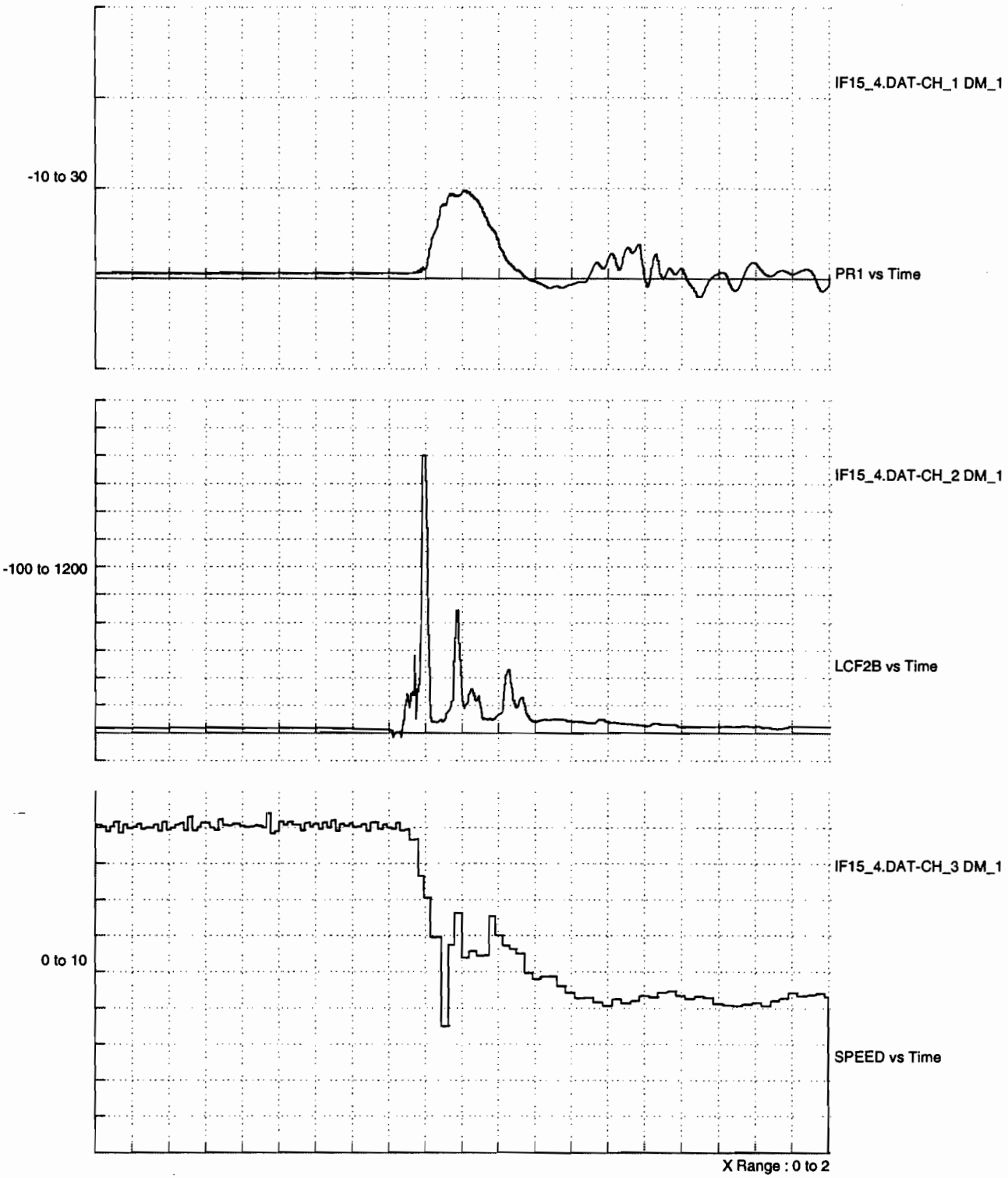

Figure 59. Surge Pressure Repeatability 9 mph

Surge Pressure Impact Data Configuration A 9 mph

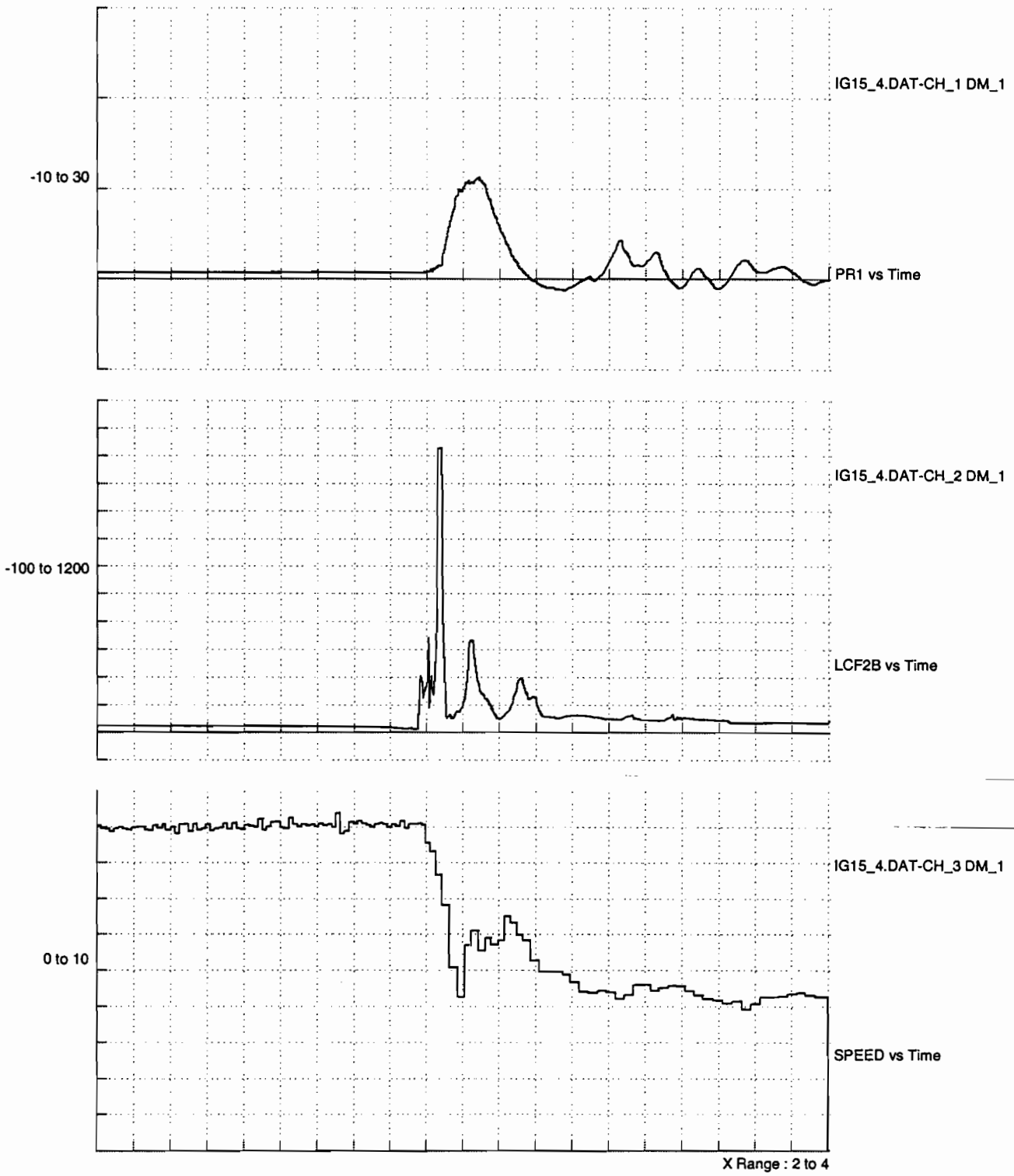

Figure 60. Surge Pressure Repeatability 9 mph

4.8 FEEST2 SHOCK WATCH DATA

The Shock Watch units recorded data continuously during the FEEST2 tests. The units recorded shock events by recording the date and time of each event with small differences in the recorded time for the same event due to differences in the individual clocks. The "g's" recorded are shock levels and may better be thought of as "impact severity" in order to reduce the temptation to infer rigid body acceleration values from this data (see Section 4.8.1). These units were not serviced or calibrated by TTC and as such no responsibility for the data quality is assumed by TTC.

The data collected by the Shock Watch units for each leg is presented in Appendix D. The data collected for leg 7 is shown in Table 22.

In general, there was an inconsistency between the A- and B-end shock levels recorded as shown by the number of "10 G" events occurring on the A-end and not on the B-end. This may have been due to the slightly different mounting locations of the units or in the attachment to the tank car.

It is interesting to note that the leg 7 Shock Watch data did not show a significant increase in the number of events recorded even though leg 7 produced the most severe VCF fatigue life environment. This again suggests that high LCF coupling events are not a major contributor to the resulting fatigue life reduction seen in leg 7. This conclusion is based on the impact test results which allowed a generalized correlation of known impact speeds with the Shock Watch data to be made. A severe LCF environment caused by impact events would have been indicated by a large number of high level shock events being recorded. Since only one 10-g event was recorded by the Shock watch units on leg 7, it is concluded that other dynamic inputs were responsible for the reduced fatigue life.

The Shock Watch data indicates that leg 9 was the most severe for producing high impact coupling events along with a higher frequency of occurrence.

Table 22. Leg 7 Shock Watch Data

B-END (SERIAL NUMBER 334)				A-END (SERIAL NUMBER 335)		
DATE	TIME	G's		DATE	TIME	G's
10/19/94	13:59	2.0		10/19/94	13:59	10.0
10/19/94	14:53	2.0		10/19/94	14:54	2.0
10/19/94	15:30	2.0		10/19/94	15:31	2.0
10/19/94	15:30	2.0		no data recorded		
10/20/94	22:23	2.0		10/20/94	22:24	2.0
10/24/94	10:31	2.0		10/24/94	10:32	2.0
10/24/94	10:39	2.0		10/24/94	10:39	2.0

4.8.1 Surge Pressure Impact Tests Shock Watch Data

The surge pressure impact testing performed at the end of leg 10 was used to correlate the Shock Watch readings with known impact conditions. Table 23 presents the data obtained along with the configuration and initial impact velocity for all of the impact tests. The abbreviation "NDR" in Table 23 indicates that no data was recorded by the Shock Watch unit for that event. Refer to Figures 16 and 17 for test configuration setups. Unfortunately, the A-end unit failed during the test and no data was recovered.

Table 23. Surge Pressure Impact Tests Shock Watch Data

IMPACT NUMBER	TEST TIME	TEST CONFIG.	SPEED (mph)	Shock Watch "G" Value B-END
1	10:05	A	2.6	2.00
2	10:07	A	2.6	2.00
3	10:08	A	2.6	2.00
4	10:10	A	2.5	2.00
5	10:11	A	3.1	2.00
6	10:15	A	3.9	2.00
7	10:16	A	4	2.00
8	10:18	A	3.8	2.00
9	10:20	A	3.8	2.00
10	10:21	A	4	2.00
11	10:24	A	6.5	2.00
12	10:27	A	6.3	2.00
13	10:30	A	6.1	2.00
14	10:33	A	6	2.00
15	10:36	A	6	2.00
16	11:27	A	6	2.00
17	11:42	A	8	6.00
18	11:45	A	7.8	6.00
19	11:48	A	8	6.00
20	11:52	A	7.9	6.00
21	11:57	A	8.1	6.00
22	13:10	B	2.5	NDR
23	13:11	B	3.9	2.00
24	13:13	B	6	NDR
25	13:17	B	8.2	4.00
26	13:24	B	9	4.00

Table 23. Surge Pressure Impact Tests Shock Watch Data – continued

IMPACT NUMBER	TEST TIME	TEST CONFIG.	SPEED (mph)	Shock Watch "G" Value B-END
27	13:40	C	2.4	2.00
28	13:42	C	3.9	2.00
29	13:45	C	5.7	6.00
30	13:48	A	7.7	10.00
31	14:46	A	9	10.00
32	15:01	A	9	10.00
33	15:05	A	8.9	10.00

Figure 61 shows the burst time history data for impact 32 which was a 9.0 mph impact in the A configuration. From this data, an estimate of the rigid body acceleration of the tank car can be derived from the SPEED vs TIME time history. From Figure 58, the change in speed (ΔV) is 4.8 mph during a time (Δt) of approximately .1 seconds. This corresponds to an average rigid body acceleration of 70.4 ft/sec^2 or approximately 2.2 g's which is a reasonable result. This illustrates that the 10 g's as recorded by the Shock Watch units have a higher frequency response (approximately 15 Hz) and as such are measuring the shock response of the tank car and the rigid body acceleration combined. When reviewing the data from the Shock watch units, the shock response as measured must not be confused with the rigid body acceleration values as illustrated above.

Every effort was made to camouflage the instrumentation that was added on the tank car. No impact events above 10 mph were captured; however, several 6 and 7 mph impacts were recorded. The highest magnitude LCF event that was captured by the burst history mode during the FEEST2 testing occurred during leg 11 and resulted in a LCF peak value of approximately 900 kips.

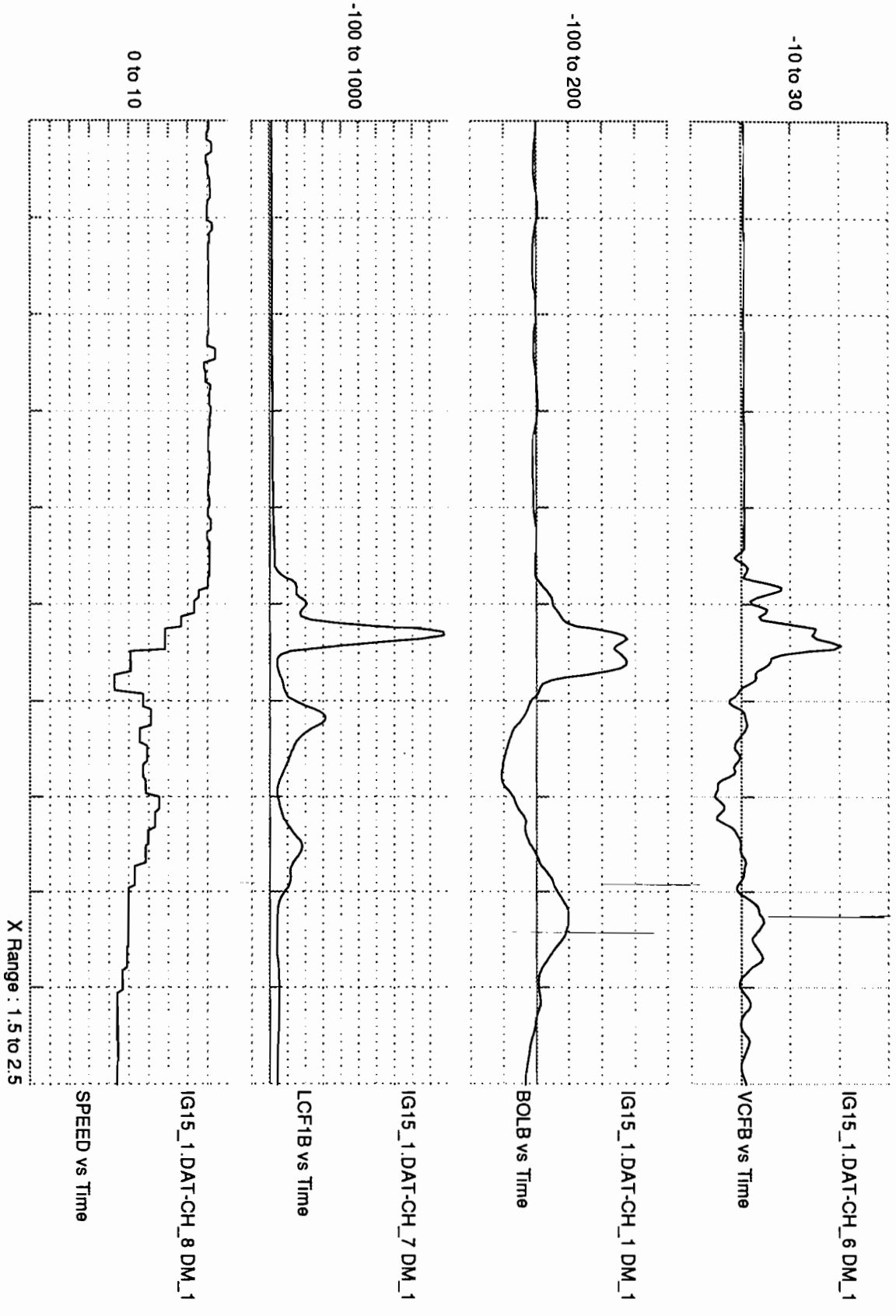

Figure 61. Surge Pressure Impact Test 9 mph Configuration A

4.9 CRITICAL REGION STRAINS

The stress levels in the critical region were measured by the strain gage rosette with measurements SG1A, SG2A and SG3A. The trigger for the rosette strain gage measurements was the measurement VCBA at a levels greater than ±120 μStrain. This is significant in that the VCBA measurement was shown to be sensitive to VCF. Sensitivity resulted in VCF events being the primary trigger source for the critical region strains and was demonstrated during the surge pressure impact tests, which resulted in only a single impact (surge pressure impact event number 30) event for the critical region strains being recorded. Data obtained from this event shows the rosette strains along with the SPEED measurement (Figure 62). Figure 63 shows the corresponding coupler forces that were developed. Figure 63 shows that a VCF peak value of approximately 63 kips was produced with a corresponding LCF of 1,000 kips. These force levels represent a severe combined loading condition.

The rosette strain data in Figure 62 was converted to von Mises stress values to allow direct comparison of the data. The corresponding von Mises stress values for this event, Figure 64, shows peak stress levels are approximately 17,000 psi. This is significant in that the critical region strain gages were located in a position that was shown to have relatively small stress risers and relatively widely spaced stress gradients. Other areas will be subjected to higher stress values due to localized stress raisers.

Using the above characteristics as a guide, the FEEST2 data obtained was reviewed to determine the primary source of the stress levels produced in the critical region. Recall that there is no direct way to correlate VCF and LCF to the critical region strain data due to measurements being acquired on separate SOMAT units. Due to the nature of the rosette strain gage response data, it is possible to identify some of the events recorded by the rosette strain gages as being the result of impacts or the low frequency VCF events shown previously.

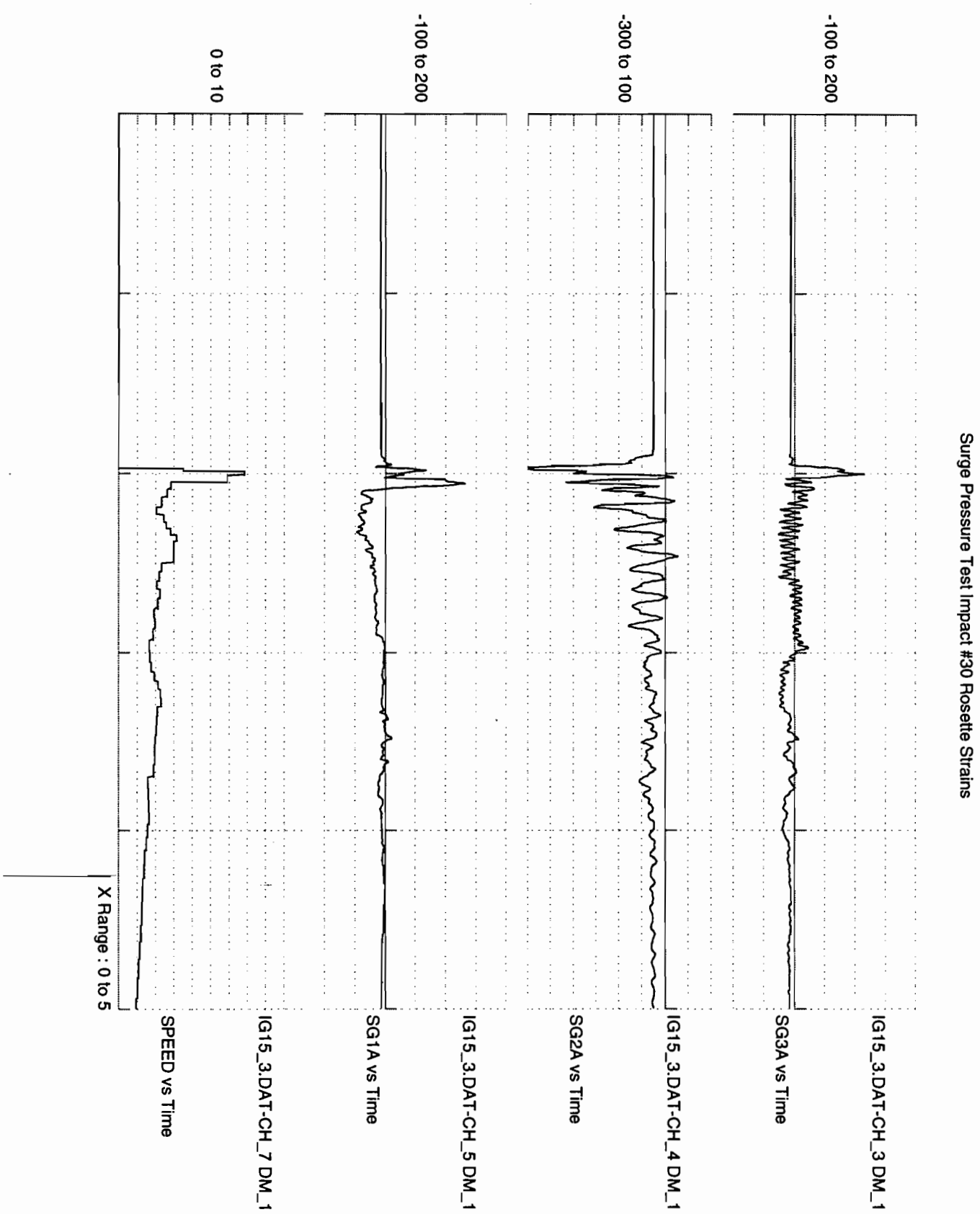

Figure 62. Critical Region Strain Response to Impact

SURGE PRESSURE TEST IMPACT DATA

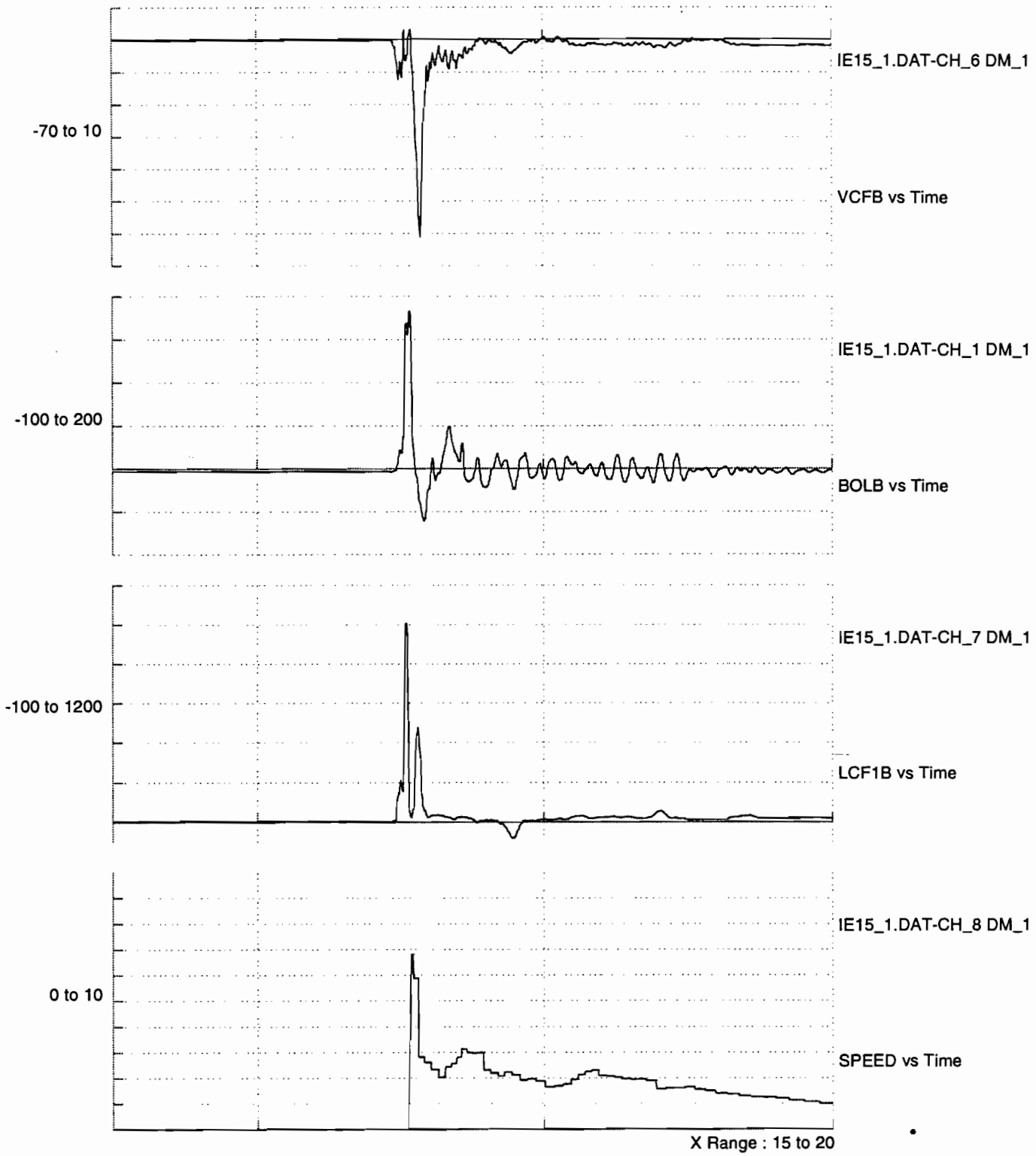

Figure 63. Coupler Force Response To Impact

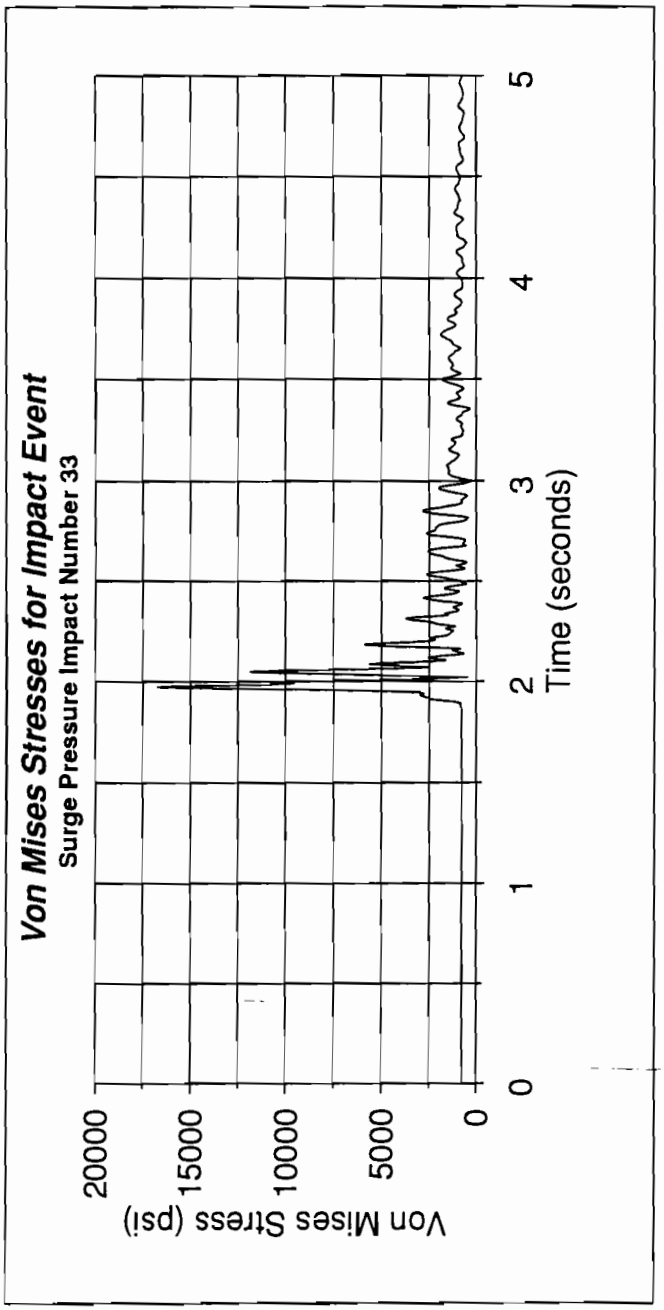

Figure 64. Critical Region Stress Response to Impact

Figure 65 shows the von Mises Stresses for an impact event that occurred during leg 10. The resulting maximum stress levels can be seen to be approximately 11,000 psi. Figure 66 shows the von Mises stress for a low frequency event also obtained during leg 10. The characteristics of this event are similar to the low frequency VCF event shown in Figure 55. The maximum stress level developed during this event was approximately 9000 psi and was representative of the vast majority of the critical region strain gage data collected.

Based on the above, the general conclusion is made that impact events produced the highest stress levels in the critical region, typical levels being on the order of 11,000 to 15,000 psi. The maximum stress levels associated with the low frequency VCF events was lower with maximum values being between 5,000 to 10,000 psi. By calculating the percent of fatigue damage associated with each peak-to-peak bin value, the basic fatigue damage characteristics of the VCF and LCF acting **independently** can be seen. Figures 67 and 68 show that the basic characteristics of the fatigue damage caused by the VCF events is very different than the fatigue damage caused by the LCF events. Figure 67 shows that the VCF events at low peak-to-peak values and high occurrence rates account for the majority of the fatigue damage due to VCF. Figure 68 shows that individual LCF events at peak-to-peak values above 400 kips have a significant con~~tribution to~~ the total fatigue damage caused by LCF events. Results show that the high occurrence rates of the low frequency VCF events and the high stress values associated with LCF impact events are the major contributors to the fatigue damage caused in the critical region.

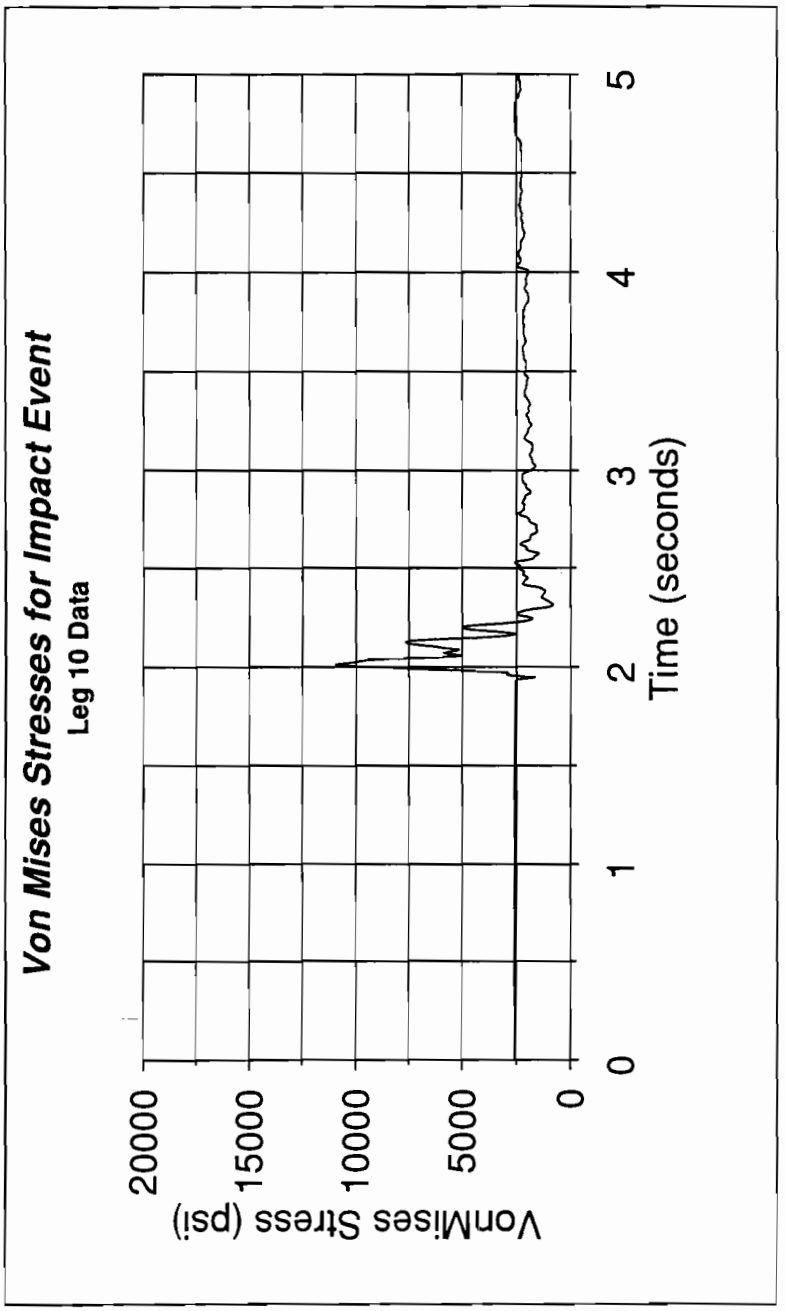

Figure 65. Critical Region Stress Response to Impact on Leg 10

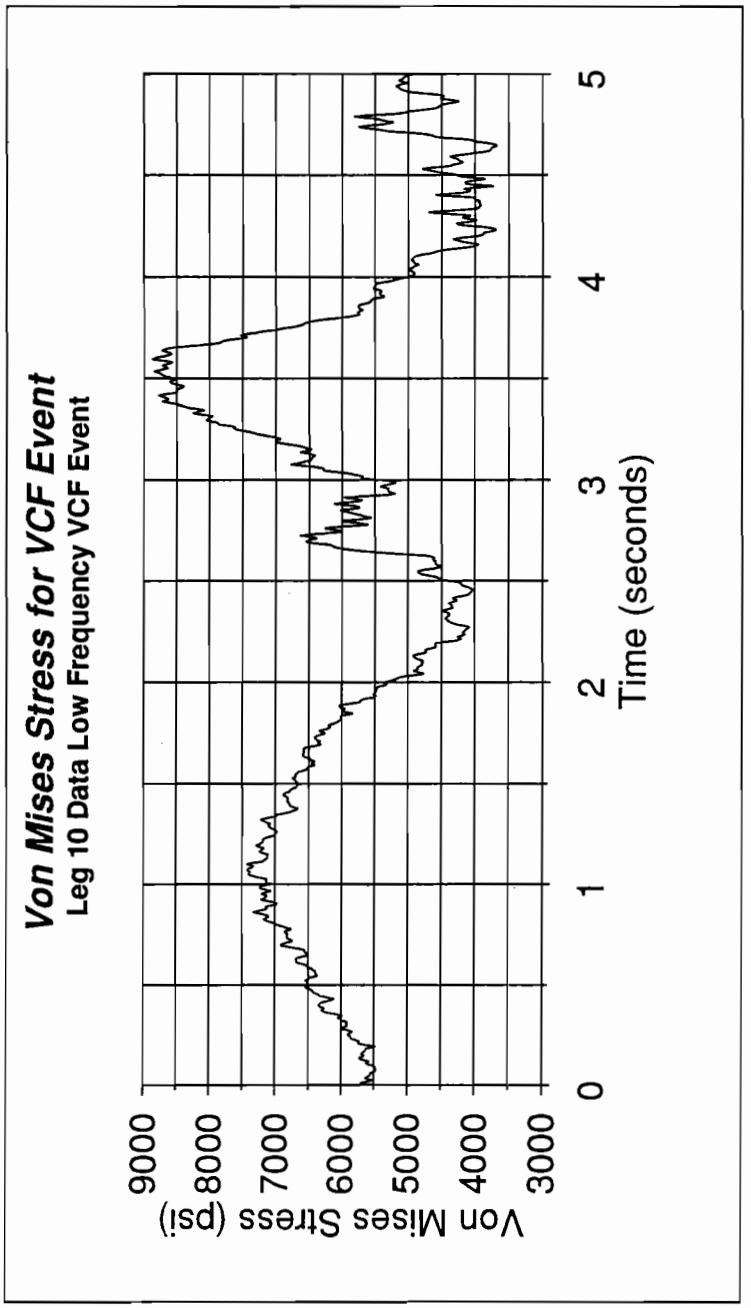

Figure 66. Critical Region Stress Response During Leg 10

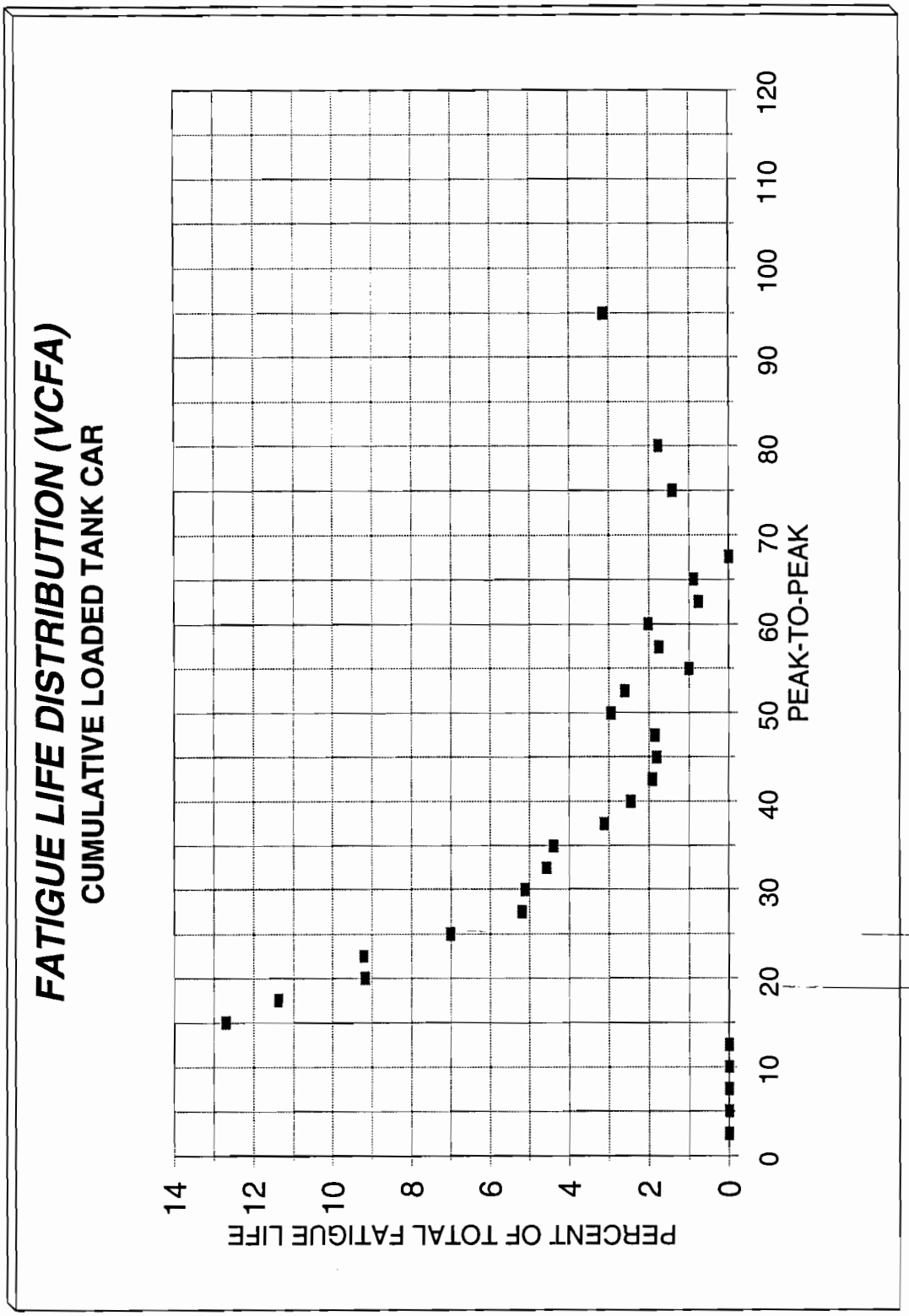

Figure 67. Loaded VCF Fatigue Life Distribution for VCFB

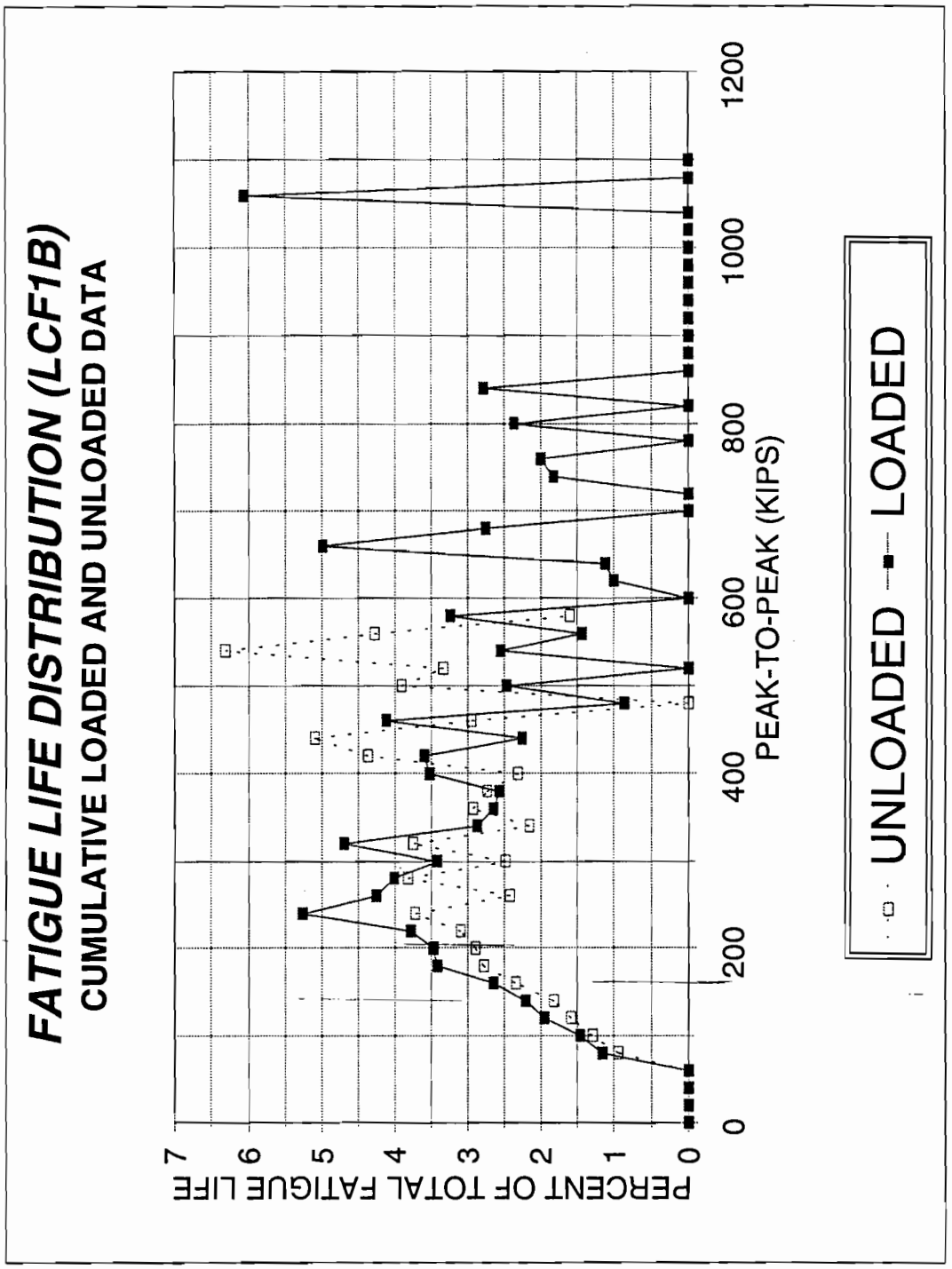

Figure 68. Loaded LCF Fatigue Life Distribution for LCF1B

4.10 IMPACT TEST DATA

Appendix G contains some of the recorded impact events that occurred during the FEEST2 OTR test. Typical LCF values range from 100 kips to over 900 kips occurring during leg 11. All of the impact data available was reviewed to determine if there were any definite relations between the LCF and VCF produced during the impacts. No trends were found in the data, and it is concluded that during impact conditions there are no predictable relationships that exit between the LCF and VCF produced. However, the existence of the simultaneous of VCF and LCF was shown in many of the impacts such as the impact presented in Figure 69. Figure 69 shows a 6.5 mph impact producing simultaneous peak LCF and VCF of 403 kips and 37 kips respectively. The highest VCF recorded due to a known impact was 47 kips. Although the peak VCF and LCF data shown in Figure 63 do not occur at the same time, the development of very high VCF is demonstrated.

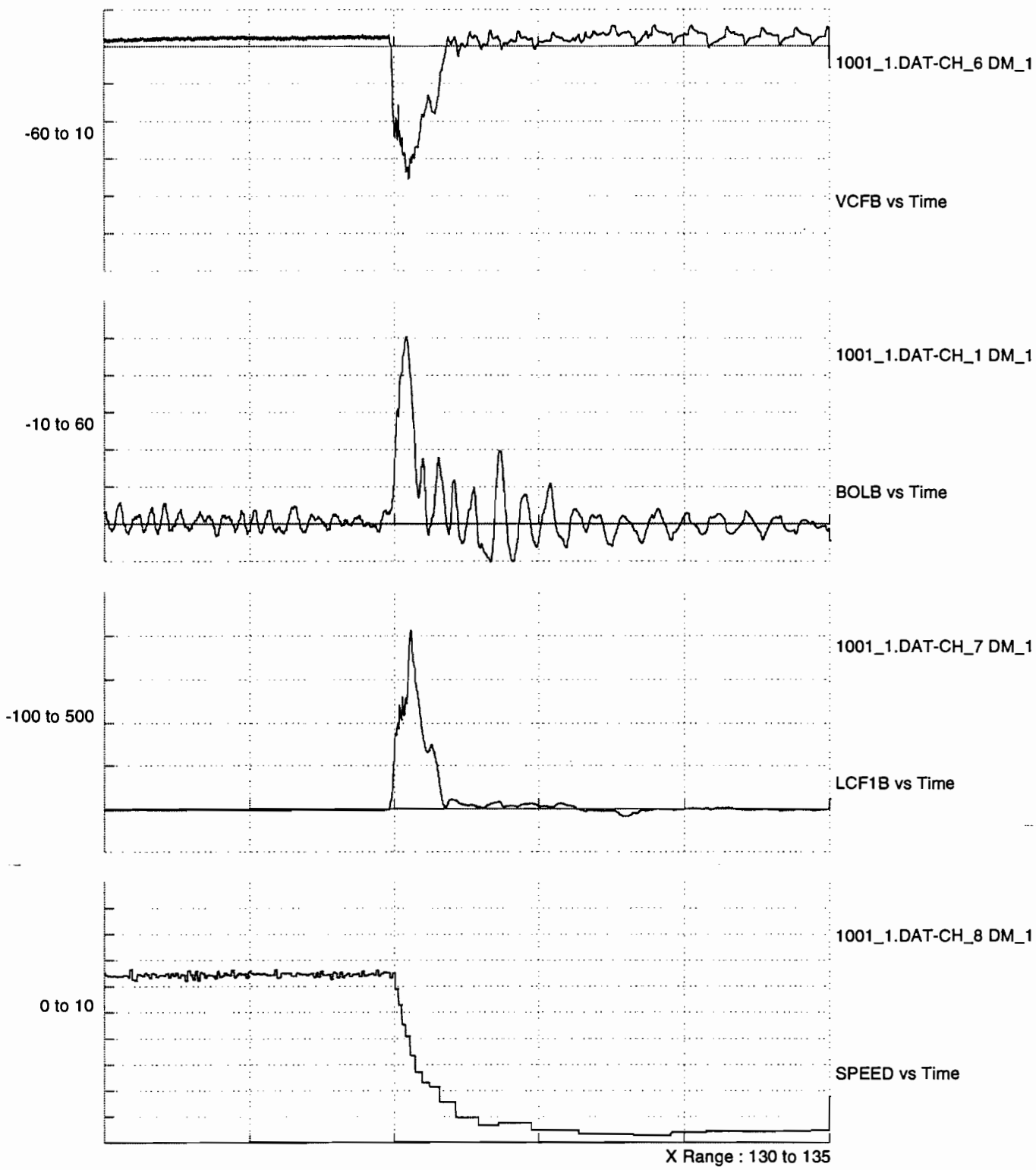

Figure 69. LCF VCF Phase Relationship During Impact

5.0 CONCLUSIONS AND RECOMMENDATIONS

The FEEST2 test resulted in obtaining VCF and LCF histograms which are representative of the coupler load environment that stub sill tank cars are subjected. In addition, a basic understanding as to possible sources for the forces producing the damaging stress levels were identified. Based on the data collected, the following recommendations are made.

1. A significant cause of fatigue damage is caused by low frequency (waveform) high occurrence rate VCF events. The possible source of these VCF events was thought to be due to differential coupler height between adjacent cars caused by vertical stiffness changes in the track. This hypothesis should be investigated further to provide a basic understanding of the source of these VCF events which would allow formulation of possible corrective measures to be taken.

2. The existence of the simultaneous application of large VCF and LCF during impact conditions was demonstrated with OTR and impact test data. Due to the high stresses produced in the critical region of the stub sill tank car by the VCF, we recommend a static design case consisting of the simultaneous application of a 60 kip vertical (up and down) load at the sill and a 1000 kip LCF (buff) be considered.

3. VCF and LCF histograms were obtained which represent the coupler force environment for a stub sill tank car.

4. Individual LCF events at peak-to-peak values above 400 kips have a significant contribution to the total fatigue damage caused by LCF events. We conclude that the high occurrence rates of the low frequency VCF events and the high stress values associated with LCF impact events are the major contributors to the fatigue damage caused in the critical region.

Appendix A

Histograms for the Loaded Portion of the OTR Testing

Appendix A presents the histograms obtained from the load portion of the OTR testing. The histograms present the number of events for each individual leg along with the FEEST1 cumulative values. In addition, the number of events per mile values are also presented. Tables A1 and A2 contain tabular listings of the vertical and longitudinal coupler force values. The values shown in Table A1 were obtained by combining the results obtained from the A-end (VCFA) and the B-end (VCFB). The values in Table A2 were obtained from the measurement LCF1B only and as such were not combined with any other values.

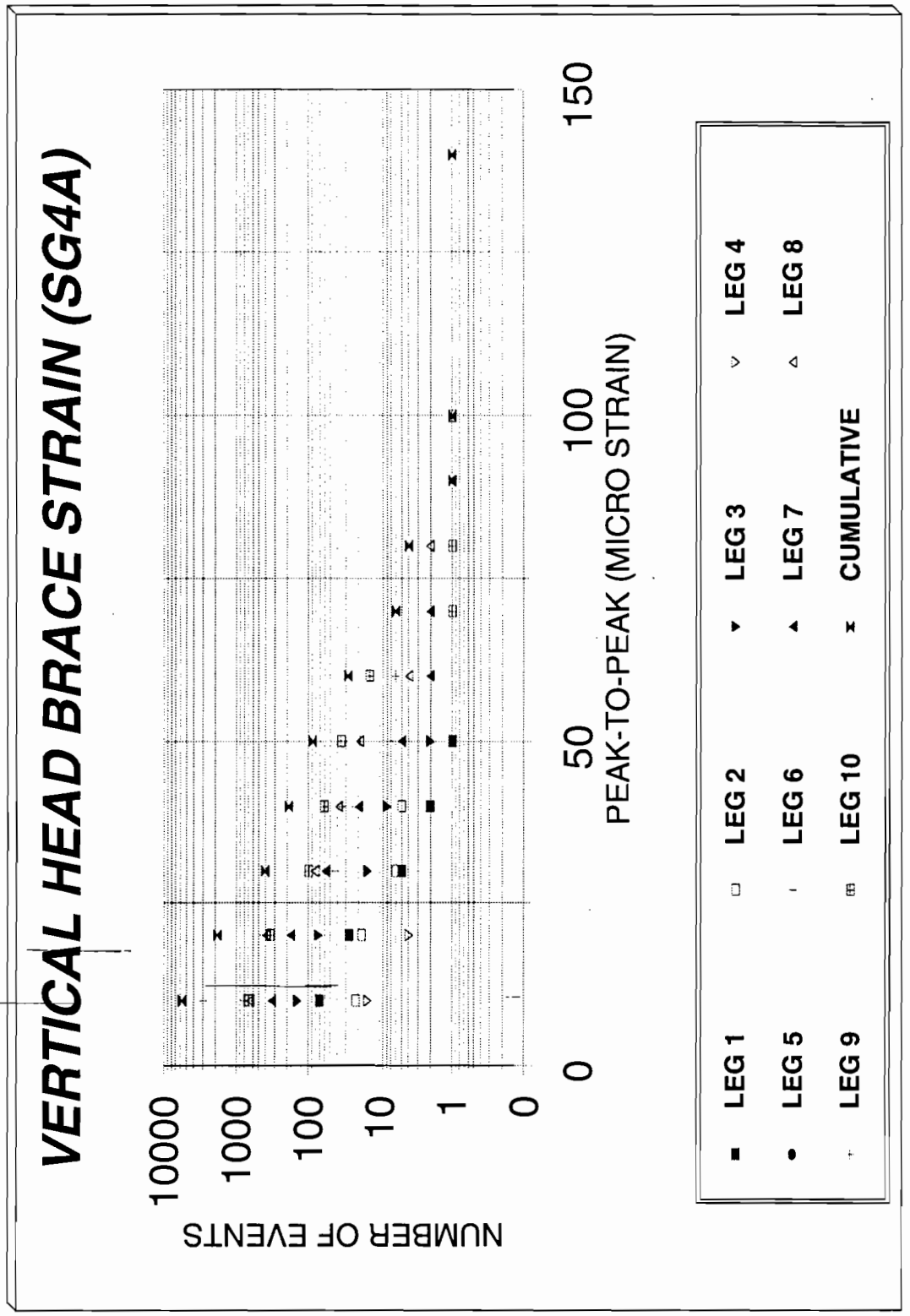

Figure A1. Loaded Portion Histograms for Measurement SG4A Number of Events

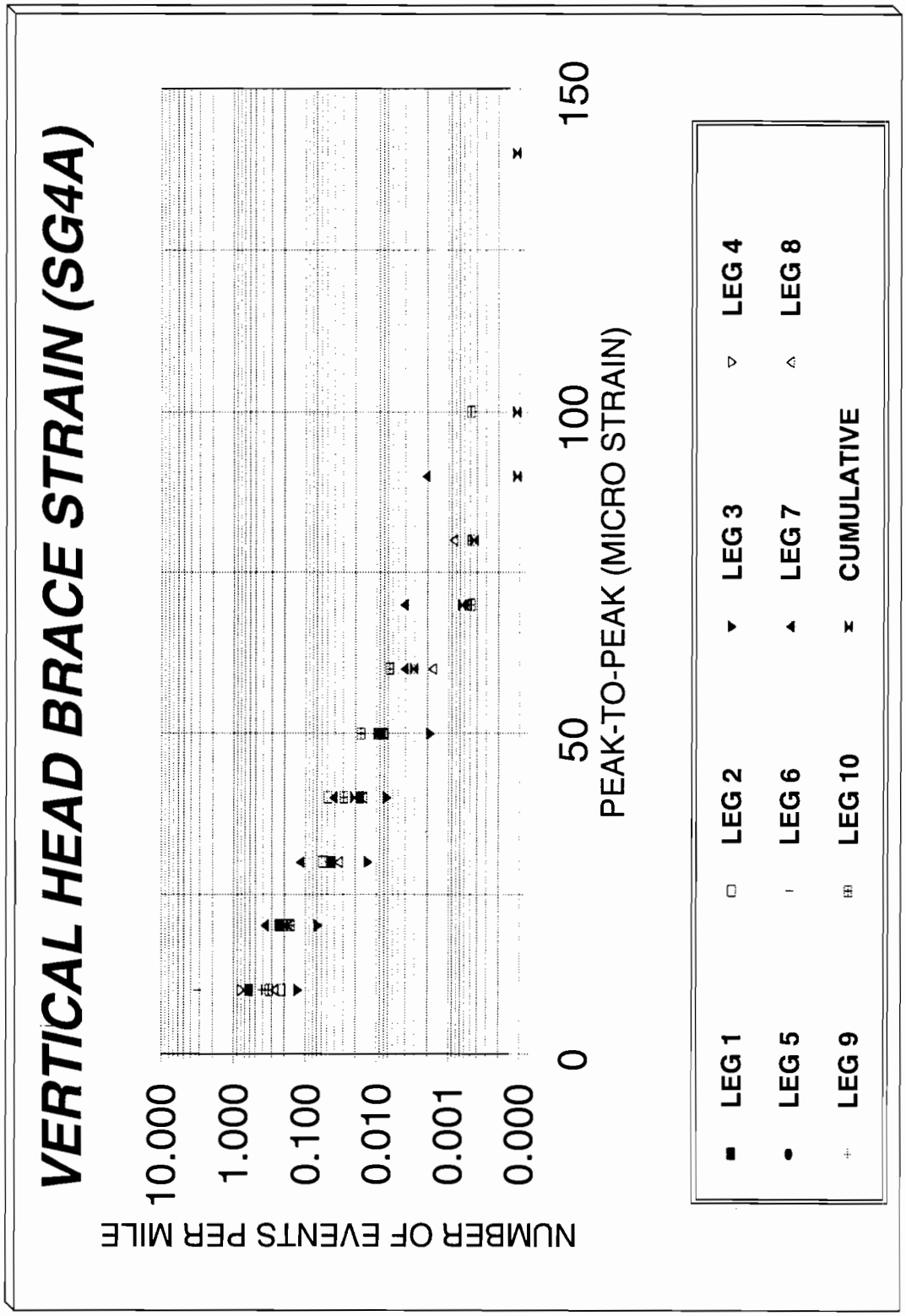

Figure A2. Loaded Portion Histograms for Measurement SG4A Number of Events per Mile

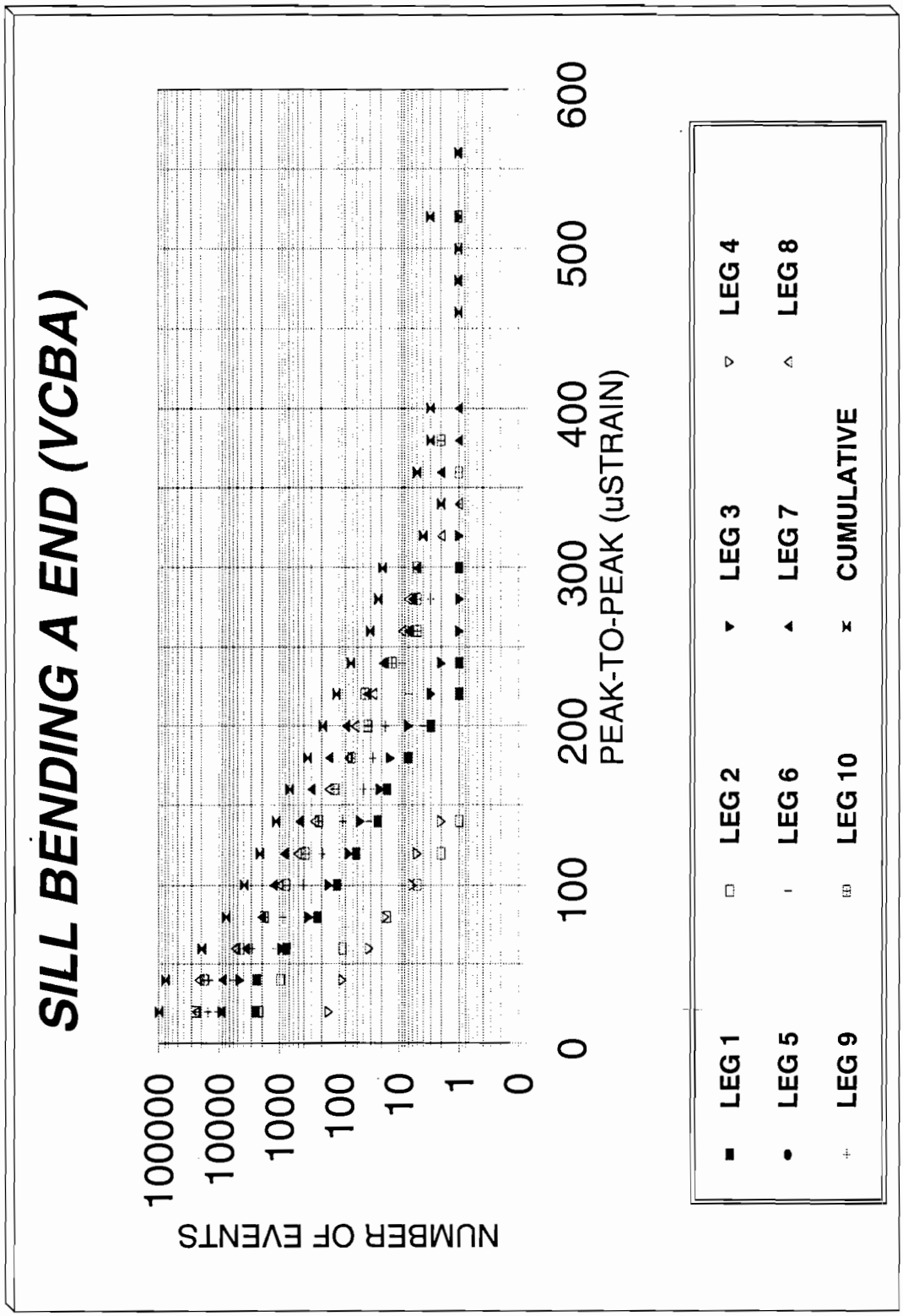

Figure A3. Loaded Portion Histograms for Measurement VCBA Number of Events

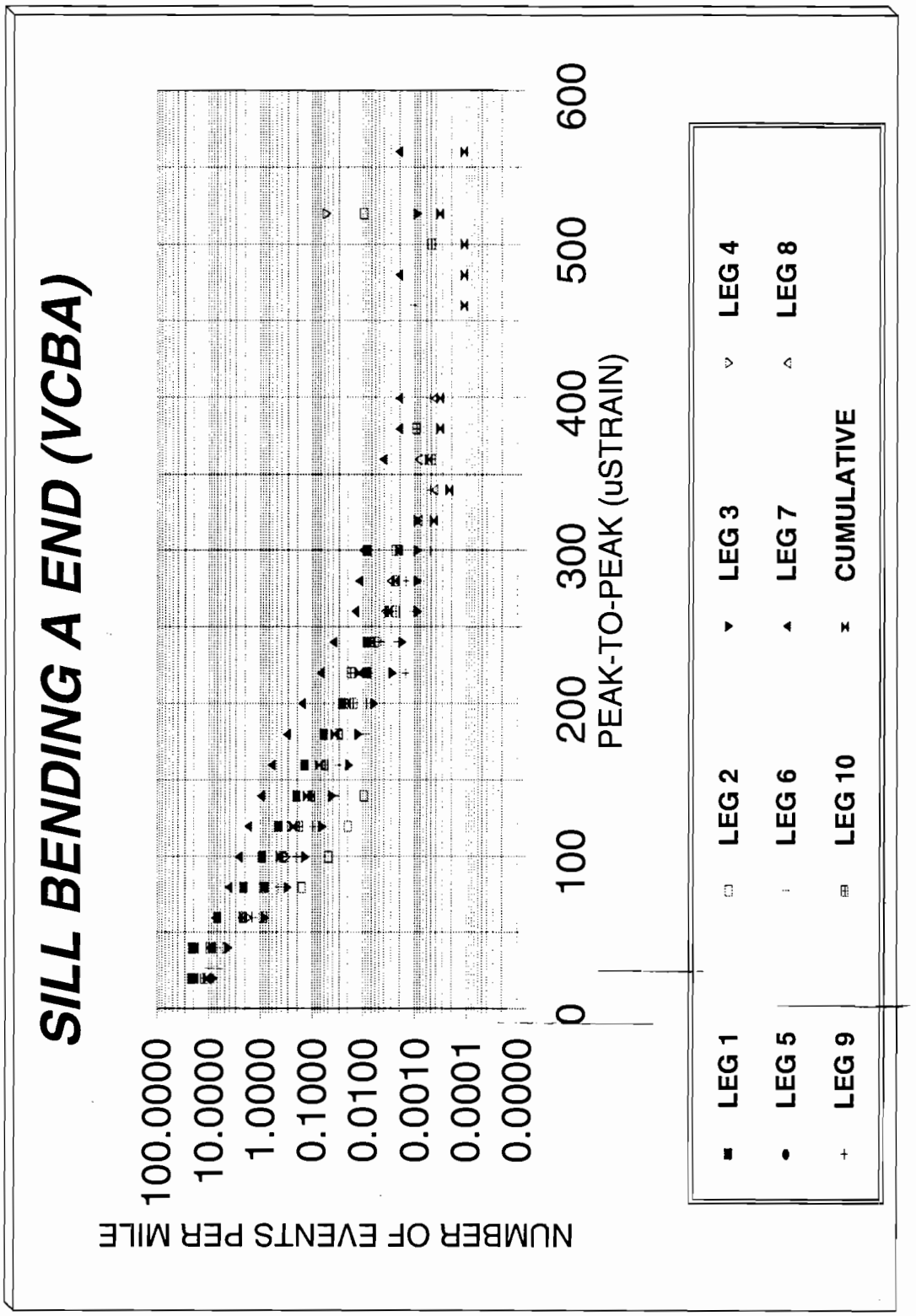

Figure A4. Loaded Portion Histograms for Measurement VCBA Number of Events per Mile

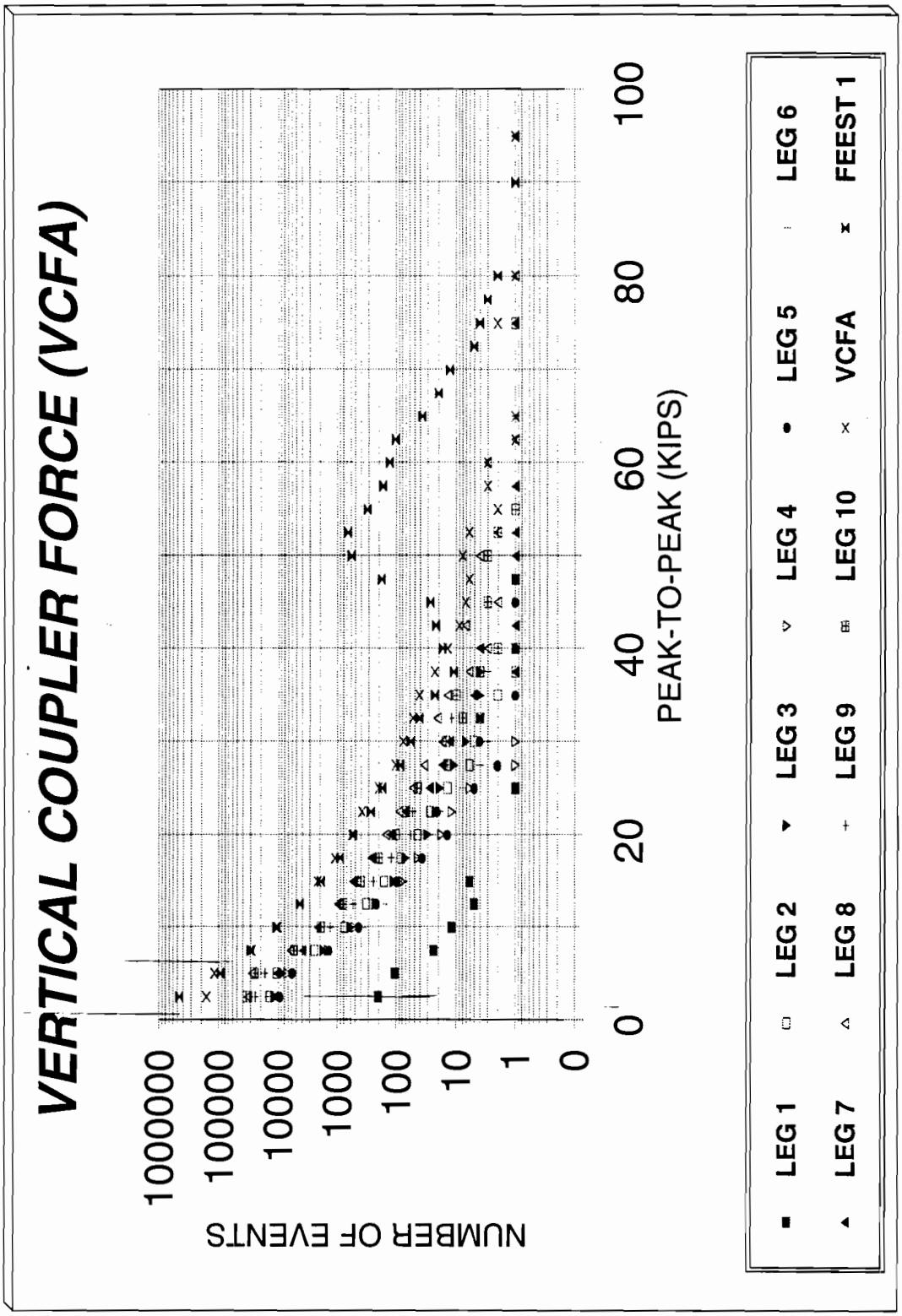

Figure A5. Loaded Portion Histograms for Measurement VCFA Number of Events

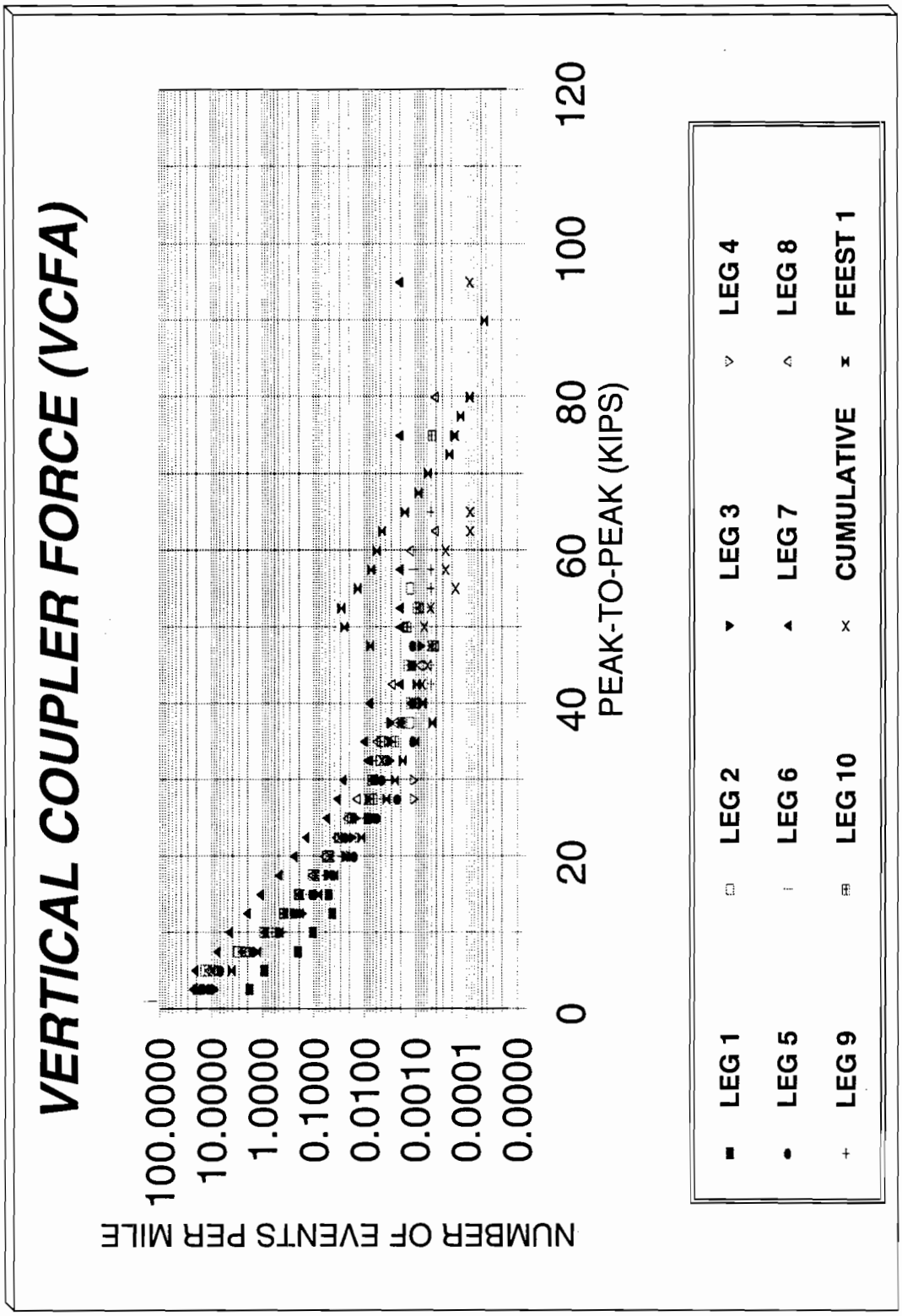

Figure A6. Loaded Portion Histograms for Measurement VCFA Number of Events per Mile

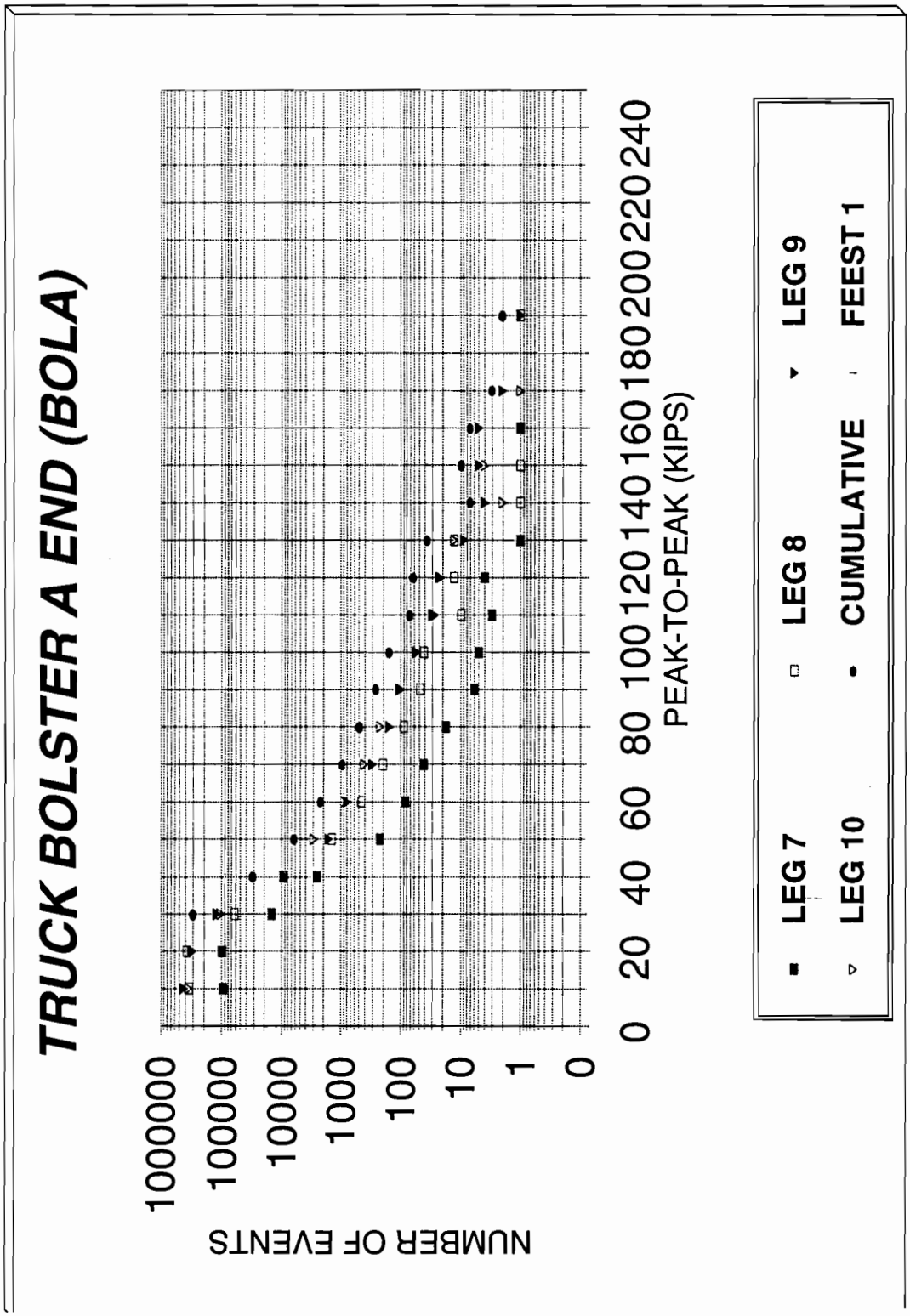

Figure A7. Loaded Portion Histograms for Measurement BOLA Number of Events

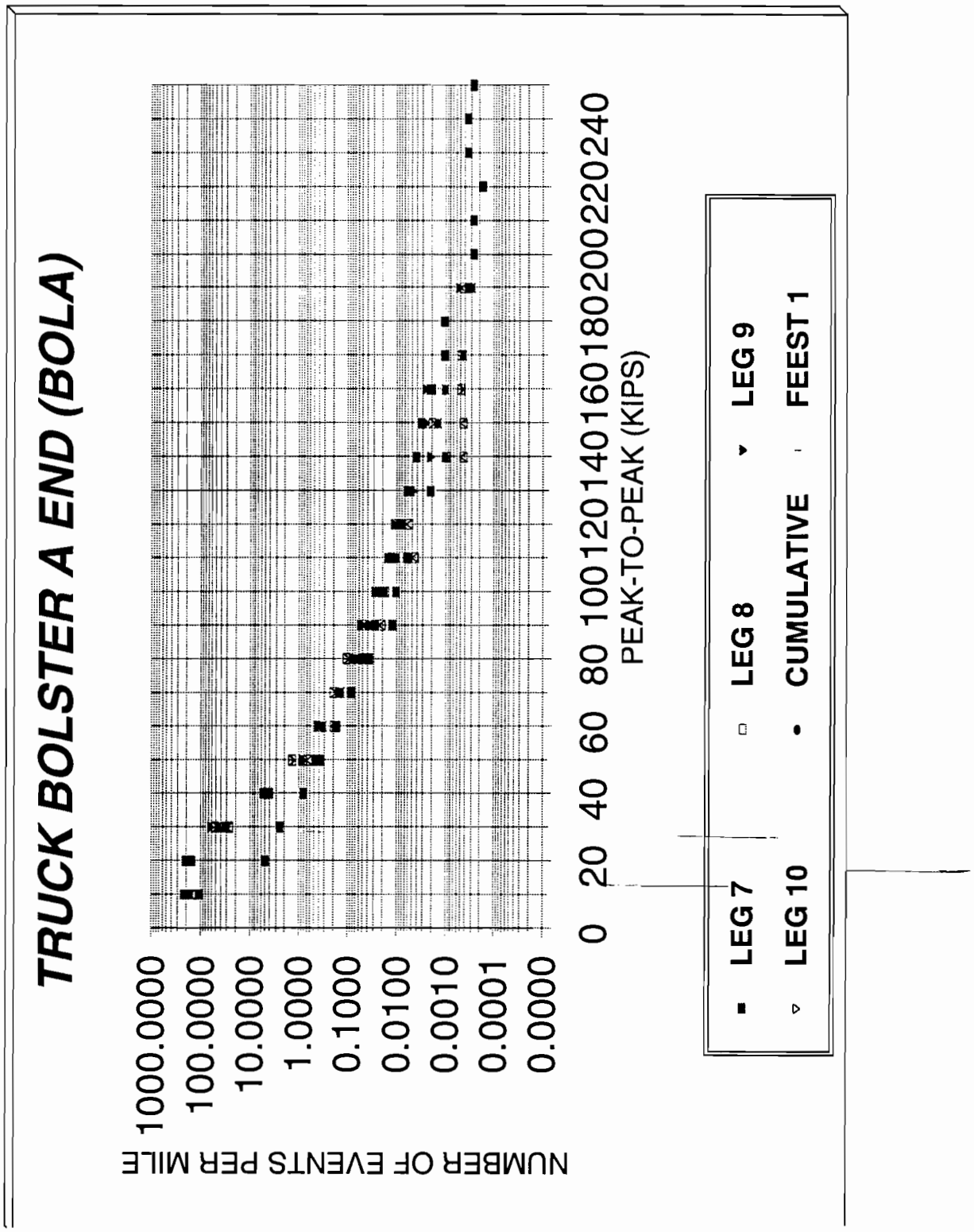

Figure A8. Loaded Portion Histograms for Measurement BOLA Number of Events per Mile

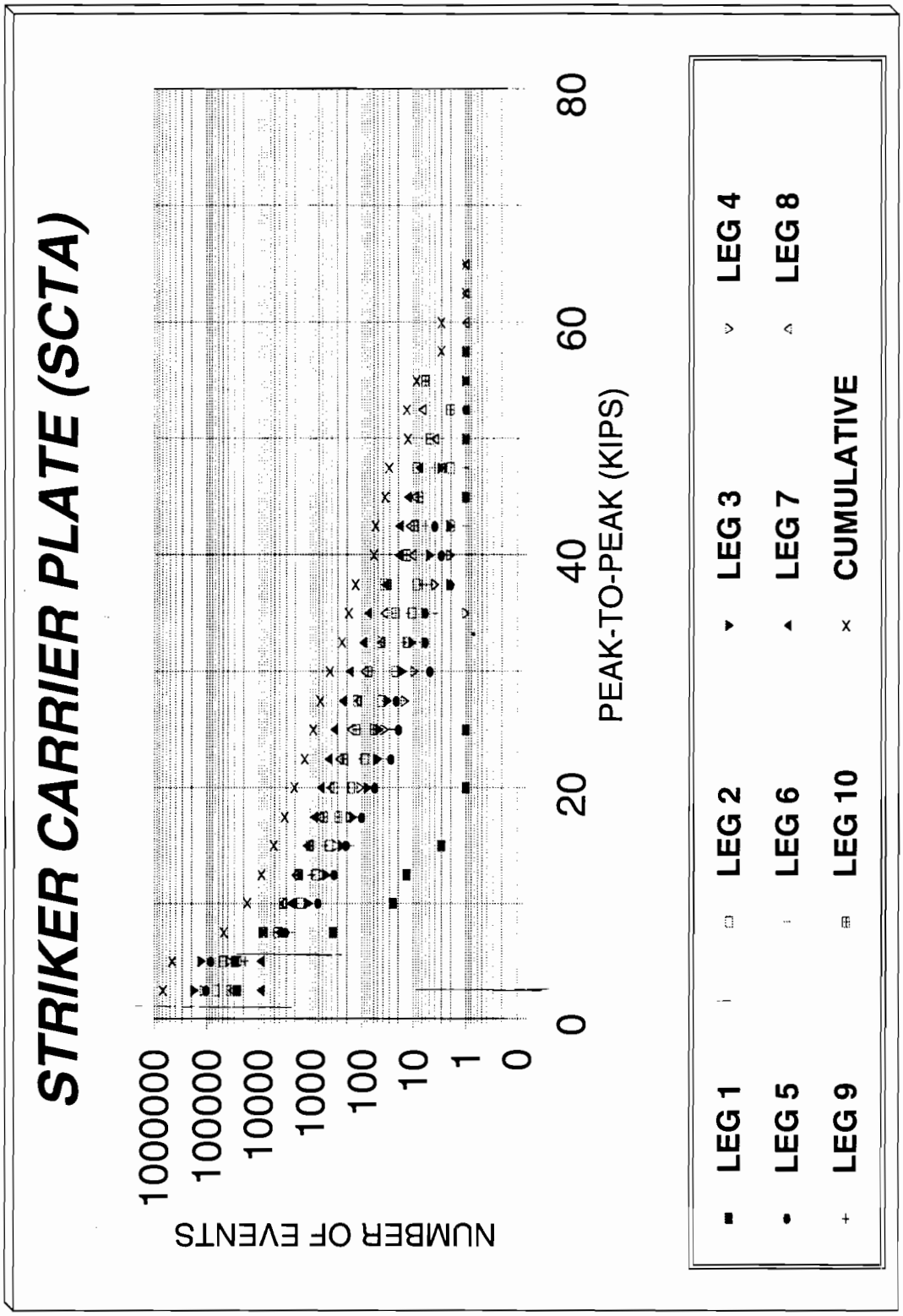

Figure A9. Loaded Portion Histograms for Measurement SCTA Number of Events

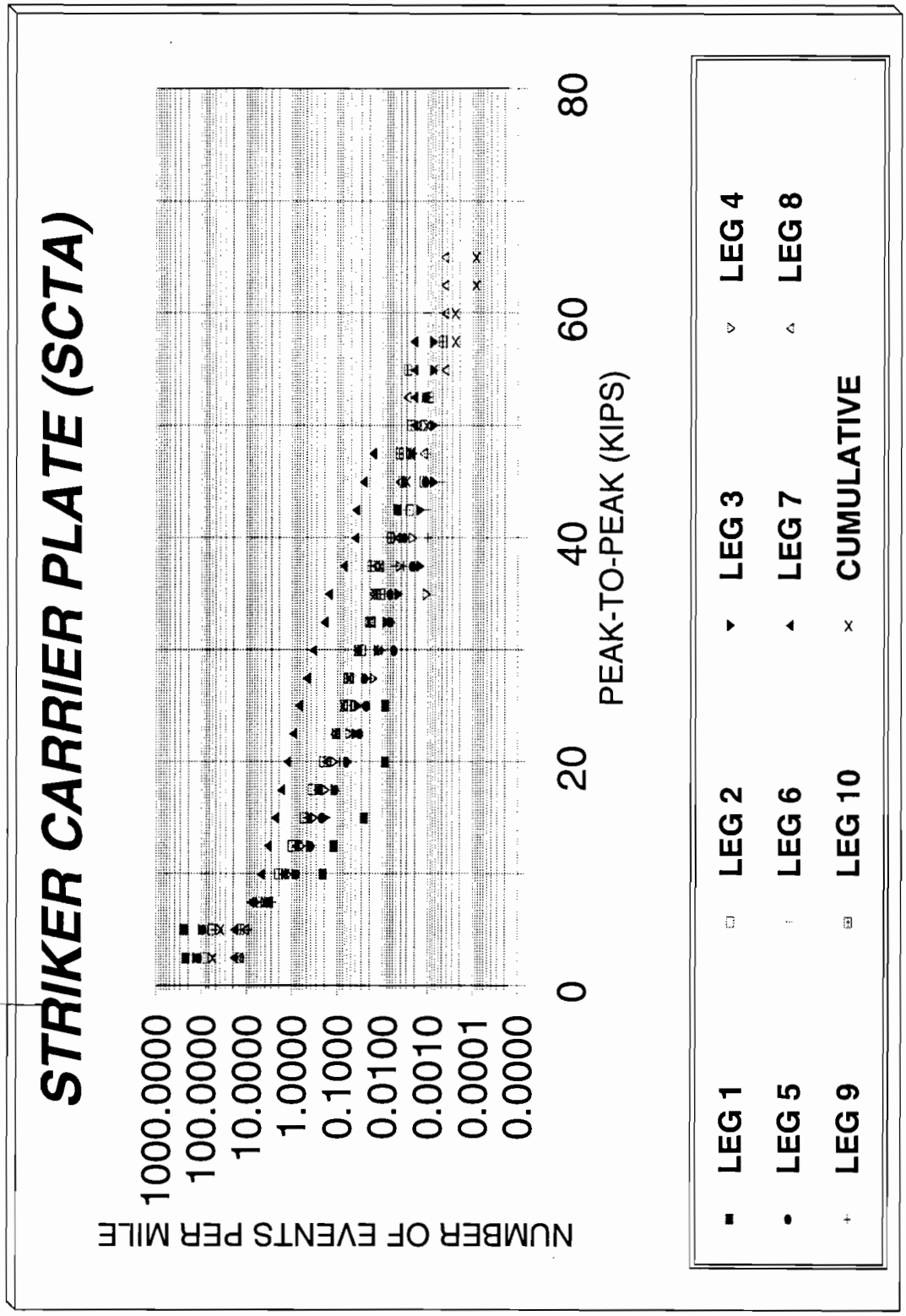

Figure A10. Loaded Portion Histograms for Measurement SCTA Number of Events per Mile

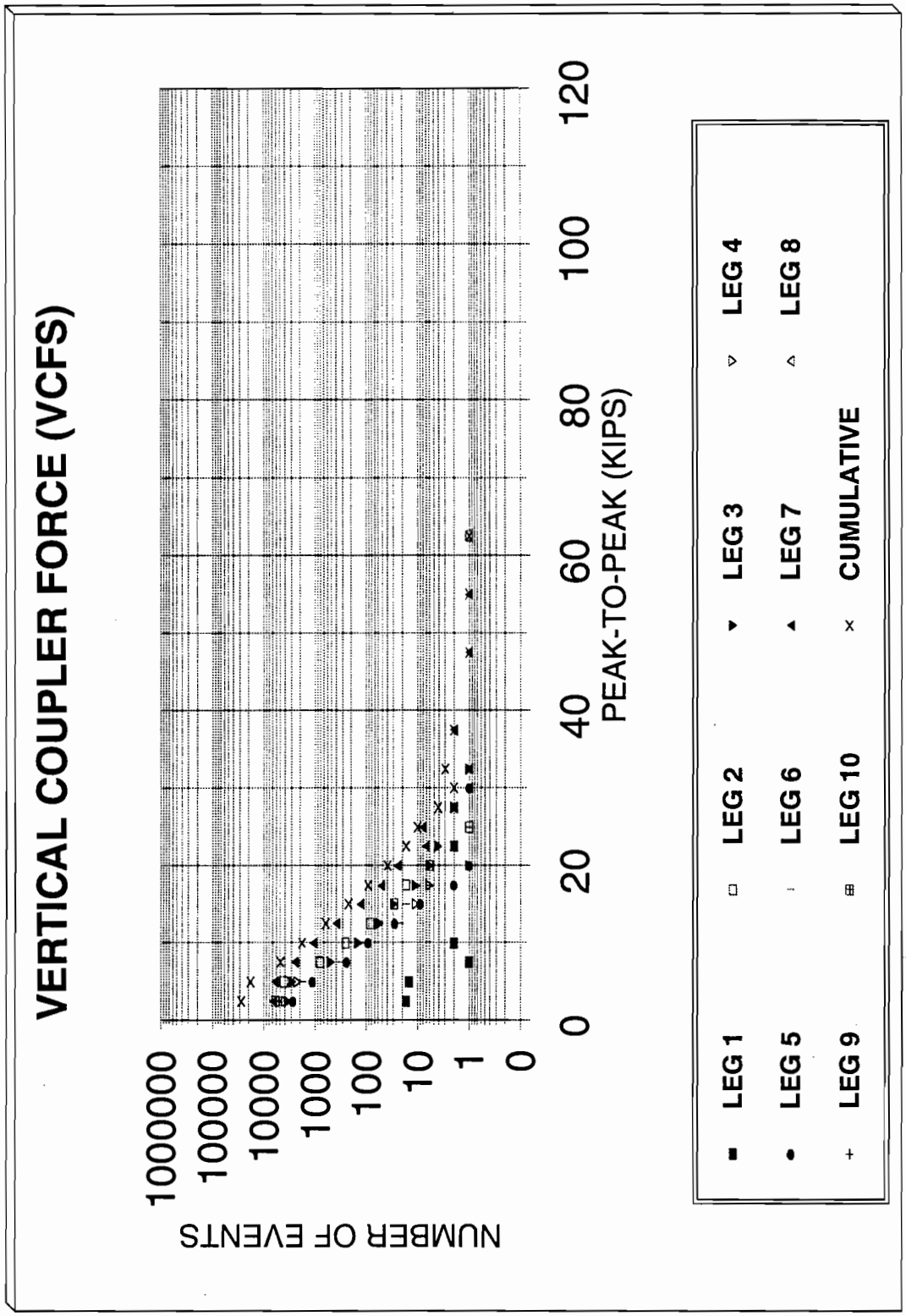

Figure A11. Loaded Portion Histograms for Measurement VCFS Number of Events

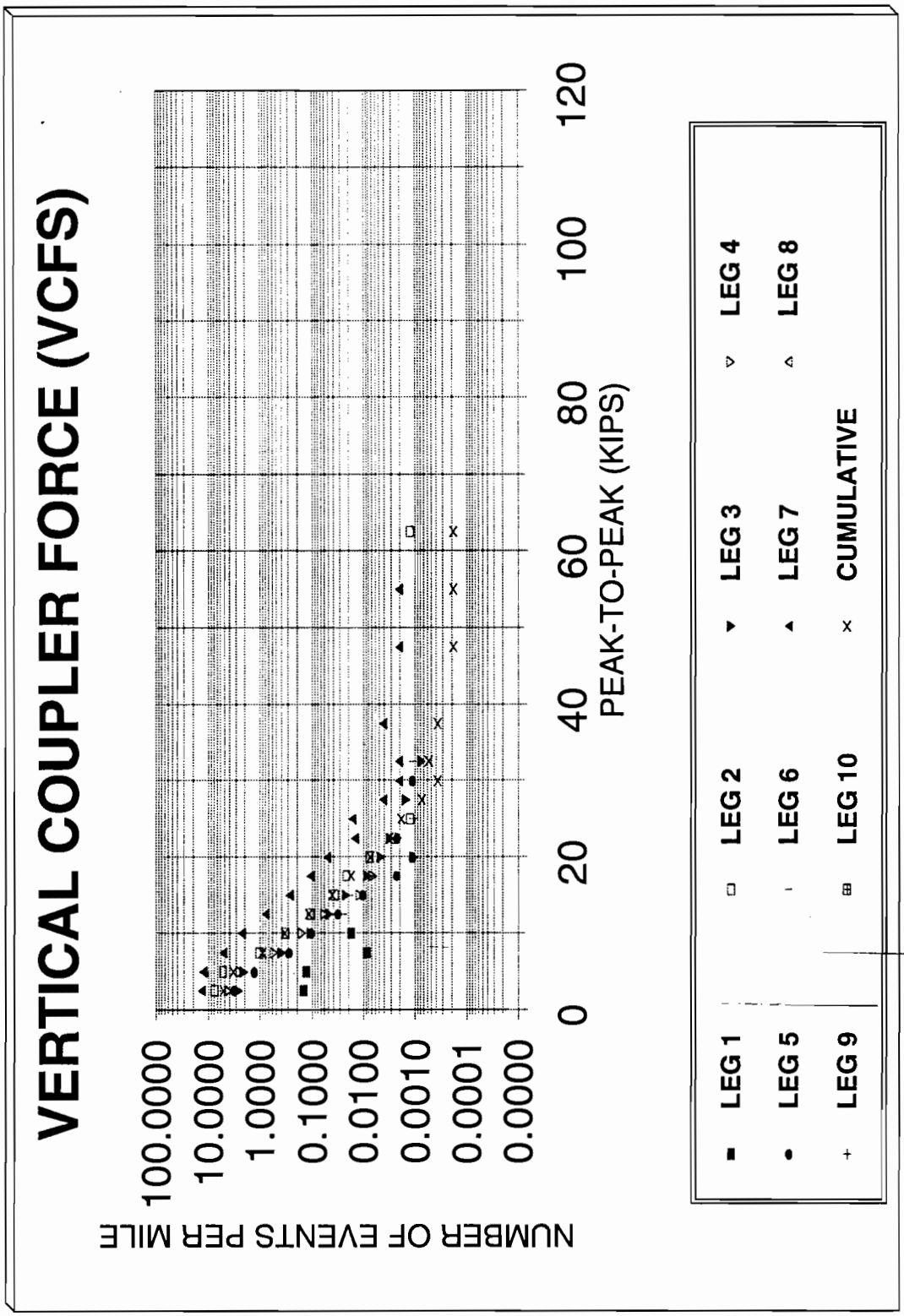

Figure A12. Loaded Portion Histograms for Measurement VCFS Number of Events per Mile

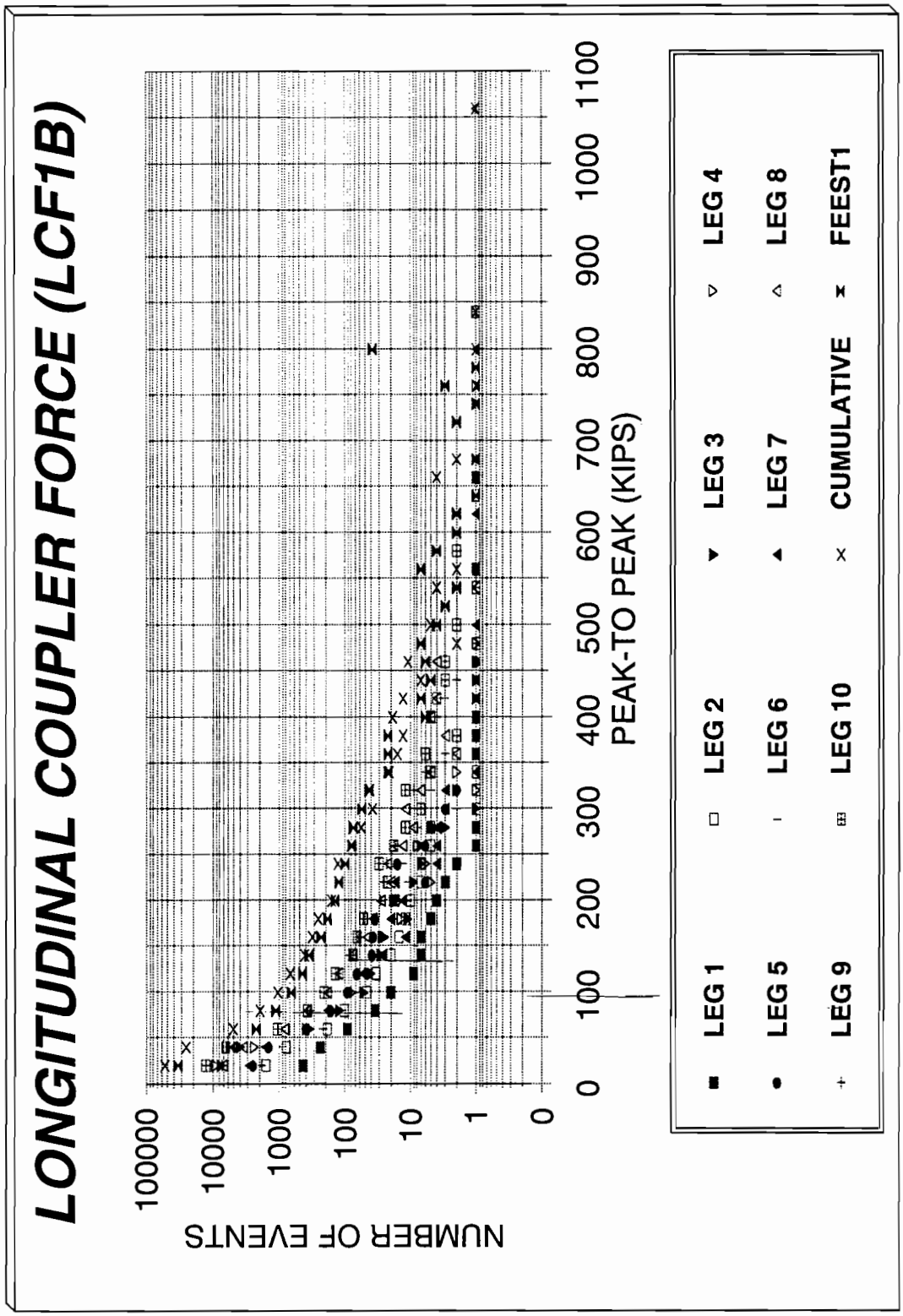

Figure A13. Loaded Portion Histograms for Measurement LCF1B Number of Events

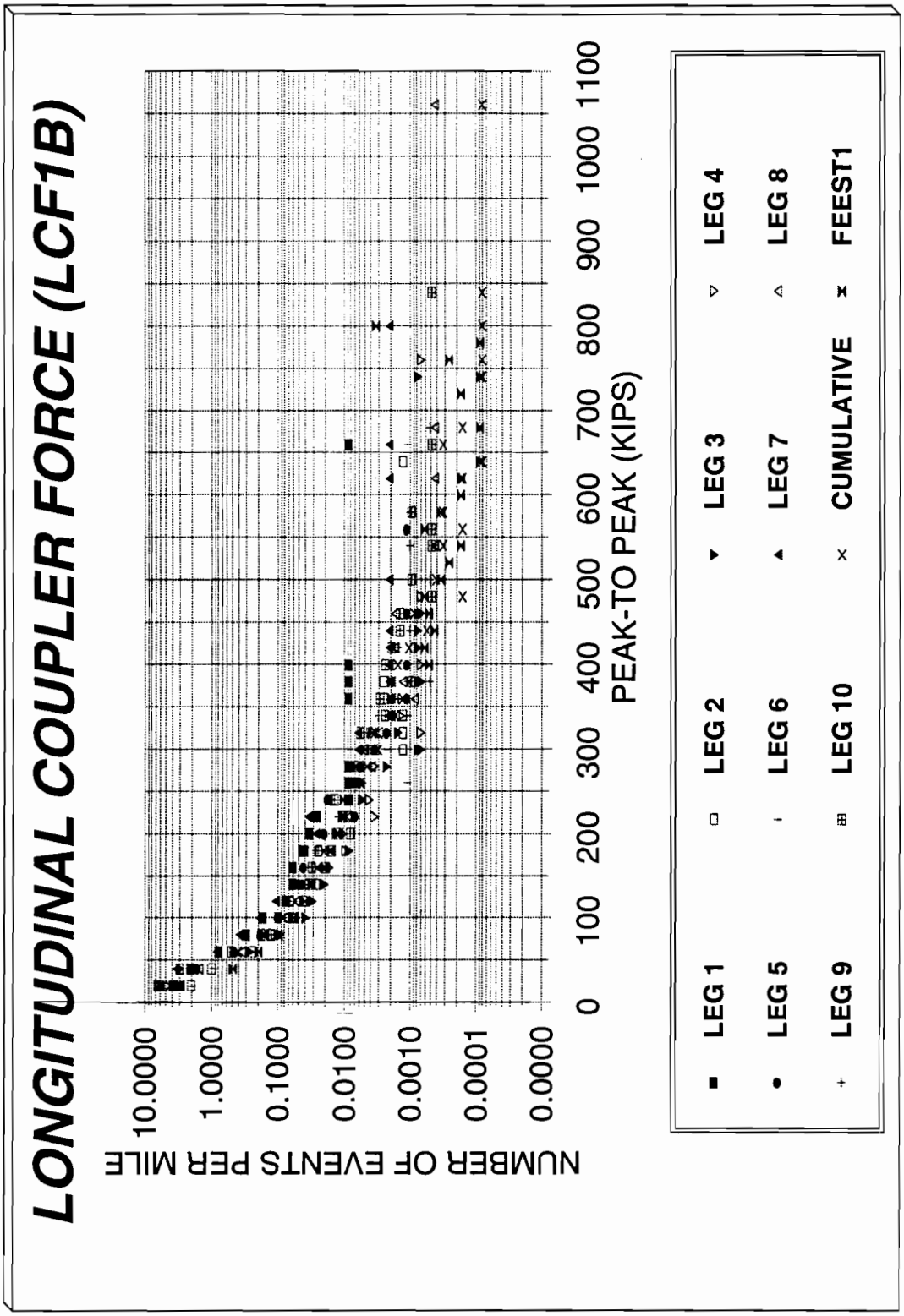

Figure A14. Loaded Portion Histograms for Measurement LCF1B Number of Events per Mile

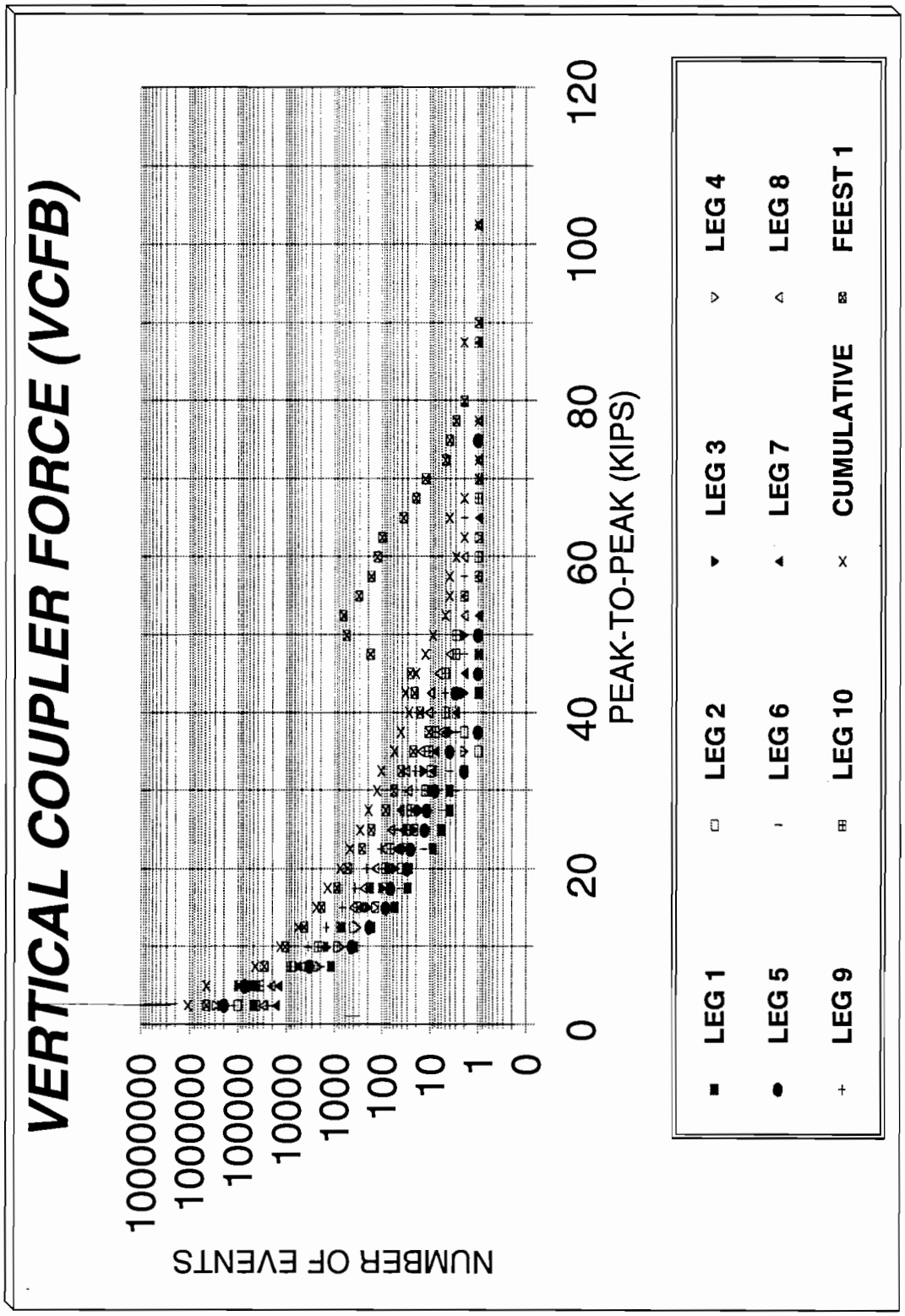

Figure A15. Loaded Portion Histograms for Measurement VCFB Number of Events

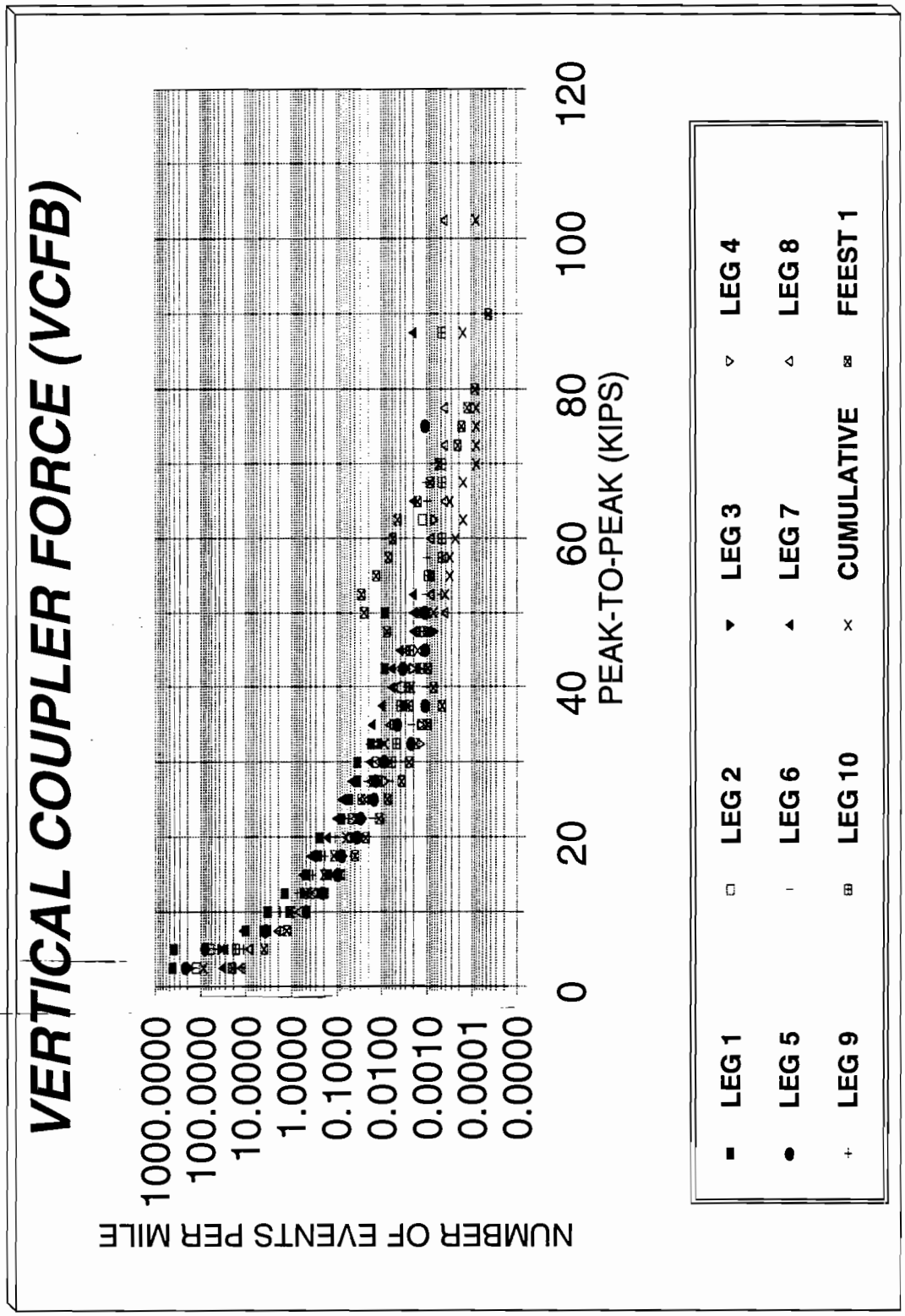

Figure A16. Loaded Portion Histograms for Measurement VCFB Number of Events per Mile

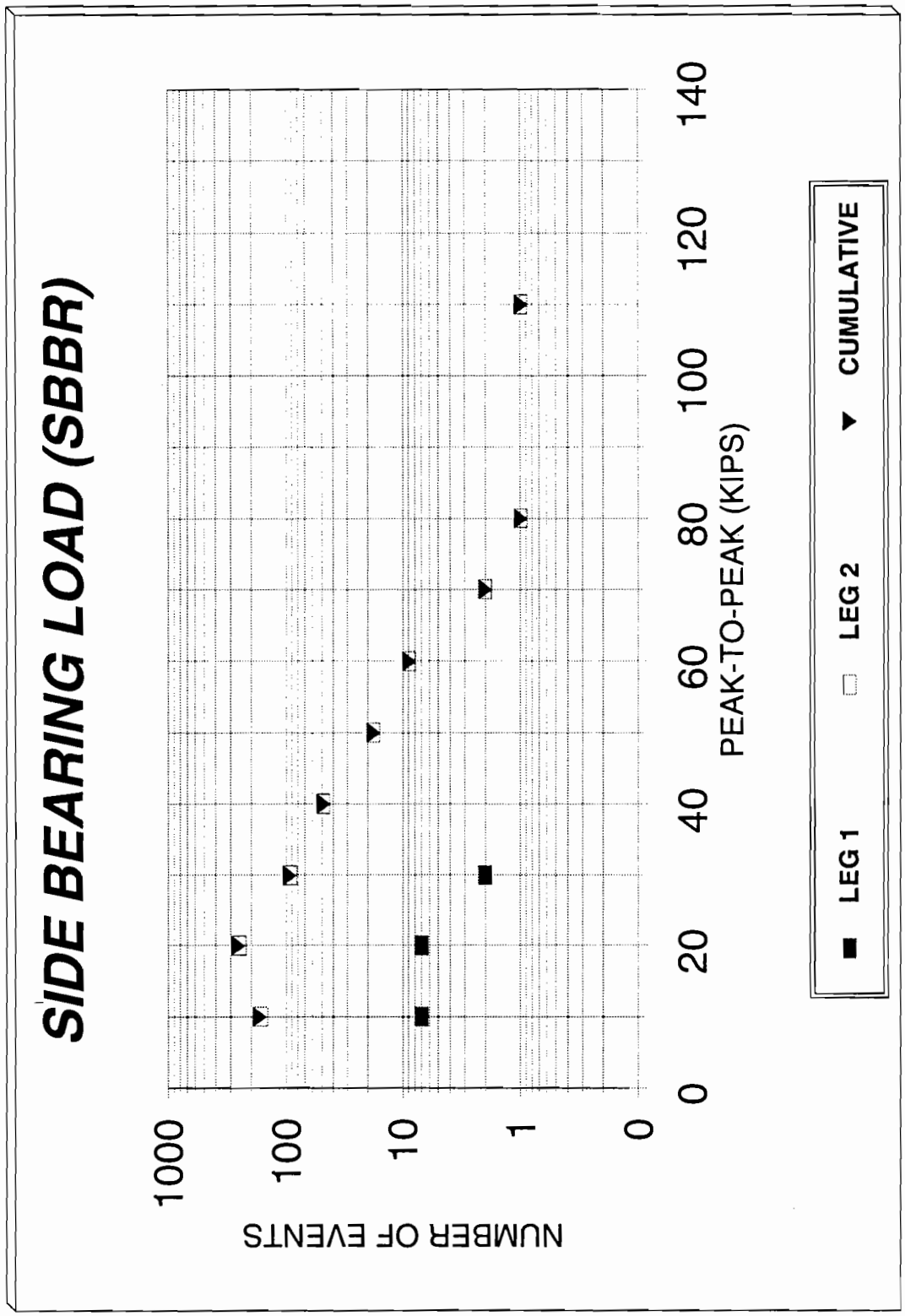

Figure A17. Loaded Portion Histograms for Measurement SBBR Number of Events

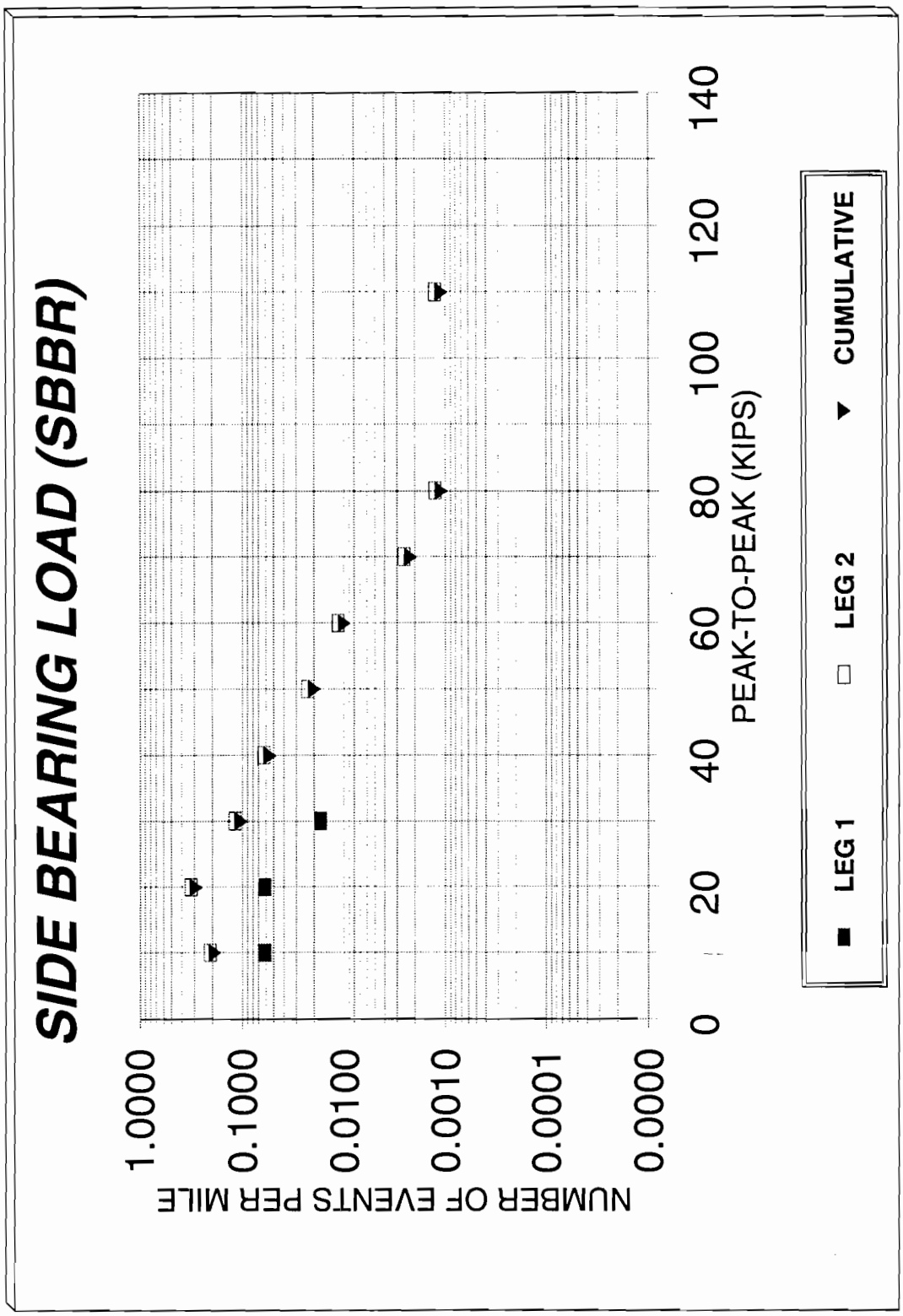

Figure A18. Loaded Portion Histograms for Measurement SBBR Number of Events per Mile

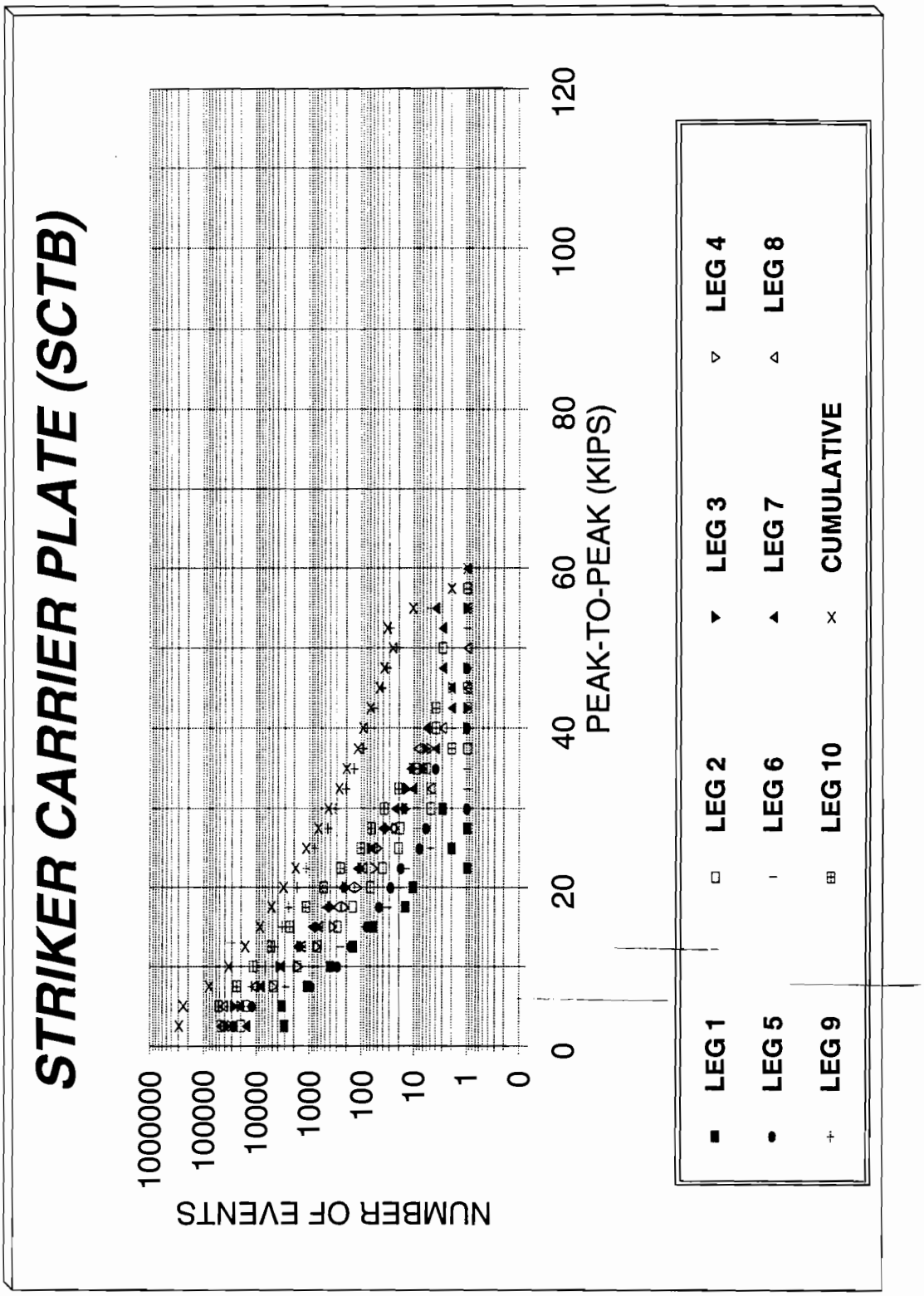

Figure A19. Loaded Portion Histograms for Measurement SCTB Number of Events